RUHR-UNIVERSITÄT BOCHUM

Wiebke Baille

Hydro-Mechanical Behaviour of Clays - Significance of Mineralogy

Bochum 2014

Heft 53

Schriftenreihe des Lehrstuhls für
Grundbau, Boden- und Felsmechanik

Herausgeber: Tom Schanz

ISSN 2190-3255

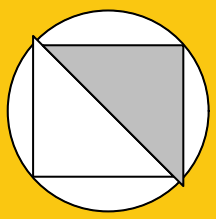

Ruhr-Universität Bochum
Schriftenreihe Grundbau, Boden- und Felsmechanik
Heft 53

Herausgeber:
Prof. Dr. -Ing. habil. Tom Schanz
Ruhr-Universität Bochum
Fakultät für Bau- und Umweltingenieurwissenschaften
Lehrstuhl für Grundbau, Boden- und Felsmechanik
44801 Bochum
Telefon: 0234/ 3226135
Telefax: 0234/ 3214236
Internet: www.gbf.ruhr-uni-bochum.de

ISSN 2190-3255

Hydro-Mechanical Behaviour of Clays – Significance of Mineralogy

Dissertation

as a requirement for the degree of

Doktor-Ingenieur (Dr.-Ing.)

at the Faculty of

Civil and Environmental Engineering

Ruhr-Universität Bochum

by

Wiebke Baille

Reviewers

Prof. Dr.-Ing. habil. Tom Schanz

Prof. Dr. Pierre Delage

Dr. Snehasis Tripathy

Bochum, December 2014

Abstract

Clays are commonly used for various geotechnical and geoenvironmental engineering applications, such as dam constructions and near-surface waste containment facilities. Montmorillonite clays have been proposed as a suitable barrier and backfilling material for the underground storage of nuclear and toxic waste in many countries. Naturally occurring expansive clays show swelling and shrinkage phenomena due to seasonal fluctuations of the ground water table which cause substantial damage to many engineering constructions. In the present work, the influence of the mineralogy and the related physicochemical and microstructural properties on the hydromechanical behaviour of various clays possessing significant proportion of one of the clay minerals from kaolinite, illite, and montmorillonite over a wide range of stress and suction was investigated. The volume change behaviour for oedometric loading condition for initially saturated clays and compacted saturated clays for maximum applied mechanical stresses up to 25 MPa was experimentally determined using a specially fabricated high stress oedometer device. The tests on compacted saturated specimens include swelling pressure measurements at confined condition due to hydration of initially compacted unsaturated specimens followed by subsequent one-dimensional compression at oedometric condition. This type of test represents the hydraulic and mechanical field condition within buffer or backfilling elements in an underground waste disposal. Further, the influence of mineralogy on the water retention behaviour and volume change due to an increase in suction was experimentally investigated. The microstructure of the clays at selected stress states was studied using ESEM and MIP. The influence of mineralogy and loading path on the volume change in the range of low and high stresses was pointed out. The experimental void ratio-stress relationships are compared to their theoretical counterparts, which were obtained using various approaches based on diffuse double layer theory. The applicability of the various approaches was discussed. The influence of mineralogy on effective stress in clays was assessed using suction stress approach. Based on the performed investigation, conclusions regarding the significance of mineralogy on the hydro-mechanical behaviour of the clays were drawn, and suggestions for future studies were made.

Zusammenfassung

Tone finden verbreitet Anwendung in verschiedenen geotechnischen und umweltgeotechnischen Anwendungen, wie zum Beispiel bei Dammbauwerken und Oberflächenabdichtungen. Bentonite wurden zur Verwendung als Dichtmaterial für geotechnische Barrieren im Rahmen der Konzepte von untertägigen Deponien zur Entsorgung von toxischem und radioaktivem Abfall vorgeschlagen. Natürlich vorkommende quellfähige Tone neigen bei saisonalen Veränderungen des Grundwasserspiegels zu Verformungen infolge von Quell- und Schrumpfvorgängen. Diese können erhebliche Schäden an Bauwerken verursachen.

In der vorliegenden Arbeit wurde der Einfluss der Mineralogie und der damit zusammenhängenden physiko-chemischen und mikrostrukturellen Eigenschaften von ausgewählten Tonen auf deren hydro-mechanisches Verhalten bei verschiedenen Belastungspfaden untersucht. Die Tone bestanden jeweils hauptsächlich aus einem der Minerale Kaolin, Illit und Montmorillonit. Es wurden die Quelldrücke unter volumenkonstanten Randbedingungen sowie das Volumenänderungsverhalten der Tone infolge mechanischer Belastung in einem speziell entwickelten Hochdruckoedometer sowohl für initial gesättigte als auch für initial ungesättigte, verdichtete Proben über einen großen Spannungsbereich untersucht, der repräsentativ für die Verwendung des montmorillonitischen Tones in Untertagedeponien in tiefen geologischen Formationen ist. Desweiteren wurde die das hydraulische Verhalten von Böden bestimmende Saugspannungs-Wassergehalts-Beziehung sowie die durch Trocknung induzierten Volumenänderungen experimentell bestimmt. Die Änderung der Mikrostruktur der Tone wurde bei ausgewählten Zuständen der Tone mittels Elektronenrastermikroskop und Quecksilberporosimetrie untersucht. Der Einfluss der Mineralogie sowie der Spannungspfade auf das Volumenänderungsverhalten wurde diskutiert. Hierzu wurden die experimentellen Daten zusätzlich im Kontext des Konzeptes der effektiven Spannungen interpretiert. Die Anwendbarkeit von verschiedenen Ansätzen basierend auf der Theorie der diffusen Doppelschicht zur Berechnung der Volumenänderung und des Quelldruckes in Tonen wurde untersucht. Es konnten wesentliche Schlussfolgerungen hinsichtlich des Einflusses der Mineralogie auf das hydro-mechanische Verhalten der Tone gezogen werden, und es wurden Vorschläge für weitere Untersuchungen unterbreitet.

Vorwort des Herausgebers

Tone finden eine breite Anwendung in den verschiedensten Bereichen der Geotechnik. Besonders bei Anwendung in der Umweltgeotechnik ist es von entscheidender Bedeutung die hydromechanischen Eigenschaften (z.B. Steifigkeit, Permeabilität, Quellpotential) von Tonen genau zu kennen. In den vergangenen Jahren werden Tone bzw. Mischungen von Tonen mit Sand auch bei Konzepten zur Endlagerung von radioaktiven Abfällen in geologischen Formationen diskutiert und auf ihre Einsetzbarkeit hin analysiert. Generell lassen sich Tone bzgl. ihrer Mineralogie in drei Hauptgruppen einteilen. Dies sind die Montmorillonite, die Illite und die Kaolinite. Natürliche Tone lassen sich entsprechend ihrer Hauptbestandteile dieser drei Tonminerale klassifizieren. Die Arbeit von Frau Baille beschäftigt sich damit, die Materialeigenschaften dieser drei Tone in Abhängigkeit ihrer Mikrostruktur zu untersuchen. Bei den Materialeigenschaften stehen der Quelldruck, die Kompressibilität und die Saugspannungs-Wassergehalt-Beziehung im Mittelpunkt. Frau Baille schlägt verschiedene neuartige Versuchsgeräte und Versuchsprotokolle vor. Erstere werden konstruiert, kalibriert und validiert. Die verwendeten Versuchsprotokolle sind innovativ und international führend. Frau Baille gelingt es unter Verwendung der klassischen physiko-chemischen Grundlagen in Form der Theorie der diffusen Doppelschichten, ihre experimentellen Ergebnisse qualitativ und quantitativ zu erklären. Die Arbeit stellt aus internationaler Sicht einen entscheidenden Beitrag zur Fortentwicklung des Wissens auf diesem Fachgebiet dar. Der von Frau Baille erarbeitete Datensatz ist in seiner Vollständigkeit international ohne Vergleich.

Ich möchte mich ausdrücklich für das langjährige Vertrauen unserer Fördermittelgeber bedanken. Stellvertretend seien hier die verschiedenen durch das BMBF geförderten Projekte genannt. Die sehr gute Zusammenarbeit mit Dr. Pitterich und Herrn Bühler vom Projektträger in Karlsruhe (PTKA-WTE) ist mustergültig.

Bochum, Dezember 2014 Tom Schanz

Acknowledgement

The research work was performed both at Laboratory of Soil Mechanics of Bauhaus-Universität Weimar and the Chair of Foundation Engineering, Soil and Rock Mechanics of Ruhr-Universität Bochum under the guidance of Prof. Dr.-Ing. habil. T. Schanz. I thank Prof. Schanz for giving me the opportunity to join his research group at Weimar and to finalise the work at Ruhr-Universität Bochum. I am grateful to Prof. Schanz and Dr. Snehasis Tripathy (Cardiff University, UK) for initiating the research topic and for their continuous support by discussions, constructive comments and suggestions.
The scientific cooperation with the geotechnical group at École des Ponts ParisTech is gratefully acknowledged. I thank Prof. Pierre Delage for the opportunity of a short research stay at École des Ponts, and for his agreement to be external reviewer of the dissertation.
I express my gratitude to Dr. rer. nat. Bernd Möser of F.A. Finger-Institut für Baustoffkunde at Bauhaus-Universität Weimar for the cooperation with regard to the investigation of the clays using the environmental scanning electron microscopy (ESEM) facilities. I thank Mrs. Lydia Schmiedel of the same institute for performing the mercury intrusion porosimetry (MIP) tests.
Further, I would like to thank Dr. Stephan Kaufhold from the Federal Institute for Geosciences and Natural Resources (BGR) in Hannover for the cooperation with respect to the physico-chemical and mineralogical characterisation of the clays.
The majority of the experiments was conducted at Bauhaus-Universität Weimar; my thank goes to Dipl.-Ing. (FH) Gabriele Tscheschlok and Frank Hoppe for their assistance in the laboratory. I thank the team of the technical co-workers Michael Skubisch, Werner Müller, Joachim Blazytko and Bernhard Sperl from the laboratory, and Ralf Schudy and Bernd Schmidt from the workshop for their help in the installation of the ClayLab after the move to Ruhr-Universität Bochum.
I thank my parents for their continuous support without any hesitation. I am deeply thankful to my husband Michel for his patience.

Bochum, Dezember 2014 Wiebke Baille

Contents

List of Figures

List of Tables

1. Introduction

1.1. Background

Clays are widely used in industrial and engineering applications because they possess specific properties due to their reactivity and catalytic activity, or inertness and stability, as well as regarding their rheological behaviour. In nature, either monomineralic clays or mixture of clay and non-clay minerals can be found. These mixtures are called common clays and represent the largest group of minerals used for engineering purposes in terms of tonnage. They are commonly used for various geotechnical and geoenvironmental engineering applications, such as road and dam constructions and fills. Further, common clays and bentonites are used in near-surface waste containment facilities consisting of a cover and a bottom liner. The former has to serve for minimizing rainwater infiltration, gas emission and erosion, whereas the latter has to prevent leaching migration of contaminants to the groundwater. Bentonites are also used for the construction of slurry trench walls, in shield tunneling, subsoil sealing, as antifriction agent for pipejacking and shaftsinking or for water and waste water purification. Further, the minerals kaolinite, illite and montmorillonite were shown to be effective in environmental control and remediation of sites contaminated with cationic heavy metal pollutants (Grim 1962, Grim 1968, Bergaya & Lagaly 2013). Naturally occurring expansive clays, mostly in arid and semiarid regions of the world, show swelling and shrinkage phenomena due to seasonal fluctuations of the ground water table which cause substantial damage to many engineering constructions.

Bentonites have been proposed as a suitable barrier and backfilling material for the underground storage of nuclear and toxic waste in many countries (Pusch 1977, Dixon & Gray 1985, Radhakrishna, Chan, Crawford & Lau 1989, Herbert & Moog 2002). Bentonites are considered to be suitable sealing materials because of their high swelling capability, low permeability upon imbibing water or electrolytes, and low ion diffusivity (Pusch 1982). The waste of different degree of toxicity is planned to be stored in underground waste repositories in deep geological formations at about 500 to 1000 m below ground level. The types of host rock considered are crystalline rocks, salt deposits and

clay-rich sediments. In some concepts, the engineered barrier system consists of a highly compacted bentonite buffer surrounding the waste canisters and of a bentonite or bentonite/sand sealing element closing the access gallery or shaft to the disposal area. Both the initially unsaturated buffer and sealing element tend to absorb water from the the surrounding saturated host rock and exert swelling pressure on the adjacent restraint assuming that volume change is simultaneously prevented by the host rock acting as confinement against the volume increase.

According to the specific applications of the clays given above, they are in either initially compacted unsaturated or initially saturated state (slurry). The boundary and loading conditions acting on the clay systems and thus, the state of the clay system itself usually undergo changes with time. Unsaturated clayey soils possessing clay minerals exhibit swelling or compression when inundated with fluids. Similarly, saturated clays composed of these clay minerals usually undergo significant volume decrease during the drying process and due to an increase in the surcharge. Therefore, the understanding of the long-term hydraulic and mechanical behaviour of the clays is extremely relevant. Considering the application of bentonite in an underground waste disposal, the relevant magnitude of applied mechanical stress on the clay can be in the order of up to 20 MPa. Similarly, a significantly larger amount of energy, or suction, is needed to bring a clay from saturated to dry state as compared to granular soils. The changes in void ratio, water content and degree of saturation induced by mechanical or hydraulic loading depend on the clay mineral type. The various clay mineral types are characterised by typical microstructural features and physicochemical properties, such as specific surface area, cation exchange capacity, and type and amount of exchangeable cations present. The macroscopic volume change behaviour is strongly related to these features. Identification of the relevant micromechanical mechanisms and the prediction of the engineering behaviour of clays based on these mechanisms and the physicochemical properties is still a challenge.

Considering the in-situ condition of the compacted bentonite as sealing material in the access galleries, shafts and in the buffer, most studies on swelling pressures have been carried out at strain-controlled boundary condition inhibiting swelling strains upon fluid imbibition (Müller-Vonmoos & Kahr 1982, Gray, Cheung & Dixon 1984, JNC 2000, ENRESA 2000). A number of laboratory studies reported in the literature focussed on studying the hydro-mechanical behaviour of clays by subjecting them to large pressures and suctions (Fleureau, Kheirbek-Saoud, Soemitro & Taibi 1993, Fleureau, Verbrugge, Huergo, Gomes Correia & Kheirbek-Saoud 2002, Al-Mukhtar, Qi, Alcover & Bergaya 1999, Marcial, Delage & Cui 2002). Most of the studies on the volume change behaviour of ben-

tonites due to the application of mechanical stress were for initially saturated clays with initial water content greater than the liquid limits of the clays. The compressibility behaviour of compacted bentonites after the swelling pressure is developed under confined conditions is a near field situation and has not been studied so far.

There have been substantial contributions on the study of the compressibility behaviour of clays by several researchers in the past who emphasized the influence of physicochemical forces on the void ratio due to an increase in the applied stress (Bolt 1956, Olson & Mesri 1970, Mesri & Olson 1971, Sridharan & Rao 1973, Mitchell 1993, Di Maio, Santoli & Schiavone 2004). Several research works have investigated the behaviour of clays at greater applied stresses than usually encountered in standard oedometer tests (>1 MPa) (Bolt 1956, Warkentin, Bolt & Miller 1957, Mesri & Olson 1971, Yong & Mohamed 1992, Al-Mukhtar et al. 1999, Marcial et al. 2002, Di Maio et al. 2004). Most of these studies focused on the compressibility behaviour of bentonites. Only few studies are known which report on the influence of mineralogy on the volume change of initially saturated clays representing various main mineral types such as kaolinite, illite, and montmorillonite (Sridharan & Rao 1973, Tessier 1984, Fleureau et al. 1993). However, in these studies, the range of applied mechanical stresses was limited to the standard range. Again, only few studies have been performed to compare the volume change of initially saturated clays due to an increase in applied mechanical stress and due to an increase in suction. However, these studies consider only the standard range of applied mechanical stress <1 MPa (Tessier 1984, Fleureau et al. 1993) or were restricted to only bentonites (Marcial et al. 2002).

Several attempts have been made in the past to determine compressibility, i.e. the void ratio-applied stress relationships, and swelling pressures of clays using diffuse double layer theory (Bolt 1956, Mesri & Olson 1971, Sridharan & Rao 1973, Sridharan & Jayadeva 1982, Pusch 1982, Yong & Mohamed 1992, Sridharan 2002). A modified diffuse double layer approach was proposed for the prediction of swelling pressures of compacted bentonites and compressibility of initially saturated clays at large applied stresses and suctions (Tripathy, Sridharan & Schanz 2004, Tripathy & Schanz 2007, Schanz & Tripathy 2005). In some of the research works dealing with the effect of physicochemical forces composed of repulsive and attractive forces on the volume change of saturated clays, considerations regarding the incorporation of these forces into the classical effective stress concept were made (Bolt 1956, Lambe 1958*b*, Sridharan & Rao 1973). Also, for the determination of effective stress in unsaturated soils several concepts have been proposed in the past, and were mostly applied to unsaturated shear strength of soils. The application of these

concepts to volume change behaviour of clays on account of applied suction and applied vertical stress in k_0- condition have not been explored yet.

1.2. Objectives

The aim of the present work is to investigate the influence of the mineralogy and the related physicochemical and microstructural properties on the hydromechanical behaviour of various clays possessing significant proportion of one of the clay minerals from kaolinite, illite, and montmorillonite over a wide range of stress and suction. The clays used were Spergau kaolin, NX illite and Calcigel bentonite, all originating from Germany.

The objectives of the investigation are as follows:

- Experimental determination of the basic and physicochemical properties of the clays studied. The physicochemical properties are required as parameter for the assessment based on theoretical considerations.
- Experimental determination of the applied stress-void ratio relationships for oedometric loading condition for (i) initially saturated clays and (ii) compacted saturated clays for maximum applied mechanical stresses up to 25 MPa. The tests on compacted saturated specimens include swelling pressure measurements at confined condition due to hydration of initially compacted unsaturated specimens followed by subsequent one-dimensional compression at oedometric condition. For Calcigel bentonite, this type of test represents the hydraulic and mechanical field condition within buffer or backfilling elements in an underground waste disposal.
- Experimental investigation of the influence of mineralogy on the water retention behaviour of the clays including measurement of water content, void ratio and degree of saturation due to an increase in suction.
- Microstructural investigation of the clays at selected stress states using ESEM and MIP.
- Assessment of the void ratio-stress relationships based on considerations using the diffuse double layer theory.
- Assessment of the influence of mineralogy on effective stress in clays using suction stress approach.

1.3. Layout of the thesis

The thesis is composed of eleven chapters. Following the introductory chapter (first chapter), the state of the art is presented in the second chapter. The state of the art covers the current knowledge regarding clay mineralogy, fabric and related interparticle forces in clay-water systems. Further, it describes the mechanisms responsible for swelling pressure development, and it provides a review on relevant aspects regarding volume change in clays due to applied mechanical loading paths and due to applied suctions. The last section of the second chapter deals with the main issues regarding effective stresses in clays.

The third chapter is divided into three sections: firstly, the detailed material characterisation is presented, followed by the description of the experimental methods applied, and the overview about the experimental programme.

Chapters four, five and six cover the presentation of the experimental results regarding the water retention behaviour including volume change due to an increase in suction, the swelling pressures, and the compressibility as obtained from high stress oedometer tests, respectively.

In chapter seven, the effect of loading type and and mineralogy on the volume change in clays at low and high stresses are discussed, based on microstructural investigations by Environmental Scanning Electron Microscopy (ESEM) and mercury intrusion porosimetry (MIP).

Chapter eight contains the assessment of the experimental results obtained in chapters four, five and six using theoretical approaches based on diffuse double layer theory. Chapter nine presents a study regarding additional repulsive pressures in compacted clays. Additionally to the three clays used, reported data of five other bentonites reported in literature were considered in this chapter.

Chapter 10 covers a study on effective stress in clays using suction stress concept. Distinction of the influence of clay mineral type on the shape of the suction stress characteristic curve, magnitudes of minimum and maximum suction stress, and further, their influence on the effective stress of clays for a large range of suction are discussed in this chapter.

The last chapter (chapter 11) presents the conclusions drawn based on the results obtained in the the foregoing chapters, and suggestions and recommendations for further studies in this field are given.

2. State of the art

2.1. General

The state of the art covers the basic knowledge about clay mineralogy, the forces involved at small-scale level, and the principal fabric of kaolin, illite and montmorillonite clays in the state of suspension and in compacted state. Further, knowledge about the swelling mechanisms in clays, the volume change behaviour of clays during one-dimensional consolidation, and during unconfined drying are presented. Finally, an overview about the application of approaches based on physico-chemical theories to describe stress-strain relationships and effective stresses in clays is given.

2.2. Clay mineralogy, solid-water interactions in clays and forces at particle level

2.2.1. Clay mineralogy

In this section, the basics of clay mineralogy and some clarification regarding the nomenclature used in this work are given, followed by a description of the crystal structure of kaolinite, montmorillonite and illite minerals, each of them representing the main constituent of the clays used in the present study (Spergau kaolin, Calcigel bentonite, and NX illite, respectively). Further, the different types of solid-water interactions in clays are presented, and, based on this, the resulting forces in the clay-water system are presented.

2.2.1.1. Terminology and basics of clay mineralogy

The term *clay* may be somewhat ambiguous since it may refer to a grain size, a rock or soil type and mineral type. To avoid ambiguity, a clear distinction has to made between

clay and *clay mineral*. The term clay can stand for a rock, sedimentary deposit and the weathering products of primary silicate minerals (Bergaya & Lagaly 2013, Moore 1996), thus, it is not related to a specific genesis. The joint nomenclature committee (JNC) of the Clay Minerals Society has defined clay as a naturally occurring material, primarily composed of fine-grained minerals, which is plastic at appropriate water contents and will harden when dried or fired.

A mineral is a chemical compound or element that is normally crystalline and that has been formed as a result of a naturally occurring, e.g. geological, processes (Nickel (1995) in Bailey, Brindley, Johns, Martin & Ross (1971)). The term clay mineral signifies a class of hydrated phyllosilicates, which are composed of a specific combination of two basic structural units, the *silica tetrahedral sheet* and the *octahedral sheet*. According to the proposed definition of JNC clay minerals are '... phyllosilicate minerals and minerals which impart plasticity to clay and which harden upon drying or firing'. The definition of clay mineral does not include the origin of the material or the size, thus, a clay mineral may be synthetic (unlike clay) and of any size.

The main properties characterizing clay minerals can be summarized as follows (Bergaya & Lagaly 2013):

- a layer structure with one dimension in the nanometre range; 1:1 layer thickness about 0.7 nm, and 2:1 layer thickness about 1.0 nm,
- anisotropy of the layers or particles
- existence of several types of surfaces: external basal (planar) surfaces, external edge surfaces, internal surfaces (interlayer surfaces)
- ease of modification of the external, and often also the internal, surface by adsorption, ion exchange, grafting,
- plasticity,
- hardening on drying or firing (valid for most clay minerals).

The terms used in the present work for the different structural levels in clay minerals are in accordance to the actual recommendations of the JNC. They are as follows: a *plane* of atoms, a tetrahedral or octahedral *sheet*, a 1:1 *layer* (= two-sheet *layer*), a 2:1 *layer* (= three-sheet *layer*).

There are two basic structural units involved in the atomic or crystal structures of clay minerals: (*i*) the *silica tetrahedral sheets* (Figure 2.1a) and (*ii*) the *aluminum* or *magnesium octahedral sheets* (Figure 2.1b). In the silica tetrahedron, a silicon atom is equidistant

from four surrounding oxygens (or hydroxyls, if needed to balance the structure). Six tetrahedra form a hexagonal network by sharing the oxygens at the base of the tetrahedra. The network is repeated indefinitely in a- and b-direction forming the tetrahedral sheet. The tips of the silica tetrahedra (oxygen or hydroxyls) all point in the same direction. In the octahedron, an aluminum, iron or magnesium atom is equidistant from six hydroxyls or oxygens. When a divalent cation is present, all the positions in the octahedral sheet are filled and the the structure is *trioctahedral*. On the other hand, with a trivalent cation in the octahedral sheet, only two-thirds of the positions are filled to balance the structure, and the structure is called *dioctahedral*. With magnesium as octahedrally coordinated cation, the sheet is called *brucite*. Is aluminum the octahedrally coordinated cation, the sheet is called *gibbsite*.

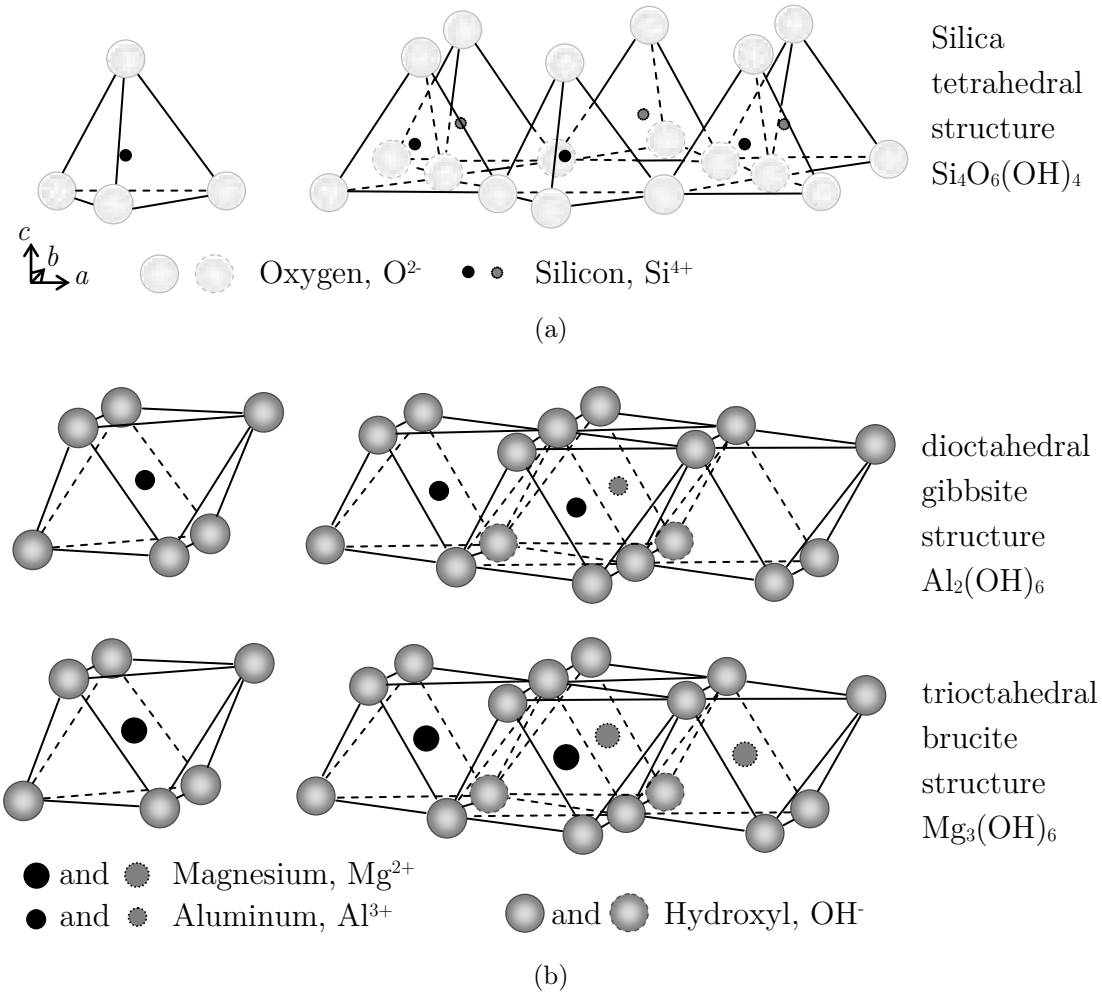

Figure 2.1.: Diagrammatic sketch of tetrahedral and octahedral units, modified after Grim (1968): (a) single silica tetrahedron (left), sheet of tetrahedra arranged in a hexagonal network (right), (b) single octahedron (left), di- and trioctahedral sheets (right).

A *layer* consists of one or more tetrahedral sheets and an octahedral sheet. There are two types of layers, depending on the ratio of the component sheets: a 1:1 layer has one tetrahedral sheet and one octahedral sheet (TO), whereas a 2:1 layer has an octahedral sheet between two opposing tetrahedral sheets (TOT). The different clay mineral groups are characterised by the manner in which successive two- or three-sheet layers are stacked and held together. Layers may be separated from one another by various *interlayer* materials: cations, hydrated cations, organic molecules, and hydroxide octahedral groups and sheets. A *unit* or *unit structure* is the total assembly of the layer and any interlayer material. Thus, a kaolinite unit structure consists of a 1:1 layer, but an illite unit structure consists of a 2:1 layer plus the interlayer potassium cations (Grim 1968). A *particle* is formed by a number of stacked layers (Tessier & Pedro 1976, Bergaya & Lagaly 2013). The number of layers contained in a single clay particle depends mainly upon the mineral type. For bentonites, the number of layers per particle varies with the amount of water available and ranges from 1 layer per particle in the extreme case of highly diluted suspensions up to several hundreds of layers per particle at dry conditions (Tessier 1984).

Substitutions of ions of one type by ions of another type having the same or different valence, while retaining the same crystal structure, is termed *isomorphous substitution* (Grim 1968). Type and amount of isomorphous substitution differs both within and among clay mineral groups. Common examples for substitutions in clay minerals are aluminum in place of silicon, magnesium instead of aluminum, and iron (Fe^{2+}) for magnesium. The actual cation distribution in the tetrahedral and octahedral sheets may develop during initial formation or subsequent alteration of the mineral. Isomorphous substitution is the source of the net negative charge of clay particles. However, it exist various interpretations about the source of surface charge in case of kaolinite, which is known to vary with chemical composition or due to structural defects (Wang & Siu 2006*a*). Cations of one type my be exchanged by cations of another type, where the cation type determines the ease of exchangeability. Exchangeability decreases for the ions given below from from left to the right: $Li^+ \rightarrow Na^+ \rightarrow K^+ \rightarrow Mg^{2+} \rightarrow Ca^{2+} \rightarrow Sr^{2+} \rightarrow Ba^{2+} \rightarrow Al^{2+}$.

2.2.1.2. Kaolinite

The kaolinite minerals are composed of alternating tetrahedral and octahedral sheets as shown schematically in Figure 2.2a. The tips of the silica tetrahedra all point towards the center of the kaolinite unit layer. In the common plane of atoms, two-thirds of the atoms are oxygens and are shared by both the tetrahedral silica sheet and the octahedral sheet. The remaining atoms in this plane are hydroxyls (OH). The octahedral sheet is a

dioctahedral gibbsite sheet (with Al^{3+} as cation). The structural formula of kaolinite is

$$(OH)_8Si_4Al_4O_{10} \tag{2.1}$$

and the charge distribution for the unit cell is indicated in Figure 2.2b. The basic units are stacked in c-direction.

The strong bonding between the layers, thus, between the Al-face site and the Si-face site, is on account of elecrostatic attraction, van der Waals forces and hydrogen bonding.

Values of measured cation exchange capacity from 3 to 15 meq/100g indicate that particles possess a net negative charge. A review of literature as given in Palomino & Santamarina (2005) or Wang & Siu (2006*b*) suggests that the surface charge at the Si-tetrahedral face site is on account of isomorphous substitution (Al^{3+} for Si^{4+}), and thus, is permanently negative. The Al-octahedral face site consists of hydroxyl groups, giving rise to a slightly pH-dependent charge which can be positive or negative. In sum, the charge of the two face sites is considered to be negative with a pH-dependent magnitude. The surfaces of the two edge sites consists of hydroxyl groups (OH_2, OH^-, O^{2-}) resulting from broken bond, and protonation or deprotonation. The edge-sites are strongly pH-dependent, resulting an an either positive or negative charge (see Fig. 2.3).

Since interlayer separation does not occur in kaolinite, balancing cations are adsorbed on the external surfaces and edges of the particles.

2.2.1.3. Montmorillonite

This section starts with a short clarification about the use of the terms *bentonite*, *montmorillonite* and *smectite*. It is becoming widely accepted that smectite refers to a group of clay minerals which is characterised by a 2:1 layer structure, a net charge deficiency resulting from isomorphous substitution of about $\xi = 0.2$ to 0.6 C/HUC (HUC refers to 'half unit cell'), balanced by external exchangeable cations, and which has weak bonding between the layers enabling water molecules and other polar molecules to enter between and separate the layers. Montmorillonite is a species of smectite group which differs in type, amount and placement of the substituted ions from other members of the smectite group (e.g., beidellite, hectorite, saponite). The term *bentonite* signifies a clay which was formed by the alteration of volcanic ash in situ, which are composed of smectite clay minerals to a great extend, and which are generally highly colloidal and plastic.

The prototype structure for smectite minerals is that of the electrically neutral, non-clay material pyrophyllite (Figure 2.4). An octahedral sheet is sandwiched between two silica

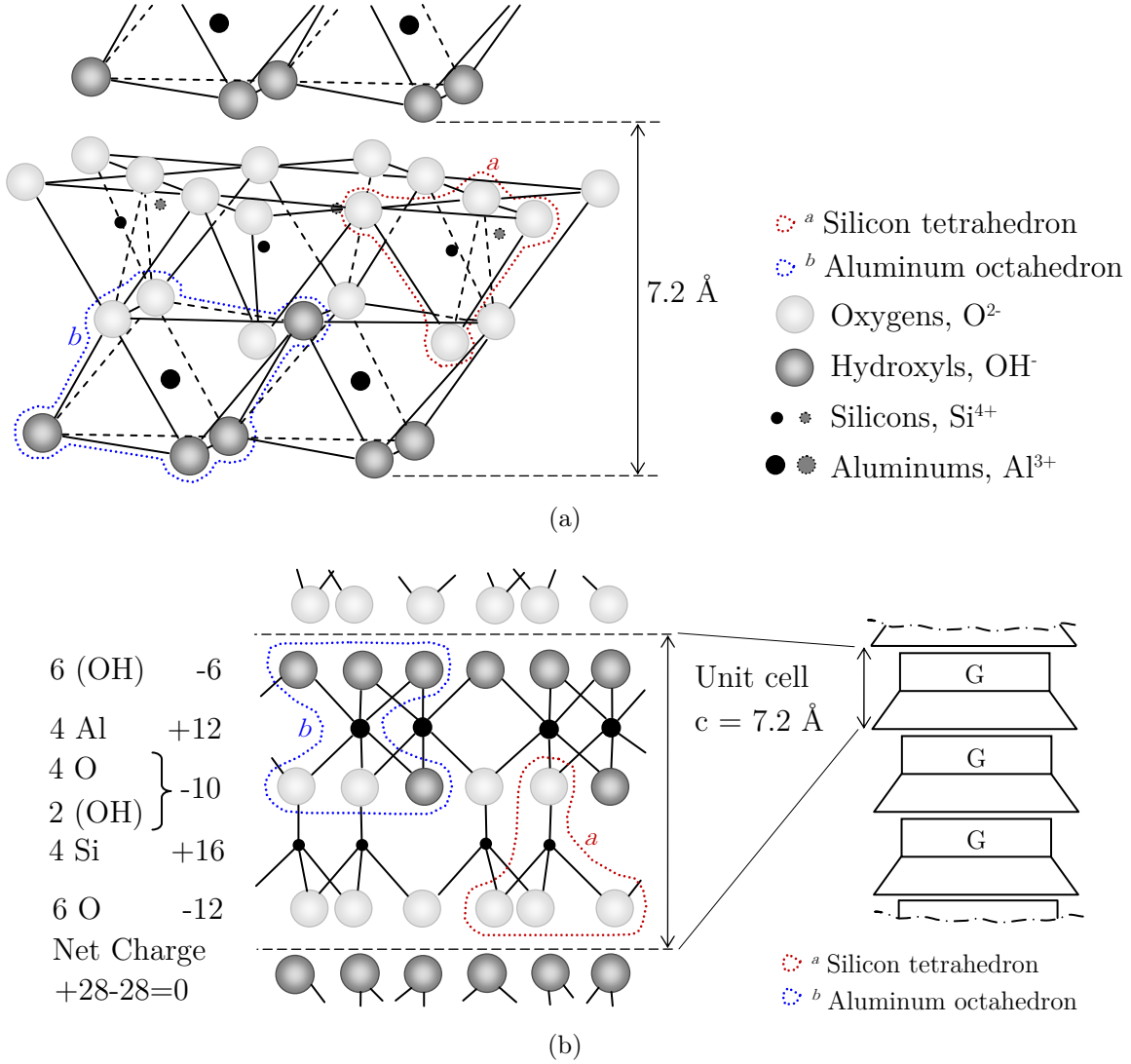

Figure 2.2.: Diagrammatic sketch and charge distribution of kaolinite, modified after Grim (1968): (a) diagrammatic sketch of the kaolinite structure, (b) charge distribution on kaolinite.

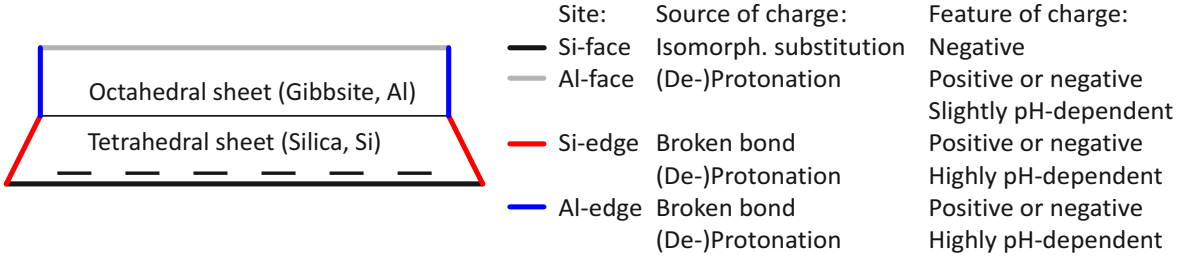

Figure 2.3.: Surface charge characteristics of kaolinite, modified after Wang & Siu (2006a).

tedrahedral sheets. The oxygen atoms of the tips of the tetrahedra of both silica sheets point towards the centre of the layer and are also common to the octahedral sheet. The hydroxyls belonging to the octahedral sheet fall directly above and below the hexagonal holes formed by the bases of the silica tetrahedra.

The 2:1 layers formed in this way are continuous in a- and b-direction and are superposed in c-direction. The oxygen plane of each unit is adjacent to the oxygen plane of the neighboring unit. This results in a cleavage and weak bonding between successive layers. The bonding forces result from van der Waals forces and cations that are present to balance the charge deficiencies in the structure. The main characteristic of smectite minerals is that water molecules and other polar molecules can enter the interlayer space and separate the layers. As a result, the crystal structure expands in c-direction, and layer-to-layer distances of more than 0.96 nm occur. In completely dehydrated smectite, the c-axis spacing varies slightly with the size of interlayer cation present. The larger the cation, the larger is the c-axis spacing.

The theoretical composition without considering isomorphous substitution, i.e., for the electrically neutral structure of pyrophyllite, is

$$(OH)_4Si_8Al_4O_{20} \cdot nH_2O(\text{interlayer}) \tag{2.2}$$

according to Figure 2.4b. Unlike pyrophyllite, there is extensive isomorphous substitution in smectite minerals, thus, their formula always differs from the above theoretical formula. Aluminum and possibly phosphorous are substituted for silicon in the tetrahedral sheet and/or magnesium, iron, zinc, nickel, lithium and other cations are substituted for aluminum in the octahedral sheet. The type of substituted ions and the amount of possible positions occupied determines the type of smectite.

For the montmorillonite subgroup of the smectite minerals, there is no substitution in the tetrahedral sheet, but substitution of each sixth Al^{3+} by one Mg^{2+} ion in the octahedral sheet, leading to a dioctahedral structure. The resulting charge deficiency is close to 0.66 C per unit cell, i.e, 0.33 per formula unit (FU) or half the unit cell (HUC). For Bavarian bentonite, a value of 0.29 C/HUC was measured (Kaufhold, Dohrmann, Ufer & Meyer 2002). The charge deficiency is balanced by exchangeable cations adsorbed between the layers and around their edges. Assuming a charge deficiency of 0.33 C/HUC corresponding to an exchange of one Mg^{2+} cation for every sixth Al^{3+} cation, one unit

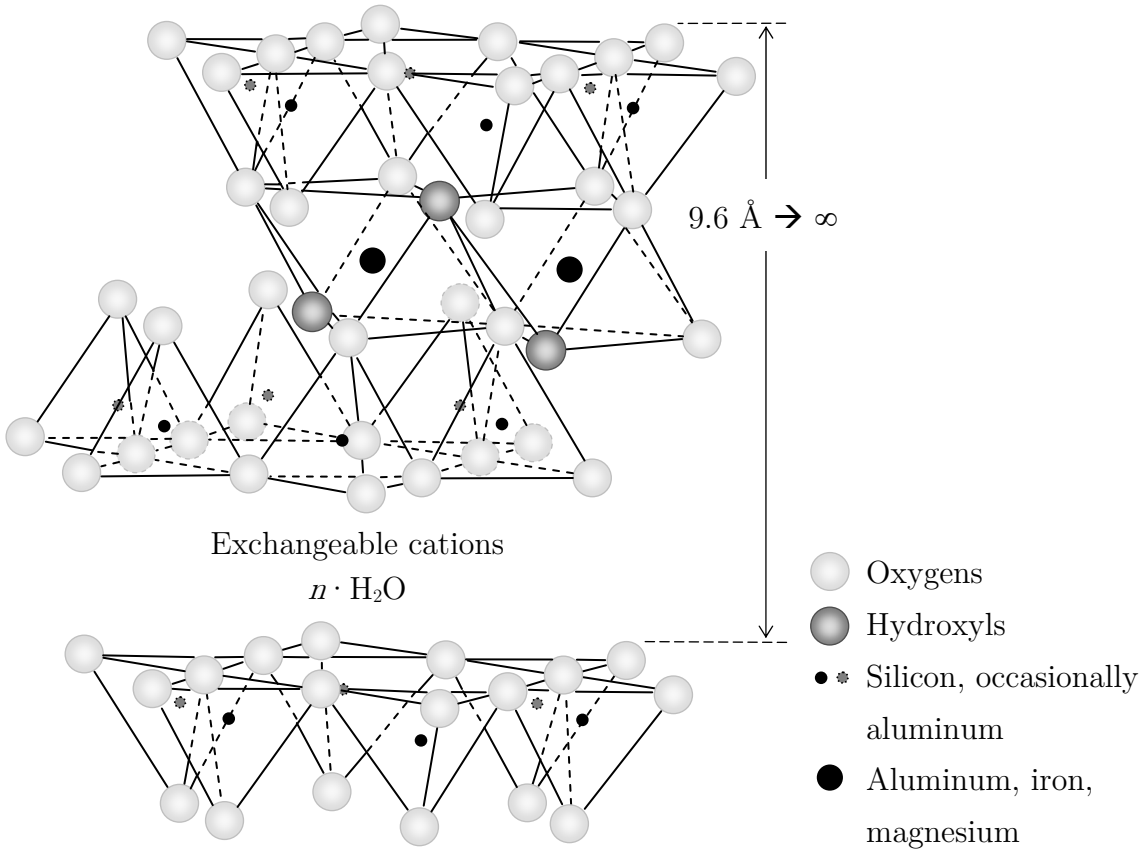

(a)

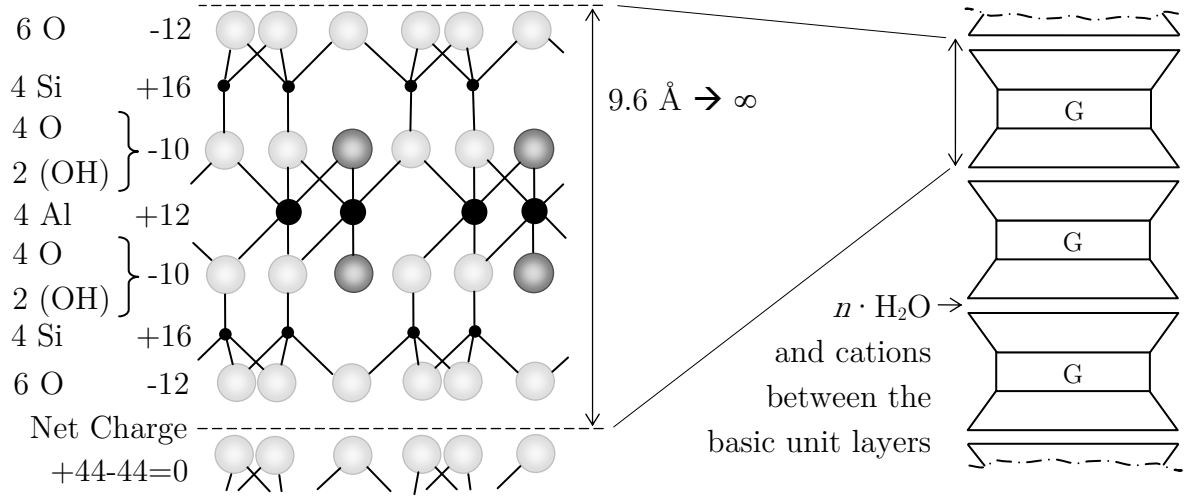

(b)

Figure 2.4.: Diagrammatic sketch and charge distribution of montmorillonite, modified after Grim (1968): (a) diagrammatic sketch of the montmorillonite structure, (b) charge distribution on montmorillonite.

cell has the formula

$$\begin{array}{ll} (OH)_4Si_8(Al_{3.34} & Mg_{0.66})O_{20} \\ & \downarrow \\ & Na_{0.66} \end{array} \tag{2.3}$$

The arrow indicates the group having the charge deficiency, which requires an external cation to balance the structure. As an example, the balancing cation has been indicated as sodium, and water or other polar molecules are not given in the formula above.

2.2.1.4. Illite

The illite mineral belong to the group of micas. Sometimes illite is also called hydrous mica. It is composed of two silica tetrahedral sheets and an octahedral sheet sandwiched between them (Figure 2.5). The structural unit of illite is basically the same as that for montmorillonite. Both belong to the three-sheet-minerals. They differ from each other in the following manner: (*i*) the charge deficiency due to substitutions is 0.65 to 0.75 C/HUC for illite and about 0.33 C/HUC for smectite, (*ii*) the position of the charge deficiency is largely in the tetrahedral sheet close to the surface of the layer, whereas for smectite it is mostly in the inner octahedral sheet of the unit layer, and (*iii*) in case of illite the balancing cation is mainly or entirely potassium. Therefore, the structural unit layers of illite are relatively fixed in position. Polar molecules cannot easily enter between the unit layers and cause expansion. The interlayer cations of illite are not easily exchangeable.

The charge deficiency given above corresponds to a substitution of about one-sixth of Al^{3+} for Si^{4+}. However, the potassium ions may ba replaced by other cations, such as Ca^{2+}, Mg^{2+}, H^+. Occasionally, slight interlayer hydration occurs. H_3O^+ may replace the potassium and may be the cause for the interlayer hydration and the reduced potassium content in illites as compared to well-crystallised muscovite mica. A usual K_2O-content in illite is about 9 to 10% (Weaver & Pollard 1973). The structural formula according to the charge distribution as shown in Figure 2.5b is

$$(OH)_4K_2(Si_6 \cdot Al_2)Al_4O_{20}. \tag{2.4}$$

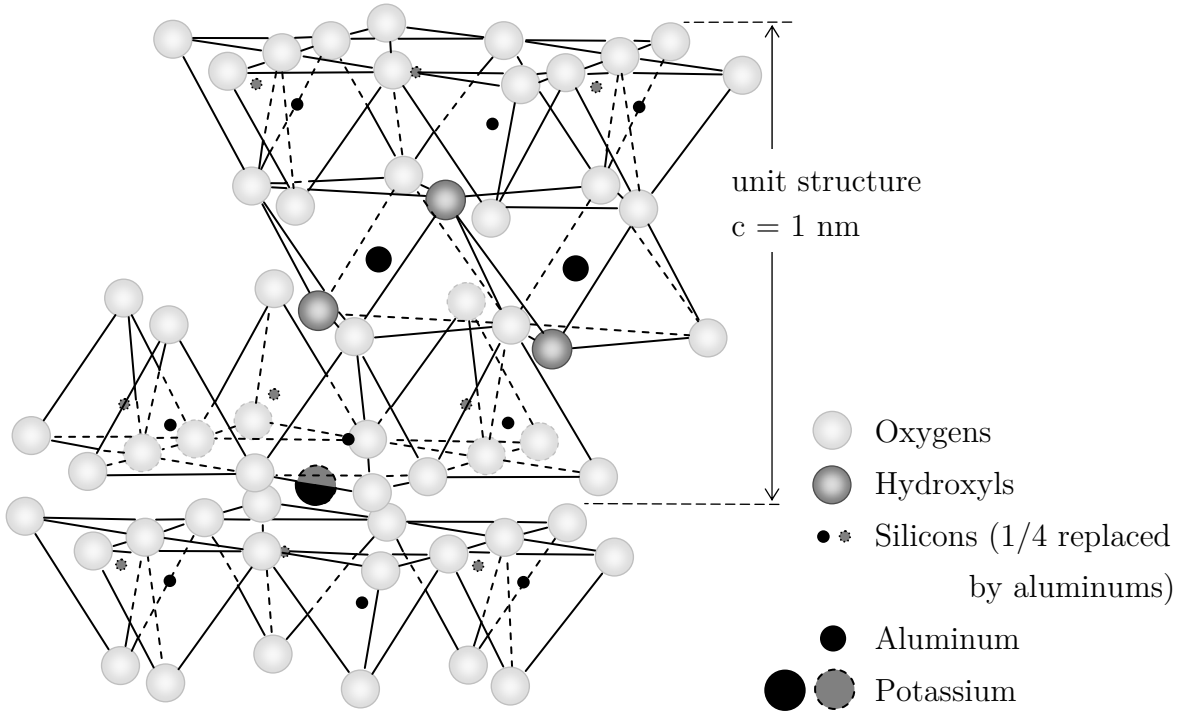

(a)

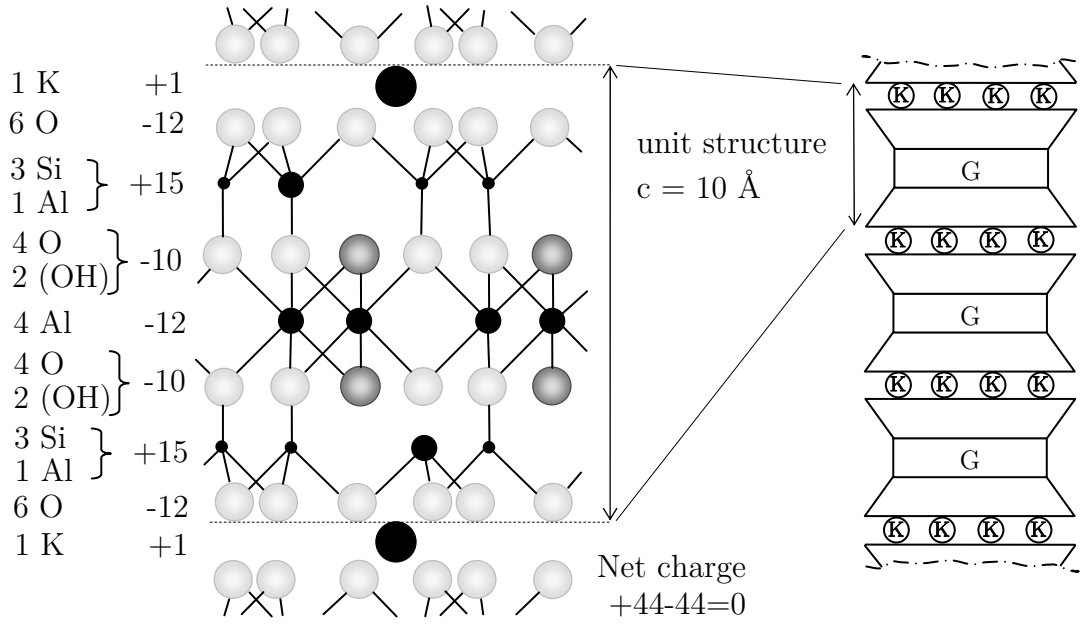

(b)

Figure 2.5.: Diagrammatic sketch and charge distribution of illite, modified after Grim (1968): (a) diagrammatic sketch of the illite structure, (b) charge distribution on illite.

2.2.2. Clay-water interactions

This section deals with the various mechanisms acting within a clay-water system. The size of clay particles is small and the resulting interfacial area between the solid and the water is large. Therefore, the interactions between water and the solid particles at micro-scale influences the hydro-mechanical behaviour of clays at macro-scale. In this section, emphasis is given to the types of water existing at or in the near of the clay-water interface, whereas later in section 2.2.3, emphasis is given on the different types of forces at interparticle level.

Water in clays may be present in various forms: structural water, adsorbed water, diffuse double layer water and free water. The term *water* used in the following is not restricted to the meaning of a (liquid) phase, but it refers to H_2O- molecules, which may be more or less bound by different mechanisms to the solid, i.e. the clay surface.

The type of water and the resulting strength of bonding depend on clay mineralogy, and the environmental conditions, such as temperature, availability of water, salinity. Figure 2.6 illustrates some of the possible mechanisms within the clay-water-system. Adsorbed water is defined as H_2O molecules attracted to internal or external surfaces of a clay particle, and adhered to these surfaces in thicknesses of one or more molecules. Elevated temperatures, typically 110 °C for 12 hours, can desorb the adhered H_2O. However, for clay minerals, a temperature of 110 °C may not liberate all the adsorbed water molecules present, and temperatures of as high as 300 °C (in special cases, even higher) may be needed for smectites (Grim 1968).

Hydrogen bonding as a type of adsorption of water molecules is illustrated in Fig. 2.6a. The external surfaces of clay minerals are usually composed of either oxygens (O) or hydroxyls (OH) (see also section 2.2.1), where the former is attracting the positive corner and the latter the negative corner of the H_2O molecules. Hydration of exchangeable cations attracted to the negatively charged clay surface is important at low water contents (see Fig. 2.6b). When the clay is dry, adsorbed cations occupy holes in the clay surface. They surround themselves with water molecules during hydration, and move to the central region between the sheets. Another model of water adsorption is presented in Fig. 2.6c. The clay particles are viewed as a negative condenser, where the positive poles of the water molecules are attracted to, thus leading to an orientation of the water molecules. The cations are moved away from the charged surface to the midplane between the parallel sheets. It was suggested that the high energy and hydration number of the aluminum in the octahedral sheet is responsible for the strong attraction of the water dipole to

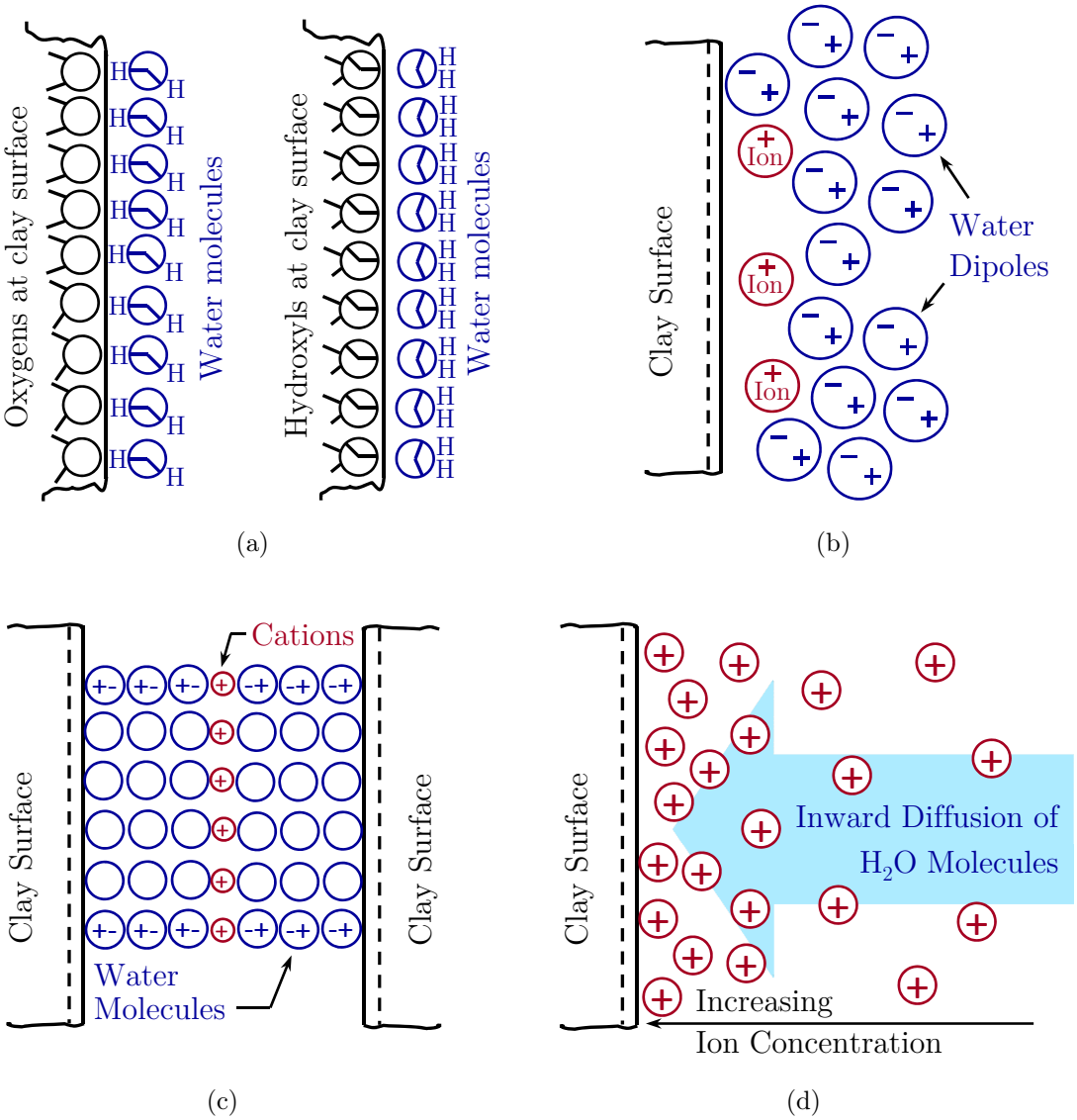

Figure 2.6.: Mechanisms of solid-water interaction (modified after Mitchell 1993): (a) hydrogen bonding, (b) ion hydration, (c) dipole attraction, and (d) osmosis.

the charged clay surface (Ingles 1968). In principle, the two latter mechanisms described (cation hydration and surface-water dipole attraction) may lead to the same configuration, i.e., adsorbed orientated water molecules close to the clay surface and cations in the midplane region.

The electrostatic attraction of cations to the negatively charged clay surface leads to a high concentration of cations in the vicinity of the particle as compared to the equilibrium concentration in the bulk solution, i.e. at some distance from the particle surface. Simultaneously, the system tends to equalize the gradient in cation concentration. Since diffusion of the cations is hindered by the electrostatic attraction to the clay particle, water molecules diffuse towards the clay surface in order to equalize the concentration. The mechanism of water attraction by osmosis (see Fig. 2.6d) is responsible for the osmotic swelling in clays according to the diffuse double layer concept.

From data of Low (1959) and Martin (1960) it is inferred that the structure, density and viscosity of the first few molecular water layers close to the clay surface at very low water contents differs from that in the same region at saturated condition.

For the sake of completeness, *structural water* (synonyms: *combined water*, *molecular water*, *structurally bound water*, *water of crystallization*, *water of hydration*) is mentioned. Structural water means that H_2O molecules or OH molecules are directly bound to cations at crystallographic sites in the crystal structure. For phyllosilicates, structural water is in the form of hydroxyl (OH) groups coordinated to cations. A temperature of 1000 °C is required to promote *dehydroxylation*.

The force field resulting from the above described interactions between solid surfaces, water and dissolved ions are subject of the following section.

2.2.3. Forces in clay-water-systems

2.2.3.1. Double layer repulsive forces

The permanent net negative surface charge of the clay particle is compensated by an equivalent amount of cations (exchangeable cations). The surface charge of the clay particle and the adsorbed compensating charge arising from the counter-ions together are called *double layer*, and due to the diffusive character of the ion charge also *diffuse double layer*. Gouy (1910) and Chapman (1913) were the first presenting a solution based on electrostatic and diffusion theory.

In a dry clay, cations in excess of those needed to balance the negative surface charge, as well as anions exist as salt precipitates. Immersed in water, the salt precipitates dissolve. Fig. 2.7a schematically shows a single clay layer immersed in water. The electrostatic attraction of the cations leads to a higher cation concentration in the vicinity of the particle as compared to some distance from the particle. Therefore, the cations tend to diffuse away from each other in order to equalize their concentration, but the diffusion is hindered by the competing mechanism of electrostatic attraction. Similarly, ions of the same sign as the negatively charged clay particle (anions) are repelled by the clay particle. Their concentration is increasing with increasing distance from the particle surface. At some distance from the particle surface, the concentration of the anions equals that of the cations. The system consisting of the particle and the ions (cations and anions) as surrounded by the boundary is electrically neutral. The water inside the boundary is the adsorbed water (see Figs. 2.6a to 2.6c) and the water bound by osmosis in order to equalize the concentration gradient existing inside the boundary (see Fig. 2.6d). The distribution of the cations and the anions with distance from the particle surface can be calculated (Fig. 2.7b). The distance at which the concentration of the cations and the anions equalizes corresponds to the boundary of the double-layer (theoretically at infinite distance). The surface enclosed by the two curves and the y-axis represents the total net charge of the diffuse layer, which is equal to the surface charge of the clay layer. It corresponds to the charge density σ (in C/m^2) (van Olphen 1977).

In a clay-water electrolyte system, repulsive double layer forces arise due to the overlap of the double layers of adjacent clay particles. Fig. 2.8 illustrates the situation for two interacting clay particles immersed in water. The interference of the diffuse cation atmospheres leads to an increase in ion concentration in the central plane between the two particles. Work must be performed in order to bring the two particles from the infinite distance to the respective smaller distance; this amount of work corresponds to the repulsive energy due to diffuse double-layer.

The calculation of the repulsive pressure due to overlapping diffuse double-layers may be done in several ways, one of them is the calculation in terms of osmotic pressure. When an aqueous solution 1 of concentration c_1 is separated by a semi-permeable membrane (only water molecules may pass) from an aqueous solution 2 of concentration c_2 and $c_1 < c_2$, the free energy of the water is less in solution 2 as compared to solution 1 for identical initial hydrostatic pressure of the two solutions. Water will flow from solution 1 to solution 2 in order to reduce the concentration imbalance; the flow of water is accompanied by a decrease of hydrostatic pressure in solution 1 and an increase in solution 2. The osmotic

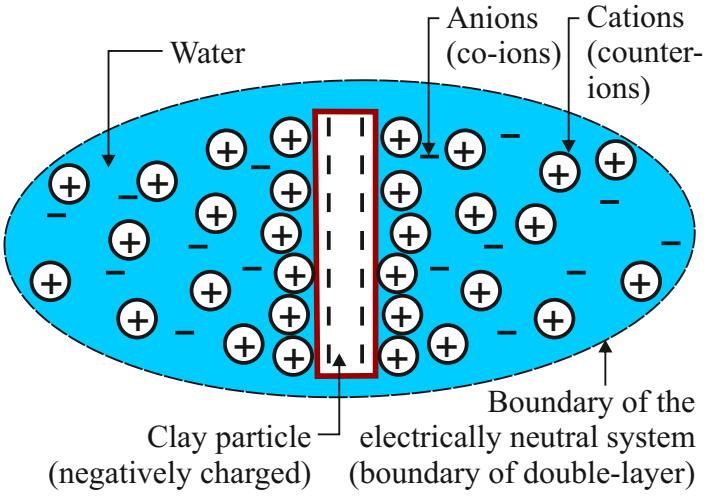

(a)

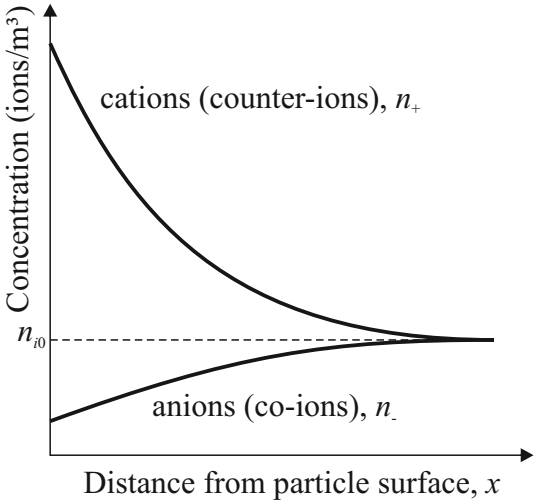

(b)

Figure 2.7.: Diffuse double layer and ion distribution and of a single dispersed particle: (a) schematic illustration, (b) charge distribution in the diffuse double layer (after van Olphen 1977).

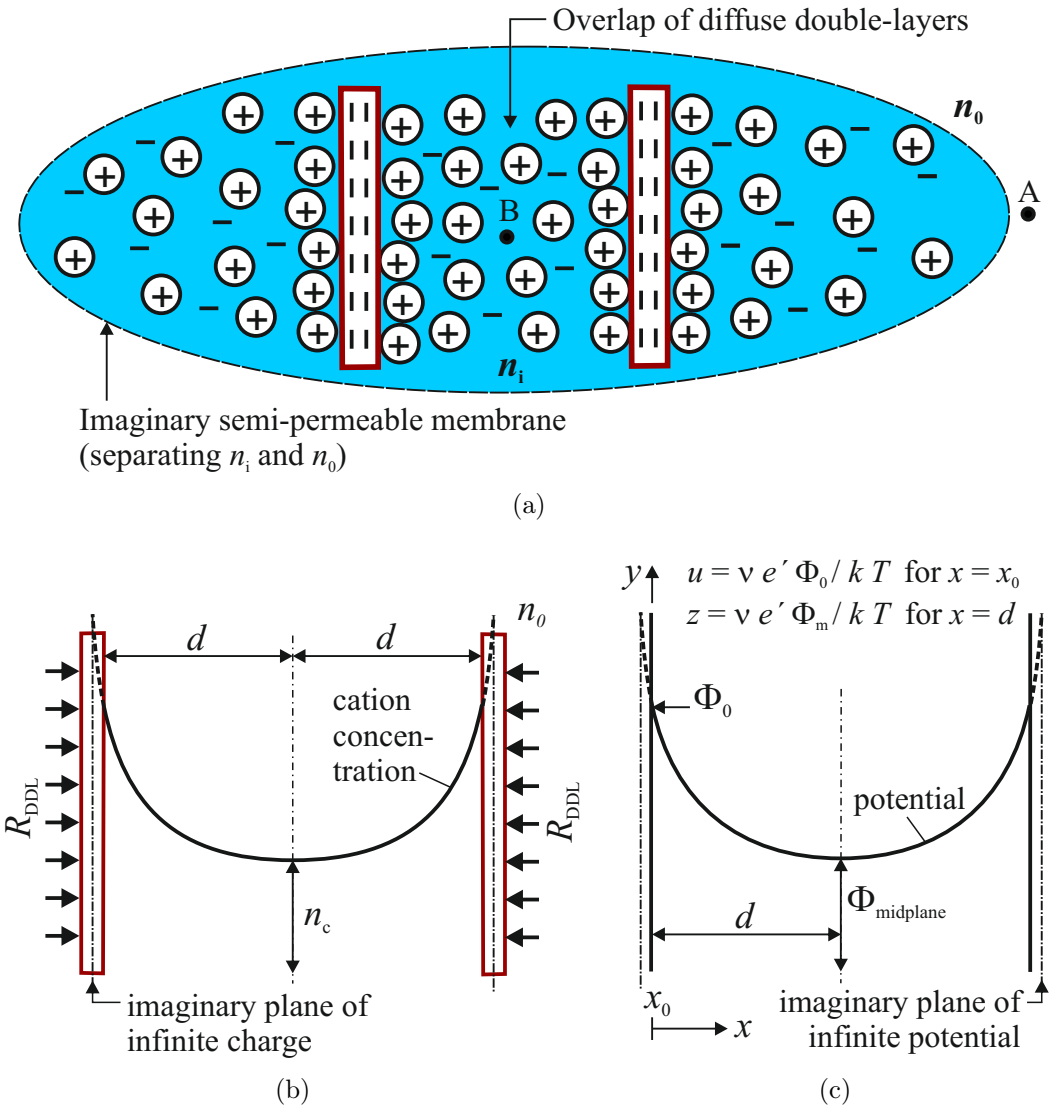

Figure 2.8.: Diffuse double-layer and ion distribution and for two parallel clay layers: (a) schematic illustration, (b) charge distribution in the diffuse double-layer, (a) potential distribution.

pressure π is the pressure applied on chamber 2 (solution 2) to prevent the flow of water from solution 1 to solution 2.

In a real clay, there is no distinct semipermeable membrane separating the regions with equilibrium bulk solution concentration from those with higher concentration. The clay particles itself act as semipermeable membrane, since they retain the cations through electrostatic forces. Therefore, it was denoted *imaginary* semipermeable membrane in Fig. 2.8a. Translating the concept of osmotic pressure on clays, the repulsive double-layer pressure R_{ddl} is equal to the difference in osmotic pressure in the central plane between particles and in the equilibrium bulk solution, provided that the diffuse-double layers of adjacent particles overlap. It can be calculated by the van't Hoff equation (eq. 2.5) (Bolt 1956),

$$R_{\mathrm{ddl}} = \pi = kT \sum n_{\mathrm{ic}} - n_{\mathrm{i0}} = RT \sum c_{\mathrm{ic}} - c_{\mathrm{i0}} \tag{2.5}$$

where n_{ic} and n_{i0} are the concentrations in particles per unit volume (m^{-3}), and c_{ic} and c_{i0} are the molar concentrations ($\mathrm{mol/m}^3$), k is the Boltzmann constant (=1.3810^{-23} J/K), R is the gas constant (=8.314 J/mol K), and T is the absolute Temperature in K.

The solution of the Poisson-Boltzmann equation (2.6) relating the electric potential, charge and distance is the basis for the computation of potential and charge as a function of distance from the particle surface,

$$\frac{d^2\Phi}{dx^2} = \frac{2n_0\nu e}{\varepsilon} \sinh \frac{\nu e \Phi}{kT} \tag{2.6}$$

where Φ is the electric potential (V), x the distance from particle surface (m), n_0 the bulk fluid equilibrium concentration (m^{-3}), ν the valency of the ions (-), e' is the electron charge ($= 1.602 \times 10^{-19}$ C), ε is the permittivity of the medium ($\mathrm{C}^2/\mathrm{J}^{-1}\mathrm{m}^{-1}$). According to the theory, interparticle distance $2d$ will increase when the ions are replaced by ions of a higher valency or when bulk solution concentration decreases. Based on the theory for single particle, for bulk fluid concentrations of 10^{-5} and 10^{-3} mol/l, the calculated thickness of the double layer was found to be about 100 nm and 10 nm for monovalent ions, and 50 nm and 5 nm for divalent ions (van Olphen 1977).

The assumptions and limitations of the diffuse double-layer theory as applied for the prediction of the compressibility behaviour and swelling pressures will be discussed in section 2.7. The set of equations used in this work for the prediction of the compressibility behaviour (void ratio vs. applied stress) and the swelling pressure-dry density relationship based on diffuse double-layer is presented in chapter 8.

2.2.3.2. van der Waals attractive forces

The van der Waals force between two particles suspended in a medium results from interactions between ions, atoms or molecules due to a dipole moment raising from the molecule itself or from induced polarization (due to the proximity of a charge). The van der Waals interaction force includes contributions from ion-dipole, dipole-dipole, dipole-polarized molecule interactions and from interactions between polarized molecules. For macroscopic bodies of different geometry, the van der Waals interaction force is obtained by the summation of interaction energies of all atoms in the bodies. In this sense, a clay particle is regarded as a macroscopic body with flat surfaces interacting with its counterpart through vacuum, air or any other medium. For this case, the van der Waals attractive force is calculated by eq. 2.7 as proposed by Hamaker (1937),

$$A = \frac{A_\mathrm{h}}{6\pi(2d)^3} \tag{2.7}$$

where A is the van der Waals attractive force ($\mathrm{N/m^2}$), A_h the Hamaker constant (J), and $2d$ the interparticle distance (m). Hiemenz (1977) in Sridharan & Jayadeva (1982) proposed eq. 2.8, which accounts for the thickness δ (m) of the clay platelets. d is half the distance between the surfaces of two parallel clay particles.

$$A = \frac{A_\mathrm{h}}{48\pi}\left[\frac{1}{d^3} + \frac{1}{(d+\delta)^3} - \frac{2}{(d+0.5\delta)^3}\right] \tag{2.8}$$

The magnitude of the attractive van der Waals force depends on the Hamaker constant A_h, and on the interparticle distance. The Hamaker constant accounts for the influence of the macroscopic bodies and the intervening medium on the van der Waals interaction energy. The evaluation of the Hamaker constant for macroscopic bodies in various media is usually done based on the Lifshitz-theory, which is a sophisticated approach accounting for the retardation effects, i.e. the frequency-dependence of dielectric properties, and the effect of the intervening medium between the interacting bodies. In general, the Hamaker constant depends on the dielectric constant of the interacting particles and the intervening medium (Sridharan 1968, Israelachvili 1992, Anandarajah & Chen 1997). Table 2.1 presents a selection of values of A_h relevant for soil systems. Sridharan (1968) established a relationship for the Hamaker constant as a function of degree of saturation; the respective values of Hamaker constant for $S_\mathrm{r} = 0$ and $S_\mathrm{r} = 1$ are given in Table 2.1. The Hamaker constant increases, when air instead of water is the pore fluid. It follows that attractive forces should increase as the clay system changes from saturated to unsaturated state. Both the double-layer repulsive forces and the van der Waal's attractive forces are considered to be long-range forces, i.e. they are considered for describing the behaviour of clays for particle distances greater than 1 to 2 nm (Ninham 1980).

Table 2.1.: Hamaker constant

Medium	Hamaker constant A_h (10^{-20}J)	
Water separating the medium		
Air	3.7	Israelachvilli (1992)
Mica	2.0	Israelachvilli (1992)
Mica	2.03	Anandarajah & Chen (1997)
Fused quartz	0.83	Israelachvilli (1992)
Quartz	1.61	Anandarajah & Chen (1997)
Montmorillonite / Kaolinite	6.11	Sridharan (1968)
Air or vacuum separating the medium		
Water	3.7	Israelachvilli (1992)
Mica	10	Israelachvilli (1992)
Mica	9.83	Anandarajah & Chen (1997)
Fused quartz	6.5	Israelachvilli (1992)
Quartz	8.73	Anandarajah & Chen (1997)
Montmorillonite / Kaolinite	19.2	Sridharan (1968)

2.2.3.3. Particle interaction forces at short range

As summarized by Santamarina (2001*a*), at short range level, two types of structural forces are acting: hydration (solvation) forces and Born repulsion. The hydration force comes into picture at distances smaller than 2 nm and depends on the characteristics of the interacting surfaces and their affinity for water. Hydration force oscillates with distance with a period of about one molecular diameter (0.25-0.28 nm for water) (Israelachvili & Pashley 1983). In clays, it is manifest by the crystalline swelling in form of discrete jumps. The hydration of divalent exchangeable cations produces a significantly greater repulsive energy than the hydration of monovalent cations (MacEwan 1954). Table 2.2 presents an overview of the radii in non-hydrated and hydrated state, r and r_h (nm), respectively, and the cation ionic potential as the ratio of valency and non-hydrated radius ν/r (1/nm). The ionic potential is a measure for the affinity to water. Born repulsion develops at smaller distances than hydration forces due to the overlapping of electron clouds of adjacent atoms. At particle level, Born repulsion opposes the interpenetration of two neighboring mineral surfaces.

Table 2.2.: Size and ionic potential of some cations

Ion	Radius (nm)		Ionic potential ν/r (1/nm)
	non-hydrated (Shannon 1976)	hydrated (Mitchell 2005)	
Li^+	0.076	0.73-1.0	13.16
Na^+	0.102	0.56-0.79	9.80
K^+	0.138	0.38-0.53	7.25
Mg^{2+}	0.072	1.08	27.78
Ca^{2+}	0.1	0.96	20.00
Sr^{2+}	0.118	0.96	16.95

Additionally, electrostatic Coulombian attraction develops at short range between negatively charged faces and positively charged edges of particles, which may favour an edge-to-face (EF) particle arrangement.

2.2.4. Net forces in clay-water-systems

The proportion of the various repulsive and attractive forces within a clay-water-system determines the net interaction curve. For a given clay-water system, the repulsive and attractive energy at any particle distance $2d$ can be computed and plotted as a function of $2d$, which is shown in Fig. 2.9a, where the energy curve due to van der Waals attraction and the double layer repulsive energy curves for three different electrolyte concentrations are shown. By summing up the (positive) repulsive and the (negative) attractive energy at any particle distance $2d$, a net interaction energy curve is obtained and shown as a dotted line in Fig. 2.9b for low concentration, in Fig. 2.9c for medium concentration, and in Fig. 2.9d for high concentration. For low and medium electrolyte concentration, the net interaction is repulsive at large distances and decreases to a minimum value with predominating attractive forces. For high electrolyte concentration, no maximum with predominating repulsive energy is observed, attractive energy is dominating at larger interparticle distances. For all concentrations, at very close particle distances, the repulsive short range forces become active and lead to a sharp re-increase of the net interaction energy into the repulsive region. When two particles approach each other, agglomeration

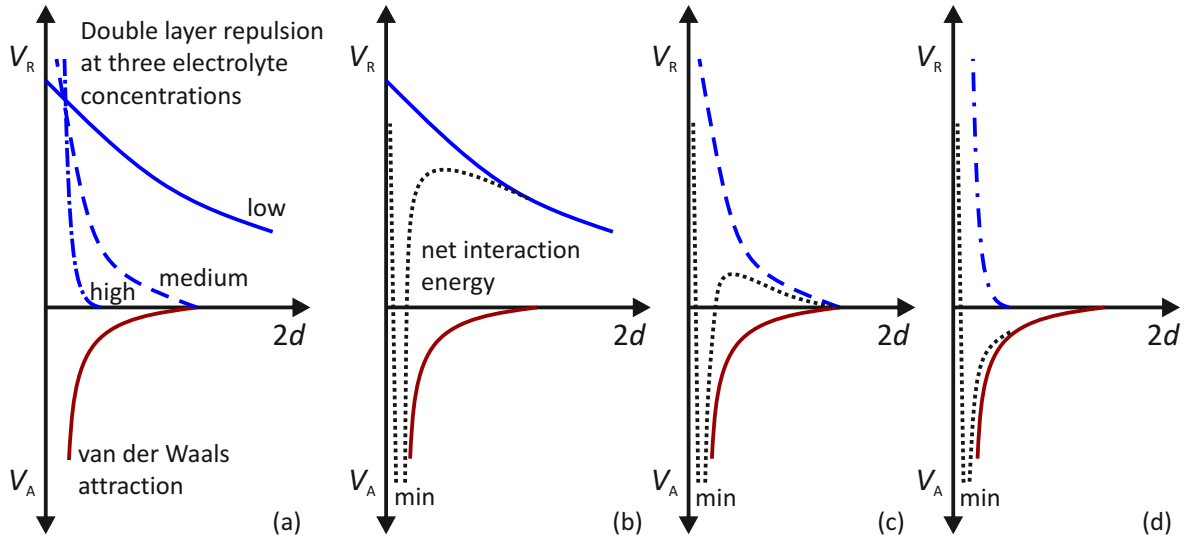

Figure 2.9.: Repulsive and attractive energy and net interaction energy as a function of interparticle distance, modified after van Olphen (1977).

takes place, when the repulsive energy barrier has overcome, and the particles reach the minimum energy state in the attractive region. Thus, the interplay of attractive and repulsive forces in the whole particle range is of great importance for the amount and type of particle association leading to a specific fabric.

The significance of the various types of forces for the present study can be summarized as follows. The type of clay, type and amount of exchangeable cations present in the clay, bulk fluid characteristics, distance between the clay platelets and temperature are some of the factors that contribute to the magnitude of the interparticle repulsive pressure (Mitchell 1993). In addition to the double layer repulsive pressure, the electrical attractive pressure and other additional repulsive pressures, such as due to the forces arising from the hydration of surface and interlayer cations, and the forces due to the overlapping of the outer electron shells of molecules (Born repulsion) may also contribute to the engineering behaviour of clays. The electrical attractive pressure has been shown to be of lesser importance within the range of overburden stress commonly dealt in geotechnical engineering (Sridharan & Jayadeva 1982). The role of attractive pressure for densely compacted expansive clays and clays loaded to very high stresses has not been given due emphasis in the past. Such information is valuable when dealing with compacted bentonites for highly toxic waste disposal programmes. On the other hand, the significance of hydration forces and Born repulsion is realised to play a paramount importance while dealing with compacted dry clays and clays compacted to very high dry densities, respectively (van Olphen 1977, Yong & Mohamed 1992).

2.3. Fabric and structure

2.3.1. Terminology

Although the soil is usually treated as a continuum for the analysis and design in geotechnical engineering, the relevance of the soil fabric and structure for the parameters such as strength, compressibility and permeability was already brought out by Terzaghi (1925) and Casagrande (1932). The term *fabric* solely refers to the arrangement of particles, whereas the term *structure* includes the effects of particle arrangement, composition and interparticle forces (Collins & McGown 1974). Fig. 2.10 clarifies about the terms used in the present work for describing the structural and fabric elements of clays. The definitions presented here are based on the reports of the JNC (joint nomenclature committee of the Clay Minerals Society) and based on Bergaya & Lagaly (2013). The definitions presented are in principle valid for all types of clays. Whenever further terms are needed they will be introduced in the respective section.

The smallest unit in clay minerals is the *layer* (two-sheet or three-sheet). Only in the extreme case of a very dilute suspension, the layers may exist individually; usually, they

stack to each other to form the *particle* (Fig. 2.10b). The layers may be stacked in a parallel manner (case a), with a lateral shifting of the layers (case c); they can also form interlayer spaces of a lenticular form (case b). The particles are arranged parallel (case d) or in a non-parallel manner (case e) to build up the *aggregate*. Several aggregates form an *assembly of aggregates*. According to van Olphen (1977), the modes of particle association are defined by various combinations of either *dispersed* or *aggregated* with either *flocculated* or *deflocculated*, where *dispersed* means no face-to-face (FF) particle association, *aggregated* means face-to-face particle association, *flocculated* can be either an edge-to-edge (EE) or an edge-to-face (EF) association between aggregates, and *deflocculated* indicates no association between particles or aggregates (Fig. 2.11).

The type of association is determined by the net energy curves of interaction. An EE-association of particles indicates, that the attraction between the edges is dominating and governs the fabric development, whereas in an EF-association the attraction between an edge and a face site of two particles is dominant. The predominance of repulsive energy is manifest in a dispersed-deflocculated fabric.

The intercalation of water molecules between layers in an aqueous dispersion leads to an increased interlayer distance. This process is called *delamination* as long as there is significant interaction between the layers maintaining the crystallographic order. When with increasing distance, no further interaction occurs between the layers or between the stacking of few layers the phenomenon is called *exfoliation*. The latter is possible in montmorillonite clays.

2.3.2. Methods of fabric investigation

Several techniques are nowadays available for fabric investigation of clays. Among the direct methods, microscopy and determination of pore size distribution (PSD) by means of mercury intrusion porosimetry (MIP) are used. They have been used in the field of soil mechanics research on clays during the last four decades for the study of natural and compacted clays (Barden & Sides 1970, Diamond 1970, Sridharan, Altschaeffl & Diamond 1971, Delage & Lefebvre 1984, Romero 1999, Delage, Marcial, Cui & Ruiz 2006). Scanning electron microscopy (SEM) provides the necessary resolution for visualising the particle arrangement within a clay. For this, the specimens have to be dry, vacuum compatible, and coated with a film of conducting material to avoid charging of the sample and loss of resolution. The Environmental Scanning Electron Microscopy (ESEM) has the advantage that samples containing liquid can be observed under a range of humidities,

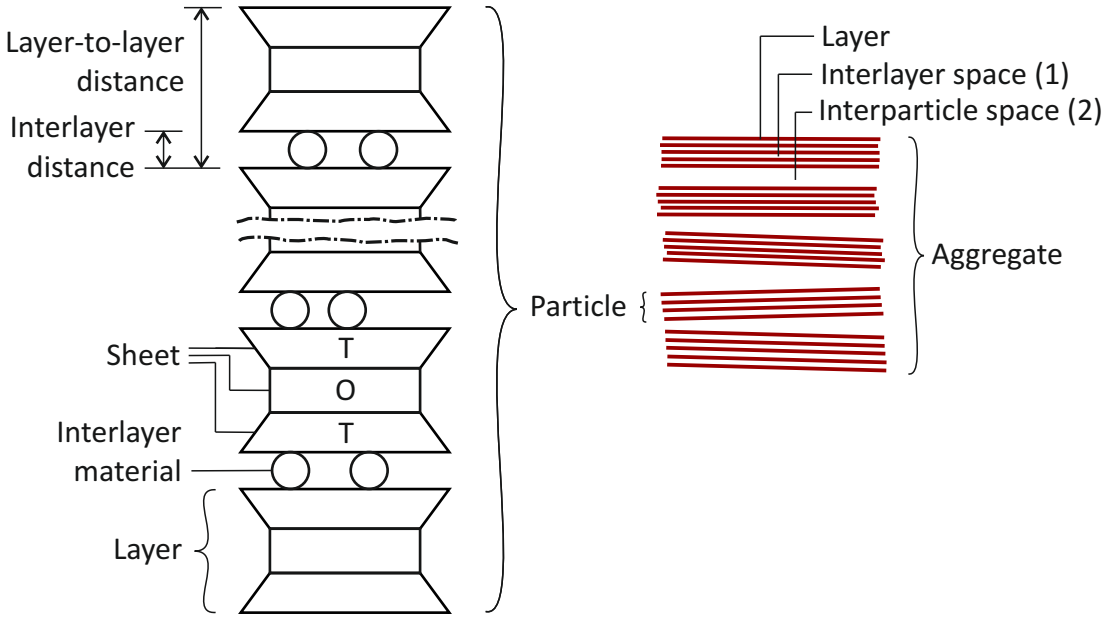

(a)

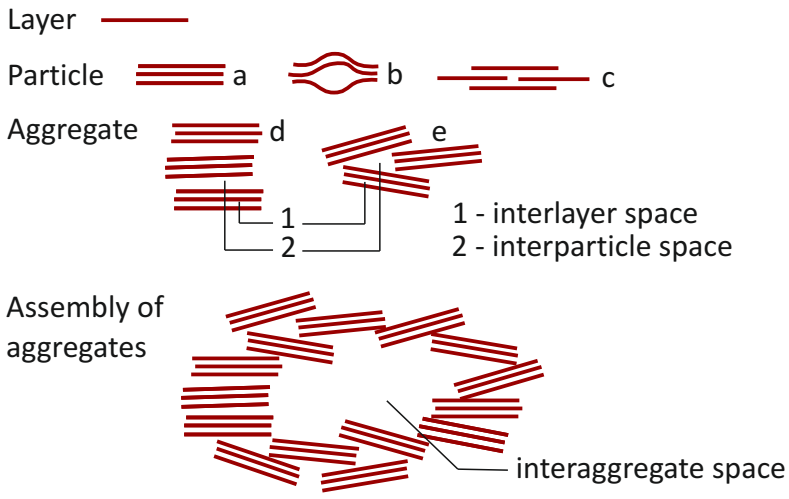

(b)

Figure 2.10.: Definition of structural and fabric elements: (a) from sheets to aggregates, (b) from layers to assemblies of aggregates: (a) parallel layer arrangement, (b) layers forming lenticular interlayer space, (c) laterally shifted layers, (d) parallel particle arrangement, (e) non-parallel particle arrangement; modified after Bergaya & Lagaly (2013).

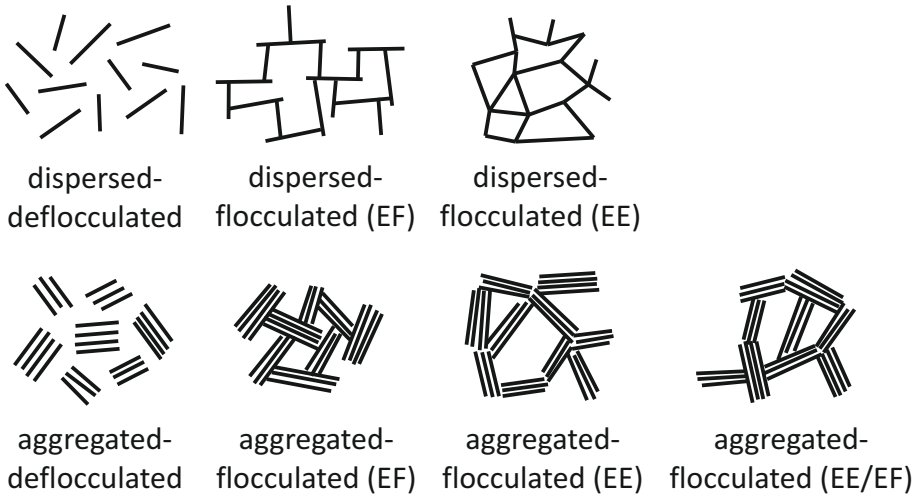

Figure 2.11.: Modes of particle association (EE: edge-to-edge, EF: edge-to-face), modified after van Olphen (1977).

pressures and temperatures. The description of the fabric investigation by means of MIP and ESEM, which were used in this work, is given in sections 3.2.7 and 3.2.6.

2.3.3. Fabric of remoulded clay in dilute solution

The hierarchy of fabric units from an assembly of aggregates down to the layer as shown in section 2.3.1 is characteristic for all clay minerals. However, the shape, size and arrangement of the particles, aggregates and assemblies depend on the mineral type (van Olphen 1963, Grim 1968, Sides & Barden 1971, Osipov & Sokolov 1978, Tessier 1984). Examples of micrographs obtained for the three mineral types are shown in Figure 2.12.

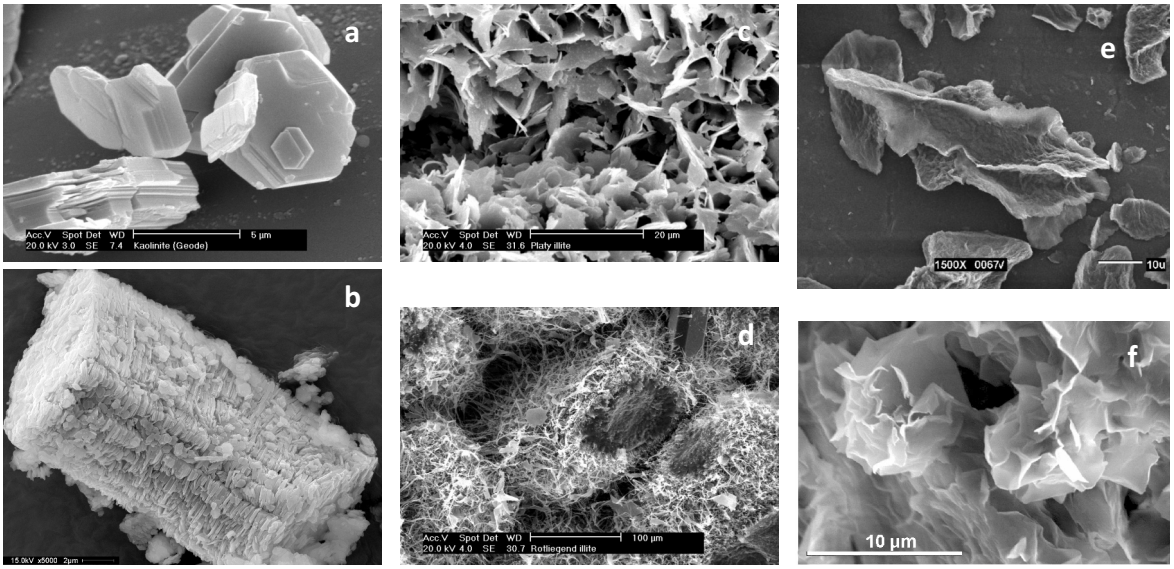

Figure 2.12.: Examples of micrographs: (a) well crystallite kaolinite from Keokuk geode, USA, (b) large kaolinite stack from Sandersville, Georgia USA, (c) platy illite from the Rotliegend, Northern Germany, (d) fibrous illite from Rotliegend Sandstone, North Sea, (e) montmorillonite quasi-crystal from Ap horizon, Webster soil, Waseca, USA, (f) montmorillonite from Miocene arkose, Madrid Basin, Spain. Images reproduced from the 'Images of Clay Archive' of the Mineralogical Society of Great Britain & Ireland and The Clay Minerals Society (www.minersoc.org/gallery.php?id=2).

Well crystallized *kaolinite* particles usually are six-sided flakes with a lateral dimension ranging from about 300 to 4000 nm and a height of about 50 to 2000 nm (Grim 1968). Tessier & Pedro (1976) observed for particles of a Calcium-kaolinite lateral dimensions of about 200 to 300 nm and a thickness of about 20 nm. Sometimes the particles are elongated in a- or b- direction. The edge surfaces are not perfectly in a right angle to the surface, but are commonly beveled. Poorly crystallized kaolinite usually occurs in smaller and thinner particles, and with less well defined hexagonal shape. Fig. 2.12a shows typical well-crystallites kaolinite particles, Fig. 2.12b shows a large aggregate containing kaolinite particles stacked face-to-face and side-by-side.

The particles of *illite* usually occur as small, poorly defined flakes forming an irregular aggregate (Fig. 2.12c). The lateral dimensions are between 100 to 300 nm, and illite particles can be as thin as 3 nm (Grim 1968). Tessier & Pedro (1976) stated that illite particles, themselves being composed of not more than 10 layers, occur in form of aggregates with face-to-face and side-by-side particle arrangement. The aggregates have a lateral extension of about 600 nm and a thickness in the order of 300 nm. Aylmore & Quirk (1967) presented measurements of surface area, porosity, and pore size distribution together with electron microscopy results and found the significant feature of a 3 nm separation between the illite surfaces within an aggregate, even at complete drying, and unaffected by the type of exchangeable cations present. This characteristic pore structure was explained by the interleaving and bending of the irregular illite particles within the aggregates. Illite particles also may be fibrous in shape (Fig. 2.12d), lath-shaped or ribbon-shaped.

In case of montmorillonite, the micrographs usually reveal a network of irregular flake shaped aggregates without distinct borders (Fig. 2.12f). Montmorillonite particles have a lateral dimension in the range from 1000 to 2000 nm and a thickness ranging from 1 nm (thickness of a single layer in the extreme case of a highly diluted dispersion) to about 1/100 of the width (Grim 1968). Fig. 2.12e shows a *quasi-crystal* of a montmorillonite. The term *quasi-crystal* was introduced by Quirk & Aylmore (1971) and assigned to an aggregate of large lateral extension (up to 5000 nm) formed by the face-to-face association of a certain number of layers. The thickness of the quasi-crystal, thus, the number of layers contained varies according to the type of exchangeable cations and the hydration state of the montmorillonite. The individual montmorillonite layers involved in a quasi-crystal vary considerably in their lateral dimensions.

The kaolinite and illite particles are rigid in nature. Depending on the interplay of the repulsive and attractive forces within the clay-water-electrolyte system, the particles and aggregates will associate in one of the specific configuration shown in Fig. 2.11. For kaolinites, the pH-value of the pore fluid was found to influence the sign of the charge at the particle edges (Palomino & Santamarina 2005, Wang & Siu 2006*b*), thus, influencing the fabric of the clay. It was stated that pH has the greatest influence at low pore-fluid concentrations, leading to an FF aggregation at low pH up to about 4, and to a dispersed, deflocculated fabric at high pH (>7). It exist a threshold concentration of the pore-fluid, where pH has no influence. At pore-fluid concentrations higher than the threshold concentration, the behaviour is primarily controlled by the concentration. For de-ionized water with a very small ion concentration, as used for the experiments in

the present work, the pH is slightly smaller than 7. For these conditions, a partly EF flocculated and partly dispersed fabric is expected.

The quasi-crystals of montmorillonites are flexible in nature (Quirk & Aylmore 1971, Tessier & Pedro 1976, Ben Rhaïem, Pons & Tessier 1987). The meaning of flexibility has to be understood with respect to its stiffness as well as to its size. The individual montmorillonite layers involved in a quasi-crystal vary considerably in their lateral dimensions. Based on transmission electron microscopy (TEM) and small-angle-X-ray-scattering (SAXS) experiments during drying and re-wetting, Ben Rhaïem et al. (1987) presented a model for the fabric of Ca^{2+}-smectite and Na^{+}-smectite suspensions submitted to 3.2 kPa suction, which is shown in Fig. 2.13. The main difference between the two smectite types is the

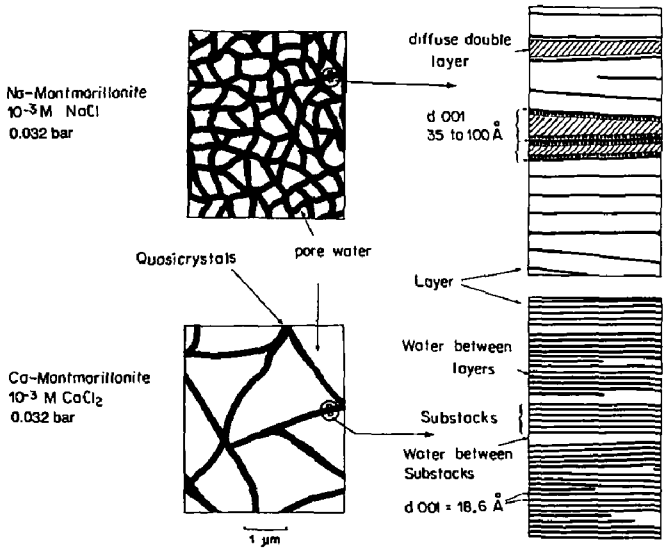

Figure 2.13.: Fabric of suspension of Na^{+}-smectite and Ca^{2+}-smectite at 3.2 kPa suction (Ben Rhaïem et al. 1987)

size of the large voids enclosed by the quasi-crystals and the number of layers contained within a crystal, which was found to be about 50 for the Ca^{2+}-smectite, and about 4 to 10 for Na^{+}-smectite for the same total thickness of the quasi-crystal. Within a Ca^{2+}-smectite quasi-crystal, few layers are forming substacks. Within the substacks, the layers are separated by a distance of about 1.86 nm; a slightly greater interlayer distance was found between the substacks. The observations have shown that during drying the number of layers contained in a quasi-crystal increases and thus, the number of quasi-crystals decreases. The change in size of the quasi-crystals during drying is manifest in a decrease of the external specific surface area. This behaviour was found to be reversible to some extent (Ben Rhaïem et al. 1987).

Tuller & Or (2003) have combined the geometrical pore space considerations of Tessier (1984) and Ben Rhaïem et al. (1987) with a formalism accounting for physico-chemical effects in an approach for predicting the constitutive hydraulic relationships for swelling porous media.

2.3.4. Fabric of compacted clays

Similarly to a sedimentary clay, where the conditions during deposition determine the initial soil structure, the placement conditions determine the initial soil structure of compacted soils. The structure is known to be influenced by the type and amount of compaction, the type and amount of pore-fluid and other additives added to the clay, and the temperature (Lambe 1958*b*). Compacted clays are initially unsaturated. The structure induced during compaction depends on moulding water content for a given dry density. The pore size distribution was found to be unimodal at optimum water content and at the wet side of optimum, whereas is was found to be bimodal at the dry side of the optimum. The aggregates are forming while mixing the clay powder with water, and the aggregates themselves associate to form assemblies of aggregates. The pore space between the aggregates is called inter-aggregate pores, and those within an aggregate are the intra-aggregate pores. The aggregates are more prone to deformation of the wet side of optimum, thus filling the larger inter-aggregate voids and creating a single class of pores. Contrary, the association of aggregates remains more stable at the dry side of optimum water content, thus, the larger inter-aggregate pores exist additionally to the pores inside the aggregate (Diamond 1970, Ahmed, Lovell & Diamond 1974, Delage, Audiguier, Cui & Howat 1996, Thom, Sivakumar, Sivakumar, Murray & Mackinnon 2007).

Compacted bentonites are comprised of pores at different structural levels (Gens & Alonso 1992, Romero, Gens & Lloret 1999, Lloret, Villar, Sànchez, Gens, Pintado & Alonso 2003, Delage et al. 2006). Pore size distribution studies of initially unsaturated compacted bentonites by Delage et al. (2006) showed that the total pore volume of compacted bentonites are comprised of the interlayer pores between the layers, the interparticle pores between the particles inside the aggregates, and the inter-aggregate pores between aggregates made up of clay mineral particles. With an increase in the water content, the swelling of bentonites is characterised by a division of the particles within the aggregate, thus increasing the interparticle spacing that is manifested on the reduction of the interaggregate pores (Saiyouri, Hicher & Tessier 2000, Saiyouri, Tessier & Hicher 2004, Delage et al. 2006, Delage 2007). These studies on bentonites have shown that the microstructure of bentonites has a dynamic character, which means that the amount of pores at one level

may reduce or increase on account of pores of another level depending on the hydraulic and stress path followed by the bentonite.

The existence of pores at least at two different structural levels is a common feature for compacted clays independent of mineralogy. However, the dynamic nature of microstructure is characteristic for bentonites.

Some aspects regarding the evolution of microstructure of clays under specific hydraulic and stress paths relevant for this work are presented in the respective sections 2.4, 2.5, and 2.6.

In the present work, the fabric of the specimens was investigated by means of MIP and ESEM at initially saturated state, at shrinkage limit state and after one-dimensional consolidation to 2 and 20 MPa in the high-stress oedometer. The results are presented in chapter 7.

2.4. Compressibility

The prediction of volume change of natural and compacted clays is essential in soil engineering practice; the calculation of the settlement of a foundation structure is an example for a traditional application, where compression due to one-dimensional consolidation processes of natural clays is relevant.

One-dimensional compressibility behaviour of clays is commonly determined from laboratory oedometer tests using saturated specimens (either undisturbed or remoulded). In general, the initial water content chosen is greater than the liquid limit for the remoulded soils, referred to herein as the initially saturated bentonite. The parameters determined from the one-dimensional consolidation tests are compression index C_c, decompression index C_s, soil stiffness E_S, and permeability k. C_c and C_s are determined by linearization of the corresponding void ratio-log σ'_v plot and usually correlate with plasticity of the clay for vertical applied stresses in the standard range of applied stress (Lambe & Whitman 1969). Marcial et al. (2002) found a bi-linear shape of the void ratio-log σ'_v plot for compression of three bentonites up to 30 MPa applied vertical stress and therefore, determined the C_c-values for two different stress ranges. The coefficient of permeability, k, is computed from the values of coefficient of volume compressibility, m_v and the coefficient of consolidation c_v, for each incremental applied stress. The c_v values are estimated from the time-settlement curve during consolidation at each step using Casagrande or Taylor's method. Usually, a decrease in c_v for increasing applied stress up

to about 600 to 800 kPa is observed (Lambe & Whitman 1969, Abdullah, Al-Zou'bi & Alshibli 1997, Marcial et al. 2002). Marcial et al. (2002) observed an increase of c_v-values with further increase beyond 1 MPa applied vertical stress, which was attributed to an increase in stiffness greater than the decrease in permeability in this stress range.

There have been substantial contributions on the study of the compressibility behaviour of clays by several researchers in the past (Bolt 1956, Olson & Mesri 1970, Mesri & Olson 1971, Sridharan & Rao 1973, Mitchell 1993, Di Maio et al. 2004). The studies have emphasised the influence of physicochemical forces affecting the void ratio changes due to an increase in the applied stress. It is generally accepted that a clay of higher liquid limit or plasticity index will show higher compressibility than low plastic clays (Lambe & Whitman 1969). Therefore, an initially saturated remoulded montmorillonite clay is usually more compressible than an illite clay and a kaolin. The volume change behaviour of a montmorillonite clay would be primarily controlled by diffuse double layer repulsive forces, whereas it is governed by the shearing resistance at particle level for kaolin clay (Sridharan & Rao 1973, Sridharan 2002).

Volume change behaviour of bentonites is known to be influenced by several factors (Sridharan & Jayadeva 1982, Chen 1988, Gens & Alonso 1992, Fredlund & Rahardjo 1993): (a) compaction density, (b) type and amount of exchangeable cations, (c) specific surface area, (d) montmorillonite content, (d) temperature, (e) properties of the bulk fluid, (f) initial and final stress states (suction and net stress), and (h) stress history. Reported studies on the compressibility behaviour of initially saturated bentonites at large pressures are limited. Bolt (1956), Warkentin et al. (1957), and Di Maio et al. (2004) carried out oedometer tests up to a vertical pressure of about 5 MPa. Mesri & Olson (1971) reported test results up to about 3 MPa, whereas Yong & Mohamed (1992) and Al-Mukhtar et al. (1999) presented experimental results up to 10 MPa, Marcial et al. (2002) up to 30 MPa.

Microstructural studies on remoulded clays consolidated up to different applied stresses have been reported in the past (Tovey & Wong 1980, Griffiths & Joshi 1990, Al-Mukhtar, Belanteur, Tessier & Vanapalli 1996, Moriwaki & Wada 2001). For kaolinite clays, an increasing degree of orientation with particle alignment normal to the principal stress direction was found with increasing consolidation pressure until 1900 kPa (Tovey & Wong 1980) and 10 MPa (Moriwaki & Wada 2001). Until an vertical applied stress of about 100 kPa, the degree of orientation was insignificant and the degree of orientation was higher in the vicinity of the drainage surface as compared to regions at some distance from the drainage surface (Tovey & Wong 1980). Griffiths & Joshi (1990) performed an MIP study of various remoulded clays having a different mineralogical composition and

stated that the deformation of clays during consolidation is mainly due to a decrease of the largest pore type (interaggregate pore), whereas the pores with a diameter smaller than about 200 nm were unaffected by the increase up to the maximum applied consolidation pressure of 1500 kPa.

Marcial et al. (2002) showed that the e-$\log \sigma'_v$ relationships (i.e., the void ratio versus log-vertical stress relationships) of initially saturated bentonites for a large pressure range (up to 30 MPa can be identified by two coefficients of compression; one in the initial pressure range and the other at large pressures. They showed that the transition from an initially steeper slope to a moderate slope occurs at different pressures depending upon the type of exchangeable cations present in the bentonite. The compressibility behaviour of the bentonites before the transition (in general, below a pressure of 1000 kPa) was attributed to two phenomena, such as: (i) the compression of a gel structure at very high void ratio, and subsequently, (ii) the compression of largest interaggregate voids. Beyond the transition and at pressures greater than about 1000 kPa, it was stated that the regular parallel arrangement of clay platelets seems to be reasonably valid. In this stress range, the stress-void ratio behaviour of bentonites is affected by the type of exchangeable cations and the number of water molecules contained in the hydration shells within the interlayer space.

Al-Mukhtar et al. (1996) presented a microstructural study of remoulded Boom clay (composed of 33% interstratified illite-smectite, 16% illite, 13 % kaolinite, 62% other minerals) consolidated to 1, 5, and 15 MPa. At 1 MPa consolidation pressure, no inter-aggregate pores greater than 150 to 200 nm were found, and at higher pressures of 5 and 15 MPa, still smaller pore sizes and a homogeneous particle arrangement was observed.

Aylmore & Quirk (1959), Aylmore & Quirk (1962) and Quirk & Aylmore (1971), based on SEM and measurements of surface area, porosity, and pore size measurements of an illite, stated that an average pore size of 3 nm prevails within the illite aggregate, even upon complete drying and unaffected by the type of exchangeable cations present. They concluded that an illite aggregate would behave with relatively strong stability as a single entity in determining the water content-energy characteristics and the mechanical properties. From this statement, it could be concluded that the stiffness as a mechanical parameter is determined by the resistance of the illite aggregate against deformation at the applied stresses.

The typical consolidation-rebound curves of clays independent of their mineralogy are showing hysteresis in void ratio. A possible explanation for the hysteresis phenomenon is that the decreasing interparticle spacing during virgin compression leads to grouping

of particles, thus, a decrease in operating specific surface area, once the attractive energy at close particle distance dominates. The attractive forces prevail to some extend during decompression, therefore, a smaller stress is needed as compared to virgin compression to keep the clay-water system at a given void ratio (Nagaraj & Srinivasa Murthy 1983). Holmes (1955) cites Schofield (1935) and Barkas (1946) who stated that hysteresis is the result of plastic readjustment of the clay particles and manifests the loss of energy during a compression-decompression cycle.

The above studies on the volume change of bentonites and other clay types were mostly for saturated condition with initial water content greater than liquid limit. The compressibility behaviour of compacted bentonites after the swelling pressure is developed under confined conditions and at very high stresses (up to 25 MPa) is a near field situation which has not been studied so far. In chapter 6, the compressibility behaviour of the clays studied (Calcigel bentonite, NX illite, Spergau kaolin) was investigated up to high applied stresses of 25 MPa, both for initially saturated and compacted saturated conditions.

2.5. Swelling pressure

Two mechanisms are mainly responsible for swelling in montmorillonitic clays: (1) the crystalline swelling, (2) the osmotic swelling. The crystalline swelling is on account of the sorption of interlayer water molecules on the clay surfaces and around the exchangeable cations, which is manifest by a stepwise increase in the interlayer distance. Crystalline swelling is the dominant mechanism at low water content; with increasing water content, the hydrated cations will dissociate from the layer surface into the solution to form the electrical diffuse-double layer (osmotic swelling) (van Olphen 1977).

As introduced in section 2.2.3.1, according to diffuse-double theory, a saturated clay-water system is in equilibrium when the difference in osmotic pressures at the central plane between two particles and in the bulk fluid is balanced by the external pressure. The external pressure is usually termed repulsive pressure or swelling pressure (Bolt 1956, Mitchell 1993). This concept was also applied to the swelling pressures of compacted bentonites (Komine & Ogata 1996, Tripathy et al. 2004). In these studies, the swelling pressure at equilibrium, i.e., at the end of saturation, was considered to be equal to the diffuse-double layer repulsive pressure. This consideration is based on the assumption that the double-layer repulsive force is the single operating force in the clay-water system. However, for bivalent montmorillonites at close clay particle distances with restricted diffuse double-layer swelling, the hydration energy due to surface and ion hydration are the

dominating factors for the swelling pressure development (van Olphen 1977, Kjellander, Marcelja, Pashley & Quirk 1988, Yong 1999).

In geotechnical laboratory testing, swelling pressures of compacted expansive clays can be determined from several methods, such as the swell and load method, the load-swell method, and the no-swell method (Sridharan, Sreepada Rao & Sivapullaiah 1986, ASTMD4546-08 2008). The latter test is known as the strain-controlled test where the volume change of the clay is not permitted (Chen 1988). Considering the use of compacted bentonites as the sealing material in the access galleries, tunnels, and also as the buffer material in the vicinity of the waste canisters, the in situ condition suggests that strain-controlled tests are more useful than the other methods of determination of swelling pressures. Therefore, most studies in the past have focussed on the determination of swelling pressures from strain-controlled tests (Müller-Vonmoos & Kahr 1982, Gray et al. 1984, JNC 2000, ENRESA 2000).

Several researchers in the past have investigated the time dependent behaviour of swelling pressures during the saturation process. Brackley (1973), Komine (1994), and Schanz & Tripathy (2009) observed that the development of swelling pressure of compacted specimens during saturation was influenced by the initial dry density, the water content and the boundary conditions. Whereas at lower initial dry densities, the swelling pressure development was smooth, the evolution of swelling pressure was characterised by a first maximum with a subsequent decrease in swelling pressure, sometimes followed by a reincrease to a second peak value. Pusch (1982) attributed the swelling pressure decrease to the loss in shear resistance in the contact region of the aggregates due to the increased interparticle distances within the aggregates during water uptake. The further swelling pressure increase is on account of a redistribution of particles from an aggregated towards a more homogeneous, dispersed state. Imbert & Villar (2006) observed similar patterns of increase-decrease-increase for specimens compacted in a range of initial dry densities from 1.3 to 1.6 Mg/m^3. Further, they stated that for a high dry density, the second swelling pressure peak value was found to be greater than the initial one, whereas this was not the case for specimens of smaller dry density. They interpreted the swelling pressure reduction as a collapse of macropores due to a suction decrease during the saturation process.

The studies cited above describe the global swelling pressure. They do not allow for a quantitative distinction between crystalline swelling and osmotic swelling during the saturation process. The hydration states of clays during crystalline swelling can be characterized by X-ray diffraction (XRD) under controlled relative humidity (RH). The amount

of water layers adsorbed is a function of RH, type of exchangeable cations, layer charge, location of layer charge (in octahedral or tetrahedral sheet), and the bulk fluid concentration (Jasmund & Lagaly 1993). The amount of intercalated molecular H_2O planes from zero (dehydrated) until three planes is evaluated based on the measured c-axis spacing. The evaluation is performed using modelling techniques to fit the experimental to theoretical XRD patterns. Various researchers have established mathematical methods for XRD profile modelling (Kakinoki & Komura 1952, Drits & Sakharov 1976, Plançon & Tchoubar 1976). Pons (1980) has presented a model for small-angle X-Ray diffraction in transmission mode.

For increasing RH values, the adsorption of the water molecules is manifest as discrete increase in the c-axis spacing. At RH of about 30 to 60%, a montmorillonite with Na^+ as exchangeable cations has one plane of H_2O molecules in the interlayer, corresponding to a c-axis spacing of 1.25 nm, whereas two planes of H_2O molecules are adsorbed in the interlayer of Ca^{2+} montmorillonite, which corresponds to a c-axis spacing of 1.45 to 1.55 nm (Grim 1968). The increase in c-spacing due to crystalline swelling does not exceed about 1.9 nm corresponding to three planes of H_2O molecules, irrespective of the type of the exchangeable cations contained in the clay (Aylmore & Quirk 1959, Blackmore & Warkentin 1960).

Various studies have emphasized major differences in the hydration behaviour of sodium montmorillonites and calcium montmorillonites (Norrish & Quirk 1954, Bolt 1956, Quirk & Aylmore 1971). Quirk & Aylmore (1971) states that in the former, a strong association between the water molecules and the layer surface occurs only in the first monolayer of the adsorbed water. The layer-to-layer distance at small concentrations ($<0.3N$ NaCl) measured in Na-montmorillonite are greater than 4.3 nm and proportional to the concentration, which allows for the development of diffuse double layers in the interlayer space. Contrary, calcium montmorillonite showed a fixed 1.9 nm layer-to-layer distance independent of the concentration of the fluid. Quirk & Aylmore (1971) postulated further that Ca-montmorillonite possesses an internal as well as an external surface. Based on a value of the external surface of Ca-montmorillonite of $\approx 100\ m^2/g$, the amount of layers contained in a particle would be about five to seven, where the layers are separated by 1 nm of water giving rise to the layer-to-layer distance of 1.9 nm.

These differences in the swelling behaviour were also observed for sodium illite as compared to calcium illite. The former showed large swelling and sensitivity to electrolyte concentration, whereas swelling of the latter was found to be insensitive to large changes in electrolyte concentration.

Warr & Berger (2007) and Devineau, Bihannic, Michot, Villiéras, Masrouri, Cuisinier, Fragneto & Michau (2006) emphasized the influence of confinement on the interlayer water adsorption and stated that the confinement hindered interlayer expansion. Warr & Berger (2007) monitored the hydration behaviour of weakly compacted ($\rho_d = 0.94$ to 1.14 Mg/m^3) Na^+- and Ca^{2+}-bentonites during infiltration of electrolyte solutions with an ionic concentration corresponding to groundwater and seawater under confined condition. The water uptake was continuous, and different amount of water layers were found to coexist, as opposed to the distinct interlayer hydration steps under controlled RH. The proportion of non-interlayer surface and pore water was found to be about 75% for Ca-bentonite and about 50% for Na-bentonite, irrespective of the ionic concentration of the infiltrating solution.

Suzuki, Prayongphan, Ichikawa & Chae (2005) separately measured crystalline swelling by XRD and the aggregate expansion by laser scanning microscopy (LSM) of Na-bentonite with initial water content of 85 and 50% at unconfined conditions subjected to NaCl-solutions of various concentration. He stated that for NaCl-concentrations up to 100 mol/m^3, double-layer swelling is the dominant process, whereas at concentrations greater than 300 mol/m^3, by both the crystalline swelling and the double-layer swelling between quasicrystals control the swelling. It was further reported, that in LSM-experiments of a Ca-bentonite, swelling started only after few days exposure to destilled water.

Likos (2004) and Likos & Lu (2006) presented an experimental set-up which allows for the continuous measurement of water content during hydration and dehydration path at controlled relative humidities between 1 and 85% RH; instead of XRD-measurements for the determination of the interlayer distance, the related volume changes in terms of axial strain were calculated from the measured water content values for the tested Na^+ and Ca^{2+}-smectites. The results were found to be consistent with earlier studies using XRD-measurements for the determination of basal spacing.

For a given water content, the higher the initial dry density, the higher is the swelling pressure (Sridharan, Sreepada Rao & Sivapullaiah 1986, Komine 1994). Sridharan, Sreepada Rao & Sivapullaiah (1986) stated that molding water content influences the fabric that may have some influence on the swelling pressure. Gens & Alonso (1992) argued that at the same compaction dry density, clay specimens having very high initial water contents or very low initial suctions tend to exhibit lower swelling pressures than that of specimens with lower water contents or higher suctions.

Compacted bentonites are comprised of pores at different structural levels (Gens & Alonso 1992, Romero et al. 1999, Lloret et al. 2003, Delage et al. 2006). Pore size distribution studies for initially unsaturated compacted bentonites by Delage et al. (2006) showed that the total pore volume of compacted bentonites are comprised of the interlayer pores between the layers, the interparticle pores between the particles inside the aggregates, and the inter-aggregate pores between aggregates. With an increase in the water content, the swelling of bentonites is characterised by a division of the particles within the aggregate, thus increasing the interparticle pore volume that is manifested on the reduction of the interaggregate pores (Saiyouri et al. 2000, Saiyouri et al. 2004, Agus & Schanz 2005*b*, Delage et al. 2006, Delage 2007). The process of division of quasicrystals is illustrated in Fig. 2.14. Thom et al. (2007), investigating the microstructure of an kaolinite by means of MIP, observed that samples subjected to isotropic compression of 400 and 800 kPa before wetted at about 37 kPa showed an aggregate expansion into the interaggregate pore space, leading to an rearrangement of particles within the aggregate. They further stated that increasing compaction pressure resulted in a considerable reduction of both the inter-aggregate and the intra-aggregate pore space, especially at low water contents.

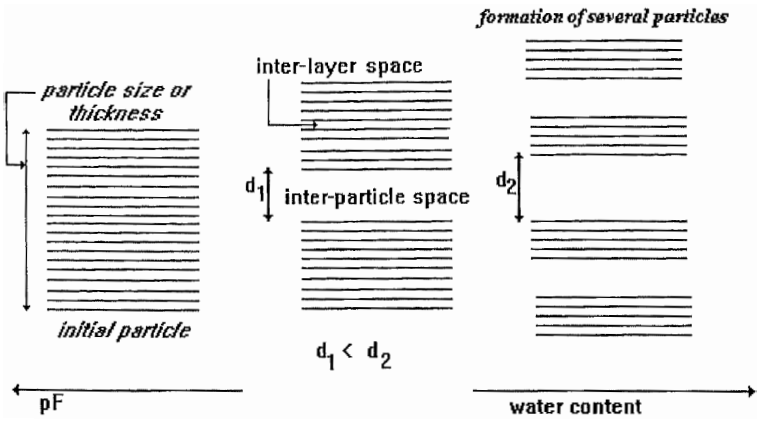

Figure 2.14.: Formation of an increased number of particles containing smaller amount of layers due to the division of the initially large quasi-crystals (Saiyouri et al. 2000).

Within an aggregate, the arrangement of the particles was shown to be nearly parallel (Blackmore & Warkentin 1960, Grim 1968, Tessier 1984, Saiyouri et al. 2000). Studies of the (001) peak on typical oriented smectite samples at low water contents obtained by neutron diffraction revealed that the clay platelets deviate ±20° about a perfectly parallel arrangement (Sposito & Prost 1982). Aggregates are in turbulent array with respect to each other (Quirk & Aylmore 1971, Aylmore & Quirk 1962). Swelling of natural soil

aggregates and compressed clay cores is isotropic (Holmes 1955), whereas the swelling within an aggregate would be unidirectional.

Commonly, clays contain a mixture of various types of exchangeable cations (Newman 1987). In studies on smectites containing Na^+- and Ca^{2+}-ions it was observed that the clay-water system exhibit preferences for one over the other cation type, leading to the presences of each cation type in different layers. This phenomenon is also called *demixing*. It was found that the break-up of the quasi-crystals during hydration preferentially takes place at interlayers containing Na^+, as illustrated in Fig. 2.15. In general, there is an increasing selectivity for a divalent cation over monovalent Li or Na cations with increasing layer charge (Laird 2006). The demixing process is also related to the long-term transformation of a Na-smectite into Ca-smectite. Warr & Berger (2007) stated that an interlayer exchange of Na- by Ca-ions would probably have a greater effect on the behaviour of a buffer or geotechnical barrier than an increase in ionic concentration of the wetting fluid by a possible sea water intrusion.

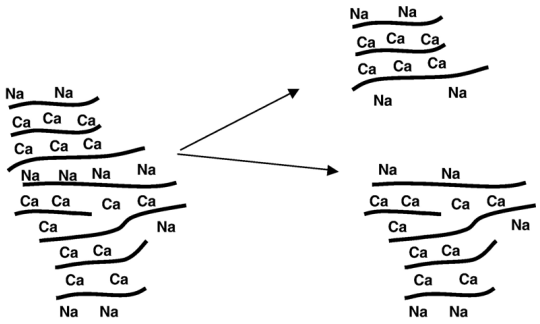

Figure 2.15.: Demixing of cations and preferential break-up of quasi-crystals at Na^+ sites (Laird 2006)

The subject of volume increase and swelling pressure due to hydration is mostly relevant for clays containing montmorillonites, because their mineralogy allows for the incorporation of water molecules in the interlayer, driven by surface and cation hydration or osmosis. Illite and kaolinite are minerals possessing a fixed c-axis spacing. According to Quirk & Aylmore (1971), these clay minerals would exhibit only inter-crystalline swelling. In other words, only the outer surfaces of the particles are active sites for possible water molecule adsorption by surface and cation hydration or osmosis.

In the present work, the swelling pressures of compacted samples of the three clays used (Calcigel bentonite, NX illite, Spergau kaolin) were determined in strain-controlled tests at constant volume. The results of the swelling pressure tests are presented and discussed in Chapter 5, and the obtained void ratio-swelling pressure relationships were compared

to the respective compression and decompression curves of the initially saturated and the compacted saturated samples in Chapter 6.

2.6. Suction

In general, the soil is a three-phase system consisting of the solid, the air and the water phase, where the latter two compose the volume of the pore space. A soil is fully saturated, when the total pore volume is filled with water; the degree of saturation S_r is then equal to one. When the degree of saturation is smaller than one, the soil is in an unsaturated state.

The concept of suction or water potential was introduced by soil scientists at the beginning of the twentieth century (Buckingham 1907, Edlefsen & Anderson 1943). At any water content, the soil pore water has a certain level of thermodynamic potential with respect to the reference potential of pure free water. Capillarity, short-range adsorption, and osmotic effects are the important mechanisms responsible for decreasing the soil water potential with respect to the reference state. Capillary effects comprise effects due to surface tension at the air-water interface and the related negative pore water pressure. Capillary effects due to surface tension only occur in unsaturated state, since they are related to the existence of air-water interfaces, whereas short-range adsorption and osmotic effects may occur both in saturated and unsaturated conditions. The potential of soil water can be expressed as energy per unit mass (chemical potential in J/kg), as energy per unit volume (pressure potential) in $J/m^3 = Pa$), or as energy per unit weight (head potential in $J/N = m$). In geotechnical engineering, *suction* is the preferred term and refers to the pressure potential ψ in kPa Ignoring the effects of temperature and gravity, eq. 2.9 describes the change in total chemical potential $\Delta\mu_t$ as the sum of its components (J/kg) (Fredlund & Rahardjo 1993, Lu & Likos 2004).

$$\Delta\mu_t = \Delta\mu_c + \Delta\mu_o + \Delta\mu_e + \Delta\mu_f \tag{2.9}$$

where $\Delta\mu_t$ is the total potential, $\Delta\mu_c$ is the potential due to capillary forces including negative pore water pressure, $\Delta\mu_o$ is the osmotic potential due to the concentration of solutes contained in the pore water, $\Delta\mu_e$ is the potential due to short-range electrical fields of the soil solid, and $\Delta\mu_f$ is the potential due to van der Waal's fields. The latter two can be summarized as due to short-range adsorption. The potentials arising from short-range adsorption and capillarity together correspond to the matric potential, leading to eq. 2.10

expressed in terms of suction:

$$\psi_{\mathrm{tot}} = \psi_{\mathrm{m}} + \psi_{\mathrm{o}} \tag{2.10}$$

where ψ_{tot} is the total suction, ψ_{m} is the matric suction, and ψ_{o} is the osmotic suction in kPa The total suction is related to the relative humidity by Kelvin's law as follows:

$$\psi_{\mathrm{tot}} = -\frac{RT}{v_{\mathrm{w0}}\omega_{\mathrm{v}}} \ln(\frac{u_{\mathrm{v}}}{u_{\mathrm{v0}}}) \tag{2.11}$$

where ψ_{tot} is the total suction (kPa), R is the universal gas constant (8.314 J/mol K), T is the absolute Temperature (K), v_{w0} is the specific volume of water (m^3/kg), ω_{v} is the molecular mass of water vapour (18.016 kg/kmol), u_{v} is the partial pressure of the pore water vapour (kPa), and u_{v0} is the saturated vapour pressure of free water at the same temperature (kPa). The ratio of the latter $\frac{u_{\mathrm{v}}}{u_{\mathrm{v0}}}$ is equal to the relative humidity RH, and eq. 2.11 can be written as:

$$\psi_{\mathrm{tot}} = -\frac{RT}{v_{\mathrm{w0}}\omega_{\mathrm{v}}} \ln(RH) \tag{2.12}$$

Thus, measuring or controlling the ambient relative humidity and temperature of a soil volume enables for determination of the total suction value within the soil.

Bolt & Miller (1958) presented equations for the calculation of the component potentials of soil water, and highlighted that within a soil volume in equilibrium, the total potential (or total suction) is constant at any point within the soil volume considered, but the magnitude of the various components of total water potential varies depending on the location relative to the clay particles, the grains and the soil-water interface.

Fig. 2.16 illustrates the features of potentials at different locations within an ideal clay system and a mixed system composed of coarse grains and clay particles. Ideal clay means a clay made up of three-sheet layers of montmorillonite type in parallel, equally spaced array with interacting double layers. In Fig. 2.16 (c), point o is located at the flat surface just inside the pure water and represents the reference state, where the total potential is zero by convention.

In Fig. 2.16 (a), three characteristic points are described for an ideal clay system: point d is situated in the equilibrium free pore solution of the clay-water system, where the ion concentration determines the osmotic potential. Point a is situated at the air-water interface of zero curvature, where the total potential is the result of the pressure in the atmosphere above the surface and the osmotic component due to the solute concentration at point a. Point c is located at the midplane between two adjacent clay particles,

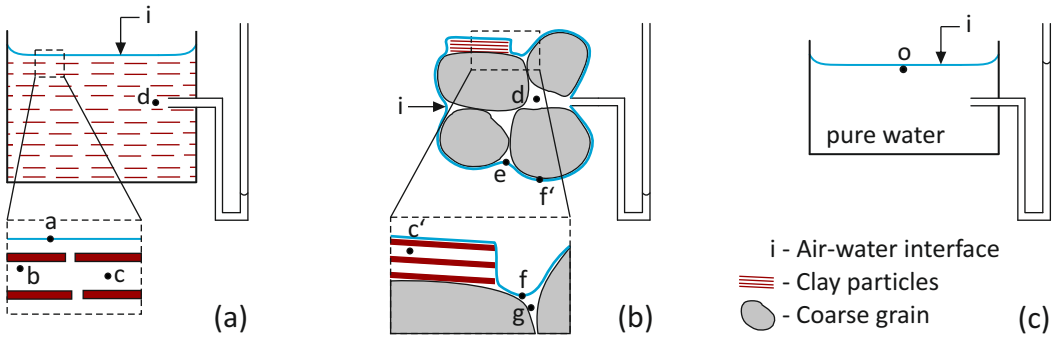

Figure 2.16.: Components of total soil moisture potential: (a) for an ideal clay-water system, (b) for a mixed system, (c) reference state, modified after Bolt (1958).

its distance from the particle is the same as that of point *a*, therefore, the magnitude of osmotic potential of points *c* and *a* is the same, but greater than that of *d*. Point *b* is located somewhere between two parallel particles, relatively close to one of them. The potential components contributing to the total potential are due to the short-range adsorption and solute concentration.

In the mixed system as shown in Fig. 2.16 (b), points *e* and *d* are outside the range of diffuse-double layer. In both points, the capillary potential and the osmotic potential due to the pore solution concentration compose the total potential. The potentials in points *c'*, *f* and *g* influence each other, in a manner that at equilibrium, the osmotic potential in *c'* is balanced by the capillary and weak osmotic potential components in points *f* and *g*.

Yong (1999) emphasized that measurements of the equilibrium energy status in terms of total or matric potential of swelling clays water may not be representative for the local potentials due to interactions in the interlayer and interparticle, but it describes the energy status of the soil water in the larger pores.

Bolt & Miller (1958) further mentioned that illite and kaolinite clays would not behave like an ideal clay system. Illite is composed of larger particles with terraced surfaces, minimizing the water uptake due to osmotic potential. Kaolinite has usually blocky particles, and may approach coarse grained soils in his behaviour.

The above considerations were made to recall the origin of suction in soils. The following paragraphs are concerned with the use of suction as a parameter to describe soil behaviour, with emphasis on clays.

For a given soil, a characteristic relationship between suction and the respective amount of water retained by the soil can be established. The suction-water content plots and the

suction-degree of saturation plots have been shown to indicate some distinctive features during a desorption process for many natural soils, primarily owing to the nature of pore size distribution in soils (Cuisinier & Laloui 2004). In Fig. 2.17a, a schematic of the soil-water characteristic curve (SWCC) is shown. For determining the SWCC, an initially saturated specimen is subjected stepwise to an increase in suction (initial drying) until complete drying, and subsequently to a re-decrease in suction (main wetting). The corresponding equilibrium water content at each suction step is measured. The term water retention curve (WRC) refers to the drying path of the SWCC, and suction-water content relationship (SWCR) relates the suction to the water content of a soil volume of any given state during soil suction history (for drying or wetting). Such curves are also called scanning curves, and they would start in the region enclosed by the main drying and the main wetting path. The initial drying path is irreversible, whereas the main wetting and main drying paths are reversible. However, hysteretic behaviour is beyond the scope of the present study.

In the SWCC, the amount of water is usually expressed as gravimetric water content w, volumetric water content θ or degree of saturation S_r. Up to the air-entry value (AEV), the soil is in the saturated state. Beyond AEV, air enters into the soil, but the water phase is still continuous until residual suction ψ_res is reached; the desaturation zone is also called funicular zone. At suctions greater than ψ_res, the air phase is continuous, the water phase is discontinuous; this region is termed residual or pendular zone.

Drying and wetting are known to induce volume change in clays, respectively, shrinkage and swelling. The swelling mechanisms related to the wetting were treated in the foregoing section 2.5. The effects of suction induced drying are the issue of this section. The shrinkage limit w_S is used in geotechnical engineering as a measure for the shrinkage behaviour of the soil, usually determined from air drying and subsequent oven drying of a specimen. Fig. 2.17b shows a schematic of a typical shrinkage curve of an initially saturated clay in terms of void ratio versus water content. The shrinkage phenomenon is characterised by two stages. During normal shrinkage, the volume change of the soil is equal to the volume of water withdrawn while the pore space remains saturated. Residual shrinkage follows the normal shrinkage stage and the volume decrease of the soil is less than the volume of water withdrawn. Thus, degree of saturation diminishes with decreasing water content, which means that the pore space becomes unsaturated. The magnitude of residual shrinkage depends upon colloidal content and the related amount of adsorbed water (Haines 1923). For any suction induced during the drying path, the shrinkage curve can be drawn, provided that equilibrium water content and volume were determined.

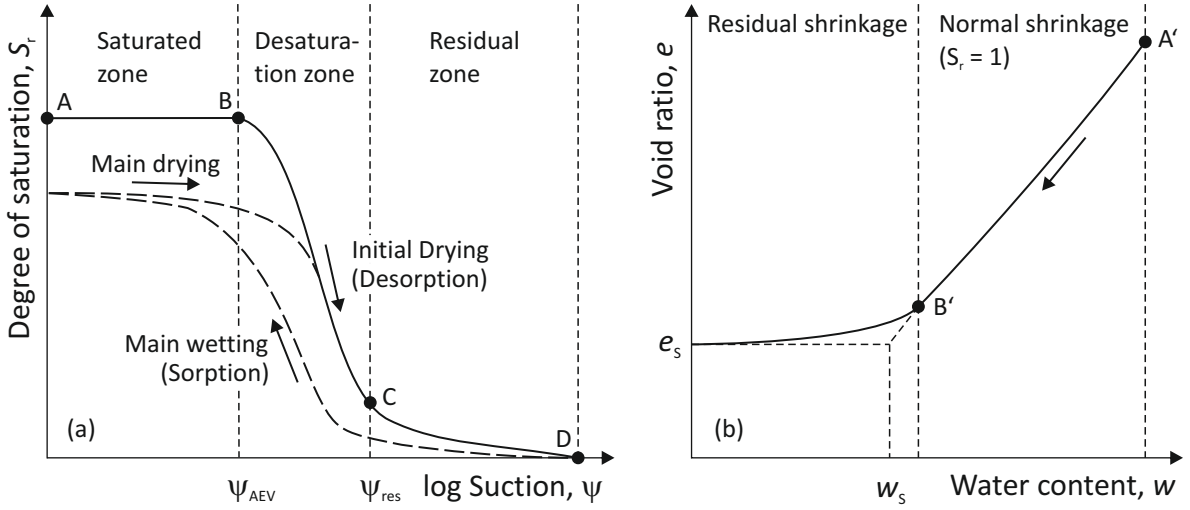

Legend: A Initial state of the soil (S_r = 1)
B Begin of desaturation; suction at B corresponds to the air-entry value ψ_{AEV}
C Transition from the desaturation zone to the residual zone; suction at point C corresponds to the residual suction ψ_{res}
D Completely desaturated state (ψ = 1000 MPa)
A' Initial state of the soil (S_r = 1)
B' Transition from linear shrinkage to residual shrinkage
w_s, e_s Water content and void ratio at shrinkage limit

Figure 2.17.: Principle shape of (a) soil-water characteristic curve (SWCC) and (b) shrinkage curve

In the laboratory, the soil-water characteristic curve is commonly established by subjecting saturated soil specimens to an increase in suction at zero external stress. The test results are valuable for determining the hydraulic conductivity of unsaturated soils (Mualem 1976, Vanapalli, Fredlund & Pufahl 1996, Leong & Rahardjo 1997, Barbour 1998, Fredlund 2006). For clays, the applied suction needed to desaturate the samples is in the range from several hundreds of kPa up to several hundreds of MPa Vapour equilibrium technique is commonly adopted to induce higher range of suction in soils from about 2 to 300 MPa (Lloret et al. 2003, Cuisinier & Masrouri 2004). Suction is imposed by controlled relative humidity using saturated salt solutions in a closed container (commonly, a desiccator). The soil suction in this case represents the total suction because of the fact that a change in the water content affects the capillarity as well as the ionic concentration of pore fluid. Since the water transfer from soils occurs in the vapour phase, the compositions of soils remain unchanged during a test (Schanz & Tripathy 2005). Further details and the procedure adopted using vapour equilibrium technique is given in section 3.2.4.

Axis-translation technique (ATT) and osmotic method (OM) are common methods for applying suctions in the range below 2 MPa. The former is able to induce matric suction up to 1500 kPa by submitting the soil to air pressure u_{a} while the pore water pressure u_{w} is kept at a positive gauge pressure (Hilf 1956). The matric suction induced correspond to $\psi_{\mathrm{m}} = u_{\mathrm{a}} - u_{\mathrm{w}}$. OM was the preferred method in the present study, since (i) it requires significantly less time for water content equilibration, and (ii) it allows for the application of a maximum suction of about 10 MPa, providing an overlapping with the suction values applied by VET. Several researchers have used the osmotic technique to study the water retention behaviour of soils (Fleureau et al. 1993, Marcial et al. 2002, Williams & Shaykewich 1969, Zur 1966). Similarly, the technique has been used to study the volume change behaviour of soils as affected by changes in the soil suction (Cui & Delage 1996, Cuisinier & Masrouri 2005, Delage, Howat & Cui 1998, Delage & Cui 2008, Dineen & Burland 1995, Kassiff & Ben Shalom 1971, Monroy, Ridley, Dineen & Zdrakovic 2007). Osmotic method uses the principle of difference in osmotic pressure between the soil-water and a polyethylene glycol-solution (PEG-solution) separated by a semi-permeable membrane (Zur 1966). The detailed description of the method and the procedure adopted is presented in section 3.2.3.

Recent developments in unsaturated soil testing have enabled establishing suction-water content SWCCs for both swelling and non-swelling soils using the dew-point technique within a reasonable time period (Leong, Tripathy & Rahardjo 2003, Likos & Lu 2001, Likos & Lu 2003, Likos & Lu 2012). Similarly, devices are also available to monitor water content

and axial deformation of soil specimens during wetting and drying processes covering the crystalline region up to RH of about 80% (Likos & Wayllace 2010). A number of laboratory techniques are available to measure volume of soil specimens during wetting and drying processes (Fleureau et al. 1993, Tripathy, Subba Rao & Fredlund 2002). Combined water content and volume measurements during wetting and drying processes generally require testing of duplicate soil specimens.

Various models have been established for the mathematical formulation of the SWCC (van Genuchten 1980, Fredlund & Xing 1994). The parameters used in these equations are obtained from fitting of experimental SWCC data.

Grim (1968) stated that water lost in clays at low temperatures may be classed in three categories, depending on its relation to the mineral components and to the texture of the clay materials: (*i*) the water in pores, on the surfaces, and around the edges of the discrete particles of the minerals composing the clay material, (*ii*) the interlayer water between the unit-cell layers of minerals, and (*iii*) for specific minerals (viz., attapulgite), water within the tubular opening between elongated structural units.

McQueen & Miller (1974) presented a conceptual model for water retention behaviour of agricultural soils. They divided the suction versus water content plot of soils into three different suction regimes. Each regime spans a certain range of suction within which the mechanism of water held in soils is accounted by the energy required to remove the soil water: (a) a suction range of 10 to 1000 MPa - tightly adsorbed regime, (b) a suction range of 33 kPa to 10 MPa - adsorbed film regime, and (c) the capillary regime that follows the adsorbed film regime for suctions smaller than about 33 kPa until the saturation state of the soil is reached. The proposed model was developed primarily in the context of studying the field capacity and wilting point of agricultural soils. As shown by McQueen & Miller (1974), limited data are usually sufficient to establish water retention behaviour of several agricultural soils. Examples shown by them indicated that the model worked very well for sandy soils.

Based on a study of a kaolinite, Vesga (2008) identified four different zones corresponding to different states of water within the soil. The development of the tensile strength and void ratio with decreasing water content was related to the following states of soil-water: (*i*) saturated and funicular state, (*ii*) complete pendular state, (*iii*) partial pendular state, and (*iv*) van der Waals state. He observed a volume re-increase at very low water contents, which was attributed to the breakage of water bridges between the particles. Similarly, Sridharan & Venkatappa Rao (1971) reported based on Leonards (1961) and Yong & Warkentin (1966) that clays were found to show a volume re-increase at low

water contents, which was attributed to an elastic rebound of particles after the water films connecting the particles were broken.

Holmes (1955) has investigated the behaviour of remoulded and natural Australian Red clay and Black clay blocks, predominantly composed of kaolinite and illite with small portions of montmorillonite, within the suction limits of 0.01 MPa and 100 MPa in a drying and wetting cycle. During drying, he observed a somewhat gradual transition from normal to residual shrinkage (see schematic in Fig. 2.17b), with the significant portion of volume change occurring during the normal shrinkage stage. The start and the size of the transition range would be governed by the pore size distribution of the soil.

Fleureau et al. (1993) compared the volume change behaviour of an initially saturated kaolinite and Ca-montmorillonite clay obtained from water retention tests with the corresponding isotropic and oedometric compression paths. They noted that the pressure-void ratio and suction-void ratio paths were very nearly similar within the saturated domain. Marcial et al. (2002) reported experimental tests of various bentonites and showed that an increase in the vertical stress and an increase in suction leads to nearly similar volume change. The differences between the compression paths and volume change due to applied suctions were attributed due to the isotropic condition while applying suction as compared to the anisotropic loading in the oedometer. Both studies have emphasized the similarity in volume change due to suction loading and mechanical loading with the validity of Terzaghi's effective stress concept within the saturated domain, i.e., up to the respective air entry suctions of the clays. For highly plastic clays the phenomenon is valid up to large suctions since up to several thousands kPa *t*he clays remain saturated. For suctions greater than air entry values, air enters the pore space, and the volume change was found to be less in the desaturated state.

Sridharan (1968) discussed the shrinkage phenomena of soils in the context of effective stress, based on experiments with kaolinite. He stated that the shear resistance mobilized between particles at the particle contacts manifest as the resistance against volume change during shrinkage. The shear resistance at particle level is a function of normal forces acting between particles and/or at the particle contacts, the frictional properties, and the electrical repulsive and attractive forces. A volume decrease occurs as long as the surface tension forces are larger than the internal shearing resistance. Thus, the shrinkage void ratio would be controlled by the effective stress in the soil. The main conclusion of this investigation was that shrinkage void ratio increases as the effective stress increases.

Studies using x-ray diffraction (XRD), environmental scanning electron microscope (ESEM), and mercury intrusion porosimetry (MIP) have provided evidence concerning the deve-

lopment of microstructure related to drying processes (Aylmore & Quirk 1962, Quirk & Aylmore 1971, Tessier 1984, Tessier 1990*b*, Montes-H, Duplay, Martinez, Geraud & Rousset-Tournier 2003). Aylmore & Quirk (1962) and Quirk & Aylmore (1971) emphasized that in an intially saturated illite, the aggregates would behave like a stable entity during drying, since a constant average separation between illite surfaces of 3 nm within the aggregate was observed, even at complete drying. Contrary, in montmorillonite clays, an increase in separation distances between the particles within an aggregate was observed. This was interpreted as an increase in the amount of layers forming an particle, leading to a smaller amount of larger particles (Aylmore & Quirk 1962, Tessier 1984, Saiyouri et al. 2000). The process can be considered to be the reverse of that shown in Fig. 2.14.

Tuller & Or (2003) have introduced a pore space geometrical model for clay fabric representation referring to the work of Tessier (1990*a*). Their modeling framework aimed at capturing the evolution of soil pore space as a function of hydration state, solution composition, soil texture and clay type. Further, they have addressed the incorporation of clay fabric with other soil textural fractions like silt and sand to develop geometrical models at mesopore space as related to measurable soil properties. Finally, they introduced hydrostatic and hydrodynamic considerations to calculate pore-scale liquid retention and saturated hydraulic conductivity.

In this study, the effects of suction increase on the water content, the void ratio, and the degree of saturation for three clays each of them with different mineralogical backgrounds comprised predominantly of minerals montmorillonite, illite, and kaolinite, were experimentally determined. Clay specimens with initial water contents slightly greater than the liquid limits of the clays were subjected to increasing suction using the osmotic method and the vapour equilibrium method. The effects of mineralogy on the shapes of the soil-water characteristic curves, the air-entry suction, and the residual degree of saturation of the clays were brought out. The fabric and structure of the clays as obtained by environmental scanning electron microscopy at saturated state and at shrinkage limit were compared. MIP studies at shrinkage limit showed the difference in pore size distributions of the clays. The volume change induced by suction increase was compared to the volume change observed in the high stress oedometer tests. The results obtained were discussed based on fabric considerations (see chapter 4 and 7).

2.7. Physico-chemical approaches

The different kinds of clay-water mechanisms and the resulting forces were presented in sections 2.2.2 and 2.2.3. It was shown that the behaviour at macroscopic scale is determined by the respective mineralogical, thus, the resulting physico-chemical properties of the clays. The theory for the quantitative description of the ion distribution adjacent to a charged surface by Gouy (1910) and Chapman (1913) was further developed by Derjaguin & Landau (1941) and Verwey & Overbeek (1948) for describing repulsive forces and energies between colloidal particles, also considering attractive forces. This theory is often referred to as Derjaguin-Landau-Verwey-Overbeck (DLVO) theory. Bolt (1956) and van Olphen (1963) presented a method for calculating the interparticle repulsive pressure in a clay-water electrolyte system. Sridharan & Jayadeva (1982) improved the procedure so that it could be readily used for understanding the engineering behaviour of clays.

This approach has been used to calculate volume change in clays taking into account the interactions at particle level raising from the diffuse double layer (Bolt 1955, Bolt & Miller 1955, Olson & Mesri 1970, Mesri & Olson 1971, Sridharan & Rao 1973, Sridharan & Jayadeva 1982). Bolt (1955), Bolt (1956), and Warkentin et al. (1957) have shown that the theoretical and experimental compressibility behaviour of clays matches well for sodium montmorillonites. Blackmore & Warkentin (1960) suggested a correction of the calculated curve of calcium-montmorillonite reported in Warkentin et al. (1957) considering a reduction in specific surface area due to formation of particles containing several layers, with the outer surface of these particles being the active site for diffuse double layer formation. Achari, Joshi, Bentley & Chatterji (1999) have used Gouy-Chapman diffuse double layer theory to predict the hydraulic conductivity of consolidated clays. Madsen & Müller-Vonmoos (1985) conducted swelling pressure tests of overconsolidated Jurassic opalinum shale and reported a good agreement between the theoretical and experimental swelling pressures of an overconsolidated Jurassic opalinum shale. Later, it was adopted also for the prediction of swelling pressures of bentonite-sand mixtures (Komine & Ogata 1996) and compacted bentonites (Tripathy et al. 2004, Schanz & Tripathy 2009), and for predicting the soil-water characteristic curves (SWCC) of bentonites (Schanz & Tripathy 2005). Tripathy et al. (2004) have proposed semi-empirical equations for the direct calculation of the swelling pressure of compacted bentonites for a given dry density based on diffuse double layer theory. Schanz & Tripathy (2009) found good agreement between the calculated and experimental swelling pressures for a Calcium bentonite up to a dry density of about 1.55 Mg/m^3. The disagreement at higher dry densities was attributed to the significant amount of divalent exchangeable cations in the clay that

produced greater hydration energy at close particle spacing, requiring the consideration of additional repulsive pressures.

The assumptions included in the classical Gouy-Chapman solution for interacting diffuse double layers are: (*i*) the ions in the double layer are point charges; there is no interaction between them, (*ii*) the charge on the layer surface is uniformly distributed, (*iii*) the layer is a plate that is large relative to the thickness of the double layer, i.e. one-dimensional condition, (*iv*) the permittivity of the medium adjacent to the layer surface is independent of position. The model based on these assumptions is illustrated in Fig. 2.18a. Further, it is usually assumed in case of clays that the surface charge σ_0 (C/m^2) is constant and determines the diffuse double layer. However, in some cases, e.g., at the edges of clay particles, the double layer would be controlled by 'potential determining ions' and by a subsequent constant surface potential Φ_0 (V). An example is the effect of the pH-value of the solution in contact with edge surfaces of kaolinite, leading to the dissociation of ions from the mineral. All equations used in this study are based on the constant surface charge.

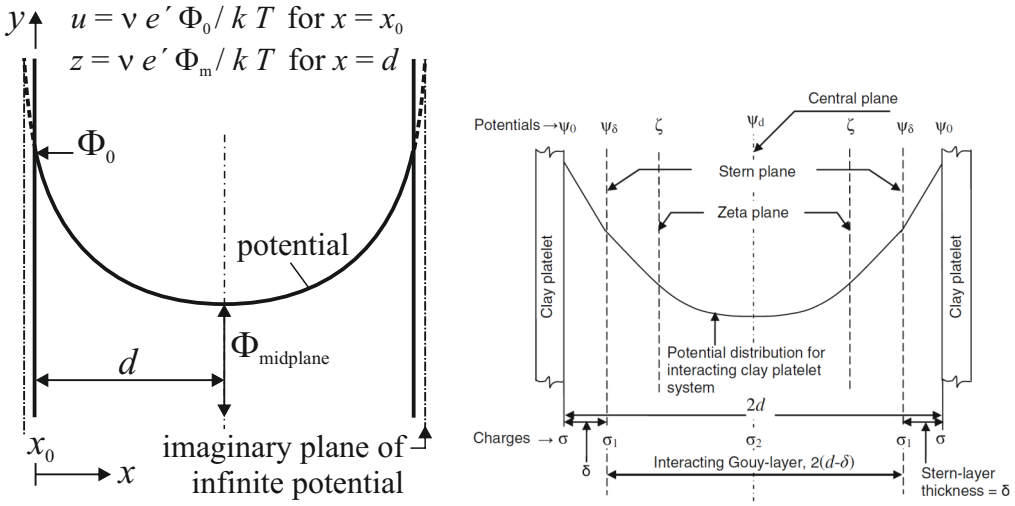

Figure 2.18.: Potential distributions for interacting diffuse double layers: (a) classical DDL-model, (b) DDL-model considering Stern-layer (after Tripathy et al. 2013a).

For the applications related to geotechnical engineering, the interparticle distance d is related to the void ratio e by eq. 2.13,

$$e = G_S \rho_w A_S d \tag{2.13}$$

where G_S is the specific gravity (-), ρ_w is the density of water (Mg/m^2) and A_S is the specific surface area (m^2/g) of the clay. The validity of this equation requires the parallel arrangement of the particles of equal size.

According to the diffuse double layer theory, an increase in electrolyte concentration, an increase of valency, and a decrease in dielectric constant reduce the thickness of the diffuse double layer, thus, result in a smaller repulsive pressure for a given interlayer distance. A temperature increase should increase the diffuse double layer thickness, however, this effect is neutralized by a simultaneous decrease in dielectric constant. Therefore, the net effect of temperature on the diffuse double layer thickness is negligible (Mitchell & Soga 2005).

Many researchers have emphasized quantitative differences between experimental data and the theoretically derived relationships (Bolt 1956, Blackmore & Warkentin 1960, Pusch 1982, Pashley 1981, Pusch, Karnland & Hökmark 1990, Güven 1992, Yong & Mohamed 1992, Sridharan 2002, Marcial et al. 2002). They were mostly attributed to the deviation of the real clay-water system from the assumed ideal system: (*i*) non-parallel particle arrangement, (*ii*) non-uniform particle size, (*iii*) ions are no point charges, but have a finite size, (*iv*) surface hydration forces at close particle distances, (*v*) existence of electrical attractive forces, (*vi*) presence of multivalent cations (*vii*), (*viii*) suppression of diffuse double layer water in the case of application of high compressive stresses.

The limited swelling of bi-valent clays can not be explained by the classical diffuse double layer theory (Pusch & Karnland 1990). Kjellander et al. (1988) presented an alternative approach (anisotrpic hypernetted chain (AHNC) theory) to account for the effects of bi-valent ions.

A possible correction to account for the finite ion size, and thus, the limited concentration of ions in proximity to the particle surface, is the Stern-theory (Stern 1924). The potential distribution considering the Stern-layer is schematically shown in Fig. 2.18b. According to the Stern-theory, the total charge in the liquid σ (C/m^2) is divided into two parts. The first part is the Stern-layer charge σ_1, which is located on a plane at the distance δ; the second part of the charge is the Gouy-layer charge σ_2 which extends from the Stern-plane in accordance to the Poisson-Boltzmann distribution. The electrical potential (ψ in mV) decreases linearly from the surface (ψ_0) to the Stern-plane (ψ_δ). Tripathy (2013) compared experimental data from one-dimensional consolidation tests to calculated void ratio vs. applied stress-relationships. It was found that the Stern theory improved the agreement at stresses greater than 100 kPa; further, the smaller void ratio decrease at high applied stresses was well captured.

The role of attractive pressures has been also discussed in literature. Sridharan & Jayadeva (1982) calculated the attractive pressures for montmorillonite and kaolinite within a pressure range of about 10 kPa to 1000 kPa using the van der Waals-Hamaker equation (see equation 2.8) and showed that the attractive pressures have negligible influence on the compressibility behaviour of saturated clays and can be ignored. Anandarajah & Chen (1997) have found that particle geometry, orientation and spacing, and the fluid properties have a significant influence on the attractive van der Waal's force.

Anandarajah & Lu (1991) and Lu & Anandarajah (1992) developed a finite-element model with two flat clay particles of definite length. In a parametric study they investigated the influence of inclination, length and surface potential on the double layer repulsive force between the two particles and deduced empirical relationships for calculating the repulsive force between clay particles. Further, Anandarajah (2000) used the discrete element method (DEM) to simulate the consolidation behaviour of a kaolinite taking into account repulsive double layer forces, attractive van der Waal's forces and mechanical contact forces. They reported good agreement between the calculated and measured void ratio change, k_0-values and anisotropy.

Leroy & Revil (2004) have proposed an electrical triple-layer model (TLM) to describe the electrochemical properties of clay minerals. They have included the specific properties of the active crystallographic surface sites and a classical description of the Stern and diffuse layers in the model. It was used to calculate electrokinetic properties such as surface conductivity. Later, Gonçalvèz, Rousseau-Gueutin & Revil (2007) modified the TLM to account for the interaction of diffuse double layers in compacted clays containing monovalent ions.

In the present work, the equations of classical diffuse double layer theory and the semi-empirical approach of Tripathy et al. (2004) were used to calculate (1) swelling pressure-dry density relationships for the compacted saturated clays and (2) void ratio-applied vertical stress relationships (see chapter 8). Further, by fitting the difference between experimentally determined swelling pressures, and the calculated net interparticle pressures $(R-A)$, a relationship for additional short-range repulsive forces for the clays was found. These results are presented in chapter 9.

2.8. Effective stresses in clays

The volume change and shear strength behaviour of soils are controlled by the effective stress. Terzaghi (1936) introduced the concept of effective stress for saturated soils, where the effective stress is a combination of the externally applied stress and the internal pressure of the fluid phase. The influence of positive pore water pressure on the effective stress has been widely adopted as the design basis in geotechnical engineering practice associated with saturated soils. The effective stress approach provides a mean for modelling the soil, which is a multi-phase porous medium, as an equivalent single-phased continuum.

Most naturally occurring clayey soils are composed essentially of one or more of the clay minerals from kaolinite, illite, and montmorillonite groups (Grim 1968). Unsaturated clayey soils possessing such clay minerals exhibit swelling or compression when inundated with fluids. Similarly, saturated clays composed of these clay minerals usually undergo significant volume decrease during the drying process and due to an increase in the surcharge. Physicochemical forces at microscopic level are responsible for these phenomena observed at macroscopic scale.

Effective stress approaches to account for the electrochemical forces have been proposed for saturated clays in the past (Bolt 1956, Lambe 1958*a*, Lambe 1960, Sridharan & Rao 1973, Morgenstern & Balasubramonian 1980). With σ being the total stress, σ_c the contact stress, σ' the effective stress, u the bulk water pressure, $(R_{ddl} - A)$ the net physicochemical stress arising from the difference of the repulsive (R_{ddl}) and attractive (A) forces, the equations for the effective stress approaches can be given in terms of stress differences with respect to a reference state (Hueckel 1992).

1. Approach based on Lambe (1958b, 1960):
   It was suggested that the total stress is the sum of the contact stress, the bulk water pressure and the net physicochemical stress (eq. 2.14a). Given the definition for effective stress in eq. 2.14b, it follows that effective stress is equal to the sum of the contact stress and the net physicochemical stress (eq. 2.14c). Thus, a net repulsive stress $(R_{ddl} - A)$ increase would lead to an increase in effective stress.

$$\Delta\sigma = \Delta\sigma_c + \Delta u + \Delta(R_{ddl} - A) \tag{2.14a}$$

$$\Delta\sigma' = \Delta\sigma - \Delta u \tag{2.14b}$$

$$\Delta\sigma' = \Delta\sigma_c + \Delta(R_{ddl} - A) \tag{2.14c}$$

2. Approach based on Sridharan & Rao (1973); Morgenstern & Balasubramonian (1980):
   Contrary to Lambe's (1958b, 1960) approach, it was argued that net physicochemical (repulsive) stress ($R_{\mathrm{ddl}} - A$) reduces the effective stress, thus, reduces the resistance against shear failure. The corresponding effective stress definition is given in eq. 2.15.

$$\Delta\sigma' = \Delta\sigma_{\mathrm{c}} = \Delta\sigma - \Delta u - \Delta(R_{\mathrm{ddl}} - A) \tag{2.15}$$

3. Approach based on Bolt (1956); Lambe (1958, 1960):
   The following definition is based on the assumption that the contact stresses and the physicochemical (repulsive) stress ($R_{\mathrm{ddl}} - A$) are equal and correspond to the effective stress. In case of clay suspensions without mineral-to-mineral contact, the effective stress is equal to the net (repulsive) physicochemical stress ($R_{\mathrm{ddl}} - A$).

$$\Delta\sigma = \Delta\sigma' + \Delta u \tag{2.16a}$$

$$\Delta\sigma' = \Delta\sigma_{\mathrm{c}} = \Delta(R_{\mathrm{ddl}} - A) \tag{2.16b}$$

Hueckel (1992), based on a discussion of the three approaches, highlighted the differences between the various models, and concluded that approach 2 seem to be applicable for clay systems with flocculated (edge-to-face, EF) contacts and lower density, whereas approach 3 seems more relevant for denser, consolidated clays systems with dominating face-to-face (FF) particle arrangement. Approaches 2 and 3 were found to be qualitatively confirmed by tests at macroscale. However, since direct measurement of the actual micromechanical forces (skeletal contact forces, repulsive and attractive forces) under various possible loading conditions is difficult, the definition of effective stress in clays, saturated or unsaturated, is still an objective of research in soil mechanics.

Soils are likely to be in an unsaturated state, usually with water and air as the fluid phases. The influence of negative pore water pressure on the engineering properties of unsaturated soils has been explored (Fredlund & Rahardjo 1993, Lu & Likos 2004). Both two stress state variables and single stress variable approaches have been implemented in analyzing the engineering behaviour of unsaturated soils (Bishop 1954, Fredlund & Morgenstern 1977, Khalili, Geiser & Blight 2004, Nuth & Laloui 2008, Lu & Likos 2004, Lu & Likos 2006, Lu, Godt & Wu 2010), to name a few. Recently, Nikooee, Habibagahi, Hassanizadeh & Ghahramani (2013) have proposed an approach taking into account the

interfacial energy and the contribution of the interfacial area between water and air. In either of these approaches, determination of the soil-water characteristic curve (SWCC) has been shown to play a crucial role (Fredlund & Rahardjo 1993, Lu et al. 2010). Of the single stress state variable approaches, the suction stress approach (Lu & Likos 2004, Lu & Likos 2006, Lu et al. 2010) has been shown to better conjugate the effective stress in describing the shear strength behaviour of unsaturated soils for the entire range of degree of saturation (Lu et al. 2010, Oh, Lu, Kim, Lee & Lee 2012).

The suction stress forms a part of the effective stress in case of unsaturated soils. The suction stress is manifest in the tensile strength of soil that originates from the available interaction energy at the soil solid surface that can be conceptualized to exist in the forms of van der Waals attractive force, double-layer repulsive force, surface tension, and solid-liquid interface forces due to pore water pressure (Lu & Likos 2006). The suction stress of soils either can be measured in the laboratory from tensile strength tests or can be calculated based on the shear strength tests, or even can be calculated based on theoretical considerations. The suction stress characteristic (SSCC) curve of a soil (i.e., the relationship between suction stress and degree of saturation or suction or water content) can be established based on the SWCC of the soil (Lu et al. 2010).

The shape of the SSCC has been shown to depend upon the soil type (Lu et al. 2010). For example, suction stress decreases and further increases with an increase in suction or a decrease in the degree of saturation for sandy and silty soils, whereas a monotonic decrease in the suction stress with an increasing in suction occurs in case of clayey soils. The range of suction and degree of saturation within which the suction stress remains at considerable magnitude is of great interest (Lu et al. 2010). The suction stress influences the shear strength and provides stability to unsaturated soils. Similarly, the impact of variations of suction stress with changes in soil suction and their influence on the effective stress is of utmost significance when analyzing the volume change behaviour of problematic soils (i.e., expansive and collapsible soils).

The physico-chemical forces are known to significantly influence the volume change behaviour of clays (Bolt 1956, Sridharan & Rao 1973, van Olphen 1977, Sridharan & Jayadeva 1982, Hueckel 1992, Mitchell 1993, Lu & Likos 2006, Tripathy, Kessler & Schanz 2006, Tripathy & Schanz 2007, Schanz & Tripathy 2009). The magnitude of interparticle repulsive and attractive forces depends upon the mineralogy, the physical and chemical properties of clays, and the pore fluid characteristics. Distinction of the influence of clay mineral type on the shape of the SSCC, magnitudes of minimum and maximum suction stress,

and further, their influence on the effective stress of clays for a large range of suction has not been fully explored yet.

In this context, based on the experimental data for water retention and one-dimensional volume change behaviour of clays with significantly different clay minerals, the influence of suction stress on the effective stress of clays is brought out in this part the study. The results are presented in Chapter 10.

3. Materials and methods

3.1. Materials used

3.1.1. General

In this section, the material properties such as particle density, grain size distribution, Atterberg limits, activity, and the mineralogical and physico-chemical characteristics are presented. The properties of the clays were determined according to DIN and ASTM laboratory standards. The clays used in this study are Calcigel bentonite, NX illite, and Spergau kaolin, each of them with different mineralogical backgrounds comprised predominantly of one of the main clay mineral groups (montmorillonite, illite, and kaolinite). These clays were chosen because they are expected to exhibit distinct behaviour.

3.1.2. Particle density and grain size distribution

The particle densities of the three clays were determined by pycnometer method according to DIN18124 (1997). The values obtained are given in Table 3.1. The grain size distributions of the clays were determined by sedimentation technique (S) (DIN18123 1996) and by laser diffraction method (LD). The results are presented in Fig. 3.1. The plots reveal that for each clay, the grain sizes obtained from laser diffraction method are slightly greater than that obtained by the sedimentation technique. This is probably due to the

Table 3.1.: Measured particle densities of the clays studied

	Calcigel bentonite	NX illite	Spergau kaolin
Particle density, ρ_S (Mg/m^3)	2.803	2.714	2.617

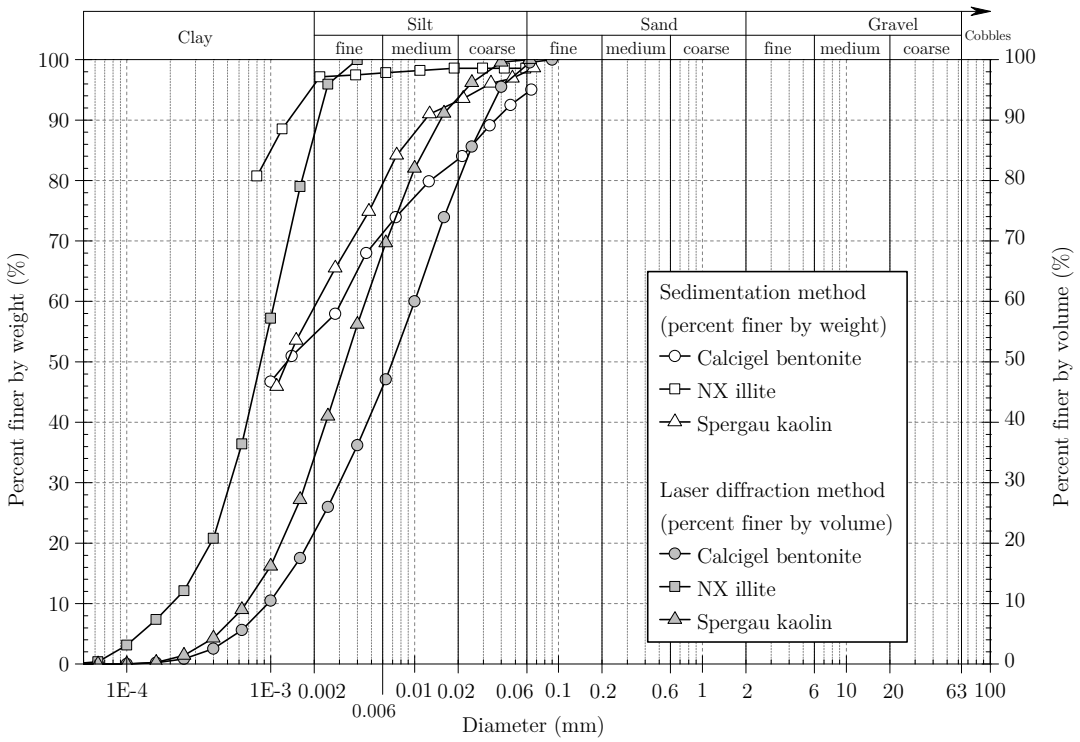

Figure 3.1.: Grain size distributions of the clays studied.

different dispersing agents used during sample preparation. Whereas Trinonylphenylphosphite (TNPP) was used in the laser diffraction method, Tetrasodium pyrophosphate (TSPP) was added to the water to avoid particle flocculation during sedimentation.

3.1.3. Atterberg limits and activity

The liquid limit, the plastic limit and the shrinkage limit of the three clays are presented in Table 3.2. The liquid limit and plastic limit values were determined according to the German standard methods DIN18122T1 (1997) and DIN18122T2 (2000). The shrinkage limit was determined according to ASTMD4943-02 (2002). The liquid limits of the clays were determined by Casagrande method. A comparison with values given in literature (Mitchell & Soga 2005) shows that in general, the Atterberg limits in this study agree very well with the range of values given for the equivalent mineral type in literature (see Table 3.3). For Calcigel bentonite, the Atterberg limits were found to be within the lower range given for montmorillonites, which is consistent with the high amount of divalent cations contained in the Calcigel bentonite (see section 3.1.8). The shrinkage limit of NX illite was found to be somewhat higher than the range given in literature (25.7% as compared to 15-17%). This indicates that NX illite is less susceptible to shrinkage than illite clays considered by Mitchell & Soga (2005).

The activity is defined as the ratio of plasticity index to the clay size fraction (percentage finer by weight of particles finer than 0.002 mm Activity $= I_P/\% < 0.002$ mm (Skempton 1953). The greater the activity, the higher is the influence of the clay fraction on soil properties and the more important are changes in type of exchangeable cations and pore fluid composition on soil properties. The activity values of Calcigel bentonite and NX illite were found to be in the range given in literature (Table 3.3), whereas the activity of Spergau kaolin was slightly smaller than the value given by Mitchell & Soga (2005).

Table 3.2.: Atterberg limits and activities of the clays studied

Clay	Calcigel bentonite	NX illite	Spergau kaolin
Liquid limit, w_L (%)	178	77.6	53.4
Plastic limit, w_P (%)	56.1	30.1	32.3
Plasticity index, I_P (%)	121.9	47.5	21.1
Shrinkage limit, w_S (%)	11.8	25.7	31.3
Activity (-)	2.2	0.5	0.4

Table 3.3.: Range of Atterberg limits and activities for the relevant mineral types, from various authors in Mitchell (2005)

Mineral	Montmorillonite	Illite	Kaolinite
Liquid limit, w_L (%)	100-900	60-120	30-110
Plastic limit, w_P (%)	50-100	35-60	25-40
Shrinkage limit, w_S (%)	8.5-15	15-17	25-29
Activity (-)	1-7	0.5-1	0.5

3.1.4. Compaction curves

The standard proctor compaction curves for the three clays were determined according to ASTMD698 (2000). The specimens were compacted dynamically with a compaction energy of 600 kNm/m^3. The proctor curves for the clays are presented separately in Figures 3.2a, 3.2b and 3.2c. The test results are compared in Figure 3.2d. The optimum water contents and maximum dry densities of the clays are presented in Table 3.4. The compaction results showed that higher the liquid limit, greater is the optimum water content and smaller is the dry density.

Table 3.4.: Optimum water content and maximum dry densities of the clays studied

Clay	Calcigel bentonite	NX illite	Spergau kaolin
Optimum water content, w (%)	40.0	35.9	22.8
Maximum dry density, $\rho_{d,\,max}$ (Mg/m^3)	1.19	1.29	1.50

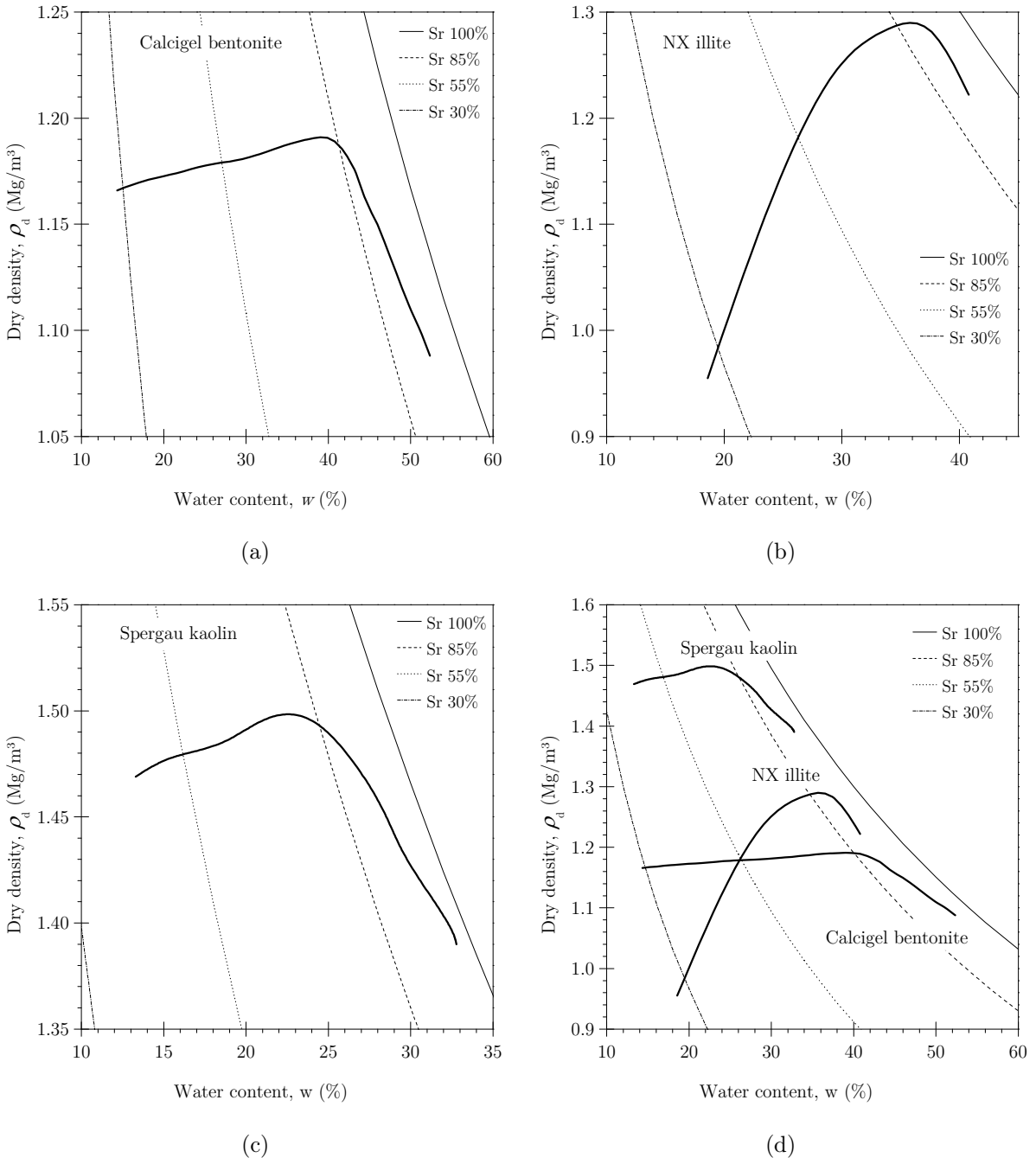

Figure 3.2.: Proctor curves of the clays studied: (a) Calcigel bentonite, (b) NX illite, (c) Spergau kaolin, and (d) comparative plot of the clays studied.

3.1.5. Mineralogy and chemical composition

X-ray diffraction (XRD) and infrared spectroscopy (IR) were used to study the mineralogy of the clays. The drawback of both methods are detection limits for specific minerals. For instance, amorphous constituents can not be identified by XRD, and the detection of silicates of minor amounts within a mineral mixture is often problematic with IR. To circumvent the detection limits, both methods were used herein for the semi-quantitative determination of the mineralogy of the clays.

The X-ray diffractometer charts of the clays are presented in Figure 3.3. The plots obtained from infrared spectroscopy are presented in Figure 3.4. Table 3.5 presents the minerals which were identified for each of the clays in a semi-quantitative manner. The clays studied were not monomineralic; however, predominantly contain minerals of specific types, such as montmorillonite, illite and kaolinite.

The chemical composition of the main elements was determined by means of x-ray fluorescence (XRF). The test results are shown in Table 3.6.

Considering the type of minerals contained in the clays, their respective structural formula, the average molar weight of one half unit cell (half unit cell = one formula unit), and the chemical composition, the amount of minerals contained in each of the clays can be quantified (Kaufhold et al. 2002). The result of the mineral quantification is presented in Table 3.7.

Table 3.5.: Mineralogic composition of the clays studied as determined by XRD and IR

Soil	Mnt	Qtz	Ms/Ill	Ill	Kln	Cb	Cal	Dol
X-ray diffraction (XRD)								
CgB	+	+-		-	-			-
NXI				+	+		-	
SpK		+-	+-		+			
Infrared spectroscopy (IR)								
CgB	x	x			$< 1\%$	$\approx 2\%$		
NXI				†	x		x	
SpK		x			x			

† illite is not detectable in IR in case of strong presence of kaolinite

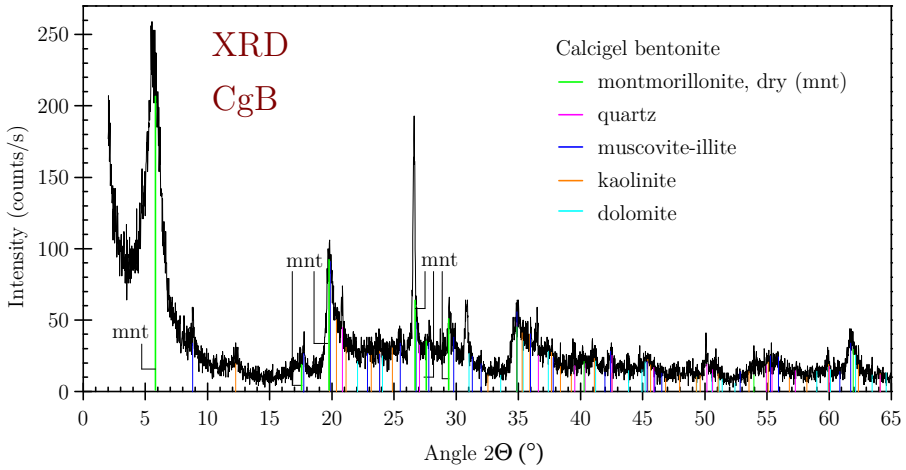

(a)

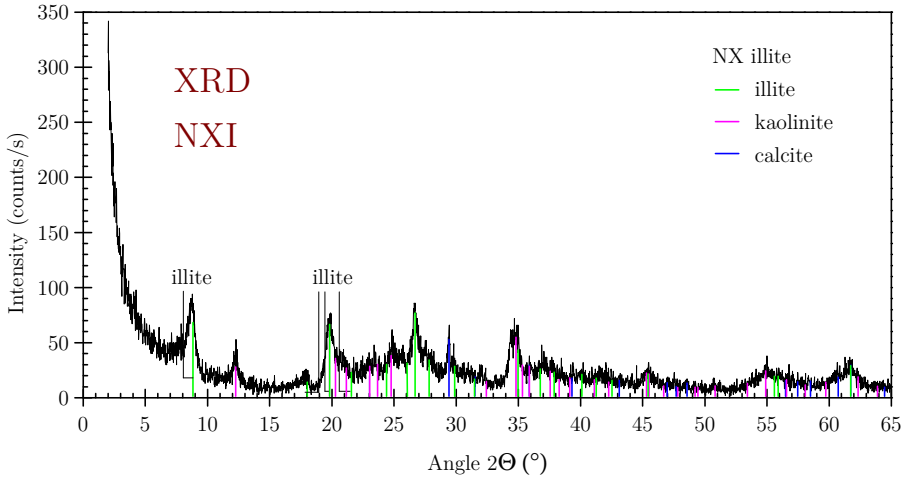

(b)

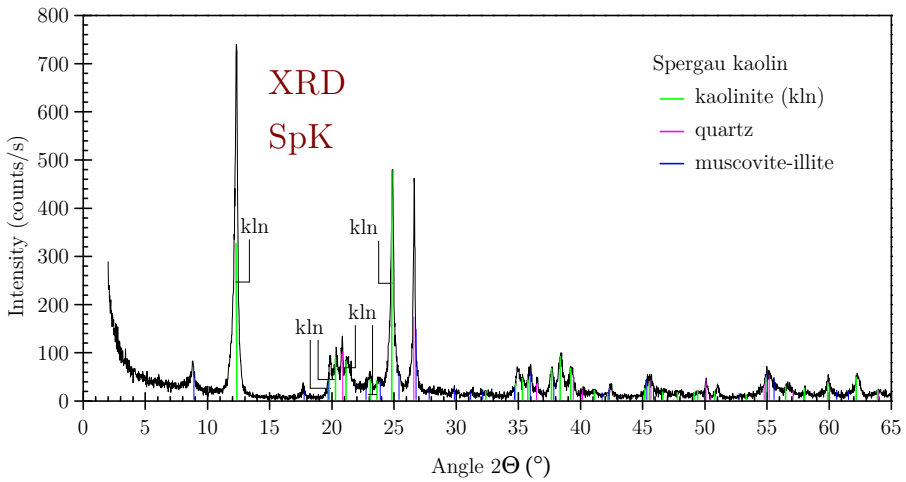

(c)

Figure 3.3.: X-ray diffraction (XRD) charts of the clays studied: (a) Calcigel bentonite, (b) NX illite, (c) Spergau kaolin.

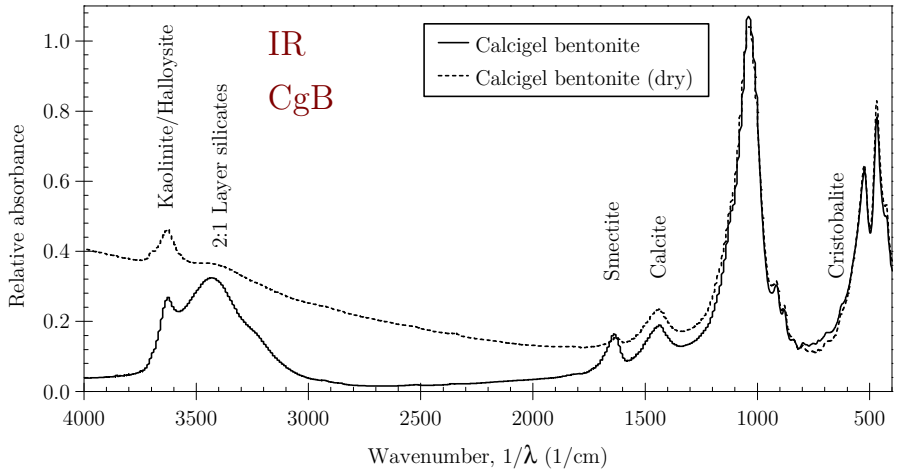

(a)

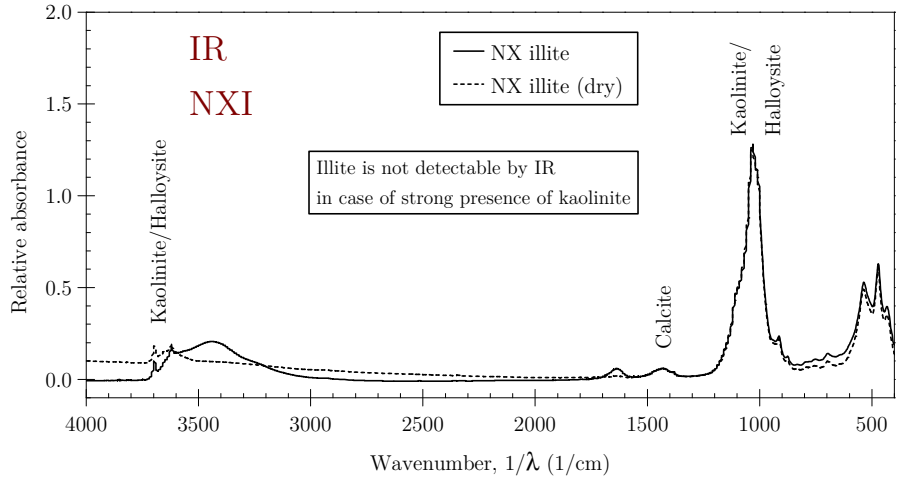

(b)

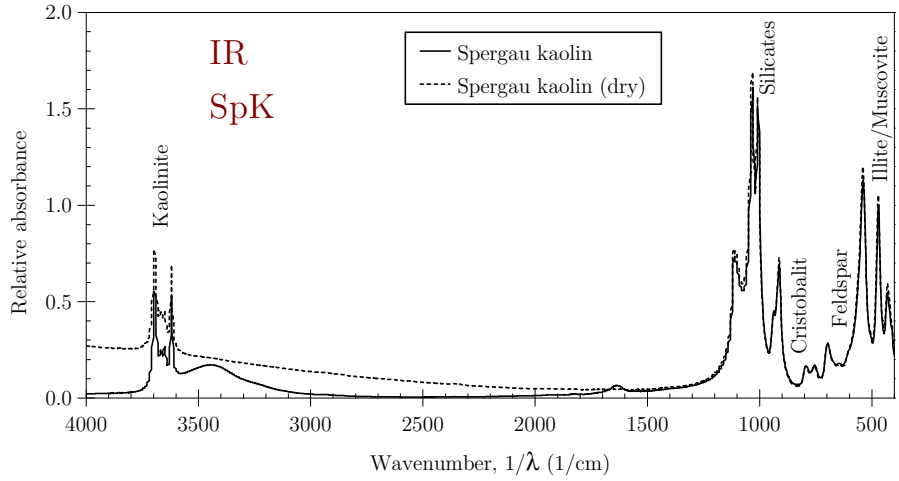

(c)

Figure 3.4.: Infrared (IR) spectra of the clays studied: (a) Calcigel bentonite, (b) NX illite, (c) Spergau kaolin.

Table 3.6.: Chemical composition of main elements of the clays studied

	Content of chemical main element, in %		
Element	Calcigel bentonite	NX illite	Spergau kaolin
SiO_2	50.2	47.30	51.56
Al_2O_3	17.34	21.30	32.66
Fe_2O_3	4.96	7.06	0.86
CaO	4.02	2.31	0.19
MgO	4.07	3.05	0.35
Na_2O	0.26	0.17	0.05
K_2O	1.44	5.73	1.37
SO_3	0.14	< 0.01	0.03
P_2O_5	0.08	0.37	0.12
TiO_2	0.37	0.82	0.58
MnO	0.04	0.08	0.01
LOI †	16.98	11.45	11.96
Sum	99.75	99.64	99.71

† Loss on ignition

Table 3.7.: Quantitative mineralogic composition of the clays studied

Clay	Mnt	Qtz	Ms/Ill	Ill	Kln	Cal	Dol	Sum
Calcigel bentonite	78	4		8	2	3.5	3	98.5
NX illite				77	10	12		99
Spergau kaolin		8		16	76			100

3.1.6. Thermal analysis

Thermal analysis is a term used for a group of analyses that determine physical parameters (e.g., energy, weight, dimension) as a dynamic function of temperature. The measured parameter changes with temperature. The observed thermal reactions upon heating serve as a diagnostic property for the qualitative and quantitative identification of substances. In this study, differential scanning calorimetry (DSC) and thermogravimetry (TG) were used.

DSC measures the amount of energy required to establish zero temperature difference between the sample and a reference material while both are heated side by side at a controlled rate. When a thermal reaction occurs in the sample, thermal energy is subtracted from or added to the sample or reference containers in order to maintain the sample at the same temperature as the reference material. The recording of this balancing energy yields calorimetric measurements of the transition energy.

Thermogravimetry is a technique whereby the sample is continuously weighed as it is being heated at a controlled rate. The weight changes are recorded as a function of temperature and yields information on the thermal stability and composition of the sample.

The results of the DSC measurements are presented in Fig. 3.5. Spergau kaolin (Fig. 3.5c) shows a minor endothermic peak at about 100 °C, followed by another endothermic peak at about 580 °C, and an exothermic peak at about 1000 °C. The latter two peaks represent the typical behaviour of kaolinite. The endothermic peak at 580 °C is attributed to dehydroxylation, whereas the exothermic peak is attributed to formation of γ-alumina.

The DSC curve of montmorillonite is characterised by a low-temperature endothermic peak between 100 to 200 °C (loss of adsorbed water), an endothermic peak between 600 and 700 °C (dehydroxylation), followed by a weak exothermic peak between 900 and 1000 °C (recrystallisation). In the the DSC plot of Calcigel bentonite (Fig. 3.5a), the characteristic peaks of montmorillonite can be recognised. The slight divergence from the typical montmorillonite behaviour expressed by multiple endothermic peaks between 520 and 840 °C is attributed to the amount of minerals other than montmorillonite contained in Calcigel bentonite.

The typical behaviour of illite is characterized by endothermic peaks between 100 and 200 °C (loss of adsorbed water), at about 600 °C, between 900 to 920 °C (dehydroxylation), and by an exothermic peak between 920 to 950 °C due to recrystallisation. Overall, the typical peaks can be recognised in Fig. 3.5b. The endothermic peak between 900 to 920 °C was not observed, indicating that dehydroxylation was already finished.

The loss of adsorbed water and dehydroxylation represented as a weight loss can also be detected by thermogravimetry (Figure 3.6). In case of NX illite and Calcigel bentonite, the weight loss observed due to removal of adsorbed water and dehydroxylation was similar. For Spergau kaolin, the weight loss due to dehydroxylation was significant whereas that resulting from loss of adsorbed water was minor.

The thermal analysis confirmed the mineralogical composition of the clays. Calcigel bentonite, NX illite, and Spergau kaolin are comprised mainly of montmorillonite, illite, and kaolinite, respectively.

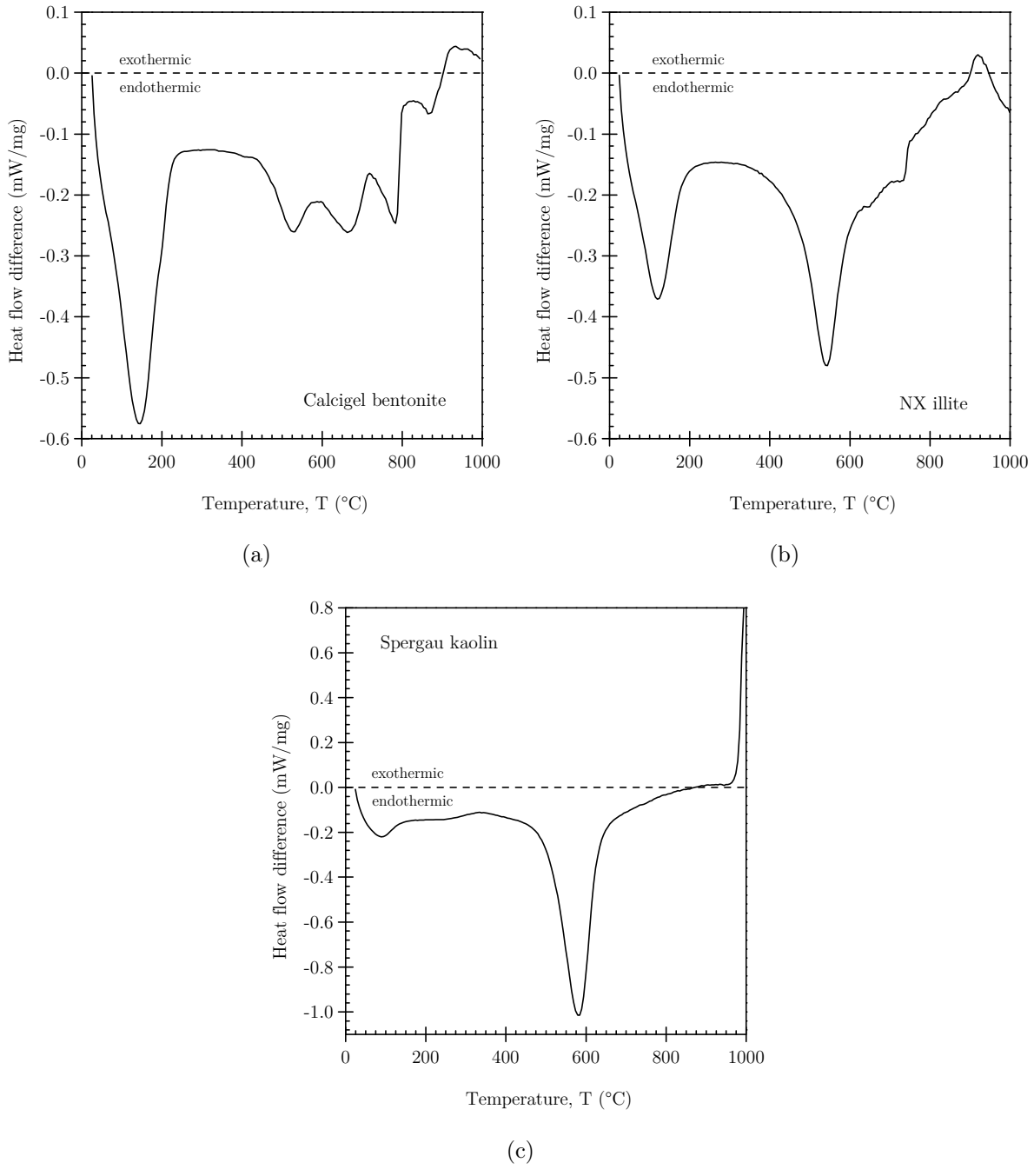

Figure 3.5.: Differential Scanning Calorimetry (DSC) of the clays studied: (a) Calcigel bentonite, (b) NX illite, (c) Spergau kaolin.

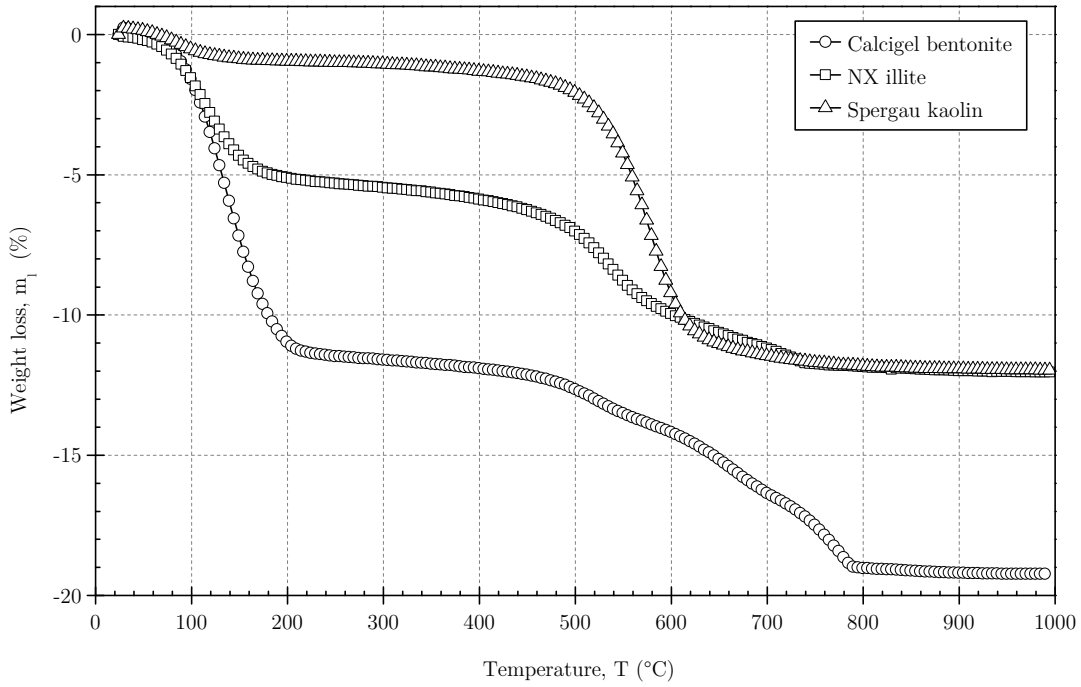

Figure 3.6.: Thermogravimetric curves of the clays studied.

3.1.7. Specific surface area

The specific surface area, A_S, is defined as the surface area per unit mass of soil and is usually expressed in m^2/g. Nonexpanding layer silicates such as kaolinites and some micas usually possess only external surfaces, whereas expanding layer silicates, such as montmorillonites and other smectites have extensive internal as well as external surface. The specific surface areas of the three clays were determined by two different methods, such as Brunauer-Emmett-Teller method (BET) and ethylene glycol monoethyl ether method (EGME). The test results are presented in Table 3.8.

The BET method is based on the principle of gas adsorption theory. The quantity of gas adsorbed on solid surfaces provides a measure of the surface area. Brunauer, Emmett & Teller (1938) derived an equation from multimolecular adsorption theory for calculating the number of adsorbate molecules in a monolayer. The BET tests were carried out using nitrogen. It is known that nitrogen, due to its molecule size, does not penetrate the interlayer surfaces of clays (Santamarina, Klein, Wang & Prencke 2002). The surface areas obtained by BET method with nitrogen therefore do not represent the total specific surface area but the external surface area.

The EGME method is based on the principle of retention of polar liquids. Based on the method of Dyal & Hendricks (1950), Carter, Heilman & Gonzalez (1965) introduced the use of ethylene glycol monoethyl ether (EGME) as the polar molecule for determining the total specific surface area of layer silicate minerals and soils. Later, Cerato & Lutenegger (2002) described the method and presented a detailed test procedure. The EGME method for estimating surface area of soils and clays has been widely accepted. Nevertheless, for calculating the specific surface area it involves the assumption that EGME covered all interlayer and external surfaces, which is difficult to prove (Carter et al. 1965).

Table 3.8.: Specific surface area values of the clays studied

Clay	Calcigel bentonite	NX illite	Spergau kaolin
A_S (m^2/g) by BET	66	96	14
A_S (m^2/g) by EGME	525	154	28

3.1.8. Cation exchange capacity

Clay particles of clay minerals possess a net negative charge. To preserve electrical neutrality, cations are attracted and held between the layers and on the outer surfaces and edges of the particles. Because they may be replaced by cations of another type, they are called exchangeable cations. The quantity of exchangeable cations is termed the cation exchange capacity (CEC). It is usually expressed as milliequivalent per 100 grams of dry clay (meq/100g). The cation exchange capacity including the type and amount of cations was determined utilizing the Cu-Triethylenetetramine method (Meier & Kahr 1999) with a weighted sample of 0.08 and 0.12 g. Additionally, the CEC values were determined by the Silver-Thiourea method with calcite saturation (Pleysier & Juo 1980, Dohrmann 1997). The values for cation exchange capacity as well as type and amount of cations available for the three clays obtained from the two methods are presented in Tables 3.9 and 3.10. The CEC determined by the two methods are in the same range. However, the values determined by Silver-Thiourea method were greater than those determined by Cu-Triethylenetetramine method for the three clays.

Table 3.9.: Exchangeable cations and CEC of the clays studied obtained from Cu-Triethylenetetramine method

	CEC and cations in meq/100g		
	Calcigel bentonite	NX illite	Spergau kaolin
Na^+	3	0	0
K^+	2	3	0
Mg^{2+}	21	5	1
Ca^{2+}	50	30	5
S value	77	38	6
T value	64	21	7
S-T	13	17	-1
T value (VIS)	63	19	-
CEC [a]	64	21	7

[a] Cu-Triethylenetetramine method (Meier & Kahr 1999)

Table 3.10.: Exchangeable cations and CEC of the clays studied obtained from Silver-Thiourea method

	CEC and cations in meq/100g		
	Calcigel bentonite	NX illite	Spergau kaolin
Na^+	2	0	0
K^+	0	3	0
Mg^{2+}	17	5	0
Ca^{2+}	29	16	2
S value	49	24	2
T value (Ag)	74	29	10
S-T	-25	-5	-8
CEC [b]	74	29	10

[b] Silver-Thiourea method (Pleysier & Juo 1980, Dohrmann 1997)

3.1.9. Summary of the properties of the clays studied

According to the Unified Soil Classification System, all three clays can be classified as inorganic clays of high plasticity (CH). In Table 3.11, the main properties of the three clays are summarized.

Table 3.11.: Summary of the main material properties of the clays studied

Clay	Calcigel bentonite	NX illite	Spergau kaolin
Classification (USCS)	CH	CH	CH
Specific gravity of soil solids, G_S	2.80	2.71	2.62
Liquid limit, w_L (%)	178	77.8	53.4
$1.1w_L$ (%)	195.8	85.6	58.7
Plastic limit, w_P (%)	56.1	32.3	30.1
Shrinkage limit, w_S (%)	11.8	25.7	25.8
Plasticity index, I_P (%)	121.9	45.5	23.3
Cation exchange capacity, CEC (meq/100g)	74	26	8
Specific surface area, A_S (m^2/g) †	525	154	28
Weighted average valency, ν (-)	1.93	2.00	1.92

† EGME method (Carter et al. 1965)

3.2. Experimental methods

In this section, the experimental devices and procedures used are presented. The section includes the detailed description of the new high stress oedometer device developed for the present study. The experimental procedures adopted for the various types of test in the new device, such as swelling pressure tests, one-dimensional compression tests, and swelling pressure tests with subsequent compression-decompression paths are described. Further, the techniques and procedures used for suction control and suction measurement are presented.

3.2.1. New high stress oedometer device

In order to simulate field conditions, the device should fulfill the following main requirements: (*i*) measurement of swelling pressures at constant volume, and (*ii*) subsequent loading of the specimen up to high stresses (20 to 30 MPa) after equilibrium of swelling pressure is reached. A review of literature on the oedometers designed for applying large pressures (>3 MPa) revealed that the existing devices are suitable either for measuring swelling pressures of clays using a force transducer for the strain-controlled condition or for applying large vertical pressures up to about 30 MPa to determine the consolidation behaviour (Romero 1999, Marcial et al. 2002). However, measurements of the swelling pressure and subsequent loading of clay specimens to very large pressures may not be possible using the available designs. Therefore, a new oedometer device was designed and fabricated to study the swelling pressure as well as the compressibility behaviour of compacted saturated bentonite specimens.

A schematic of the new high pressure oedometer device with detailed itemised components and a photograph of the test set up are shown in Fig. 3.7. A thick bottom stainless steel base (no. 3) houses a porous stainless steel plate (no. 7) and the bottom water chamber (no. 19). The central part of the device (no. 2) holds a thick-walled specimen ring of height 20 mm and 50 mm in diameter (no. 4) that accommodates a compacted clay specimen (no. 5), and a pressure pad with a porous stainless steel plate (no. 6). The top part carries the loading piston (no. 10) attached with a force transducer (no. 8). The force transducer used in this study had a maximum loading capacity of 50 kN with a precision of 0.001 kN. A strain gauge (no. 9) with a precision of 0.001 mm and a total run of 25 mm was connected directly to the loading piston to record the vertical deformation. The bottom and central part are connected with the help of heavy screws (no. 17), whereas the top part is directly screwed onto the central part. The force transducer together with the loading piston becomes fixed between the pressure pad (no. 6) and the upper restraint (no. 12).

In case of compacted specimens, the top part of the device was rotated to apply a seating pressure of 10 kPa. The force transducer enabled measuring the swelling pressures and monitored the applied vertical pressures. The device was designed in such a way that upward vertical movement above the initial height of the specimen can be restricted, whereas the loading piston can move downwards. Hence, soil specimens can be loaded after the equilibrium swelling pressures are reached to study the compressibility behaviour. During the unloading process, height changes are restricted above the initial height of the specimen.

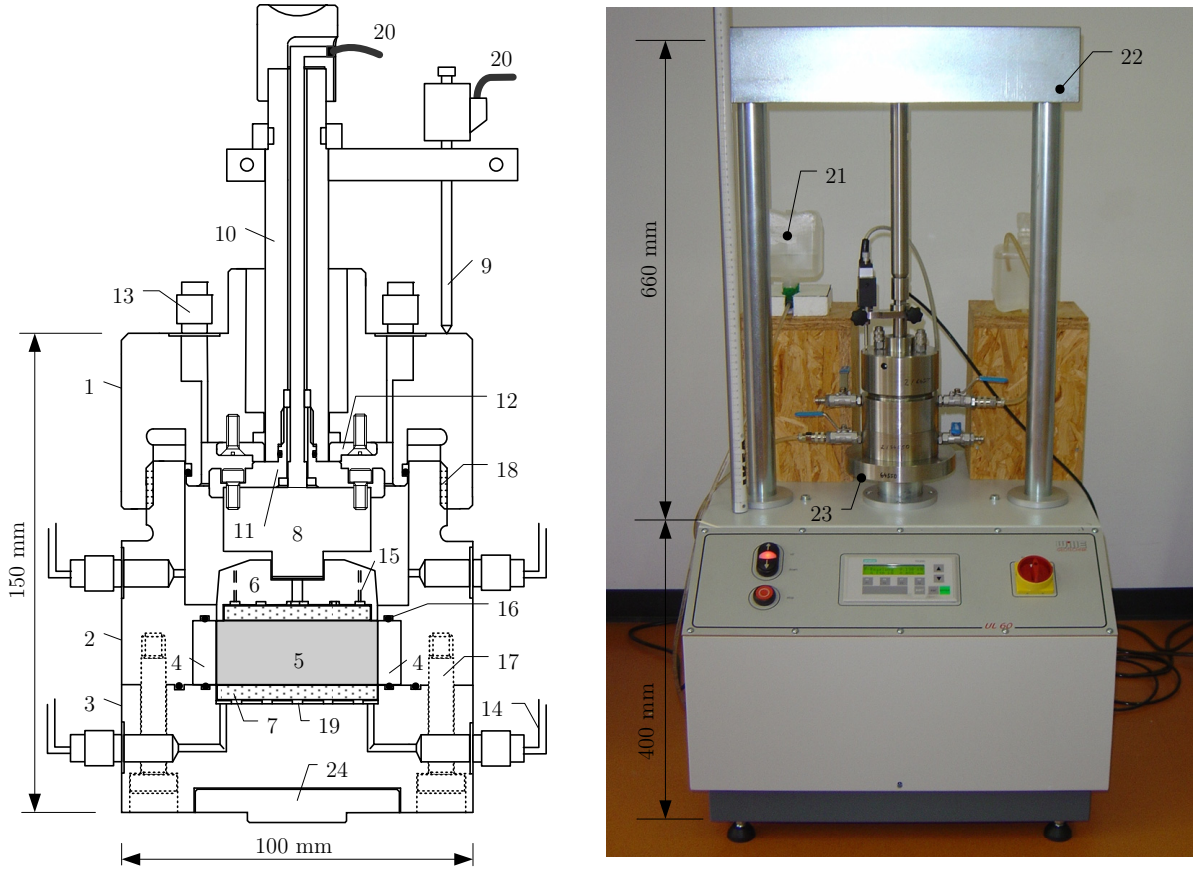

1 Top part	6 Pressure pad with top porous plate	10 Loading piston	15 Vent	20 Electrical cables
2 Central part		11 Adapter for 8	16 O-ring	21 Fluid reservoir
3 Bottom part	7 Bottom porous plate	12 Upper restraint	17 Heavy screw	22 Loading frame
4 Specimen ring	8 Force transducer	13 Provision for vapour supply	18 Thread	23 Base plate
5 Soil specimen	9 Strain gauge	14 Water or vapour supply	19 Water chamber	24 Adapter for 23

Figure 3.7.: New high pressure oedometer device with schematic of the cell (left) and photograph of the test set up (right); Baille et al. (2010).

The wall of the oedometer hosts tubing at top and bottom (no. 14) that were connected to fluid reservoirs (no. 21) for circulating fluid and to keep the specimen saturated during swelling, loading, and unloading processes. During the tests, distilled water was supplied to the top and bottom porous plates from the water reservoirs with a constant water head of 2 kPa. Filter papers were used at the top and bottom of the bentonite specimens. The specimen ring was lubricated prior to the specimen preparation to minimise the side friction.

Prior to testing for bentonite specimens, the pressure-deformation characteristic of the new device was studied using a steel dummy following the procedure suggested by ASTMD2435-96 (1996). Several independent loading-unloading and cyclic loading-unloading tests were carried out. The pressure-deformation plots for the two new devices used in this study (device no. 1 and 2) were found to be very nearly similar for various independent and cyclic loading-unloading cycles (Fig. 3.8). For clarity, test results for only some selected loading-unloading cycles for the devices used are presented in Fig. 3.8. The measured de-

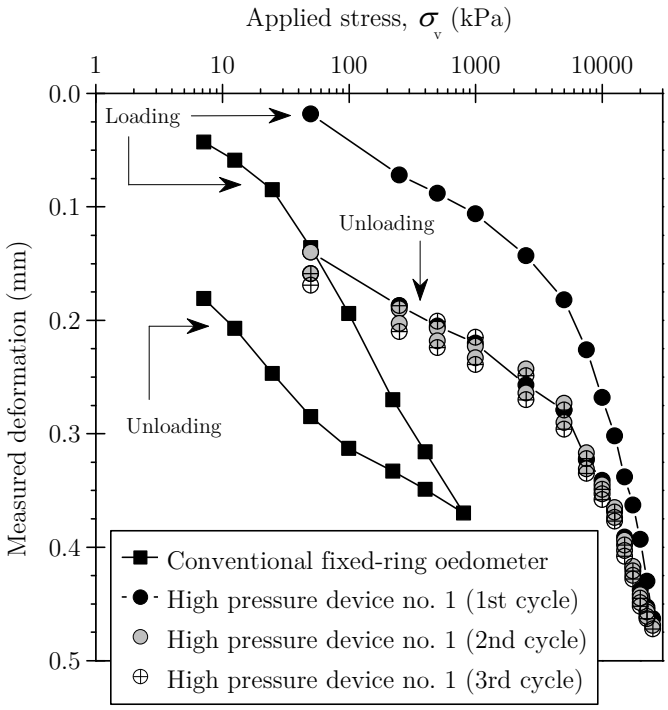

Figure 3.8.: Compressibility of the high pressure oedometer.

formations during any loading-unloading cycles included the deformation of the loading piston, the transducer, the oedometer cell, and the loading frame, and thus represent the total deformation of the system. The calibration results indicated that during the first loading cycle the system was plastically hardened. The deformation of the system

during the subsequent cyclic loading-unloading cycles was found to be reversible. Additionally, the pressure-deformation characteristic of the system for any independent first loading-unloading cycle was found to be repeatable. In Figure 3.8, the stress-deformation behaviour of a conventional fixed-ring oedometer subjected to one cycle of loading and unloading is shown for comparison. It shows that in general, the deformation of the conventional oedometer was greater than that of the new oedometer devices within a vertical pressure of 1000 kPa.

It was assumed that the system deformation induced during the swelling pressure development and due to an increase in the vertical pressure during the consolidation tests are similar. Therefore, the pressure-deformation data for the first loading cycle was referred to for calculating the corrected specimen densities at the end of the swelling pressure tests, and for calculating the corrected heights and void ratios of the specimens during each loading step in the consolidation tests. Similarly, the pressure-deformation path obtained during the first unloading cycle was used for calculating the corrected heights and void ratios of the specimens during the decompression tests.

3.2.2. UPC isochoric cell

According to the experimental programme, a number of constant volume swelling pressure tests (without subsequent one-dimensional compression) were carried out. For this purpose, the UPC isochoric cell, which was developed at the Technical University of Barcelona (UPC) in Spain, was used additionally (Romero 1999). The UPC isochoric cell allows performing constant volume tests on compacted specimens controlling total suction by vapour transfer. In this study, one-step swelling pressure tests were carried out, where the compacted specimens were hydrated using de-ionised water.

The cell mainly consists of a bottom and top part, which are screwed together. The bottom part houses a coarse metal porous disc. The top part contains the specimen ring, the upper porous disc, and the load cell. The bottom and top porous discs are connected to water/vapour supply. In this study, the specimens were hydrated from the bottom using de-ionised water. The load cell has a capacity of maximum 22 kN corresponding to about 11 MPa for the specimen diameter of 50 mm. It is screwed into the top part of the cell to ascertain constant volume conditions throughout the test and is connected to a readout unit.

3.2.3. Osmotic method

In order to cover a wide range of suction it was necessary to adopt two different available methods for inducing suction in the clays. A review of the literature suggested that the osmotic technique has been mainly used for applying suctions up to 1.5 MPa, but studies on the applications of the osmotic technique for higher suctions are limited (Delage & Cui 2008). Marcial et al. (2002) used the osmotic method for determining the retention behaviour of initially saturated bentonites up to 9 MPa. Delage et al. (1998) stated that osmotic method can be used for applying high suctions up to 10 MPa.

The method uses the principle of difference in osmotic pressure between two different solutions separated by a semi-permeable membrane (Zur 1966). The clay specimens are kept in contact with polyethylene glycol-solution (PEG-solution) of a known concentration by a semi-permeable membrane. The membrane is permeable to water and ions but not to the large PEG-molecules. On either side of the membrane, the ionic concentration of both soil-water and the PEG-solution tend to equilibrate with elapsed time. Since the PEG-molecules may not pass through the membrane, an osmotic potential is established within the system. Water molecules hence are forced to move through the membrane outside to the PEG solution. However, the ions in the soil-water may as well pass freely through the membrane, in the event of equalisation, osmotic suction due to the PEG-molecules corresponds to matric suction in the soil (Zur 1966). The following equations demonstrate this fact. In eqs. 3.1 to 3.4, the superscript '1' denotes the PEG-solution, the superscript '2' denotes the soil volume, both are separated by the semi-permeable membrane, and together they form a closed system.

The total suction at each side of the membrane can be written as the sum of the osmotic and matric component:

$$\psi^1_{\mathrm{tot}} = \psi^1_{\mathrm{o}} + \psi^1_{\mathrm{m}} \quad \text{and} \quad \psi^2_{\mathrm{tot}} = \psi^2_{\mathrm{o}} + \psi^2_{\mathrm{m}} \tag{3.1}$$

The total suction is equal at both sides, therefore:

$$\psi^1_{\mathrm{o}} + \psi^1_{\mathrm{m}} = \psi^2_{\mathrm{o}} + \psi^2_{\mathrm{m}} \tag{3.2}$$

Matric suction in the PEG-solution is zero ($\psi^1_{\mathrm{m}} = 0$), the osmotic suction in the PEG-solution (ψ^1_{o}) is composed of the component from the PEG-molecules (π^1_{PEG}) and that from the salts (π^1_{salt}). The osmotic suction of the soil is only due to the salts, therefore, eq. 3.2 can be rewritten as:

$$\pi^1_{\mathrm{PEG}} + \pi^1_{\mathrm{salt}} = \pi^2_{\mathrm{salt}} + \psi^2_{\mathrm{m}} \tag{3.3}$$

Since the salts may pass freely through the membrane, their concentration, and thus, osmotic suction component is equal. Therefore, eq. 3.4 remains :

$$\pi^1_{\mathrm{PEG}} = \psi^2_{\mathrm{m}} \tag{3.4}$$

The membrane and the size of the PEG molecules are defined by their molecular weight cut-off (MWCO) and molecular weight (MW) values. The MW value of the chosen PEG is generally preferred to be greater than the MWCO of the membrane to prevent the PEG-molecules to pass through the semi-permeable membrane. In the current study, PEG 20 000 was used for suction range of 30 to 3000 kPa, whereas PEG 6000 was used for applying a suction of 9000 kPa. The clay specimens were subjected suctions of 30, 100, 300, 1000, 3000, 9000 kPa using the osmotic method. The equivalent concentrations of the PEG-solution for the given suctions were determined using the calibration curves given by Williams & Shaykewich (1969) and Delage et al. (1998). The latter have performed a calibration of PEG-solutions using PEG of MW 1500 to MW 6000 for an extended suction range up to 12.6 MPa.

Figure 3.9 shows a schematic of the experimental set up for the osmotic tests. In all, six containers were used, each of them was filled with PEG-solution of a certain concentration corresponding to the suction values of 30, 100, 300, 1000, 3000, 9000 kPa. The containers were placed in a temperature controlled water bath. Throughout the tests, a

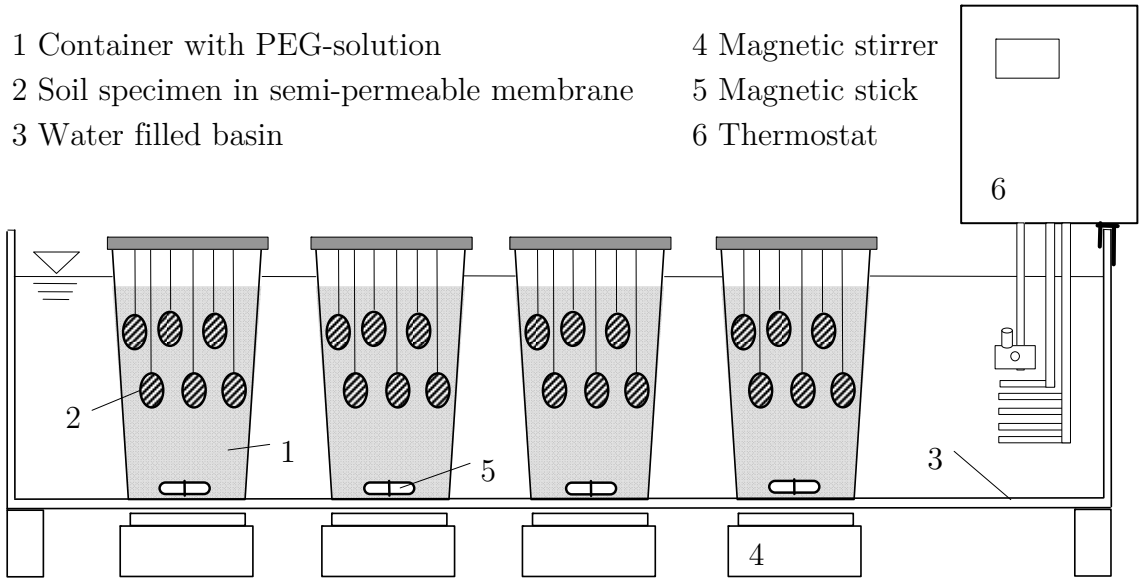

Figure 3.9.: Schematic of the experimental setup for osmotic method

temperature of 20 ± 0.1 °C was maintained in the water bath with the help of a thermostat. Below the water bath, magnetic stirrers were placed at suitable positions so as to

ensure a homogenous PEG-solution in the specimen containers. The clay specimens were prepared by filling tube-shaped membranes with 15 to 30 g of the clay slurry, closing the membranes, and then fixing them to the top cap of the container in such a way that the clay filled membranes were submerged in the PEG-solution. Clay specimens were allowed to equilibrate with the PEG solutions for several days. Duplicate specimens of the clays were tested at all suctions considered in this study. At the end of the tests, the specimens still in the semi-permeable membranes were taken out of the PEG-solution and the membrane was carefully removed. The volume of the clay specimens in the osmotic method was not measured, whereas the final water contents at each suctions were determined by oven drying the clay specimens at 105 °C.

The times required for equilibration at the least and the highest suctions (i.e., 30 kPa and 9 MPa were determined separately in advance for each of the clay (Figure 3.11a). The equilibration time was found to be about 25 h and 60 h for specimens of Spergau kaolin and NX Illite, respectively, at both suction values. For Calcigel bentonite specimens, the equilibration time was found to be about 150 h at suction of 30 kPa, whereas only about 60 h were required at suction of 9 MPa.

3.2.4. Vapour equilibrium technique

Vapour equilibrium technique is commonly adopted to induce higher range of suction in soils (Lloret et al. 2003). The method can be applied in the range of suction of 2 to 300 MPa. Suction is imposed by controlled relative humidity using saturated salt solutions in a closed container (commonly, a desiccator). The soil suction in this case represents the total suction because of the fact that a change in the water content affects the capillarity as well as the ionic concentration of pore fluid. Since the water transfer from soils occurs in the vapour phase, the compositions of soils remain unchanged during a test (Schanz & Tripathy 2005). Agus (2005), based on an analysis of errors induced by temperature variations, stated that the fluctuation of temperature of 0.5 °C at 850 kPa has an error of 30%, whereas at a suction of 2 MPa the error would be reduced to 10% for the same temperature variation.

The salt solutions used, the corresponding values of relative humidity, and the equivalent suction values are presented in Table 3.16. The relative humidity of the saturated salt solutions was monitored by a chilled mirror hygrometer (Leong et al. 2003). Differences were observed with regard to the actual relative humidity values in some cases, whereas the targeted relative humidity was well achieved in others. With regard to the actual relative

humidity (or suction) to be taken for presenting the test results, purity of the technical grade salts was questioned and was inconclusive in taking a decision. Chilled mirror hygrometer is known to measure relative humidity of salt solutions within a precision of 0.1% and therefore was relied upon for the actual relative humidity values (see also section 3.2.5).

The experimental setup for the vapour equilibrium technique is shown in Fig. 3.10. In all, 9 specimens were tested in each desiccator: three specimens of Calcigel bentonite, three of NX illite, and three specimens of Spergau kaolin. The initially saturated clay specimens were carefully transferred to specially fabricated containers. The specimen container is comprised of a plastic ring (specimen ring) and a plexiglass base. The height of the specimen ring varied between 10 to 15 mm, whereas the diameter of the specimen ring was 46.2 mm in all cases. It was expected that size of the specimen would slightly affect the equilibration time. Since the specimen containers were completely filled with the clay slurries, the initial volume of the specimens correspond to the volume of the container. The specimens were carefully transferred to the desiccators after the preparation. The mass of the specimens was monitored by regularly weighing them about once per week.

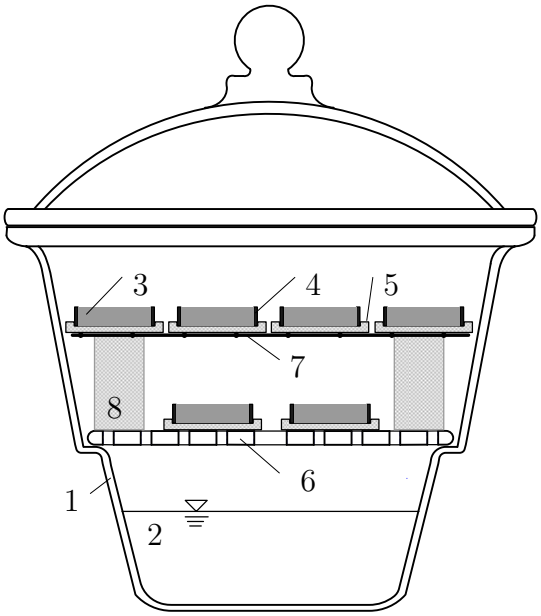

1 Desiccator
2 Saturated salt solution
3 Specimen
4 Specimen ring
5 Plexiglass base
6 Perforated ceramic plate
7 Perforated grid
8 Socle

Figure 3.10.: Schematic of the experimental setup for vapour equilibrium method

The drying process was found to be accompanied by a decrease in volume of the clay specimens. As a result, the specimens were found to be detached from the ring. The diameter and height of the specimens were measured using a precise calliper. The volume of the specimens could then be calculated. Since the shape of the specimens did not remain

perfectly cylindrical during the shrinkage process, the transient volume measurements can be regarded as an indicative only. Equilibrium was considered to be reached when there was no change in mass of the specimens for a given applied suction. Fig. 3.11 shows the typical time versus water content change plot in linear time scale for the clays studied at suction of 2.0 MPa in VET and at 0.03 and 9 MPa in OM. Equilibrium time plots for all specimens tested in VET at the various suctions are contained in Annexe B. The clay specimens were taken out of the desiccator after the equilibrium was reached in each case. Two out of the three specimens were considered for volume measurement using wax method (ASTMD4943-02 2002), whereas the other was selected for water content measurement by oven drying method.

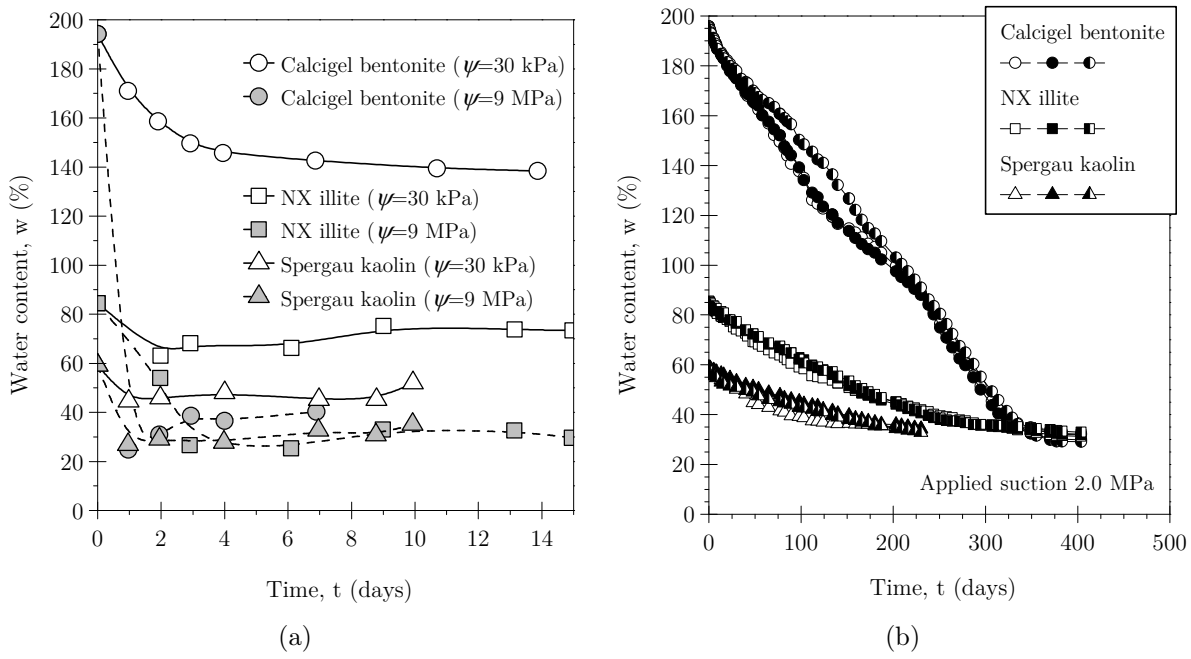

Figure 3.11.: Equilibration time in osmotic method and vapour equilibrium technique: (a) Osmotic method at 30 kPa and 9 MPa, (b) Vapour equilibrium technique at 2 MPa.

3.2.5. Chilled mirror hygrometer

Chilled mirror hygrometer, also known as water activity meter, is a means for measuring total suction of soil specimens. As compared to other measurement techniques for total suction, such as non-contact filter paper method, thermocouple psychrometry, it is a fast and reliable method for a large suction range (Leong et al. 2003, Agus & Schanz 2005*a*). The device uses the dewpoint technique for estimating the relative humidity,

RH. Dew point is reached when water condenses from vapour phase to liquid phase. At the dewpoint, the relative humidity is 100%.

The device used in this study was a water activity meter, model series 3TE from Decagon Devices, Inc. A schematic of the device is shown in Figure 3.12. During measurement,

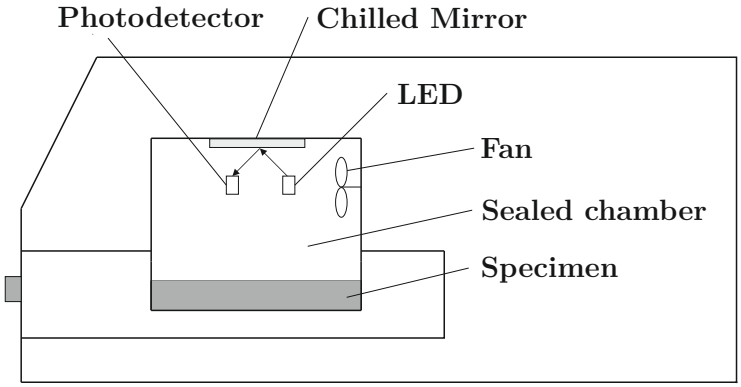

Figure 3.12.: Schematic of the chilled mirror hygrometer

the soil sample is enclosed in a sealed chamber and fills about half the capacity of the small specimen container. Water vapour in the soil pores equilibrates with the water vapour in the air space above the soil sample. A fan is installed inside the chamber which circulates air in order to reduce equilibrium time. A mirror whose temperature is precisely controlled by a thermoelectric (Peltier) cooler is fixed inside the chamber. A beam of light, usually from a light-emitting diode (LED), is continuously directed onto the mirror. It is reflected by the mirror onto a photodetector cell which is able to sense the change in reflectance intensity of the mirror due to condensation of water vapour on the surface of the mirror. The temperature at which condensation occurs is maintained constant by a microprocessor circuit and measured by a thermocouple on the mirror. The dewpoint temperature is then related to the ambient relative humidity. The value of relative humidity and the corresponding temperature are displayed at the end of the measurement. Using Kelvin's equation (see eq. 2.12), the total suction can be calculated from the measured relative humidity.

The accuracy of the device used is in the order of ±0.3% of relative humidity. The measurement range is from about 3% (≈450 000 kPa) to about 99.9% (≈100 kPa). Scatter in measurement increases for relative humidities greater than 99% (≈ 1000 kPa) (Lu & Likos 2004). Leong et al. (2003) stated that using the chilled mirror dew-point technique, it is likely that the error in total suction measurement is less than 150 kPa for the range of suctions of the soil samples tested, considering the accuracy of the relative humidity measurement of 0.1% for a suction range of about 140 to 2500 kPa.

3.2.6. Fabric investigation - mercury intrusion porosimetry

A volumetric pore size distribution can be obtained from adsorption and desorption isotherms or by forced intrusion of a non-wetting fluid into the soil system. The latter includes the evaluation of pore size based on the drying path of the soil water characteristic curve where air is the non-wetting fluid, or mercury intrusion porosimetry (MIP) with mercury as non-wetting fluid. Kelvin's law provides the thermodynamic basis for the above methods. As given by eqs. 3.5a and 3.5b (Lu & Likos 2004, p. 150), the capillary pore radius is inversely proportional to matric suction $u_a - u_w$ or the intrusion pressure u_p. Further, it depends on surface tension T_s and the contact angle θ.

$$r = \frac{2T_s \cos\theta}{u_a - u_w} \tag{3.5a}$$

$$r = -\frac{2T_s \cos\theta}{u_p} \tag{3.5b}$$

Equation 3.5b is also known as Washburn's equation, since he originally conceived the mercury intrusion method.

A detailed description of the mercury intrusion porosimetry technique (MIP) for geotechnical application is given by Diamond (1970) and Sridharan et al. (1971). During the test, the mercury is forced to enter the pores of the dry soil specimen by a stepwise pressure increase. The volume of mercury which enters the specimen at a certain pressure is recorded. The relation between the intrusion pressure u_p and the pore entrance radius r is given in equation 3.5b. The test results are usually depicted in plots were the intruded pore volume is plotted against the pore entrance radius or diameter. The intruded pore volume is either plotted as cumulative volume or as log differential intrusion curve ($dV/d\log r$). The latter represents the pore size density function. While evaluating data obtained from MIP, the following constraints need to be considered: (*i*) completely isolated pores can not be intruded by the mercury and thus are not measured, (*ii*) pores having an 'ink bottle' shape are only accessible at a pressure corresponding to the smaller entrance radius, and the intruded pore volume would be attributed to the small entrance radius, and not to the bigger true pore radius; for detecting the constricted pore volume, a subsequent re-intrusion of the mercury after a pressure release was suggested (Pellerin 1979), (*iii*) the maximum pressure applicable by the device defines a minimum limit of measurable pore diameter. Depending on the clay type tested, not all of the pores might be detected (Diamond 1970).

MIP technique requires the dehydration of the soil specimen. In case of highly plastic clays, standard oven drying alters the pore system of the specimens due to shrinkage. To avoid this, freeze-drying technique is applied to remove water from the soil. Hereby, the soil water is quickly freezed and than removed by sublimation from the specimen. Delage & Pellerin (1984) showed in the frame of an investigation of the structure of a sensitive Champlain clay that sample disturbance induced by freezing-drying is minimized under conditions enabling very fast freezing without crystallisation of the frozen water. Penumadu & Dean (2000) found that an isotropic compaction occurs during the initial pressure steps of the test, leading to an overestimation of the diameter of the most frequent pores. However, for relatively stiff specimen, this effect was found to be minor. Further, based on own measurements, he suggested a value of 160° for the contact angle between mercury and the kaolin surface. Usually, a value of 139 to 141° is applied for clays (Diamond 1970, Delage & Lefebvre 1984).

3.2.7. Fabric investigation - environmental scanning electron microscopy

Scanning electron microscopy (SEM) refers to the type of image generation, which consists in scanning the sample and detecting characteristic information of the sample at the scanning positions. An electron beam is used to interact with the sample surface. Different types of initiated signals may be detected: backscattered electrons (BE) are those ones of the electron beam detected by positively charged atomic nuclei of the sample surface, while secondary electrons (SE) are those ones bounced out of their position in the sample surface through collision with accelerated primary electrons (PE) of the electron beam. These signals generate the different gray scale values of the image. The X-ray signal also originating during the scanning process may be used to determine the chemical composition of a material by energy dispersive x-ray spectroscopy (EDX). A drawback of SEM technique is that the electrical charging of the surface due to exposure of a non-conductive material to an electron beam needs to be prevented by a thin conducting coating layer, which may disturb the sample. Further, the sample chamber is under vacuum to avoid the interaction of the electrons with atoms of the gaseous environment around the sample. Thus, the investigation of the fabric of humid samples is not directly possible, since the applied vacuum would alter the fabric of the initially humid sample of interest.

To circumvent this problem, the freeze-drying method can be used to produce a dry specimen without alteration of the fabric of the initially humid specimen. Or, the envi-

ronmental scanning electron microscopy (ESEM) has to be used which allows for detecting signals within a gaseous environment in the sample chamber. The temperature, pressure and humidity within the sample chamber can be controlled and adjusted to the sample condition so as to prevent severe fabric alteration during the test. By choosing the appropriate conditions in the sample chamber, a possible fabric change will be minimized.

3.3. Experimental programme

The following section presents the experimental programme which was conducted to obtain void ratio-applied vertical stress and void ratio-suction relationships for various initial specimen conditions and at various test boundary conditions. The experiments performed were constant volume swelling pressure tests, one-dimensional consolidation tests of initially saturated specimens, one-dimensional consolidation tests of compacted, saturated specimens. The applied vertical stresses hereby covered stress range up to 25 MPa. The desorption behaviour including change in water content, volume and degree of saturation was experimentally determined for the three clays from initially saturated specimens. At specific states of the specimens, the fabric of the clays was investigated by means of mercury intrusion porosimetry (MIP) and/or environmental scanning electron microscopy (ESEM). The following sections provide an overview about the initial conditions of the specimens tested during the different experiments.

3.3.1. Constant volume swelling pressure tests

Constant volume swelling pressure tests were performed for several specimens of each clay type. The high stress cell and the isochoric cell were used to perform the constant volume swelling pressure tests (see sections 3.2.1 and 3.2.2).

Tables 3.12, 3.13 and 3.14 contain the initial conditions of the compacted specimens of Calcigel bentonite, Spergau kaolin and NX illite, respectively, for which constant swelling pressure tests were performed. The initial compaction conditions including dry density, ρ_d, void ratio, e, water content, w, and degree of saturation, S_r are given. The corrected dry densities and void ratios of the specimens after the completion of the swelling pressure tests (shown within brackets in Table 3.12, 3.13 and 3.14) were calculated based on the system deformations at the corresponding swelling pressures. The initial compaction conditions (dry density ρ_d and water content w) of all specimens with respect to the Proctor curve are illustrated in Fig. 3.13. Additionally, total suction of the specimens was

determined using chilled mirror hygrometer. These values are also given in the respective tables.

The specimens were statically compacted directly in the specimen ring to the desired dry density and were mounted into the cell used. The tests were carried out as one-step swelling pressure tests, i.e., the compacted specimens were wetted with de-ionized water. The swelling pressure developed during the wetting process was monitored. The test duration was adopted according to the measured swelling pressure values; the test was stopped when equilibrium of swelling pressure was reached. For some specimens, the equilibrium swelling pressure was not observed within a reasonable testing period; in these cases, the test was stopped before equilibrium was reached. The results of the constant volume swelling pressure tests are presented in sections 5.2 and 5.3.

Selected specimens were submitted to a loading and unloading path after the swelling pressure test stage (see section 3.3.2.2). These specimens are indicated in Tables 3.12, 3.13 and 3.14 by the superscript ^{b}. The loading and unloading cycle was carried out directly after the end of swelling pressure measurement, without removing or dismantling the specimen from the high stress cell. The Calcigel bentonite specimens CB 1, CB 2, CB 3, CB 4, CB 5, CB 6 and CB 7 (see Table 3.12) had the same initial water content of 9.5% but were compacted to various dry densities. Specimens CB 8, CB 9 and CB 10 were compacted with higher water contents of w = 25.4, 40.4, and 50.0%, respectively. The compaction conditions of CB 8, CB 9 and CB 10 correspond to the Proctor curve (see section 3.1.4). The swelling pressure tests of CB 2a, CB 5a, and CB 6a were performed in a second test series, therefore, the initial hygroscopic water content values (w = 10.5, 10.9, and 10.3%, respectively) and the initial total suctions slightly differ from that of specimens CB 1 to CB 7.

For Spergau kaolin, seven specimens were tested at lower water content values of w = 0.9% (CK 1a, CK 1b and CK 4), w = 2.77% (CK 1c, CK 2 and CK 3) and w = 7.12% (CK 1). Specimens CK 5 and 6 were compacted with higher water content values of w = 30.97% and 22.57%, respectively. They are located on the wet side and at maximum of the Proctor curve.

Seven swelling pressure tests were performed with compacted NX illite specimens, having a similar water content close to 4%, except CI 4 with an initial water content of 0.9%. All specimens are located on the dry side of the proctor curve. No specimens with higher water content were tested in case of NX illite.

The total suctions of the clay specimens were measured using the chilled mirror dew-point technique (Leong et al. 2003). The measurements of total suction were done on powder

Table 3.12.: Initial conditions of the compacted Calcigel bentonite specimens

No.	Initial compaction details				Total suction[d], ψ_{tot} (MPa)
	Dry density [a], ρ_d (Mg/m^3)	Void ratio [a], e (-)	Water content, w (%)	Degree of saturation, S_r (%)	
CB 1	1.11 (1.10)	1.53 (1.54)	9.5	17.38	126
CB 2 [b]	1.17 (1.17)	1.39 (1.40)	9.5	19.13	126
CB 2a	1.20 (1.19)	1.34 (1.35)	10.5	21.94	≈ 92[c]
CB 3	1.24 (1.24)	1.25 (1.26)	9.5	21.28	126
CB 4	1.43 (1.41)	0.98 (0.99)	9.5	27.14	126
CB 5 [b]	1.54 (1.53)	0.82 (0.83)	9.5	32.44	126
CB 5a	1.58 (1.56)	0.78 (0.79)	10.9	39.13	≈ 92[c]
CB 6 [b]	1.64 (1.63)	0.62 (0.72)	9.5	37.46	126
CB 6a	1.65 (1.65)	0.70 (0.70)	10.3	41.2	≈ 92[c]
CB 7 [b]	1.73 (1.70)	0.62 (0.65)	9.5	42.90	126
CB 8 [b]	1.16 (1.16)	1.41 (1.42)	25.4	50.44	7.30
CB 9 [b]	1.22 (1.22)	1.29 (1.30)	40.4	87.69	0.36
CB 10	1.12 (1.11)	1.52 (1.53)	50.0	92.10	0.00

[a] Values within brackets: corrected dry densities or void ratios after the swelling pressure tests

[b] Tests with subsequent compression-decompression path after swelling pressure test, see section 3.3.2.2

[c] Tripathy et al. (2006), (unpublished)

Table 3.13.: Initial conditions of the compacted Spergau kaolin specimens

No.	Initial compaction details				Total suction[d], ψ_{tot} (MPa)
	Dry density [a], ρ_d (Mg/m^3)	Void ratio [a], e (-)	Water content, w (%)	Degree of saturation, S_r (%)	
CK 1 [b]	0.92 (0.93)	1.84 (1.82)	7.12	10.13	≈ 3.5[c]
CK 1a	1.09 (1.08)	1.41 (1.43)	0.90	1.68	≈ 90[c]
CK 1b	1.10 (1.13)	1.38 (1.32)	0.90	1.70	≈ 90[c]
CK 1c	1.27 (1.23)	1.06 (1.12)	2.77	6.85	≈ 15.9[c]
CK 2 [b]	1.38 (1.37)	0.90 (0.91)	2.77	8.06	≈ 15.9[c]
CK 3 [b]	1.51 (1.50)	0.73 (0.74)	2.77	9.94	≈ 15.9[c]
CK 4 [b]	1.59 (1.59)	0.65 (0.65)	0.90	3.64	≈ 90[c]
CK 5 [b]	1.43 (1.42)	0.83 (0.84)	30.97	96.74	≈ 0.36[c]
CK 6 [b]	1.53 (1.52)	0.71 (0.72)	22.57	82.39	≈ 0.72[c]

[a] Values within brackets: corrected dry densities or void ratios after the swelling pressure tests

[b] Tests with subsequent compression-decompression path after swelling pressure test, see section 3.3.2.2

[c] Tripathy et al. (2006), (unpublished)

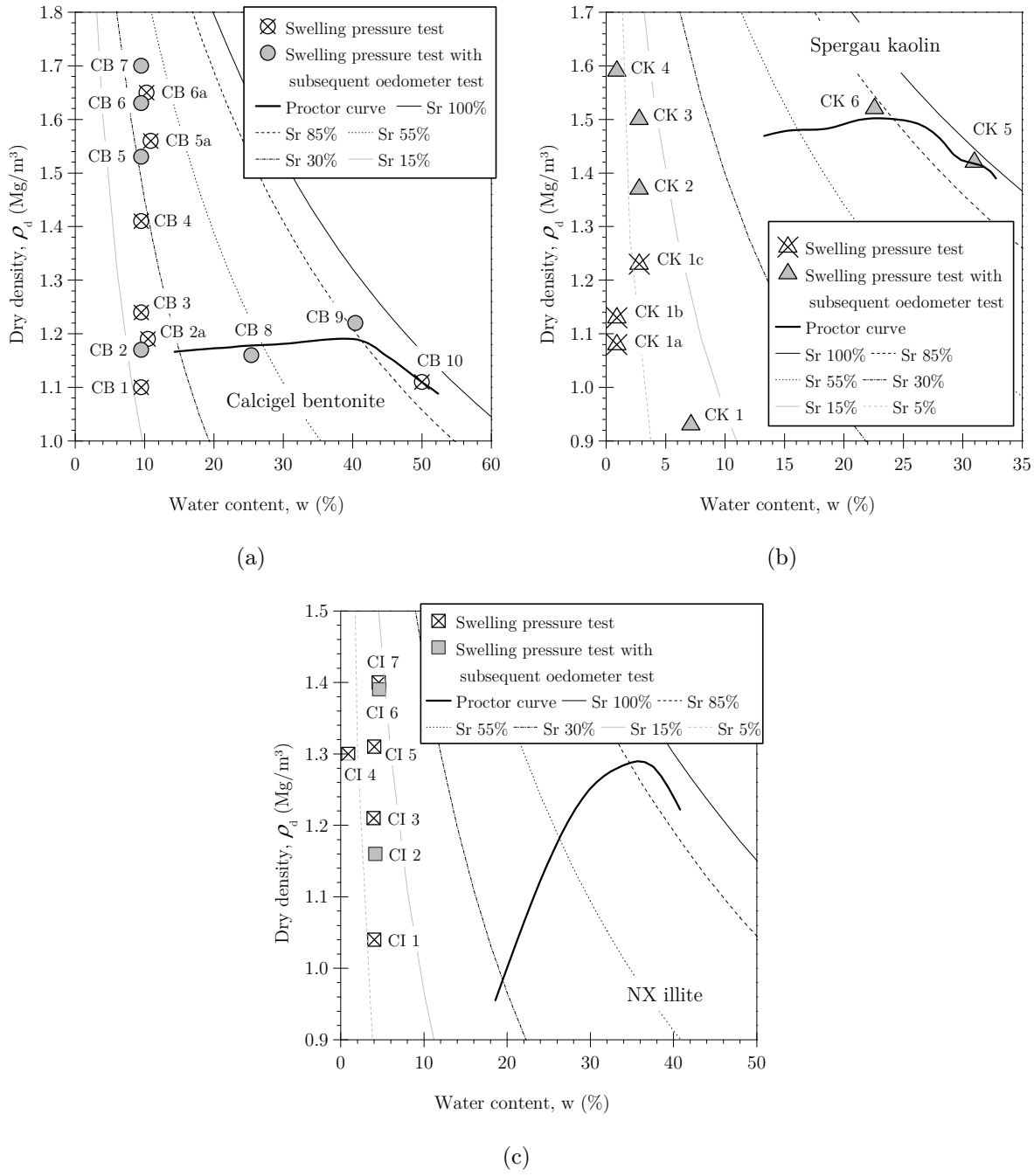

Figure 3.13.: Initial conditions of the compacted specimens and proctor curve: (a) Calcigel bentonite, (b) Spergau kaolin, (c) NX illite.

Table 3.14.: Initial conditions of the compacted NX illite specimens

No.	Initial compaction details				Total suction[d], ψ_{tot} (MPa)
	Dry density [a], ρ_d (Mg/m^3)	Void ratio [a], e (-)	Water content, w (%)	Degree of saturation, S_r (%)	
CI 1	1.06 (1.04)	1.57 (1.60)	4.02	6.95	$\approx 120^c$
CI 2 [b]	1.16 (1.16)	1.33 (1.33)	4.18	8.49	$\approx 120^c$
CI 3	1.32 (1.21)	1.05 (1.25)	3.98	10.28	$\approx 120^c$
CI 4	1.43 (1.30)	0.90 (1.09)	0.91	2.73	$\approx 352^c$
CI 5	1.32 (1.31)	1.05 (1.07)	4.04	10.45	$\approx 120^c$
CI 6 [b]	1.40 (1.39)	0.94 (0.95)	4.65	13.43	$\approx 92^c$
CI 7	1.45 (1.40)	0.88 (0.93)	4.56	14.13	$\approx 92^c$

[a] Values within brackets: corrected dry densities or void ratios after the swelling pressure tests

[b] Tests with subsequent compression-decompression path after swelling pressure test, see section 3.3.2.2

[c] Tripathy et al. (2006), (unpublished)

specimens. The values of the initial total suction of Spergau kaolin, NX illite, and Calcigel bentonite specimens CB 2a, 5a and 6a were interpolated from water content-total suction measurements performed in chilled mirror hygrometer at various water contents (Tripathy et al. 2006).

The static pressure applied during preparation of the specimens increased with an increase in the targeted dry density. After releasing the static compaction pressures, it is likely that some residual lateral stresses remained within the specimens. A possible influence of the residual lateral stresses on the measured swelling pressures and compressibility behaviour of the bentonite are not considered in the study.

The compacted bentonite specimens were hydrated with distilled water in the new oedometer devices. Duplicate specimens were tested to verify the degree of saturation at the end of swelling pressure tests. The results clearly showed that the specimens were fully saturated at the end of swelling pressure tests. It was noted that equilibration of swelling pressures in time-swelling pressure plots was an indicator for completion of the saturation process. In all cases, more than one week was required for saturating the specimens.

3.3.2. One-dimensional consolidation tests

3.3.2.1. Initially saturated clays

One-dimensional consolidation tests were performed on initially saturated specimens, which were submitted to a loading-unloading cycle. For Calcigel bentonite, two specimens (SB 1 and SB 2) were tested in the new high pressure oedometer devices. For the sake of comparison of test results, one specimen (SB 3) was tested in a conventional fixed ring oedometer. One specimen was tested for Spergau kaolin (specimen SK) and NX illite (specimen SI).

The initial water content of the specimens, w corresponded to $1.1w_{\mathrm{L}}$. The clay powder was mixed with the equivalent amount of de-ionized water to reach the desired water content. Before starting the compression tests, the clay-water mixtures were left in a closed container for at least seven days in order to obtain a homogeneous clay-water mixture with equilibrated water content. The initial water content and void ratio values of the initially saturated specimens are given in Table 3.15. Specimen SB 3 was subjected

Table 3.15.: Initial conditions of the initially saturated specimens

	Calcigel bentonite			Spergau kaolin	NX illite
	SB 1	SB 2	SB 3	SK	SI
Initial water content, w (%)	192.0	191.7	189.9	58.8	86.0
Initial void ratio, e (-)	5.54	5.64	5.32	1.54	2.41

to a maximum vertical pressure of 800 kPa. The unloading in this case occurred at 100 kPa and 800 kPa. The saturated Specimens SB 1, SB 2, SK and SI were loaded to a maximum vertical pressure of 21 MPa followed by unloading to a pressure of 50 kPa. The load increment ratio (LIR) adopted was 1.0 up to a pressure of 800 kPa, whereas a LIR of 0.5 was adopted at higher pressures. The one-dimensional consolidation tests (loading and unloading path) lasted for about 29 weeks for specimens SB 1 and SB 2, whereas about 22 weeks were required for specimen SB 3. The total test duration for the NX illite specimen SI was 19 weeks and that for the Spergau kaolin specimen SK was 12 weeks.

3.3.2.2. Compacted saturated clays

After the swelling pressure measurements were completed, few compacted specimens were loaded up to a maximum pressure of 25 MPa and then unloaded. The selection of the

specimens for the compression-decompression tests was based on the initial compaction conditions to cover a wide range of initial void ratio at the same water content (specimens CB 2, CB 5, CB 6, CB 7; CK 1, CK 2, CK 3, CK 4; CI 2 and CI 6). Additionally, tests were carried out at higher water content values to study the effects of initial water content on the compressibility of Calcigel bentonite and Spergau kaolin. The specimens tested were CB 8, CB 9 and CK 5 and CK 6, respectively.

For the compacted saturated specimens submitted to a loading-unloading cycle, the equivalent data pairs of corrected void ratio, e, and swelling pressure, p_s, correspond to the starting point of the loading-unloading path in a void ratio-applied vertical stress plot. The vertical stress for each loading step represents the total stress acting on the clay specimen, that is, the final measured swelling pressure plus the applied vertical stress in the consolidation test (see Fig. 6.4a).

3.3.3. Suction induced desorption and volume change of initially saturated clays

In order to cover a wide range of suction for determining the water content-suction relationship of the three clays it was necessary to adopt two different available methods for inducing suction in the clays. Osmotic method and vapour equilibrium technique were chosen for this purpose. The experimental set-ups as well as the procedure adopted were described in the foregoing sections 3.2.3 and 3.2.4. Clay specimens were subjected to suctions of 30, 100, 300, 1000, 3000, and 9000 kPa using the osmotic method, and to suctions of 2, 6.9, 20.5, 36.4, 56.1 and 218.7 MPa using the vapour equilibrium technique. The suctions were chosen so that both methods overlap in a limited suction range.

At each suction value and for each clay type, multiple specimens were tested: two in case of osmotic suction, and three in case of vapour equilibrium technique. The initial condition of all specimens corresponded to slurry state with water content $w = 1.1w_L$ (see Table 3.15). The equivalent targeted suction values were applied in one step to the initially saturated specimens.

The experimental programme including the main experimental boundary conditions for determining the suction-water content relationship by osmotic method and vapour equilibrium technique is summarised in Table 3.16. The relative humidity (RH) of the saturated salt solutions was monitored by a chilled mirror hygrometer (CMH) (Leong, Tripathy & Rahardjo 2004). Chilled mirror hygrometer measurements was relied upon for the actual relative humidity values.

Table 3.16.: Experimental programme for the water retention test

Osmotic method						
PEG (MW)	20 000	20 000	20 000	20 000	20 000	6000
Membrane (MWCO)	1000	1000	1000	1000	1000	1000
Concentration (g PEG/100g H_2O)	5.22	9.53	16.5	30.2	52.2	96.3
Suction (MPa)	0.03	0.1	0.3	1	3	9
Vapour equilibrium technique						
Saturated salt solution	K_2SO_4	KNO_3	KCl	NaCl	$NaNO_2$	LiCl
RH, Reference † (%)	97	94	86	76	66	12
RH, CMH ‡ (%)	98.5	95	85.9	76.4	66	19.8
Calculated suction, Ref. (MPa)	4.1	8.4	20.4	37.1	56.1	286.3
Calculated suction, CMH (MPa)	2.0	6.9	20.5	36.4	56.1	218.7

† Relative humidity (RH) for the equivalent salt solution at 20 °C from reference

‡ Relative humidity (RH) for the equivalent salt solution as measured by chilled mirror hygrometer (CMH)

3.3.4. Fabric investigations

The fabric of the specimens at specific states was investigated by means of electron microscopy (ESEM) and mercury intrusion porosimetry (MIP). MIP tests were performed on Spergau kaolin, NX illite and Cacigel bentonite after the shrinkage limit test, i.e., after oven drying. For Spergau kaolin, the pore size distribution was also obtained at saturated state corresponding to a water content of $1.1w_L$. Since the MIP test requires the specimens to be in a dehydrated state, freeze-drying method was adopted for the saturated specimen in order to preserve the respective particle arrangement during the drying process.

Specimens of the three clays at saturated state ($w = 1.1w_L$) and at shrinkage limit state were investigated by means of environmental scanning electron microscopy (ESEM). Further, the fabric of initially saturated Calcigel bentonite and Spergau kaolin specimens which were submitted to 2 MPa and 20 MPa applied vertical stress in the one-dimensional test was investigated by ESEM.

4. Unconfined water retention and shrinkage behaviour

4.1. General

The following section covers the experimental results regarding unconfined water retention and shrinkage behaviour of the initially saturated clays of different mineralogical background due to suction increase. Clay specimens with initial water contents slightly greater than the liquid limits of the clays were subjected to increasing suction using the osmotic method and the vapour equilibrium method. In the first section of this chapter, the desorption behaviour of the clays, i.e. the effect of applied suction on water content, degree of saturation and void ratio as well as the shrinkage curve for each clay are presented. The results are compared to the water content vs. matric suction curves of the clays determined from mercury intrusion porosimetry (MIP) results. In the second part, the shrinkage behaviour is discussed in relation to the measured void ratios and water content values at Atterberg limits and air-entry.

4.2. Desorption characteristics

The desorption behaviour of the clays is summarised in Figs. 4.1, 4.2, and 4.3 for Spergau kaolin, NX illite and Calcigel bentonite, respectively. The effect of applied suctions on the water content (Figs. 4.1a, 4.2a, 4.3a), on the void ratio (Figs. 4.1b, 4.2b, 4.3b), and on the degree of saturation (Figs. 4.1c, 4.2c, 4.3c) of the clays is presented. The shrinkage curves of the clays are shown in Figs. 4.1d, 4.2d, and 4.3d.

From plots (a) and (c) in Figs. 4.1, 4.2, and 4.3, the apparent dissimilarities between the responses of the clays to an increase in suction and its effects on the water content and degree of saturation can be clearly noted. In general, either two or three zones were observed: (i) in zone I (indicated by AB), with an increase in suction, there was a decrease

in water content, whereas the degree of saturation of clays remained at 100%, (*ii*) in zone II (indicated by BC), the rate of decrease in water content varied significantly depending upon the type of clay; this zone was accompanied by a decrease in degree of saturation for all clays, and (*iii*) in zone III (indicated by CD), the rate of decrease in water content and degree of saturation further decreased. Zone III could not be detected for Calcigel bentonite and only to some extend for NX illite, which indicates that the continuity in the water phase persisted in case of Calcigel bentonite even at large suctions. According to the conceptual model of McQueen & Miller (1974), zone I and II correspond to the capillary zone, and zone III to the adsorbed film and tightly adsorbed regime. In zone I, the water phase is continuous, in zone II, their is continuity in both water and air phase and in zone III, the air phase is in continuity and the water phase is discontinuous.

The suction at air-entry, ψ_{AEV}, was determined based on the best-fit of the ψ-S_{r} data using van Genuchten's (1980) model as the inverse of the fitting parameter α. The air-entry values were found to be 3.8 MPa, 17.4 MPa and 51 MPa for Spergau kaolin, NX illite and Calcigel bentonite, respectively. The air entry value of Spergau kaolin was found to be slightly higher than that determined for White clay ($\approx$ 1.5 MPa) by Fleureau et al. (1993). Referring to the works of Aylmore & Quirk (1962), Tessier (1984), and Villar (2000), Marcial et al. (2002) stated that the air-entry value of smectite suspensions is close to 100 MPa, which is greater than the air-entry value determined for Calcigel bentonite in this study. Concerning illite clays, an air-entry value of about 1.5 MPa was found for an Na-illite (Bruand & Prost 1987), which is smaller than that determined in this study for the NX illite.

The residual degree of saturation is defined as the degree of saturation at which an increase in suction does not produce a significant change in the degree of saturation. This point correspond to point C. Zone III, and thus, the residual degree of saturation according to the definition above could not be detected for Calcigel bentonite, although the water content at the highest suction applied was only 6.7%. The values of the residual degree of saturation for NX illite and Spergau kaolin were found to be about 30% and 10%, respectively. The residual water content for NX illite and Spergau kaolin was found to be about 7% and 5%, respectively. The absence of zone III for Calcigel bentonite is due to the fact that the water content decrease is still accompanied by an sufficient amount of void ratio decrease so that the degree of saturation remains large for high suctions.

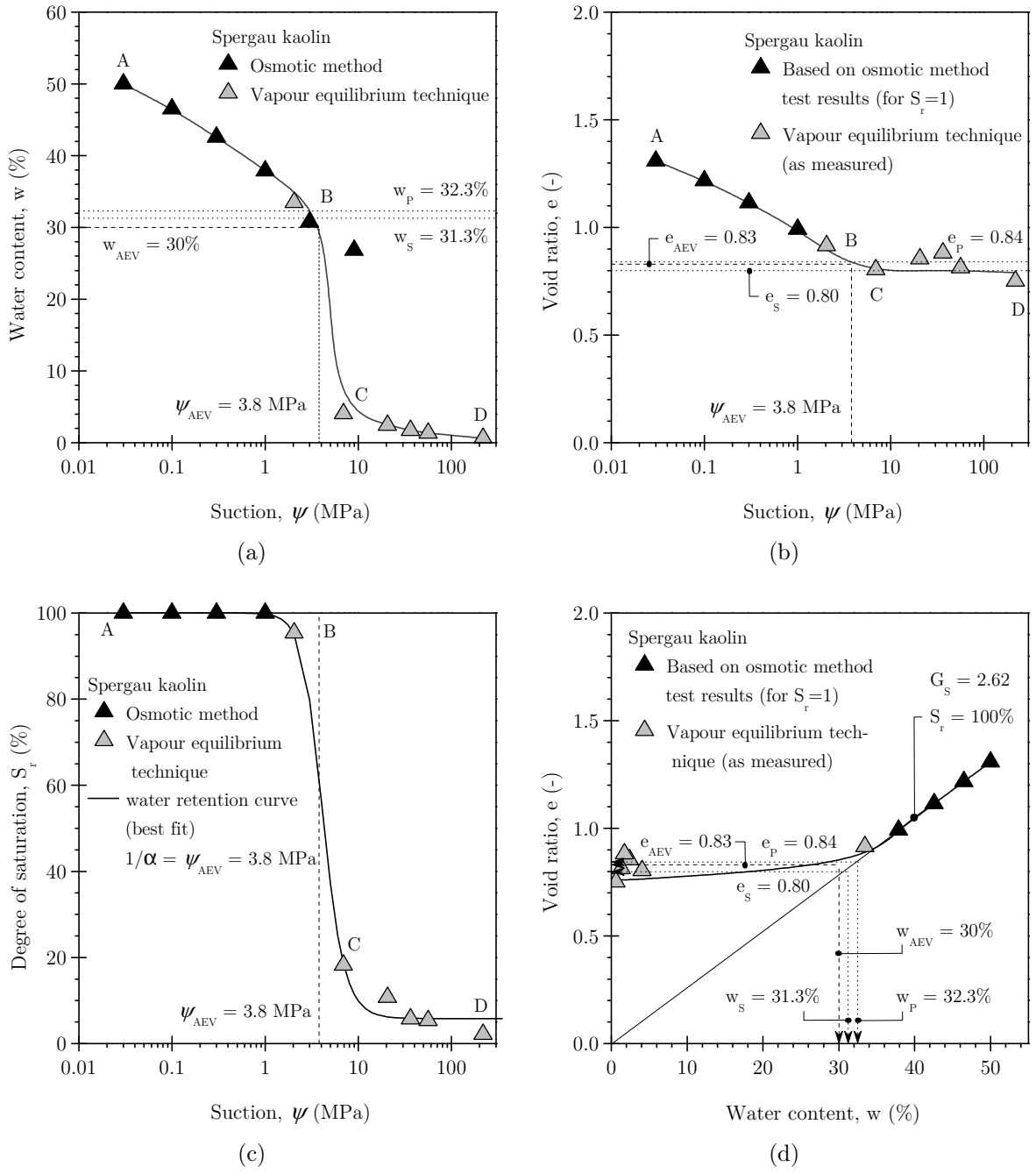

Figure 4.1.: Desorption behaviour of Spergau kaolin: (a) suction versus water content plot, (b) suction versus void ratio plot, (c) suction versus degree of saturation plot, and (d) water content versus void ratio plot.

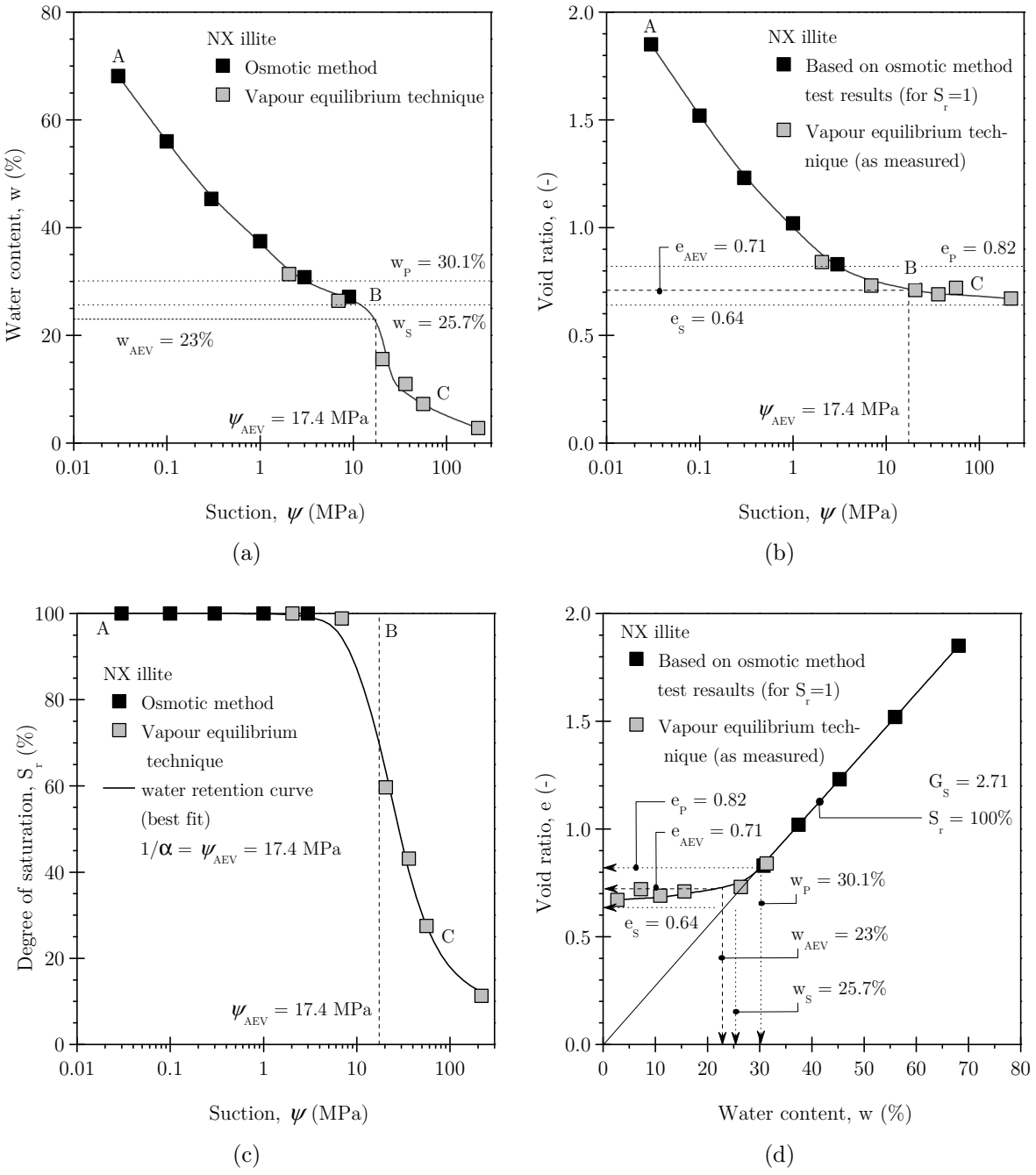

Figure 4.2.: Desorption behaviour of NX illite: (a) suction versus water content plot, (b) suction versus void ratio plot, (c) suction versus degree of saturation plot, and (d) water content versus void ratio plot.

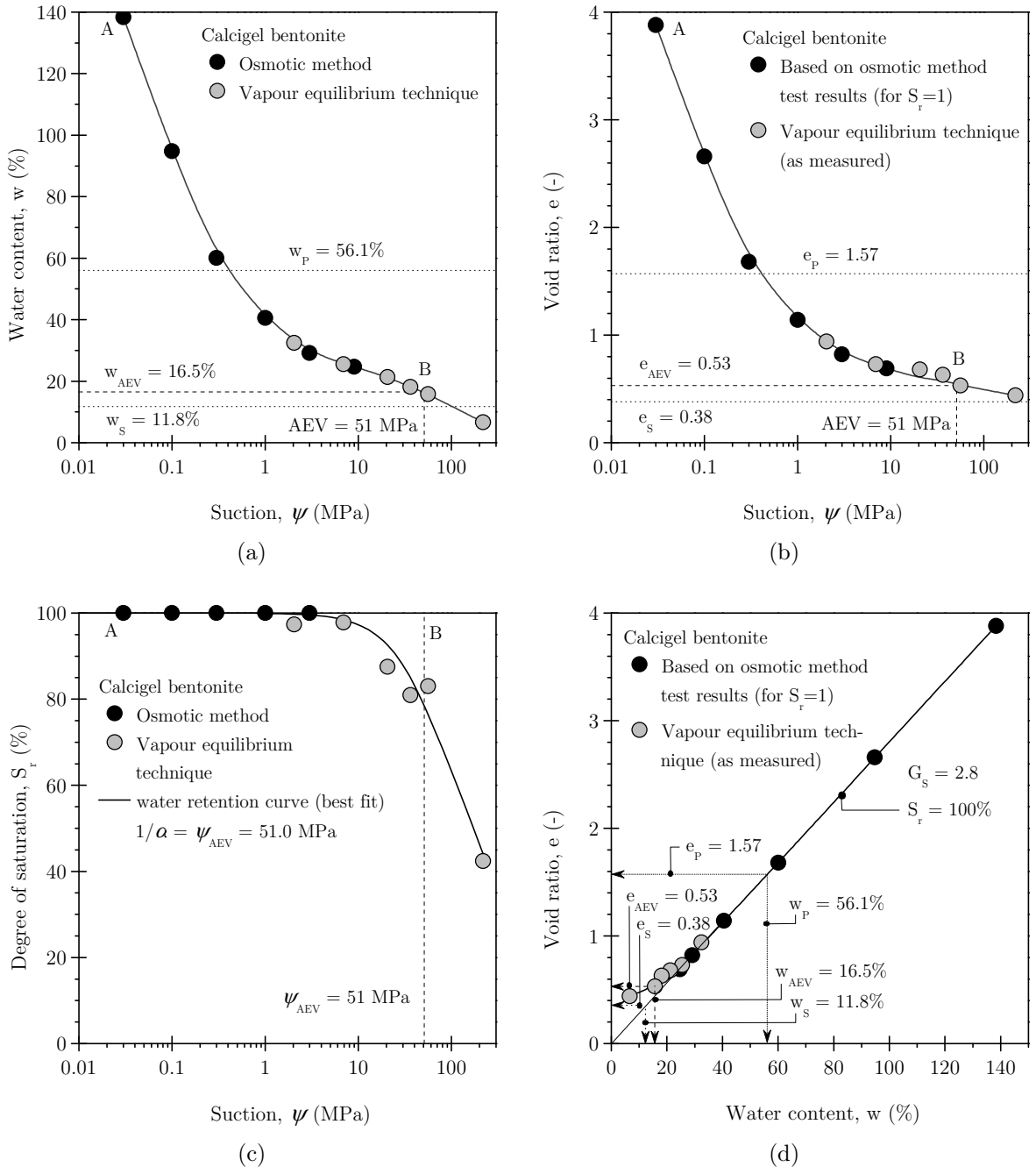

Figure 4.3.: Desorption behaviour of Calcigel bentonite: (a) suction versus water content plot, (b) suction versus void ratio plot, (c) suction versus degree of saturation plot, and (d) water content versus void ratio plot.

MIP data can be used to estimate the water content versus matric suction curve using eq. 4.1

$$\psi_m = (u_a - u_w) = -\frac{T_w \cos\varphi_w}{T_{HG} \cos\varphi_{HG}} \tag{4.1}$$

where ψ_m is matric suction, T_w is the surface tension of water (0.072 Nm at 25 °C), T_{HG} is the surface tension of mercury (0.484 Nm at 25 °C), φ_w is the contact angle between water and the clay surface ($\varphi_w = 180°$), and φ_{HG} is the contact angle between mercury and the assumed pore surface ($\varphi_{HG} = 141.3°$)The results of the estimation are shown in Fig. 4.4. It is to be noted that the estimation of the water content vs. matric suction relationship

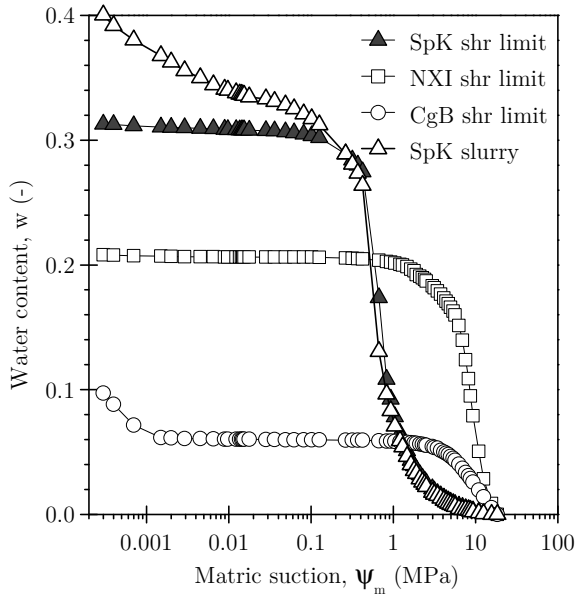

Figure 4.4.: Water content vs. matric suction curves of the clays studied as determined from MIP.

does not include effects of adsorption, thus represents effects due to capillarity. The curves indicate air-entry values of about 300 kPa for Spergau kaolin, and about 5 MPa for NX illite and Calcigel bentonite. These values are significantly smaller than those obtained from the water retention tests (see Figs. 4.1, 4.2 and 4.3), indicating the importance of forces other than resulting from capillarity.

4.3. Shrinkage behaviour and Atterberg limits

The water content and void ratio values at air-entry suctions of the clays were obtained from the suction-water content and the suction-void ratio plots (Figs. 4.1 to 4.3). Simi-

larly, the void ratios at liquid limit, plastic limit and shrinkage limit were obtained from Figs. 4.1d, 4.2d and 4.3d. Table 4.1 shows the salient features during suction increase for the clays studied.

In case of Spergau kaolin, it can be seen that the values of water content and void ratio at plastic limit (w_P, e_P), shrinkage limit (w_S, e_s) and air-entry (w_{AEV}, e_{AEV}) are nearly similar. For NX illite and Calcigel bentonite it was observed that the differences between the water content and void ratio at plastic limit and at shrinkage limit were significant. The void ratio values at air-entry (e_{AEV}) of the clays were found to be within the corresponding values at plastic and shrinkage limit. They were closer to the shrinkage limit than to the plastic limit in case of Calcigel bentonite and NX illite, and e_{AEV} of Spergau kaolin was closer to plastic limit than to shrinkage limit. The water content at air entry w_{AEV} of NX illite and Spergau kaolin is slightly smaller than the water content at shrinkage limit, whereas w_{AEV} of Calcigel bentonite was found to be between w_P and w_S. For all three clays, water content and void ratio at air entry were found to be close to the according values at shrinkage limit, which is concurrent with literature (Fleureau et al. 1993). The results suggest that the difference in water content at plastic limit and at shrinkage limit ($w_P - w_S$) is an indicator for the desaturation behaviour: the smaller is $|w_P - w_S|$, the smaller, i.e. the more narrow, is the suction range in which desaturation occurs. Or in other words, the smaller $|w_P - w_S|$, the more steep is the suction-degree of saturation relationship.

Table 4.1.: Salient features during suction increase for the clays studied

Salient features	Calcigel bentonite	NX illite	Spergau kaolin
Suction at plastic limit, ψ_P (MPa)	0.4	2.5	3.5
Water content at plastic limit, w_P (%)	56.1	30.1	32.3
Void ratio at plastic limit, e_P (for $S_r = 1$)	1.57	0.82	0.84
Suction at air-entry, ψ_{AEV} (MPa)	51.0	17.4	3.8
Water content at air-entry, w_{AEV} (%)	16.5	23.0	30.0
Void ratio at air-entry, e_{AEV}	0.53	0.71	0.83
Water content at shrinkage limit, w_S (%)	11.8	25.7	31.3
Void ratio at shrinkage limit, e_s ‡	0.38	0.64	0.80
Residual degree of saturation, S_{res} (%)	-	30.0	10.0

‡ Experimentally determined following ASTM (2003)

The relevance of air-entry value for the volume change during unconfined water retention tests is highlighted in Fig. 4.5, which presents the void ratio and water content normalised with the respective values at air entry (e/e_{AEV} and $[w/w_{\mathrm{AEV}}]/[e/e_{\mathrm{AEV}}]$) versus the normalised suction ψ/ψ_{AEV}. The plots qualitatively highlight the effect of air-entry on the void ratio and water content changes of the three clays. For Spergau kaolin and NX illite, both representing the rigid type of fabric, the void ratio more or less ceased to decrease at $\psi/\psi_{\mathrm{AEV}} = 1$, whereas further volume decrease occurred at suctions greater than the respective air-entry suction for Calcigel bentonite, due to its flexible nature. In Fig. 4.5b, the ratio of normalised water content and void ratio $[w/w_{\mathrm{AEV}}]/[e/e_{\mathrm{AEV}}]$ is plotted against the normalised suction ψ/ψ_{AEV}. The region at $\psi/\psi_{\mathrm{AEV}} < 1$ represents the normal shrinkage stage of the clays, where the amount of total volume decrease is equal to the volume of water drained out. This behaviour is identical for all three clays and they follow the horizontal line at 1. Beyond air entry, i.e. for $\psi/\psi_{\mathrm{AEV}} > 1$, the ratio $[w/w_{\mathrm{AEV}}]/[e/e_{\mathrm{AEV}}]$ depends on the type of clay. The curve of Spergau kaolin shows a distinct bilinear behaviour, where zone II and III can be clearly recognised, whereas the figure indicates that for both NX illite and Calcigel bentonite, the residual zone III was not fully covered by the maximum suction applied.

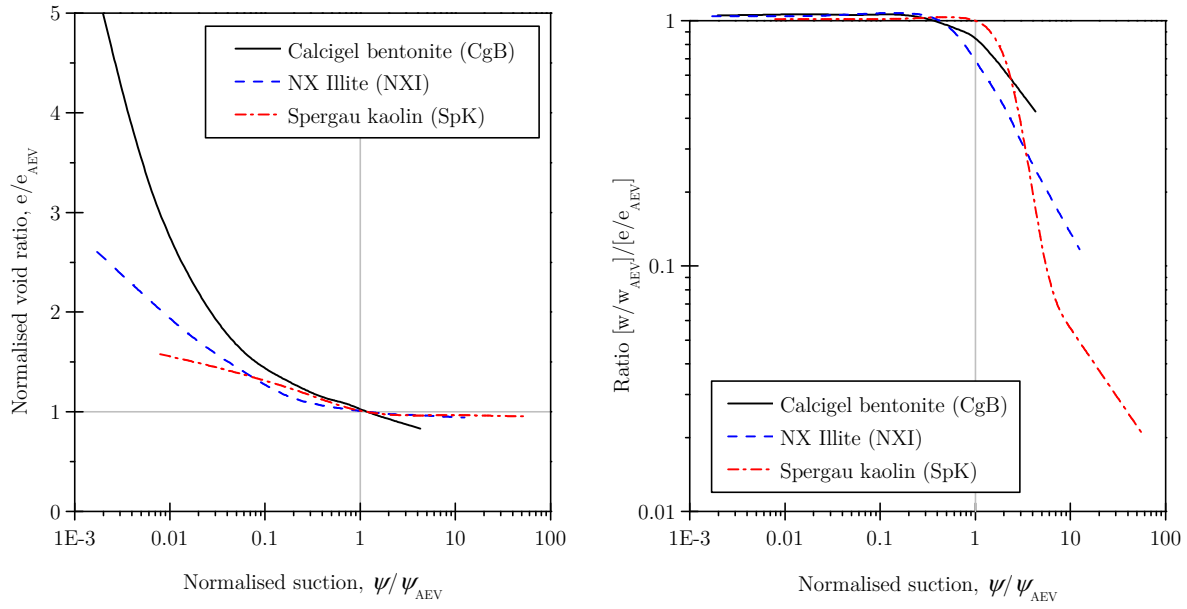

Figure 4.5.: Normalised plots for hydraulic loading: (a) normalised void ratio vs. normalised suction, (b) $[w/w_{\mathrm{AEV}}]/[e/e_{\mathrm{AEV}}]$ vs. normalised suction.

4.4. Summary

The water retention and shrinkage behaviour of clays with significant proportion of one of the minerals montmorillonite, illite and kaolinite was experimentally studied. Osmotic and vapour equilibrium techniques were used for establishing drying water retention characteristic curves for a suction range from 30 kPa to 220 MPa. Volume measurements of the clays during the drying process enabled establishing the shrinkage curves and the suction-degree of saturation relationships. The respective air-entry values of the clays were determined. Mineralogy was found to significantly influence the shape and salient features of the water retention curves of the clays. Concurrent with earlier studies, the test results revealed that significant void ratio decrease occurred at suctions smaller than the air-entry values, whereas suctions greater than the air-entry values were less effective in causing volume change. For all three clays, water content and void ratio at air-entry were found to be close to the respective water content and void ratio values at shrinkage limit. The difference in water content at plastic limit and at shrinkage limit $w_P - w_S$ can be regarded as an indicator for the desaturation behaviour: the smaller is $w_P - w_S$ the more steep is the suction-degree of saturation relationship.

5. Swelling pressure

5.1. General

In the following section, the results of the constant volume swelling pressure tests for the three clays are presented and discussed. The experimental programme, the equipment used and the experimental procedure were already described in chapter 3. The measured swelling pressure values of all specimens tested together with their equivalent compaction details are summarised in Table 5.1. Firstly, the influence of initial compaction conditions on the measured swelling pressure is brought out. The second part of this chapter deals with the time dependent behaviour of the compacted specimens during wetting under constant volume condition. The discussion of the results aims at both bringing out the specific behaviour for each of the clays depending on the initial compaction conditions and a comparison of the behaviour in the light of the different mineralogic properties of the three clays.

5.2. Swelling pressure-dry density relationship

The results of the constant volume swelling pressure tests for the three clays are summarised in Table 5.1 and are illustrated separately in Figs. 5.1a, 5.1b, and 5.1b for Calcigel bentonite, Spergau kaolin and NX illite, respectively. Fig. 5.1d shows the measured swelling pressures of all clay specimens tested.

Table 5.1.: Details of the compacted specimens and measured swelling pressures

No.	Initial compaction details				Total suction, ψ_{tot} (MPa)	Swelling pressure, p_s (MPa)
	Dry density, ρ_d (Mg/m^3)	Void ratio, e (-)	Water content, w (%)	Degree of saturation, S_r (%)		
Calcigel bentonite						
CB 1	1.10	1.54	9.5	17.38	126	0.174
CB 2	1.17	1.40	9.5	19.13	126	0.250
CB 2a	1.19	1.35	10.5	21.94	≈ 92	0.222
CB 3	1.24	1.26	9.5	21.28	126	0.310
CB 4	1.41	0.99	9.5	27.14	126	0.795
CB 5	1.53	0.83	9.5	32.44	126	1.160
CB 5a	1.56	0.79	10.9	39.13	≈ 92	1.555
CB 6	1.63	0.72	9.5	37.46	126	1.380
CB 6a	1.65	0.70	10.3	41.20	≈ 92	2.685
CB 7	1.70	0.65	9.5	42.90	126	9.200
CB 8	1.16	1.42	25.4	50.44	7.30	0.160
CB 9	1.22	1.30	40.4	87.69	0.36	0.172
CB 10	1.11	1.53	50.0	92.10	0.00	0.080
Spergau kaolin						
CK 1	0.93	1.82	7.12	10.13	≈ 3.5	0
CK 1a	1.08	1.43	0.90	1.68	≈ 90	0
CK 1b	1.13	1.32	0.90	1.70	≈ 90	0
CK 1c	1.23	1.12	2.77	6.85	≈ 15.9	0
CK 2	1.37	0.91	2.77	8.06	≈ 15.9	0.091
CK 3	1.50	0.74	2.77	9.94	≈ 15.9	0.206
CK 4	1.59	0.65	0.90	3.64	≈ 90	0.602
CK 5	1.42	0.84	30.97	96.74	≈ 0.36	0.069
CK 6	1.52	0.72	22.57	82.39	≈ 0.72	0.229
NX illite						
CI 1	1.04	1.60	4.02	6.95	≈ 120	0.085
CI 2	1.16	1.33	4.18	8.49	≈ 120	0.088

Table 5.1.: Specimen details and swelling pressures: continuation

No.	ρ_d (Mg/m^3)	e (-)	w (%)	S_r (%)	ψ_{tot} (MPa)	p_s (MPa)
CI 3	1.21	1.25	3.98	10.28	≈ 120	0.185
CI 4	1.30	1.09	0.91	2.73	≈ 352	0.230
CI 5	1.31	1.07	4.04	10.45	≈ 120	0.144
CI 6	1.39	0.95	4.65	13.43	≈ 92	0.864
CI 7	1.40	0.93	4.56	14.13	≈ 92	1.624

For the Calcigel specimens at water content of 9.5%, the total suction measured was 126 MPa. This value of suction was obtained on clay powder at 9.5% water content and also on clay specimens prepared at the predetermined densities using a specially fabricated mould. The clay specimens were extruded from the specimen mould so as to be tested in the chilled mirror dew-point device. It was noted that at constant water content of 9.5% the variation of dry density practically had no influence on the total suction values of the specimens. Romero et al. (1999) and Tarantino & De Col (2008) reported that for compacted clays at very low water contents and with bi-modal pore-size distribution, an increase in the degree of saturation due to an increase in the dry density upon compaction is due to a decrease in the void ratio associated with the macro-pores. The water residing in the micro-pores of clays does not contribute significantly to the measured suctions. Clay specimens CB 1 to CB 7 had the same initial suction but different initial void ratios. The specimens prepared at higher water contents showed lower suctions (specimens CB 8 and CB 9). The total suction measured was null for specimen CB 10 indicating the limitation of the chilled mirror device in measuring very low suctions (Leong et al. 2003).

Overall, for any given water content, the total suction measured was highest for Calcigel bentonite, followed by NX illite and Spergau kaolin specimens showed the least total suction measured.

For Calcigel bentonite, the measured swelling pressure values were in the range between 0.08 MPa for CB 10 and 9.2 MPa for CB 7 (see Figure 5.1a). The results showed that with increasing dry density, the swelling pressure values increased. Ignoring the small differences in the corrected void ratios (Table 5.1), the swelling pressures of specimens CB 1 and CB 10 ($e = 1.54/1.53$), specimens CB 2 and CB 8 ($e = 1.40/1.42$), and specimens CB 3 and CB 9 ($e = 1.26/1.30$) can be compared. It was noted that specimens having higher initial water contents and lower initial suctions (specimens CB 10, CB 8, and CB 9) exhibited lesser swelling pressures as compared to the specimens that had

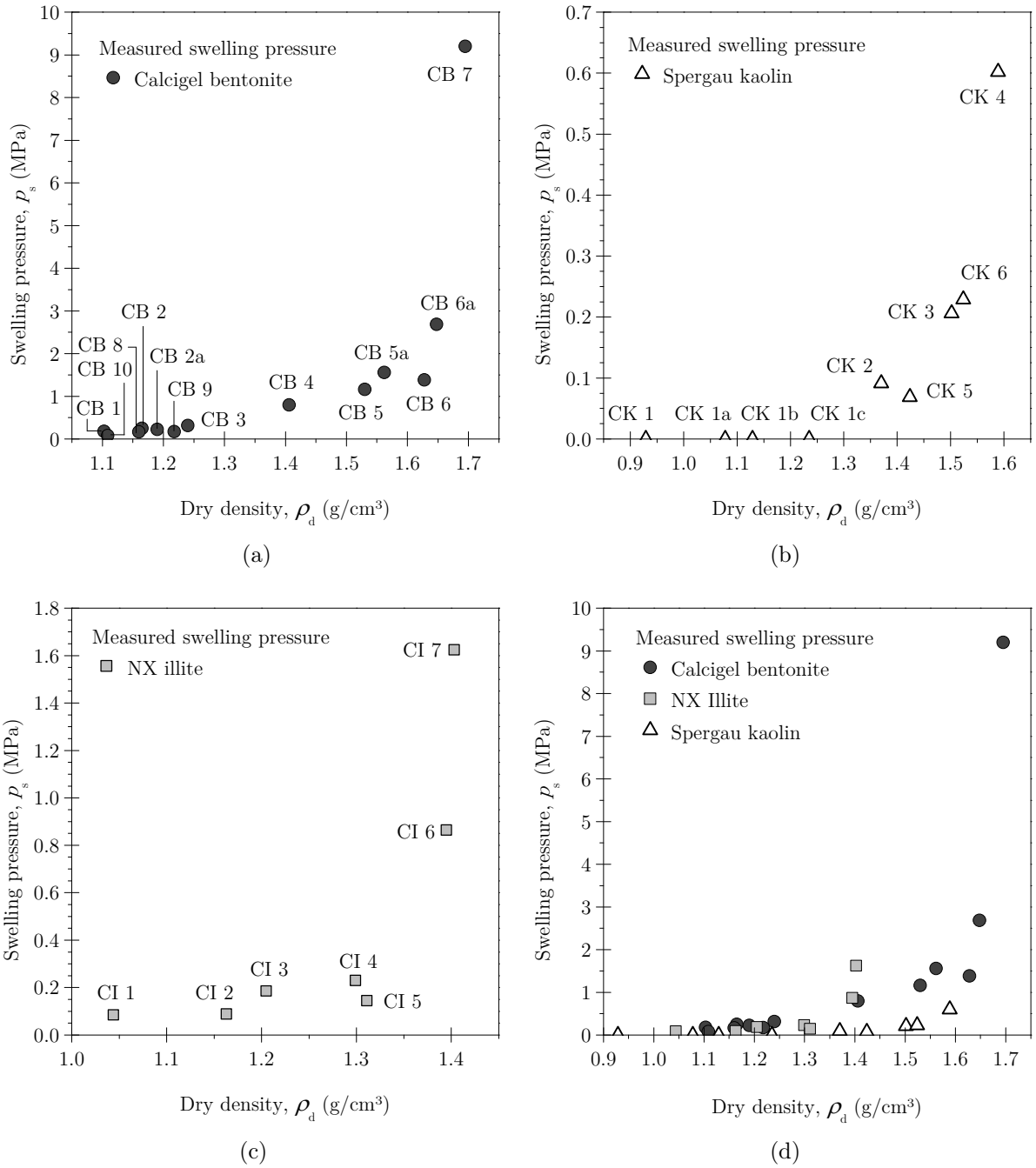

Figure 5.1.: Measured swelling pressure versus dry density: (a) Calcigel bentonite, (b) Spergau kaolin, (c) NX illite, and (d) comparison of the three clays.

lower initial water contents and higher initial suctions (specimens CB 1, CB 2, and CB 3, respectively). The measured swelling pressure values of specimens CB 2a, CB 5a and CB 6a are consistent with those of the other specimens (Fig. 5.1a). Only CB 6 shows a smaller swelling pressure as compared to specimen CB 5a. However, in general, the measured swelling pressures of the compacted Calcigel bentonite specimens are consistent with each other and to findings from literature.

For dry densities smaller than about 1.3 g/cm^3, no swelling pressures were measured for Spergau kaolin, and swelling pressures of maximum 200 kPa were found for NX illite. This behaviour is expected for these clay minerals, where interlayer swelling is not possible due to the strong bonding forces between the layers in these minerals. If at all, formation of a diffuse double layer could only occur at the outer surface of the particles. However, the negligible and small experimental swelling pressures in the low density range for Spergau kaolin and NX illite relative to those of Calcigel bentonite are found to be in agreement with the smaller values of cation exchange capacity and specific surface area of Spergau kaolin and NX illite. The magnitude of the measured swelling pressures for NX illite and Spergau kaolin beyond a dry density of about 1.3 g/cm^3 for the former and beyond 1.5 g/cm^3 for the latter was unexpectedly high for these clay types. This effect is attributed to the compaction conditions with an initial dry density in the range of the maximum Proctor density and greater. These densities produced very small distances between the adjacent particles at their contacts, where short range repulsive forces due to hydration and Born repulsion are relevant. No significant effect of initial water content on the swelling pressures measured for Spergau kaolin was found. For NX illite, all tests were performed with a similar water content.

5.3. Development of swelling pressure with time

In the following section, emphasis is given to the swelling pressure development with time. For each of the clays, the results are presented in absolute values of swelling pressure, p_s, versus time and in terms of normalised swelling pressure, $p_s/p_{s,max}$, versus time. The equivalent plots for Calcigel bentonite can be found in Figs. 5.2 and 5.3, for Spergau kaolin in Figs. 5.4 and 5.5, and for NX illite in Figs. 5.6 and 5.7. Referring to the time-swelling pressure plots for the Calcigel bentonite specimens at higher dry densities (Figs. 5.2a and 5.2b), the following observations were made: specimen CB 7 shows a distinctive behaviour with a non-monotonous swelling pressure development with two maxima. After reaching the first maximum of 6.5 MPa in about 2000 min of saturation

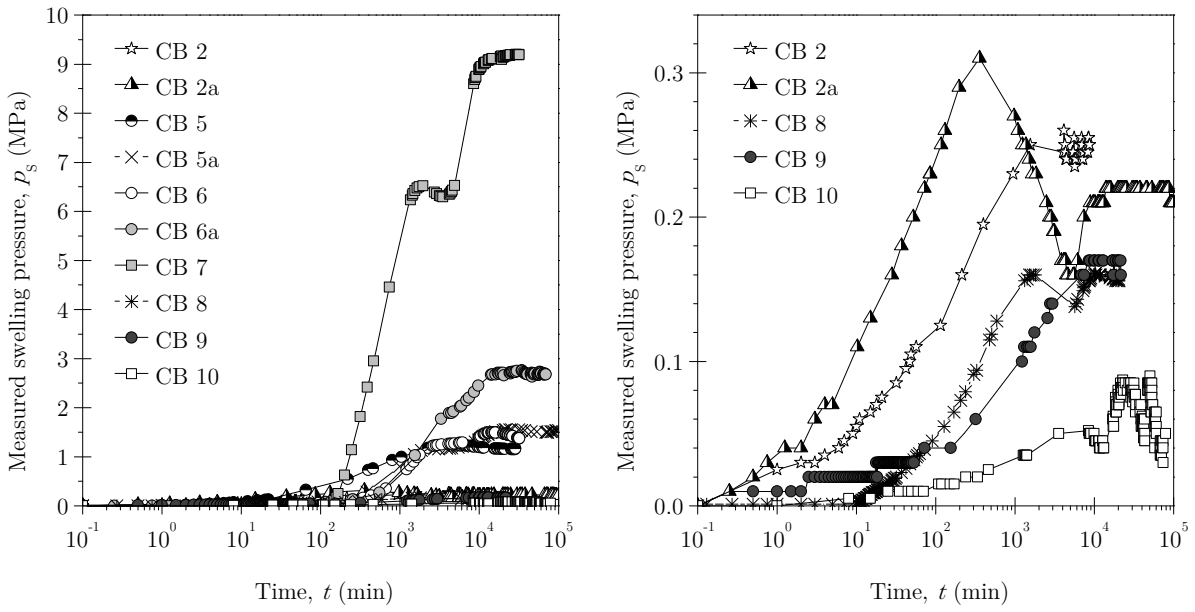

Figure 5.2.: Time-swelling pressure curves of compacted Calcigel bentonite specimens: (a) Swelling pressure scale from 0 to 10 MPa, and (b) Swelling pressure scale from 0 to 0.34 MPa.

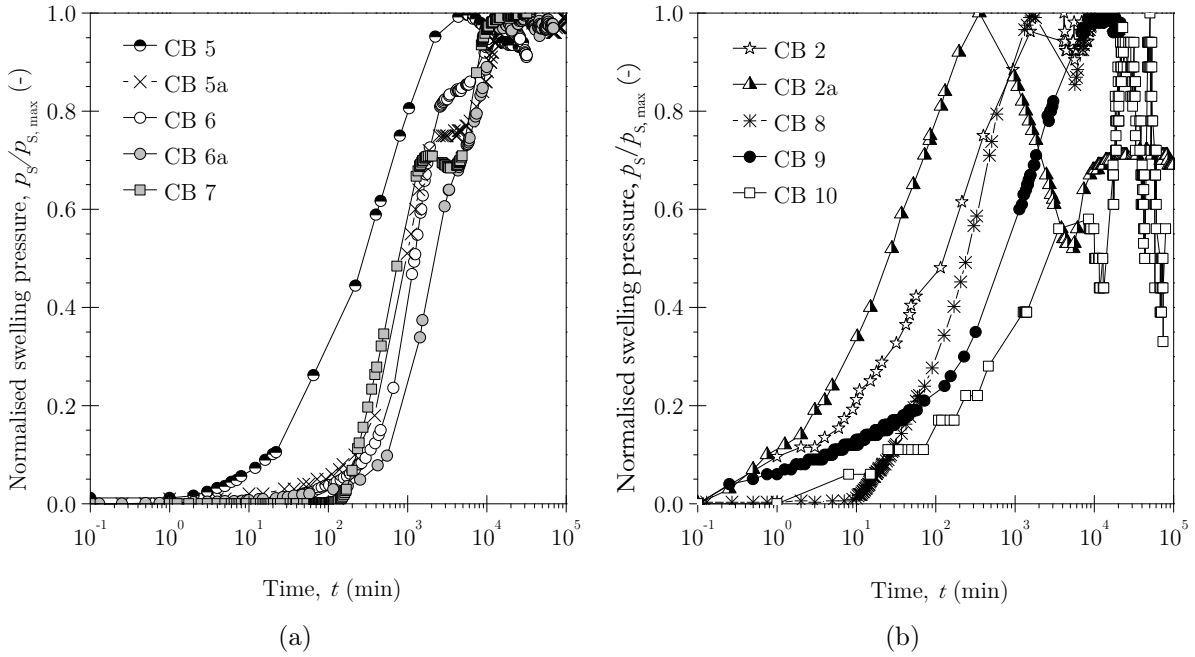

Figure 5.3.: Time-normalised swelling pressure curves of compacted Calcigel bentonite specimens: (a) Specimens CB 5, CB 5a, CB 6, CB 6a, and CB 7 ($\rho_d > 1.5$ Mg/m^3), and (b) Specimens CB 2, CB 2a, CB 8, CB 9, and CB 10 ($\rho_d < 1.5$ Mg/m^3).

period, the swelling pressure decreased slightly and further increased to attain the second maximum of 9.2 MPa after about more than 20 000 min. The time-normalised swelling pressure curves of CB 5a, CB 6, CB 6a and CB 7 (Fig. 5.3a) were found to be very close, thus, the qualitative time-swelling pressure development of the specimens was found to be similar.

The swelling pressure vs. time curves of the low density specimens CB 2a, CB 2a, CB 8, CB 9 and CB 10 were plotted in Figs. 5.2b and 5.3b. The pattern of the normalised swelling pressure curves is a less uniform and less smooth than the specimens with higher dry density.

The time dependent swelling pressure development of the compacted Spergau kaolin specimens is illustrated in terms of absolute values in Fig. 5.4 and qualitatively in Fig. 5.5. The time-swelling pressure curves of specimens CK 1, CK 1a, CK 1b, and 1c are shown in Fig. 5.4, their measured swelling pressure fluctuated around zero throughout the test. Therefore, the curves of these specimens are omitted in Fig. 5.5. The specimens CK 2,

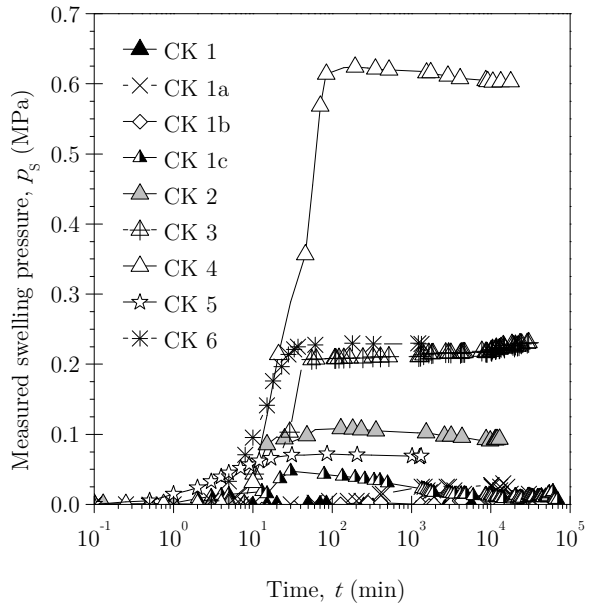

Figure 5.4.: Time-swelling pressure curves of compacted Spergau kaolin specimens.

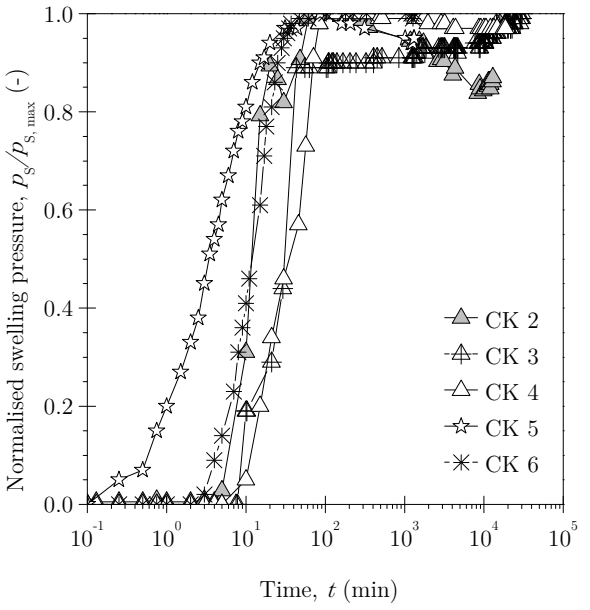

Figure 5.5.: Time-normalised swelling pressure curves of compacted Spergau kaolin specimens.

CK 3, CK 4, CK 5, and 6 followed a similar pattern. After about 3 to 10 min, a sudden linear increase in swelling pressure until a certain value, this pressure remained more or less constant until the end of the test. Overall, the swelling pressure development was very fast as compared to Calcigel bentonite. The maximum swelling pressure was reached

within 30 to 80 min. The total test duration was about 1330 min (= 22 h) for specimens CK 5 and 6, whereas it was 13 000 min (= 9 d) for CK 2, 18 700 min (= 13 d) for CK 4, and 30 200 min (= 21 d) for CK 3.

Figure 5.6a presents the time-swelling pressure plot of all compacted NX illite specimens. In Figure 5.6b, the same plot is presented at a smaller scale for specimens CI 1, CI 2, CI 3, CI 4 and CI 5. For more clarity, the normalised swelling pressure versus time plots are presented separately in Figure 5.7a for the specimens with initial dry density greater than 1.3 Mg/m^3 (CI 4, CI 5, CI 6, CI 7) and in Figure 5.7b for the specimens with initial dry density smaller than 1.3 Mg/m^3 (CI 1, CI 2, CI 3). Specimens CI 6 and CI 7

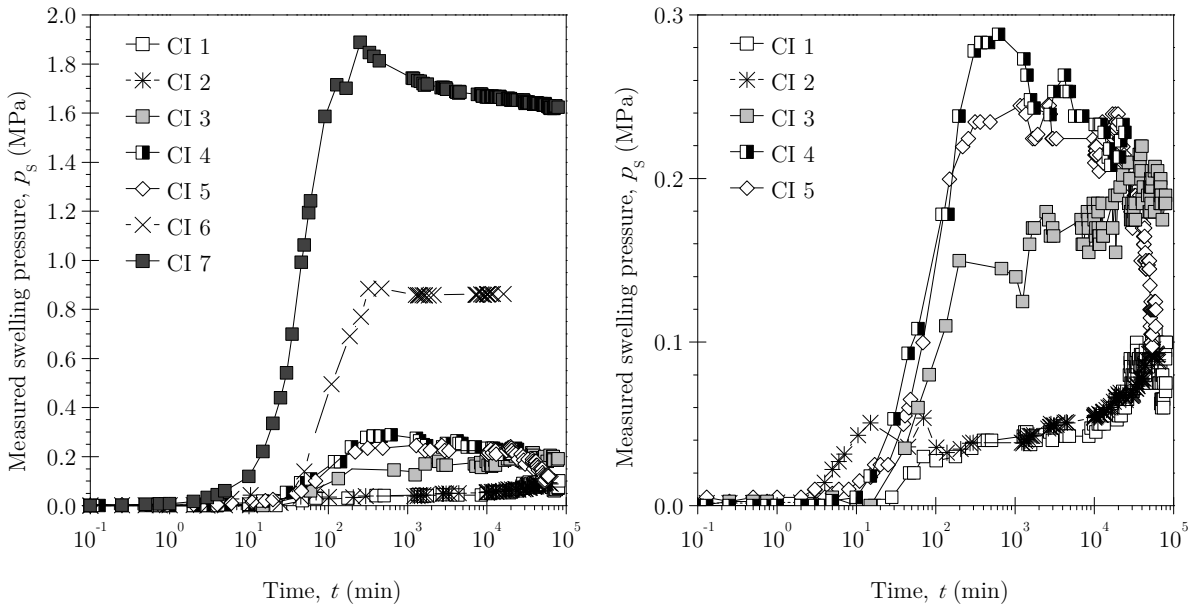

Figure 5.6.: Time-swelling pressure curves of compacted NX illite specimens: (a) Swelling pressure scale from 0 to 2 MPa, and (b) Swelling pressure scale from 0 to 0.3 MPa.

exhibited a characteristic swelling pressure development similar to that observed in case of Spergau kaolin. After 10 to 30 min, the swelling pressure suddenly increased linearly until maximum swelling pressure was reached. After the break point, the swelling pressure of CI 6 decreased slightly to about 96% of maximum swelling pressure and then showed a constant behaviour until the end of the test after 17 100 min (= 12 d). The swelling pressure of CI 7 decreased down to about 86% of the maximum swelling pressure until the end of the test at 79 300 min (= 55 d). Qualitatively, the behaviour of specimens CI 4 and CI 5 is similar to that of CI 6 and CI 7 until reaching the maximum swelling pressure. No

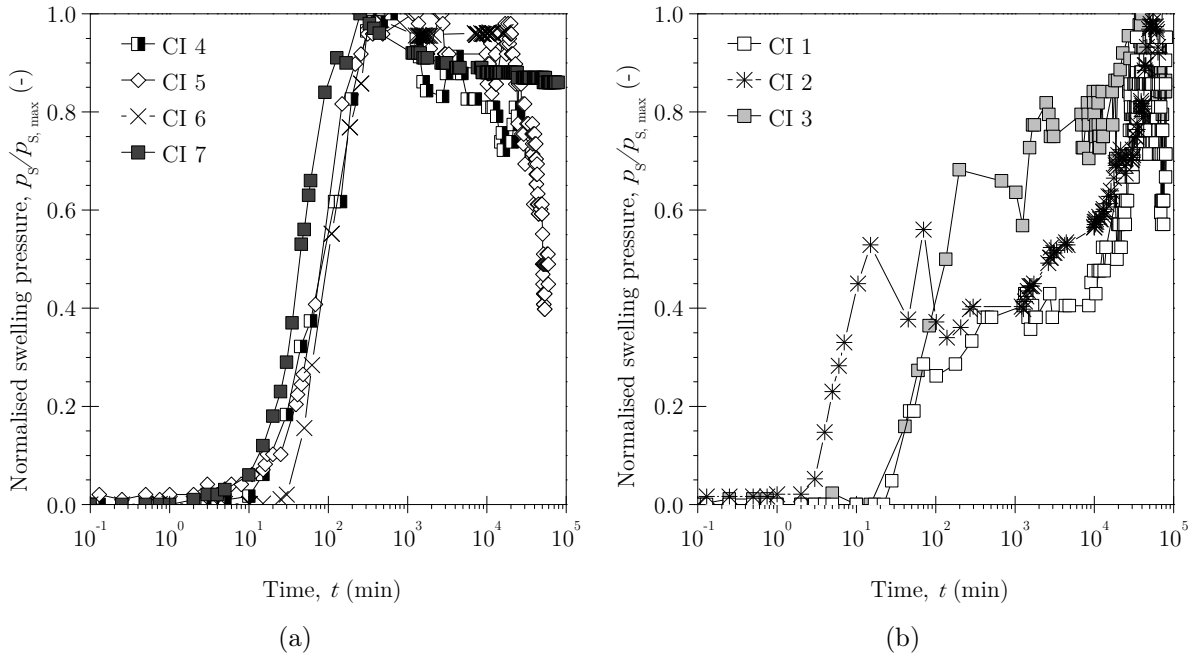

Figure 5.7.: Time-normalised swelling pressure curves of compacted NX illite specimens: (a) Specimens CI 4, CI 5, CI 6, and CI 7 ($\rho_d > 1.3$ Mg/m^3), and (b) Specimens CI 1, CI 2, and CI 3 ($\rho_d < 1.3$ Mg/m^3).

distinctive swelling pressure equilibrium was established by CI 4 and CI 5, even within the relatively long test duration of 24 440 min (= 17 d) and 59 300 min (= 41 d), respectively.

Specimens CI 1, CI 2, and CI 3 did not show a smooth swelling pressure development: the development of swelling pressure started within 3 to 20 min with a linear increase until 30%, 50%, and 70% of the maximum swelling pressure of CI 1, CI 2 and CI 3, respectively. The linear increase was then followed by an irregular behaviour where the swelling pressure increased but at a slower rate as before. The second stage of swelling pressure development was characterised by an oscillating behaviour of the time dependent swelling pressures measured. In total, the swelling pressure tests lasted 80 555 min (= 56 d), 63 525 min (= 44 d) and 79 030 min (= 55 d) for CI 1, CI 2 and CI 3, respectively.

For bentonites, the transient behaviour showing one or more peaks is usually attributed to the internal redistribution of pore space. In case of Spergau kaolin, the steep linear shape indicates that such a redistribution does not take place, since interlayers may not separate. The non-monotonous swelling pressure development for NX illite is possibly related to the fabric with aggregates made up of irregularly arranged particles. After filling the larger pores between the aggregates, water enters inside the aggregates leading to some kind of particle rearrangement.

5.4. Summary

Initial compaction conditions clearly affected the swelling pressure of Calcigel bentonite specimens. At the same water content, the swelling pressure increased with an increase in the dry density. At the same dry density, the swelling pressure was found to decrease with an increase in water content indicating that the influence of molding water on the fabric of the clay can be quite significant. The test results are concurrent with reported studies on swelling pressures of compacted expansive clays. As expected, NX illite and Spergau Kaolin have shown zero or negligible swelling pressures at smaller initial dry densities. However, for specimens compacted at greater dry densities, swelling pressure development was observed. Initial water content had no effect on the swelling pressures measured. The swelling pressure development with time of Spergau kaolin and NX illite was found to be different from that of Calcigel bentonite. Irrespective of the mineral type, the clays showed significantly greater swelling pressures at high dry densities, which are attributed to short range repulsive forces being dominant at close particle spacings.

6. One-dimensional compressibility behaviour

6.1. General

The following section covers the presentation and discussion of the experimental results with respect to the one-dimensional compressibility behaviour under oedometric conditions up to large stresses of maximum 25 MPa. Firstly, the compression-decompression behaviour of the initially saturated clays is dealt with; the differences between the three clay types will be brought out. The void ratio-swelling pressure relationships obtained from the constant volume swelling pressure tests and also the compression-decompression paths of the compacted saturated specimens will be compared to the compression-decompression paths of the initially saturated clays. The time-deformation data of the initially saturated specimens and of the compacted saturated specimens were further considered for calculating the coefficient of volume change, m_v, the coefficient of consolidation, c_v, and the saturated coefficients of permeability, k, at all compression stress steps. From the data obtained, the effect of applied vertical stress and void ratio on the coefficient of consolidation and the permeability of the clays will be highlighted.

6.2. Compression-decompression paths of initially saturated clays

The compression-decompression tests of the initially saturated specimens were performed according to the experimental programme given in Table 3.15 in section 3.3.2.1. In Fig. 6.1, the compression-decompression paths of the initially saturated clay specimens are shown in a separate plot (Figs. 6.1a, 6.1c and 6.1b) and as well in a comparative plot (Fig. 6.1d). In Fig. 6.2, the time-compression curves of the three initially saturated clays SB 1, SI and SK are compared.

Two specimens of Calcigel bentonite (SB 1 and SB 2) were tested in the new high pressure oedometer devices. For the sake of comparison of test results, one specimen (SB 3) was tested in a conventional fixed ring oedometer. The compression-decompression paths of the initially saturated bentonite specimens (Figure 6.1a) showed that the variations in e-$\log \sigma'_v$ relationships for all specimens were within the experimental error due to the variation in the initial water contents. The results of SB 1 were considered as the representative saturated compression-decompression behaviour and compared with the compression-decompression paths of Spergau kaolin and NX illite. The initial void ratios of the initially saturated specimens varied according to the liquid limit values between 5.54 for Calcigel bentonite (SB 1), 1.54 for Spergau kaolin and 2.41 for NX illite.

Qualitatively, the shapes of the compression paths of Calcigel bentonite (Fig. 6.1a) and NX illite (Fig. 6.1b) resemble each other. At stresses greater than about 50-100 kPa, the e-$\log \sigma'_v$ relationships of the specimens SB 1 and SI were found to be distinctly curved and and concave upward. Contrary to SB 1 and SI, the compression path of the Spergau kaolin specimen SK was found to be slightly curved and concave downward at stresses smaller than about 400 kPa, whereas a linear behaviour was observed at stresses greater than about 400 kPa (Fig. 6.1c). The compression-decompression paths of all three clays were found to be irreversible even at large vertical stresses. Comparing the compressibility of the three clays, the following observations were made: the Calcigel bentonite compression path remained above that of NX illite nearly throughout the whole stress range; with increasing applied stresses their paths approached each other and they had the same void ratio at maximum applied stress of 21 MPa. The compression path of Spergau kaolin remained below that of NX illite and Calcigel bentonite at all loading steps; the void ratio attained at maximum applied stress of 21 MPa was 0.54 as compared to 0.70 for Calcigel bentonite and NX illite. In general, Calcigel bentonite and NX illite showed more resistance to compression than Spergau kaolin. The decompression path of Calcigel bentonite was found to be linear, that of NX illite was found to be linear until a vertical stress of about 800 kPa; at stresses smaller than 800 kPa, the curve was slightly curved and concave downward. Spergau kaolin was slightly curved and concave upward in a stress range from 21 MPa to about 800 kPa, and was found to be slightly curved and concave downwards at stresses smaller than about 400 kPa.

The time-compression curves of the three initially saturated clays SB 1, SI and SK are shown in Fig. 6.2. The compression for any loading step is represented by the ratio $\varepsilon_{v,t}/\varepsilon_{v,final}$ given in %, where $\varepsilon_{v,t}$ is the volumetric strain at any time during the loading step and $\varepsilon_{v,final}$ is the final volumetric strain at the end of the loading step. The shapes of

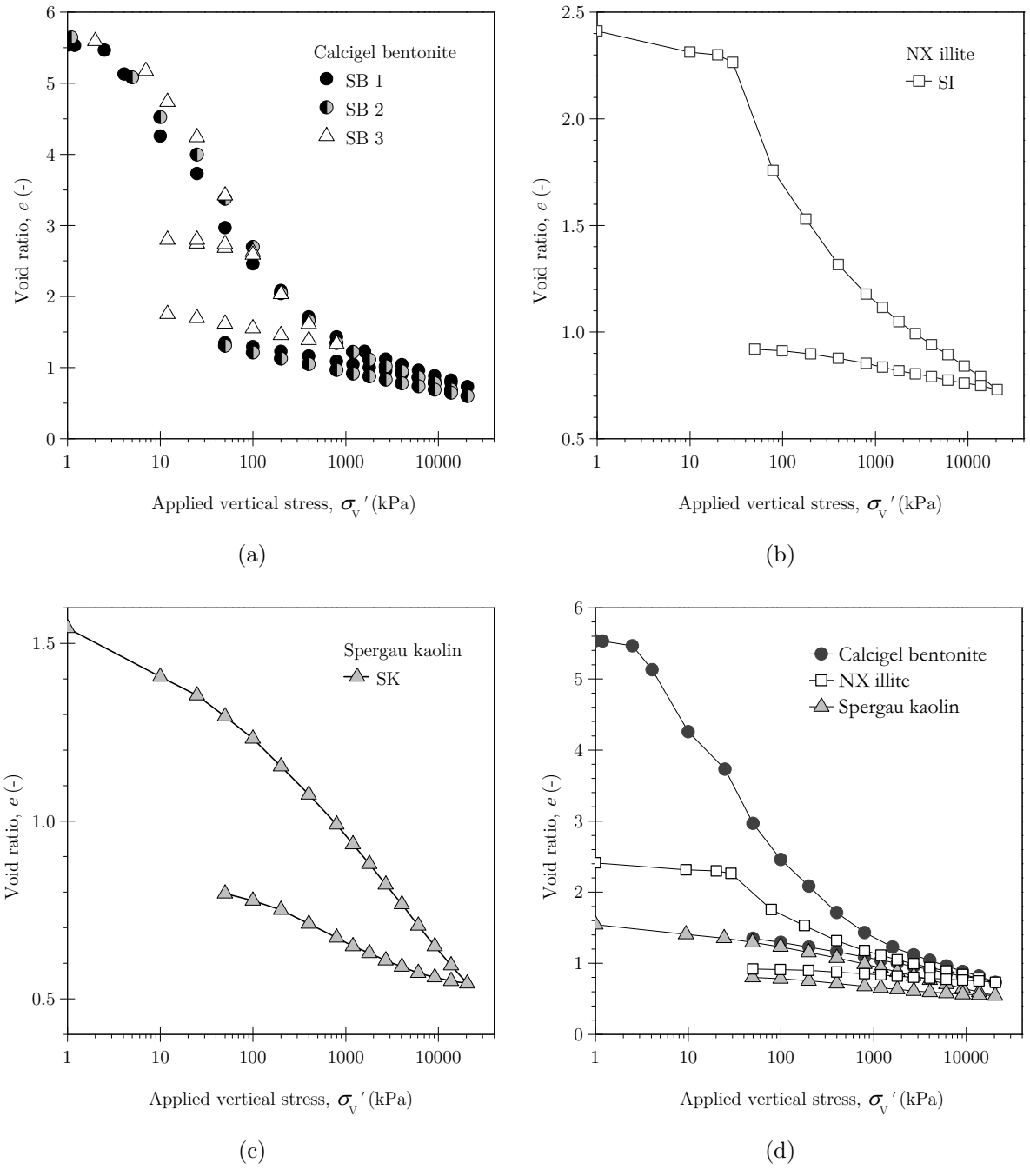

Figure 6.1.: Compressibility of initially saturated specimens: (a) Calcigel bentonite, (b) NX illite, (c) Spergau kaolin, and (d) comparative plot of the three clays.

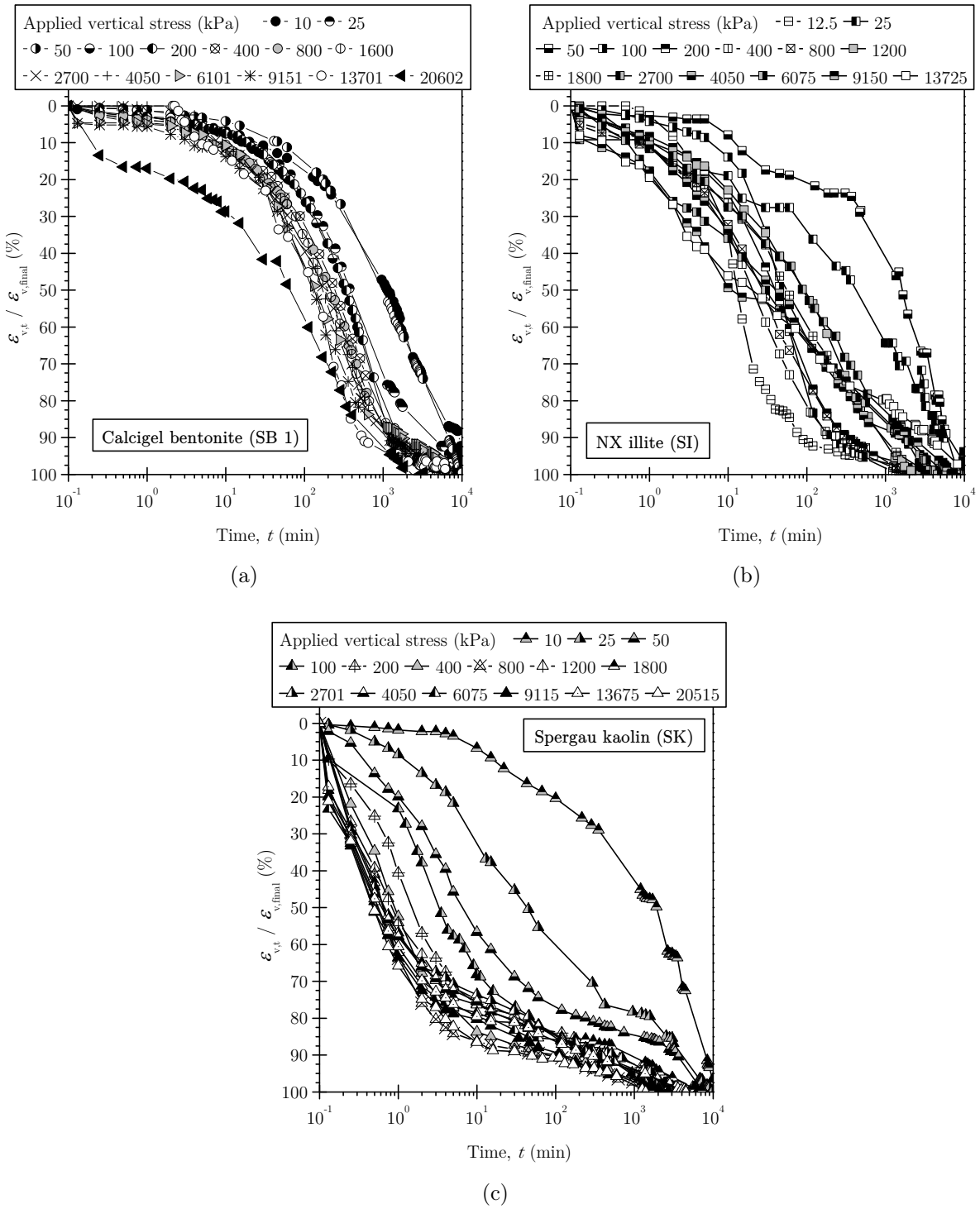

Figure 6.2.: Time-compression curves of initially saturated specimens: (a) Calcigel bentonite (SB 1), (b) NX illite (SI), (c) Spergau kaolin (SK).

the time-compression curves of Calcigel bentonite and NX illite are qualitatively similar and they resemble the classical s-shaped consolidation curve. A somewhat different behaviour was observed for Spergau kaolin. For vertical stresses greater than 400 kPa, about 70 to 90% of the compression occurred during the first 1 to 10 min after the start of loading. Then compression slowed down and continued at slower rate until the end of the loading step. Further time-compression and time-decompression data, where the compression and decompression were expressed as cumulative settlement measured during the test, are given in Annexe A. A possible explanation for the shape of the time-settlement curves of Spergau kaolin at higher stresses is, that, once the larger water filled voids have been squeezed out, the particles are in direct contact and further deformation is minimized.

6.3. Comparison of compression-decompression paths of initially saturated clays and swelling pressure-void ratio relationships of compacted saturated clays

In Fig. 6.3, the measured swelling pressures of the compacted clay specimens are compared to the equivalent compression-decompression path of the initially saturated specimen. The data is presented in Figs. 6.3a, 6.3b and 6.3c for Calcigel bentonite, NX illite and Spergau kaolin, respectively. As is apparent from Fig. 6.3a, the swelling pressure-void ratio data for the compacted saturated specimens CB 1 to CB 10 remained distinctly below that of the compression path of SB 1 and SB 2. On the other hand, the swelling pressure data points remained either above or below that of the decompression path of SB 1 and SB 2. In Fig. 6.3c, presenting the data of Spergau kaolin, the points of specimens CK 1, CK 1a, CK 1b and CK 1c are given for the sake of completeness. Zero swelling pressure was measured for these specimens and according to their void ratio during the constant volume swelling pressure tests the points are aligned on the 10^{-1} kPa-line in Fig. 6.3c. Since no swelling pressure was measured, the meaning of the location of their points with respect to the compression-decompression curve of specimen SK is limited. The compacted Spergau kaolin specimens CK 2, CK 3, CK 4, CK 5 and CK 6 remained distinctly below that of the compression path of specimen SK. On the other hand, the swelling pressure data points of specimens CK 3, CK 4, CK 5 and CK 6 remained very close to that of the decompression path of specimen SK, either slightly above (CK 5) or below (CK 3, CK 4 and CK 6). Specimen CK 2 is located above, and less close to the

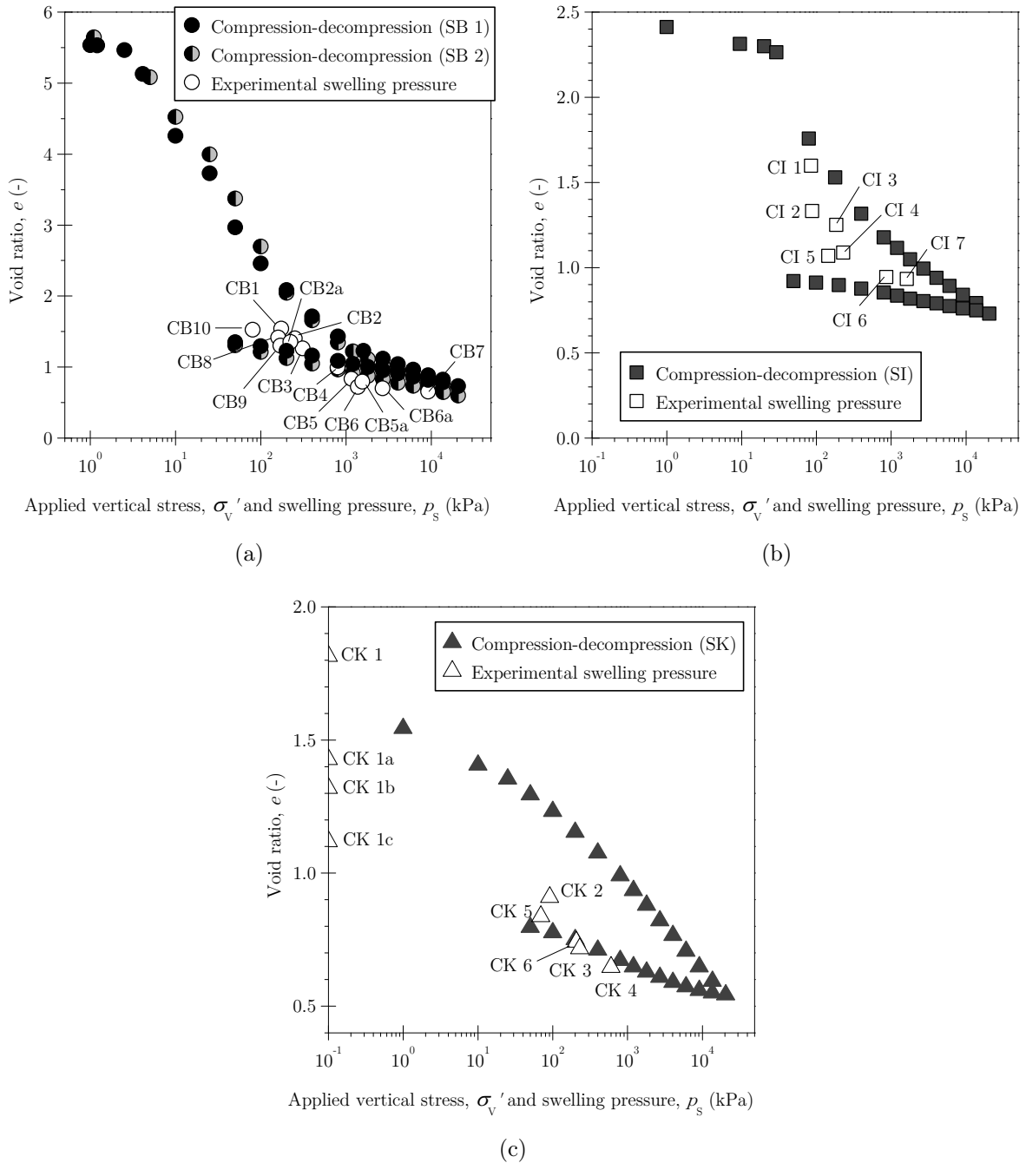

Figure 6.3.: Applied vertical stress and swelling pressure-void ratio relationships: (a) Calcigel bentonite, (b) NX illite, (c) Spergau kaolin.

decompression path of SK, as compared to CK 5. In general, this behaviour was also observed in case of the compacted Calcigel bentonite specimens (see Fig. 6.3a).

The behaviour of the compacted NX illite specimens is somewhat different. The points of the compacted specimens CI 1 to CI 6 are located between the compression and the decompression line of the initially saturated specimen SI. Specimen CI 1 was found be very close to, and slightly below the compression line, all the other compacted specimens were found to be distinctly below the compression line and above the decompression line.

Comparing the swelling pressures and the compression path of SB 1 and 2, at any given void ratio, the difference between the loading pressure (i.e., the applied vertical stress) in case of the initially saturated specimens SB 1 and SB 2 and the swelling pressure of compacted specimens increased with a decrease in the void ratio. This difference was about 325 kPa for specimen CB 1, whereas for specimen CB 7, the difference between the pressures was found to be about 11.46 MPa. The test results clearly showed that the e-$\log \sigma'_v$ relationships are strongly dependent on the stress paths and the initial compaction conditions that significantly influence the fabric and structure of the bentonite (Sridharan, Sreepada Rao & Sivapullaiah 1986, Gens & Alonso 1992).

For Spergau kaolin, at any given void ratio, the difference between the applied vertical stress of specimen SK and the measured swelling pressures of the compacted specimens increased with decreasing void ratio. The differences were about 1,210 kPa and 2,030 kPa for specimens CK 2 and CK 5, respectively, whereas it was about 8,500 kPa for specimen CK 4. Again, for the NX illite specimens, a similar trend was observed. The difference between the applied vertical stress of specimen SI and the measured swelling pressures of the compacted specimens increased with a decrease in void ratio. Whereas for specimen CI 1 this difference was about 35 kPa, it was about 1085 kPa for CI 4 and about 3050 kPa for CI 7. Overall, these differences were found to be smaller as compared to Calcigel bentonite and Spergau kaolin.

6.4. Comparison of compression-decompression paths of initially saturated and compacted saturated clays

The compression-decompression paths of the compacted saturated clay specimens are contained in Fig. 6.4. For comparison, the compression-decompression lines of the initially

saturated specimens are included in these Figures. Figs. 6.4a and 6.4b represent the data for the Calcigel bentonite specimens CB 2, CB 5, CB 6, CB 7 and specimens CB 8 and CB 9, respectively. For more clarity, only one initially saturated specimen (SB 2) is presented in the plot for Calcigel bentonite. The results of NX illite and Spergau kaolin are shown in Figs. 6.4c and 6.4d, respectively. The following observations were made for each clay type with respect to the compression-decompression paths of the initially saturated and the compacted saturated specimens.

For Calcigel bentonite, the compression-decompression paths of the compacted saturated specimens were found to remain distinctly below that of specimen SB 2 even at very large stresses. At stresses greater than about 100 kPa, the e-$\log \sigma'_{\mathrm{v}}$ relationship of SB 2 was found to be distinctly curved and concave upward; however, in case of the compacted saturated specimens, the concavity in e-$\log \sigma'_{\mathrm{v}}$ relationships was found to be indistinct, whereas the paths were found to be slightly curved and concave downward at smaller pressures immediately after the corresponding swelling pressures. The dissimilar shapes of the e-$\log \sigma'_{\mathrm{v}}$ relationships are due to differences in the fabric of the bentonite owing to the initial compaction conditions. At large pressures, the e-$\log \sigma'_{\mathrm{v}}$ plots for the compacted saturated specimens showed nearly linear relationships. The compression-decompression paths were found to be irreversible even at large vertical pressures. The discussions on the reported micro-structures of initially saturated bentonites (Marcial et al. 2002), unsaturated compacted bentonites (Delage et al. 2006), and compacted saturated bentonites (Saiyouri et al. 2004) under section 2.4 may be recalled. At pressures smaller than about 1,000 kPa, the difference in the void ratios of the initially saturated specimen and the compacted saturated specimens can be attributed to: (i) the difference between the fractions of the total void ratio contributed by the pores bounded by the stacked clay platelets in case of initially saturated specimen and the interaggregate pores for the compacted saturated specimens, and (ii) the difference between the fractions of the total void ratio contributed by the interlayer pores in both cases. At pressures greater than 1,000 kPa, the differences in the void ratios are primarily on account of dissimilar interlayer pores.

In case of NX illite, the compression-decompression paths of the compacted specimens CI 2 and CI 6 remained also distinctly below that of the initially saturated specimen SI throughout the whole stress range. The deformations of both the initially saturated and the compacted saturated specimens were found to be irreversible, even at high stresses. At stresses greater than about 30 kPa, the compression path of specimen SI was found to be distinctly curved and concave upward. The compression paths of the compacted specimens CI 2 and CI 6 were found to be slightly curved and concave downward at

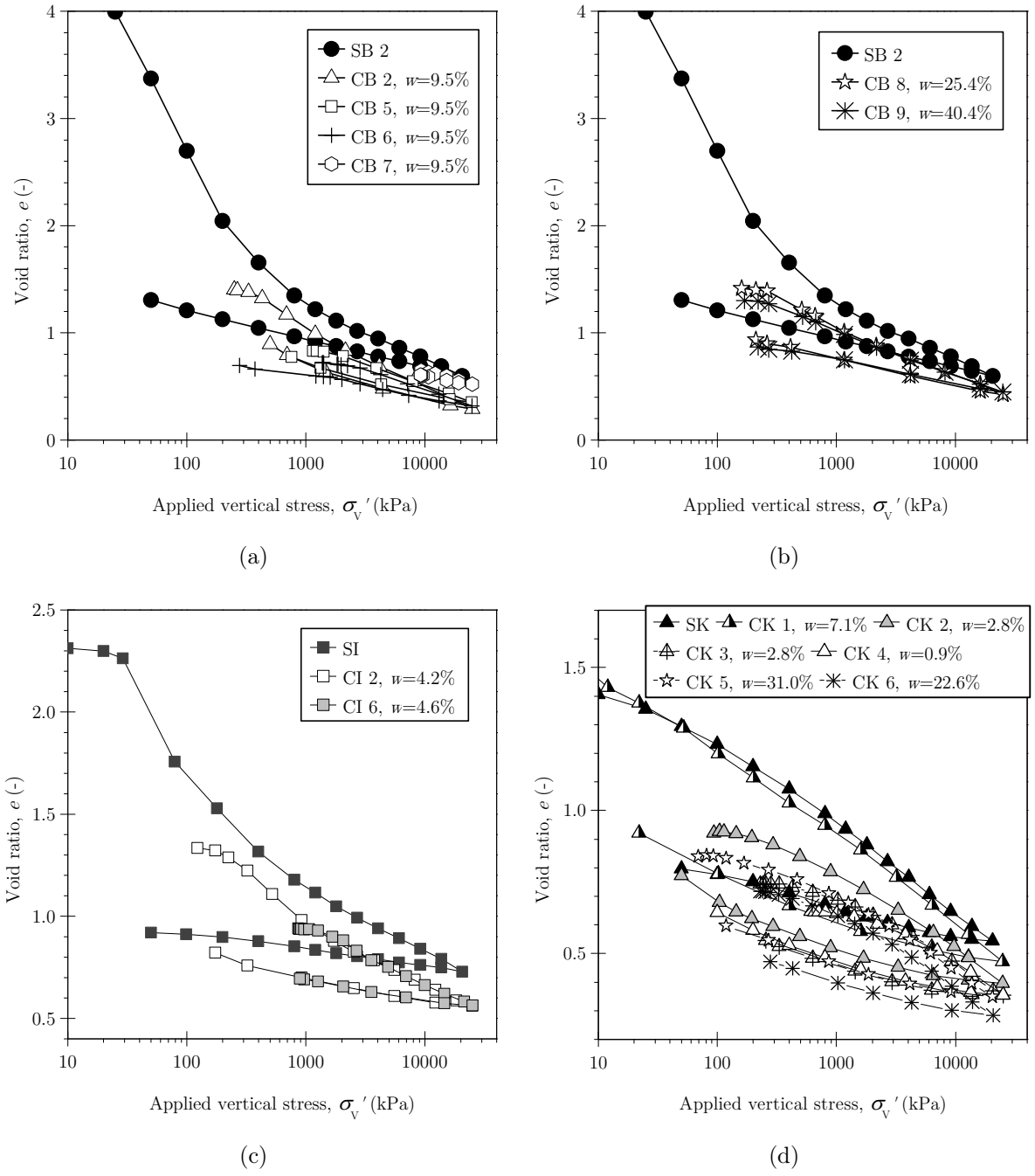

Figure 6.4.: Compressibility behaviour of the compacted saturated specimens:(a) Calcigel bentonite with initial water content 9.5%, (b) Calcigel bentonite with initial water content 25.4% and 40.4%, (c) NX illite, (d) Spergau kaolin.

smaller pressures immediately after the measured swelling pressures. At higher stresses, the path was found to be curved and concave upward for CI 2, whereas the concavity was less distinct for specimen CI 6. The shape of the decompression paths of CI 2 and CI 6 was indistinct; the path of CI 6 was nearly linear; the one of CI 2 was slightly curved and concave upward at stresses lower than about 1 MPa. The decompression path of SI was found to be linear at higher stresses, and slightly curved and concave downward at stresses smaller than about 900 kPa. Further, at stresses greater than about 2 MPa, the compression-decompression path of CI 6 is more or less identical to that of CI 2, despite the difference in the initial dry density.

Again, the compression-decompression paths of the compacted saturated specimens CK 2 to 6 were found to remain below that of the initially saturated specimen SK. The compression path of specimen CK 1 remained close to that of specimen SK; CK 1 was found to run parallel and slightly below of SK at vertical stresses greater than about 100 kPa. Except specimen CK 1, which showed a nearly linear behaviour, the compression paths of the compacted Spergau kaolin specimens were found to be curved and downward concave at lower stresses (until about 400 kPa for CK 2 and until about 3 MPa for CK 4), whereas at higher stresses the e-$\log \sigma'_{\mathrm{v}}$ relationships of the compacted saturated specimens were found to be linear. The decompression paths of the compacted specimens were showing an upward oriented concavity. In case of specimens CK 5 and 6, both having higher initial water content of $w = 31.0\%$ and $w = 22.6\%$, respectively, the concavity is less distinct at smaller stresses less than 800 kPa. The upward oriented concavity of the decompression line of the initially saturated specimen SK was found to turn into a slightly concave downward curved line at stresses smaller than about 400 kPa. The deformations of both the initially saturated and the compacted saturated specimens were found to be irreversible, even at high stresses.

6.5. Compression indices

In the following section, the compression and decompression indices (C_{c} and C_{s} values) determined from the oedometer compression tests of the initially saturated as well as of the compacted saturated clay specimens will be presented and discussed. Table 6.1 contains the experimentally determined values of the compression and decompression indices for each specimen, whereas in Table 6.2 the calculated compression and decompression indices based on relationships with plasticity index, I_{P}, and liquid limit, w_{L}, are presented. The experimental C_{c} and C_{s} values were determined by linearization of the equivalent e-$\log \sigma'_{\mathrm{v}}$

plot. Additionally to the specimens tested in the high stress cell, the compression indices of the initially saturated Calcigel bentonite specimen SB 3, which was tested in a standard oedometer device, will be also presented. The C_c values for Calcigel bentonite specimens

Table 6.1.: Compression and decompression indices of Calcigel bentonite, Spergau kaolin and NX illite

Calcigel bentonite								
Sp.	SB 2	SB 3	CB 2	CB 5	CB 6	CB 7	CB 8	CB 9
C_c	1.88[a], 0.53[b]	1.93[c]	0.53	0.40	0.37	0.32	0.44	0.42
C_s	0.26	0.24[d], 0.19[e]	0.28	0.22	0.20	0.19	0.25	0.23
Spergau kaolin								
Sp.	SK	CK 1	CK 2	CK 3	CK 4	CK 5	CK 6	
C_c	0.26[f], 0.33[b]	0.29[f], 0.32[b]	0.28	0.27	0.28	0.28	0.28	
C_s	0.10	0.11	0.11	0.10	0.11	0.11	0.10	
NX illite								
Sp.	SI	CI 2	CI 6					
C_c	0.63[g], 0.35[b]	0.50[h], 0.29[i]	0.28					
C_s	0.09	0.11	0.09					

[a] C_c for stresses from 10 to 400 kPa; [b] C_c for stresses >800 kPa; [c] C_c from 7 to 400 kPa;

[d] C_s at vertical stress of 800 kPa; [e] C_s at vertical stress of 100 kPa;

[f] C_c from 100 to 400 kPa; [g] C_c from 80 to 400 kPa;

[h] C_c from 223 to 923 kPa; [i] C_c for stresses >923 kPa

SB 2 and SB 3 within a vertical stress of 400 kPa were found to be 1.88 and 1.93, respectively. These values were found to be in agreement with the reported range of C_c values (1.0 to 2.6) for bentonites with various exchangeable cations (Lambe & Whitman 1969). On the other hand, for specimen SB 2, a C_c value of 0.53 was obtained for stresses greater than 800 kPa. The compression index calculated using Skempton's correlation for remoulded and undisturbed soils was found to be 1.18 and 1.51, respectively. Again, from a relationship with plasticity index ($C_c = I_P/74$, where I_P is the plasticity index) (Mitchell 1993), C_c was found to be 1.65. Although the latter two values are close to the values obtained from experimental results for stresses smaller than 400 kPa, at stresses greater than 800 kPa the results suggest that the correlation of compression index with soil plasticity has limited applications. The compression index for specimen SB 2 (1.88)

Table 6.2.: Calculated compression and decompression indices for Calcigel bentonite, Spergau kaolin and NX illite as a function of plasticity index, I_P, and liquid limit, w_L

	Calcigel bentonite	Spergau kaolin	NX illite
$C_c = I_P/74$ [a]	1.65	0.31	0.61
$C_c = 0.007(w_L - 10\%)$ [b]	1.18	0.30	0.47
$C_c = 0.009(w_L - 10\%)$ [c]	1.51	0.39	0.61
$C_s = I_P/370$ [a]	0.33	0.06	0.12

[a] C_c-I_P and C_s-I_P relationship (Mitchell 1993)

[b] C_c-w_L relationship (Skempton's relationship) for remoulded soils

[c] C_c-w_L relationship (Skempton's relationship) for undisturbed soils

within a stress of 400 kPa was found to be greater than Ca Fourges clay (1.0) and smaller than Na Kunigel (4.18) and Na-Ca MX80 (5.22), reported by Marcial et al. (2002). Similarly, at stresses greater than 800 kPa, the C_c value of specimen SB 2 (0.53) was found to be greater than Ca Fourges (0.25), Na Kunigel (0.26), and Na-Ca MX80 (0.42). The differences in the C_c values for the bentonites for pressures smaller than 400 kPa are in concurrent with the liquid limits of the clays, mineralogical composition, and type and amount of exchangeable cations present in the clays. At higher stresses, the range of stress considered to determine C_c was suspected to significantly affect the compression index of the bentonites. This is because the determination of the exact stress at which the transition from a steeper slope to a moderate slope occurs was found to be indistinct in the e-log σ'_v plot.

The C_c value for specimen SB 2 for vertical stresses smaller than 400 kPa was found to be much greater than those of the compacted specimens (Table 6.1). Therefore, the C_c values of the compacted saturated specimens were compared with the C_c of specimen SB 2 at vertical pressure greater than 800 kPa (0.53). For the specimens compacted at water content of 9.5%, the compression index for the entire applied range of stress was found to vary within 0.32 to 0.53 with the least value obtained for CB 7. The C_c values were found to be smaller than that of specimen SB 2, except CB 2 that showed a similar compression index to that of SB 2. For the same initial water content (specimens CB 2, 5, 6, and 7), an increase in the dry density caused a decrease in the compression index. Similarly, the C_c values were also found to be affected by the initial water content of the specimens. The compression index of specimen CB 8 ($w = 25.4\%$) was 0.44, whereas the C_c value of specimen CB 2 ($w = 9.5\%$) was 0.53. This indicates that initial compaction conditions

have a significant influence on the compressibility of compacted saturated bentonites. At higher stresses, the decreased particle spacing increases the repulsive forces in clays that offer a greater resistance to compressive stresses (Sridharan, Rao & Murthy 1986). The repulsive forces at smaller particle spacing may also stem from various mechanisms other than the double layer repulsion, i.e., Born's repulsion and hydration forces (Tripathy & Schanz 2007).

The C_c values of the initially saturated Spergau kaolin specimen were determined for a stress range from 100 to 400 kPa and greater than 800 kPa and were 0.26 and 0.33, respectively. The C_c value at lower stresses was in agreement with the reported range of C_c values from 0.19 to 0.26 for kaolinites with different exchangeable cations (Lambe & Whitman 1969), whereas the C_c value for stresses greater than 800 kPa was slightly higher than the values reported in Lambe & Whitman (1969). The experimental C_c values (0.26 and 0.33) were also found to be close to the values obtained from correlation with plasticity index (0.31) and liquid limit (0.30 and 0.39), even at higher stresses greater than 800 kPa (see Tables 6.1 and 6.2).

The C_c values of the compacted saturated specimen CK 1 (0.29 and 0.32) were found to be similar to that of specimen SK in the equivalent stress range. The C_c values of specimens CK 2, CK 4, CK 5, CK 6, and of specimen CK 3 were 0.28 and 0.27, respectively. These values were also similar to those calculated from correlation with I_P (0.31) and Skempton's relationship for remoulded soils (0.30). Further, the C_c values for the compacted Spergau kaolin specimens were nearly identical, except for CK 1. The C_c value of CK 1 with a very low initial dry density of 0.93 Mg/m^3 was 0.32 (for stresses $>$ 800 kPa), which is only slightly higher than the C_c values of CK 2, CK 3, CK 4, CK 5, and CK 6. This indicates that at least in the dry density range represented by CK 2, CK 3, CK 4, CK 5, and CK 6, the compression indices were not affected by the differences in initial dry density. Ignoring the small differences in initial dry density, the C_c values of CK 5 ($\rho_d = 1.42$ Mg/m^3, $w = 31.0\%$) and CK 2 ($\rho_d = 1.37$ Mg/m^3, $w = 2.8\%$) and of CK 6 ($\rho_d = 1.52$ Mg/m^3, $w = 22.6\%$) and CK 3 ($\rho_d = 1.50$ Mg/m^3, $w = 2.8\%$) can be compared. Despite the higher water contents of CK 5 and CK 6, their C_c values (0.28) were found to be nearly the same as those of CK 2 (0.28) and CK 3 (0.27). The results indicate that, contrary to Calcigel bentonite, the C_c value was not affected by the initial water content.

In case of NX illite, the compression indices were determined for the initially saturated specimen SI and for the compacted specimens CI 2 and CI 6, which had different initial dry densities (1.16 and 1.39 Mg/m^3, respectively), but nearly the same water content

(4.2 and 4.6%). For specimen SI, the C_c values were found to be 0.63 in the stress range from 80 to 400 kPa and 0.35 at stresses greater than 800 kPa. The C_c value at lower stresses (0.63) was found to be in agreement with the reported range of C_c values (0.5 to 1.1) for illite clays with various exchangeable cations (Lambe & Whitman 1969), whereas C_c determined at higher stresses (0.35) was smaller than the C_c range given in literature (Lambe & Whitman 1969). Similarly, the C_c value of 0.63 was found to be close that obtained from correlation with plasticity index and from Skempton's relationship for undisturbed soils (0.61 both), whereas the C_c value determined at stresses greater than 800 kPa was smaller than the values obtained from the correlations (see Tables 6.1 and 6.2).

The compression index determined for compacted illite specimen CI 2 at stresses smaller than 923 kPa was found to be 0.50, which is close to the C_c value calculated using Skempton's relationship for remoulded soils (0.47). The C_c values determined for both compacted specimens within stresses up to 25 MPa were nearly identical (0.29 and 0.28). Thus, the different initial dry densities of CI 2 and CI 6 did not affect the C_c values. No NX illite specimen with higher initial water content was tested here; therefore, no statement with respect to the effect of higher initial water content can be made.

6.6. Decompression indices

The swelling index (i.e., slope of the e-$\log \sigma'_v$ plot during unloading or decompression) is presented in this study as the decompression index, C_s (Table 6.1). The decompression indices for the compacted specimens of the three clays are corresponding to a maximum applied vertical pressure of 25 MPa.

For Calcigel bentonite, the decompression indices for specimen SB 3 (which was tested in a conventional oedometer) are corresponding to vertical pressures of 800 kPa ($C_s = 0.24$) and 100 kPa ($C_s = 0.19$), whereas for specimen SB 2, the value shown ($C_s = 0.26$) is corresponding to the vertical pressure of 21 MPa. For specimens CB 2 to CB 7, the C_s value decreased slightly with an increase in the initial dry density. The C_s value of specimen CB 7 was found to be the least (i.e., 0.19), identical to that for specimen SB 1, unloaded at 100 kPa. It is to be noted that specimen CB 7 had a swelling pressure of 9.2 MPa. Specimens CB 2 and CB 8 had nearly the same initial dry density with different initial water contents. The results indicated that the decompression index slightly decreased with an increase in the initial water content for these specimens. The initial dry density and water content of specimen CB 9 were greater than that of CB 8; however,

it showed a lesser C_s than that of specimen CB 8. The results showed that the initial dry density and water content slightly affected the decompression index for the specimens tested. The C_s values for montmorillonites with different exchangeable cations in various electrolyte concentrations are shown to vary from 0.03 to 3.6 (Olson & Mesri 1970). The decompression index value reported by Olson & Mesri (1970) for calcium montmorillonite in 10^{-3} M bulk solution is 0.34. Following the relationship $C_s = I_P/370$ (Olson & Mesri 1970), a decompression index of 0.33 was obtained. The experimental C_s value of specimen SB 3 was found to be 0.26 that is somewhat smaller as compared to the above values. The decompression behaviour was found to be in accordance with Mesri & Olson (1971)'s test results on Ca montmorillonites. The decompression indices calculated from their results are 0.24 to 0.26 corresponding to a void ratio increase from about 1.25 to 2.0, and for a pressure decrease from about 3000 kPa to 1.6 kPa, similar to the values reported in this study. The C_s values for specimen SB 1 that was unloaded at two different pressure levels (i.e., 100 kPa and 800 kPa) were found to be 0.19 and 0.24 (Table 6.1). These values are somewhat smaller than that obtained from the decompression path of specimen SB 3 (i.e., 0.26). The variation of C_s for specimens SB 1 of 0.19 and 0.24 signifies that the microstructure of bentonites is affected by the maximum supported stress and is primarily attributed to the difference in fabric and structure of the clay, according to the maximum supported stress. The C_s values for all specimens tested in this study also indicated that the irregularities in the fabric and the structure of the clay owing to the initial compaction conditions were eliminated to a great extent once the bentonite specimens were subjected to very large pressures.

For Spergau kaolin, the C_s values were found to be 0.10 (SK, CK 3 and CK 6) and 0.11 (CK 1, CK 2, CK 4, and CK 5), thus, they are nearly identical for all Spergau kaolin specimens tested. Obviously, the initial dry density and water content did not affect the decompression index. The C_s values for kaolinites with different exchangeable cations in various electrolyte concentrations are shown to vary from 0.05 to 0.08 (Olson & Mesri 1970). The decompression index value reported by Olson & Mesri (1970) for calcium kaolinite in 10^{-4} M bulk solution is 0.07. Following the relationship $C_s = I_P/370$ (Mitchell 1993), a decompression index of 0.06 was obtained. The experimental C_s values of the Spergau kaolin specimens were found to be 0.10 and 0.11 that is somewhat greater as compared to the above values.

In case of NX illite, the experimental decompression indices were found to be 0.09 (SI, CI 6) and 0.11 (CI 2). An influence of the initial dry density and water content can not be detected from these results. The decompression indices given in Olson & Mesri (1970)

for illites with different exchangeable cations in various electrolyte concentrations range from 0.04 to 0.65. The C_s value reported by Olson & Mesri (1970) for calcium illite in 10^{-3} M bulk solution is 0.31. Lambe & Whitman (1969) provides C_s values in the range of 0.1 to 0.27 for illites with varying exchangeable cations and with varying liquid and plastic limits. 0.21 and 0.18 are the C_s values reported for a calcium illite ($w_L = 100\%$, $w_P = 45\%$) and a magnesium illite ($w_L = 94\%$, $w_P = 46\%$), respectively. Following the relationship $C_s = I_P/370$ (Mitchell 1993), a decompression index of 0.12 was obtained. The experimentally determined decompression indices fit well into the range reported in literature and they are nearly equal to the C_s value obtained with the relationship $C_s = I_P/370$ (Mitchell 1993).

6.7. Coefficient of consolidation

The coefficient of consolidation, c_v, was determined from the corrected time-compression plots for all specimens tested, following Casagrande's log-time method. The results are presented in c_v versus $\log \sigma'_v$ plots and in c_v versus e plots in Fig. 6.5 and 6.6, respectively.

For initially saturated Calcigel bentonite (Figs. 6.5a and 6.6a), it was noted that c_v decreased and further increased with an increase in the vertical stress or a decrease in the void ratio for the initially saturated specimens SB 1 and SB 2. Similar observation has been reported by Marcial et al. (2002) for other bentonites under similar testing conditions.

In case of compacted saturated specimens, with an increase in the vertical pressure or a decrease in the void ratio, c_v decreased and then remained nearly constant. At any given vertical pressure and void ratio, the higher the compaction dry density, the greater is c_v (specimens CB 2, CB 5, CB 6 and CB 7). Similarly, an increase in the water content was found to reduce c_v (CB 8 and CB 9). The effect of initial compaction conditions on c_v was found to be nearly indiscernible at void ratios smaller than 0.5 indicating that there was a tendency of the bentonite specimens to attain similar fabric and structure at large pressures.

The c_v values of the initially saturated and the compacted saturated NX illite specimens were found to decrease and then increase with an increase in vertical stress (Fig. 6.5b) or a decrease in void ratio (Fig. 6.6b), where the initial decrease of c_v is less significant for the compacted saturated specimens CI 2 and CI 6. At void ratios smaller than 0.8, the c_v values of the three specimens fall together on the same line, but were found to linearly increase with decreasing void ratio.

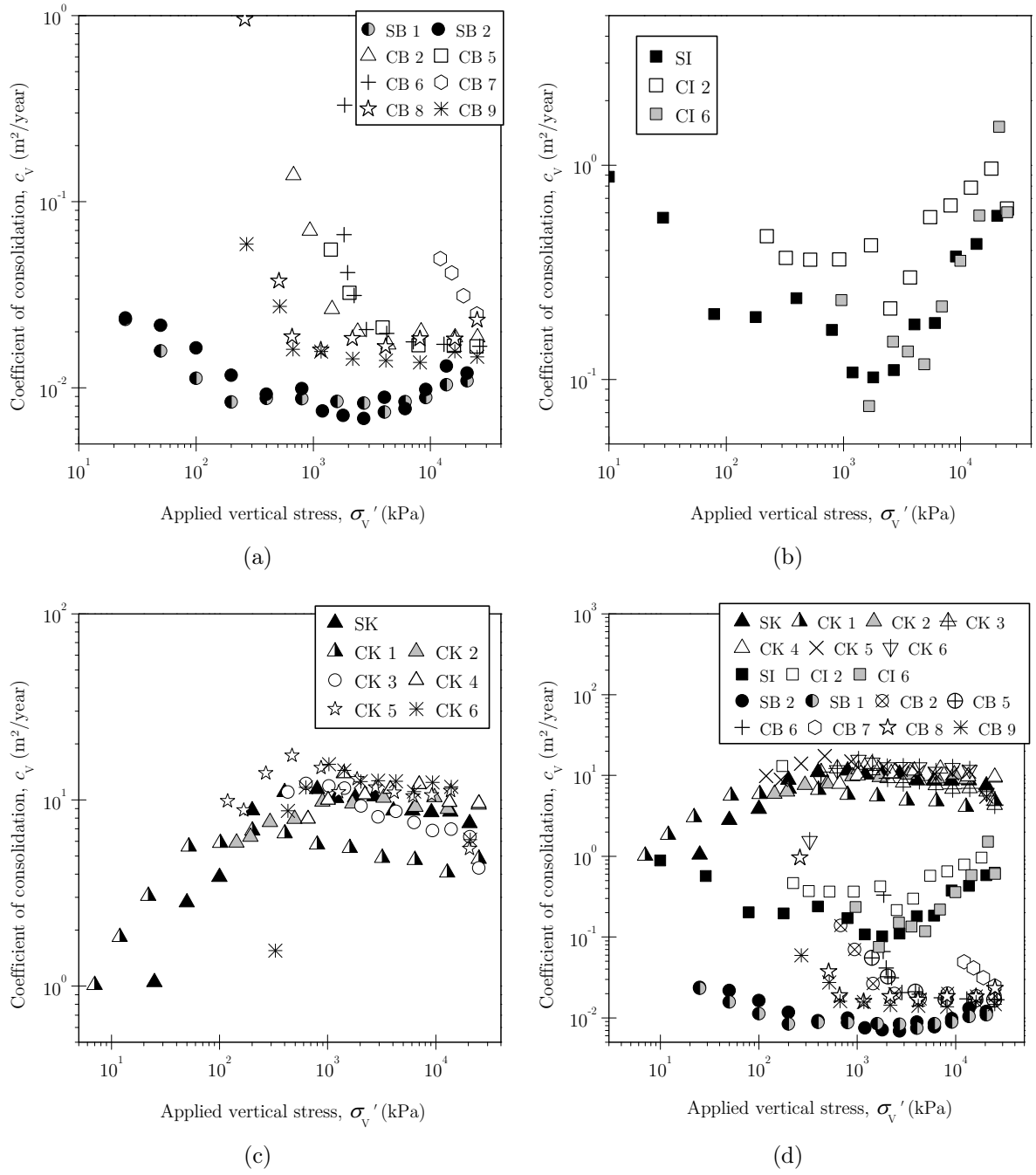

Figure 6.5.: Effect of vertical pressure on coefficient of consolidation: (a) Calcigel bentonite, (b) NX illite, (c) Spergau kaolin, (d) comparative plot of the three clays.

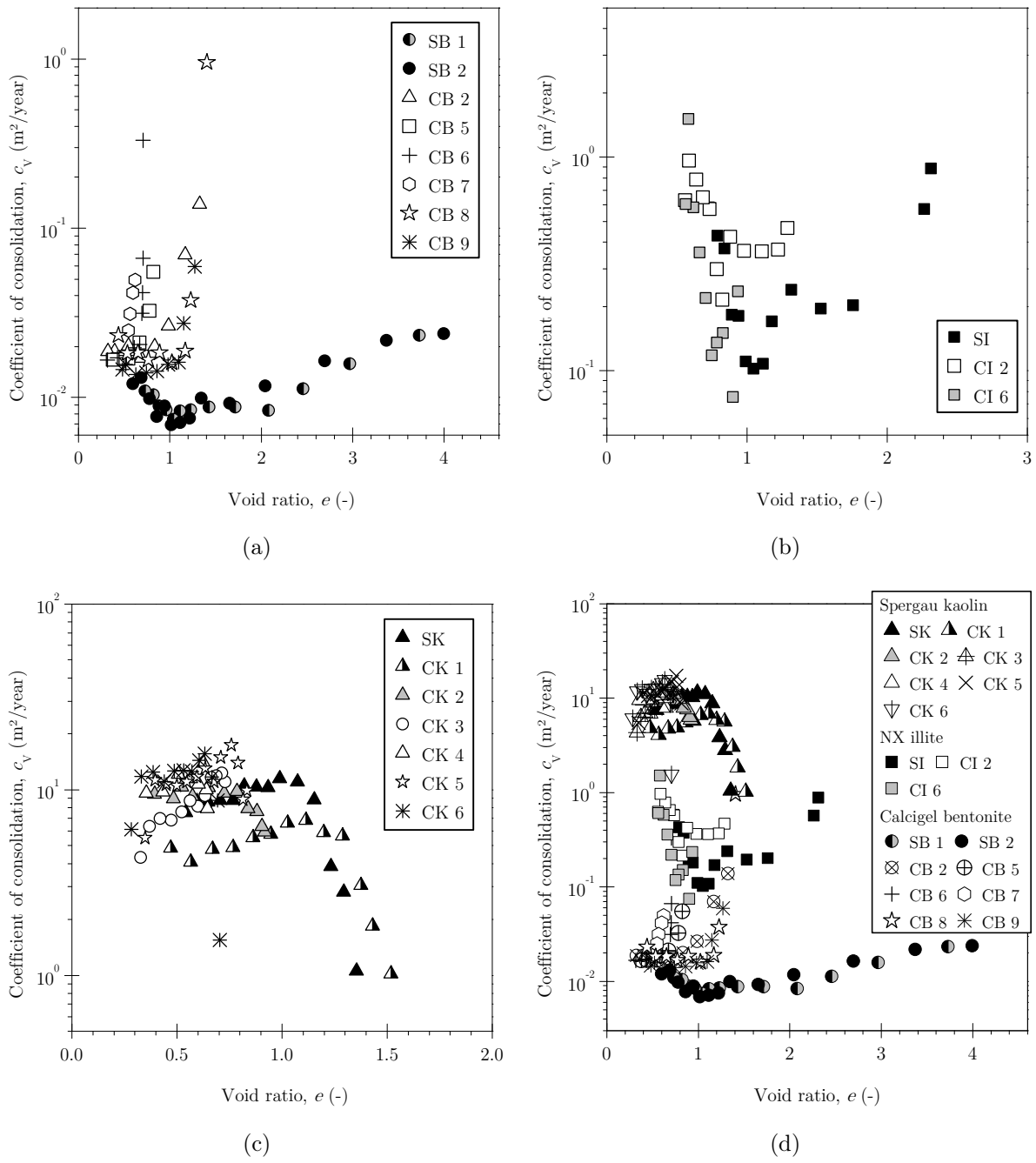

Figure 6.6.: Effect of void ratio on coefficient of consolidation: (a) Calcigel bentonite, (b) NX illite, (c) Spergau kaolin, (d) comparative plot of the three clays.

Spergau kaolin did show a somewhat different behaviour: the c_v values increased with an increase in vertical stress or a decrease in void ratio and further slightly decreased at vertical stresses greater than 500 to 1000 kPa or at void ratios smaller than 1.2 to 0.6 (Figs. 6.5c and 6.6c). An initial increase in c_v-value with decreasing void ratio is not reported in literature. The inaccuracy of the device in controlling the stresses for the initial loading steps is greater, this might cause a greater error in the determination of the c_v-value. A slightly greater scatter between the c_v-values of Spergau kaolin as compared to Calcigel bentonite and NX illite at very small void ratio was observed. Overall, no general tendency for an influence of the initial compaction conditions on the c_v value was found.

Figs. 6.5 and 6.6 show the comparative plot for the three clays. Qualitatively, differences in the shapes of the curves of the three clays can be recognized. Whereas the curves of Calcigel bentonite and NX illite are concave upwards, the points of Spergau kaolin result in a downwards oriented concave curve. For void ratios smaller than about 1, a slight decrease of c_v-value was observed. Quantitatively, over the range of vertical stresses applied and for the whole range of void ratio, Spergau kaolin shows the greatest c_v value, followed by NX illite and Calcigel bentonite. The results obtained are in concurrent with the Atterberg limits and clay mineralogy of the clays. The c_v value is the key parameter for estimating the rate of dissipation of pore pressures. It is related by eq. 6.1 to the coefficient of permeability k, the void ratio e_0, and the coefficient of compressibility a_0, defined as $-\frac{\Delta e}{\Delta \sigma'}$. Since a_0 is interrelated to the coefficient of volume compressibility m_v and the stiffness E_S, eq. 6.1 can be also written in the form of eq. 6.2 or eq. 6.3, respectively. The unit volume weight of water γ_w is assumed to be constant.

$$c_v = \frac{k(1+e)}{\gamma_w a_0} \tag{6.1}$$

$$c_v = \frac{k}{\gamma_w m_v} \tag{6.2}$$

$$c_v = \frac{k E_S}{\gamma_w} \tag{6.3}$$

From eq. 6.3 it follows that coefficient of consolidation c_v should increase with increasing permeability k and increasing stiffness E_S.

6.8. Coefficient of permeability

The coefficient of permeability, k, was computed from the values of coefficient of volume compressibility, m_v and the c_v values, for each incremental pressure. The results are presented in k versus e plots for each clay type individually (Fig. 6.7a to 6.7c), as well as in a comparative plot (Fig. 6.7d).

The void ratio-k relationships for specimens SB 1 and SB 2 were found to be distinctly bilinear (Fig. 6.7a). A rapid decrease in the permeability of specimens SB 1 and SB 2 was observed at void ratio of about 1.7. The permeability for the initially saturated bentonite varied between 10^{-10} m/s and 10^{-14} m/s for a pressure range between 0.025 MPa (corresponding to $e = 4$) and 21 MPa (corresponding to $e = 0.6$). The permeability of the compacted saturated specimens varied between 10^{-11} m/s and 10^{-14} m/s. At any void ratio, the permeability of the initially saturated specimens was found to be lower than that of the compacted saturated specimens indicating that compacted saturated bentonite is more permeable than the initially saturated bentonite. The void ratio-k relationships for the compacted saturated specimens were found to be nearly linear. In general, within the range of pressure and void ratio considered for the compacted saturated specimens, the variation of permeability was found to be about an order of magnitude for a decrease in the void ratio of 0.4.

The void ratio-k relationship obtained for the initially saturated specimen SI as well of the compacted saturated specimen CI 2 was found to be linear, whereas no distinguished shape can be attributed to the void ratio-k relationship of specimen CI 6. This is attributed to the high initial dry density and high stiffness of this specimen: the experimental points were found to be in a narrow void ratio range between 1 and 0.5, where the coefficient of permeability varied between $6 \cdot 10^{-13}$ m/s and 10^{-13} m/s. The permeability for specimen SI varied between 10^{-9} m/s and 10^{-12} m/s for a pressure range between 0.025 MPa (corresponding to $e = 2.3$) and 21 MPa (corresponding to $e = 0.7$). At any void ratio, the permeability was highest for the compacted saturated specimen CI 2, followed by the initially saturated specimen SI and the compacted saturated specimen CI 6.

The compacted saturated specimens as well as the initially saturated specimen of Spergau kaolin showed distinct linear void ratio-k relationships (Fig. 6.7c). Except for specimen CK 1, the coefficient of permeability of the compacted saturated specimens was found to be higher than that of the initially saturated specimen throughout the whole void ratio range. The permeability for the initially saturated bentonite varied between 10^{-9} m/s

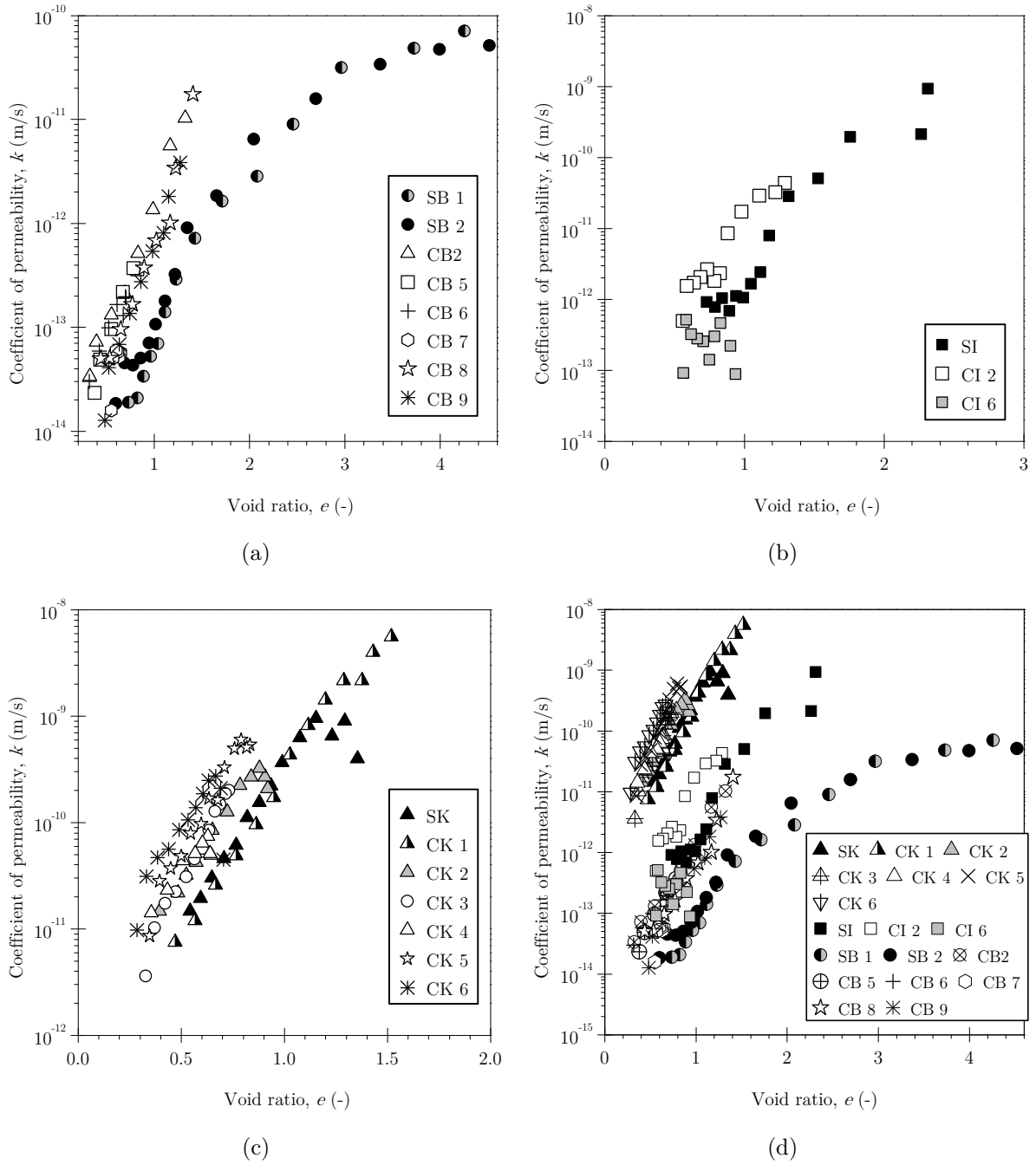

Figure 6.7.: Void ratio versus coefficient of permeability: (a) Calcigel bentonite, (b) NX illite, (c) Spergau kaolin, (d) comparative plot of the three clays.

and 10^{-11} m/s for a pressure range between 0.025 MPa (corresponding to $e = 1.15$) and 21 MPa (corresponding to $e = 0.55$).

The comparative plot (Fig. 6.7d) reveals that at any void ratio, the coefficient of permeability of the initially saturated specimens is highest for Spergau kaolin followed by NX illite and Calcigel bentonite. The same is valid for the compacted saturated specimens: k is highest for Spergau kaolin, smallest for Calcigel bentonite.

Beside the quantitative differences in the determined permeability values, the difference in shape of the void ratio-k relationship of the initially saturated specimens of the three clays is remarkable. The linear behaviour of the e-k curve of Spergau kaolin and NX illite indicate that the decrease in permeability is due to the reduction of the available pore space due to compression. With increasing vertical stress, the void ratio, i.e., the pore space available for saturated flow decreases proportionally. In case of Calcigel bentonite, the bilinear behaviour reflects the increase in stiffness at high stresses or low void ratios.

6.9. Summary

The swelling pressures and one-dimensional compressibility behaviour of compacted clays were studied. Several initial compaction conditions of the clays were considered. A newly developed high stress oedometer device was used to measure the swelling pressures of compacted specimens upon saturation under constant volume condition. Further, the compacted saturated specimens were submitted to one cycle of loading and unloading. The maximum applied vertical stress during the consolidation tests was 25 MPa. The void ratio-swelling pressure data and the compression-decompression paths of the compacted saturated specimens were compared with the compression-decompression path of the corresponding initially saturated clay specimen subjected to a maximum vertical pressure of 20.6 MPa. The effects of initial compaction conditions and the vertical pressures on the compression index, the decompression index, the calculated coefficient of consolidation, and the saturated coefficient of permeability were brought out in detail. The following conclusions were drawn from the study.

The void ratio-swelling pressure data and the corresponding compression paths of the compacted saturated Calcigel bentonite specimens remained distinctly below that of the void ratio-vertical pressure compression path of the initially saturated specimen even at very large pressures. The differences in the void ratios of the compacted saturated specimens and the initially saturated specimen at pressures smaller than 1000 kPa is attributed

to the differences in the micro- and macro-structural void ratios of the initial saturated and compacted saturated specimens, whereas at pressures greater than 1000 kPa, the void ratio differences are primarily due to the dissimilar interlayer void ratios. Similarly, compression paths of the compacted saturated NX illite and Spergau kaolin specimens remained in general distinctly below that of the void ratioŰvertical pressure compression path of the initially saturated specimen even at very large pressures. This is attributed to the compaction conditions of the specimens with density values above the Proctor curve.

The e-$\log \sigma'_{\mathrm{v}}$ relationship for the initially saturated Calcigel bentonite specimen subjected to a vertical pressure of 21 MPa showed two distinctly different values of C_{c} similar to that reported in the literature. The e-$\log \sigma'_{\mathrm{v}}$ relationships for compacted saturated bentonite specimens were found to be nearly linear for the range of pressure considered in the study. The C_{c} values of the compacted saturated bentonite specimens were found to decrease from 0.53 to 0.32 with an increase in the initial dry density from 1.17 $\mathrm{Mg/m^3}$ to 1.70 $\mathrm{Mg/m^3}$. On the other hand, the initial compaction conditions marginally affected the decompression index that remained between 0.19 and 0.26 indicating that the influence of initial compaction conditions on the fabric and structure of bentonite was very nearly eliminated at large pressures.

The e-$\log \sigma'_{\mathrm{v}}$ relationship for the initially saturated Spergau kaolin specimen showed that the C_{c} values were only slightly affected by the stress range. For the initially saturated NX illite specimen, a bilinear behaviour was observed, where the C_{c} value was found to halve in the high stress range. For the compacted saturated Spergau kaolin and NX illite specimens, the C_{c} values were only marginally affected by the initial compaction conditions. Likewise, no effect on the decompression index was found, indicating that the influence of initial compaction conditions on the fabric and structure of Spergau kaolin and NX illite was very nearly eliminated at large stresses.

The compression indices of the initially saturated clay specimens were found to be in concurrent with the liquid limits of the clays, mineralogical composition, and type and amount of exchangeable cations present in the clays. For Calcigel bentonite and NX illite, only the compression indices determined at lower stresses were found to be comparable with those calculated from correlations with plasticity index or liquid limit, whereas in case of Spergau kaolin all C_{c} values determined were found to be close to the calculated ones.

In case of Calcigel bentonite, with an increase in the applied pressure or a decrease in the void ratio, c_{v} was found to decrease for both initially saturated specimen and compacted saturated specimens; however, at large pressures, c_{v} increased for the initially saturated

specimen, whereas it remained nearly constant for the compacted saturated specimens. The effect of initial compaction conditions on c_v was found to be nearly indiscernible at void ratios smaller than 0.5 indicating the similarity in the fabric and structure of the bentonite specimens at very large pressures. Qualitatively, a similar behaviour was found for the NX illite specimens, with c_v values being about an order of magnitude greater than those of Calcigel bentonite. The behaviour was found to be different for Spergau kaolin, where the c_v-value was found to decrease and with increasing applied pressure or a decrease in the void ratio; the initial increase of c_v-value observed for the specimens with smaller dry density require a verification.

The variation of coefficient of permeability with the void ratio was found to be distinctly bilinear for the initially saturated Calcigel bentonite specimen, whereas for the compacted saturated specimens the relationship was found to be nearly linear and remained within a narrow band. The coefficient of permeability of NX illite and Spergau kaolin were found to vary linearly with void ratio within a band. For the three clays studied, the compacted saturated specimens were found to be more permeable than the initially saturated specimens at all void ratios considered in this study.

7. Effect of loading type and mineralogy on volume change in clays

7.1. General

In this chapter, the volume change behaviour of Calcigel bentonite, NX illite and Spergau kaolin are compared. The initially saturated clays were subjected to either a change in total axial stress in k_0 condition or an increase in suction. The effect of loading type and the effect of clay mineralogy on the observed volume change behaviour both at low and high applied stresses and suctions are brought out. The results obtained are discussed in the context of fabric investigations by environmental scanning microscopy (ESEM) and mercury intrusion porosimetry (MIP) at initially saturated state, at shrinkage limit and at different applied vertical stresses.

7.2. Fabric of the initially saturated clays

Before the presentation and discussion of the observed volume change behaviour, the following paragraphs are dedicated to the description of the initial fabric of the clays at saturated state. Fig. 7.1 shows the photomicrographs of the initially saturated clays, i.e., at water content corresponding to $1.1w_{\mathrm{L}}$. Figs. 7.2, 7.3 and 7.4 illustrate the different levels of fabric from particles formed by layers up to the aggregates, for Spergau kaolin, NX illite and Calcigel bentonite, respectively. Fig. 7.5 provides a comparative illustration of the fabric of the three clays at initially saturated state.

Figs. 7.1a and 7.1b show the photomicrographs of Spergau kaolin. About 20 kaolinite particles of a thickness of 25 to 75 nm and a length of about 500 to 1600 nm are arranged

face-to-face to form the aggregate of a thickness of about 250 to 1200 nm. Considering a layer-to-layer thickness of 0.72 nm for kaolinite (Grim 1968), the particle thickness of Spergau kaolin corresponds to a number of 35 to 100 layers per particle. Large pores of a diameter of more than 2000 nm as well as smaller pores having about 200 to 600 nm diameter exist. Pore space between particles inside an aggregate seems to be negligible. The dashed lines designate borders of aggregates in edge-to-face contact.

An illite particle (see Fig. 7.3) is composed of only up to 10 layers and has a length of about 250 nm. Few particles form an aggregate of a lateral extension of about 400 nm and a thickness of not more than 100 nm (Grim 1968, Tessier 1984). In the photomicrographs of NX illite (Fig. 7.1c and Fig. 7.1d), aggregates of thickness ranging from 60 to 500 nm were found. Further, the smaller size of the NX illite aggregates as compared to the Spergau kaolin aggregates can be recognised. The irregular particle arrangement creates a pore space inside the aggregate of about 3 nm extension (Quirk & Aylmore 1971). The lateral extension of the aggregates is about 350 nm and the thickness is about 100 nm. Pores having a diameter of about 100 to 500 nm were found between the aggregates.

The appearance of the Calcigel bentonite slurry (see Fig. 7.1e) corresponds well to the model established by Ben Rhaïem et al. (1987) for Ca-smectites, where quasi-crystals of montmorillonite form a three-dimensional network and separate large pores from each other (see Fig. 7.4). In Fig. 7.1e, arrows indicate the quasi-crystals as walls of the pores, and bars indicate the dimension of the large pores, the latter were found to be about 1000 nm in size. According to Ben Rhaïem et al. (1987), the quasi-crystal of Ca-montmorillonite is constituted by approximately 50 layers, which again are organised in parallel array in substacks composed by about 7 hydrated layers (Ben Rhaïem et al. 1987). It is possible that one particular layer is interleaved in more than one "pile" of juxtaposed layers and the perfect overlap of adjacent layers may be interrupted by discontinuities. The interleaving of quasi-crystals of Calcigel bentonite is visible in Fig. 7.1f.

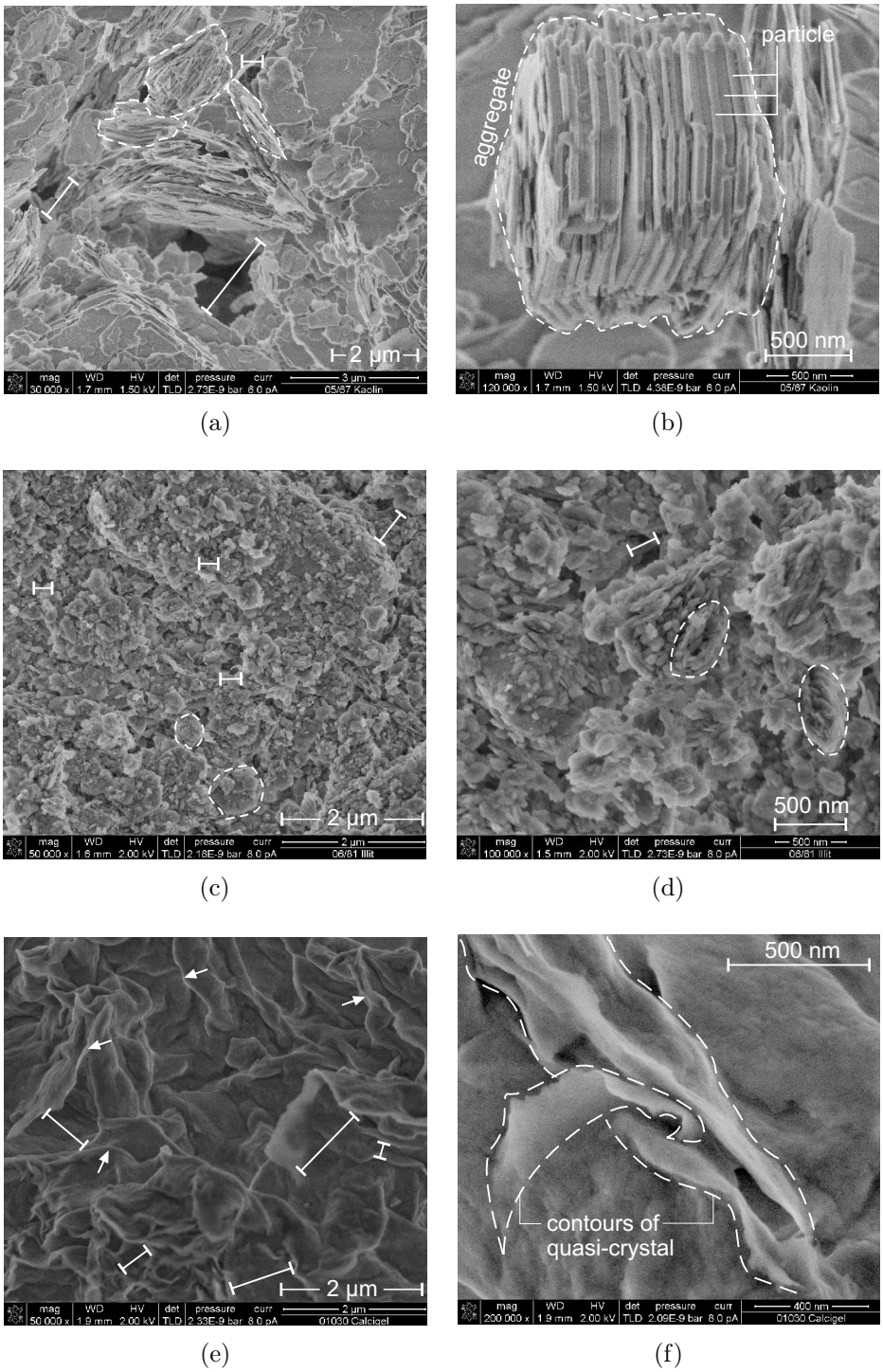

Figure 7.1.: ESEM photomicrographs at initially saturated state corresponding to $1.1w_{\mathrm{L}}$ [dashed lines: boundary of an aggregate; arrows: point towards quasi-crystals forming walls of large pores; bars: extension of voids]: (a), (b) Spergau kaolin; (c), (d) NX illite; (e), (f) Calcigel bentonite.

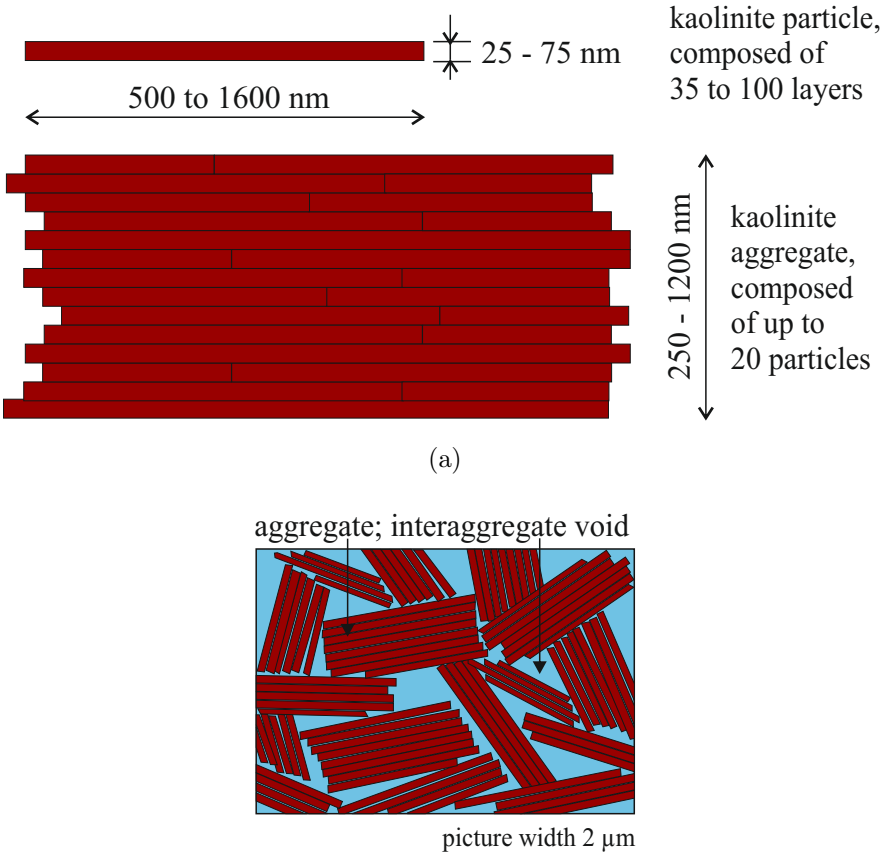

Figure 7.2.: Schematic of kaolinite fabric: (a) particle and aggregate, (c) global fabric.

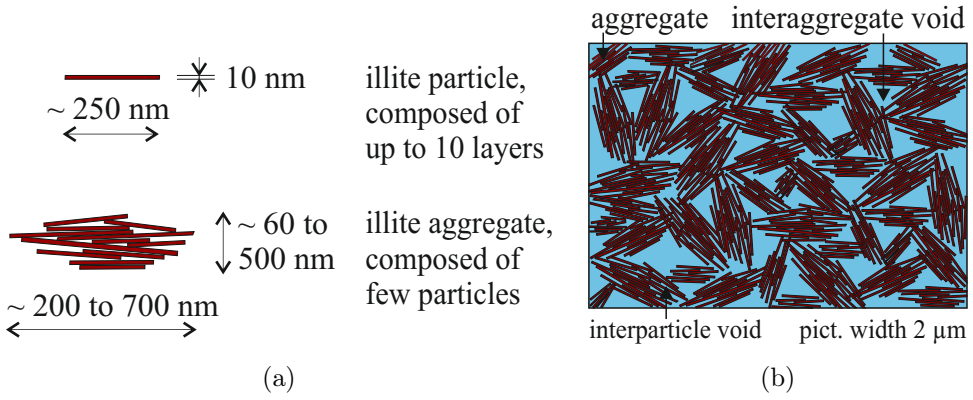

Figure 7.3.: Schematic of illite fabric: (a) particle and aggregate, (b) global fabric.

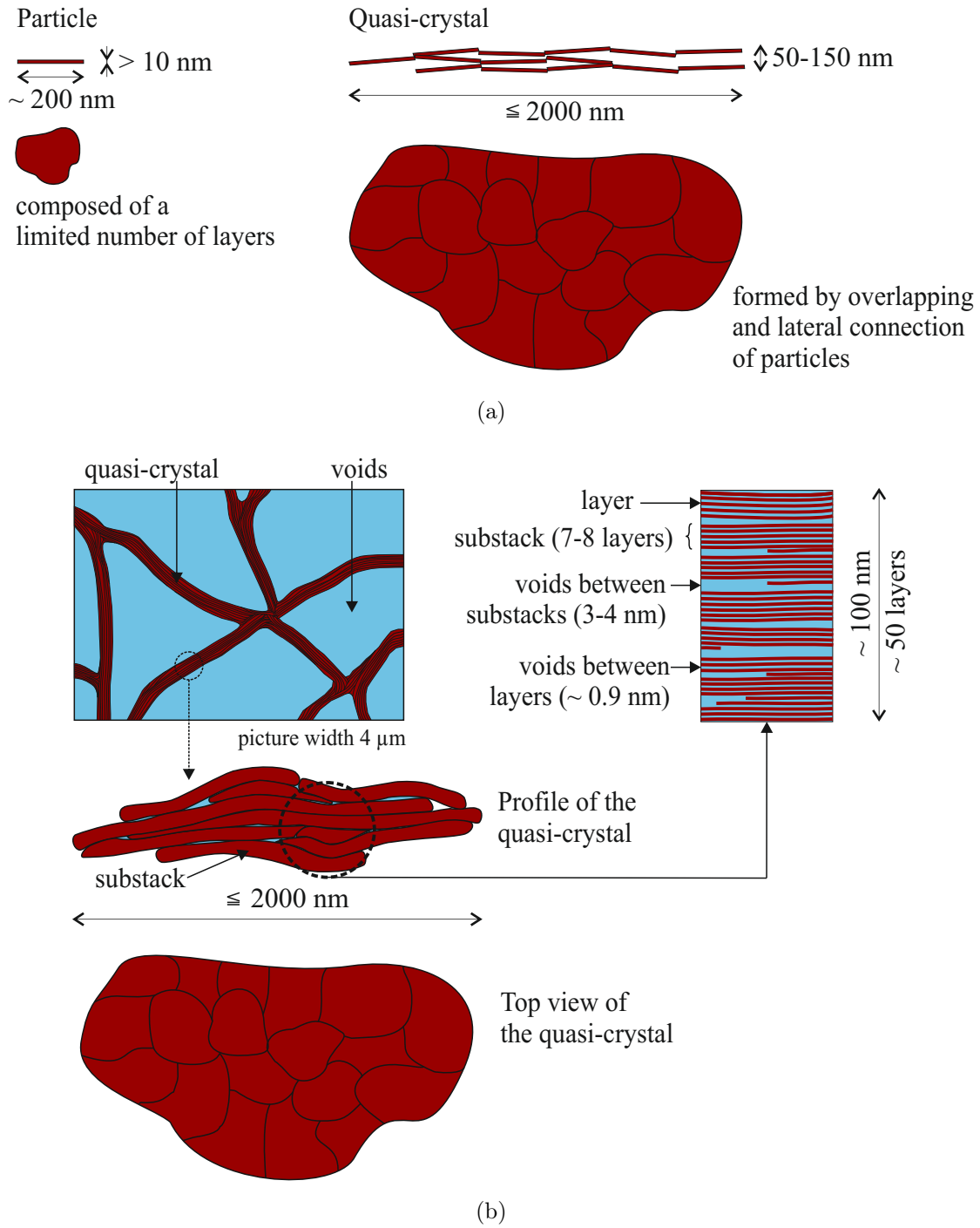

Figure 7.4.: Schematic of Ca-montmorillonite fabric: (a) particle and quasi-crystal, (b) global fabric. Modified after Tessier (1984) and Ben Rhaïem et al. (1987).

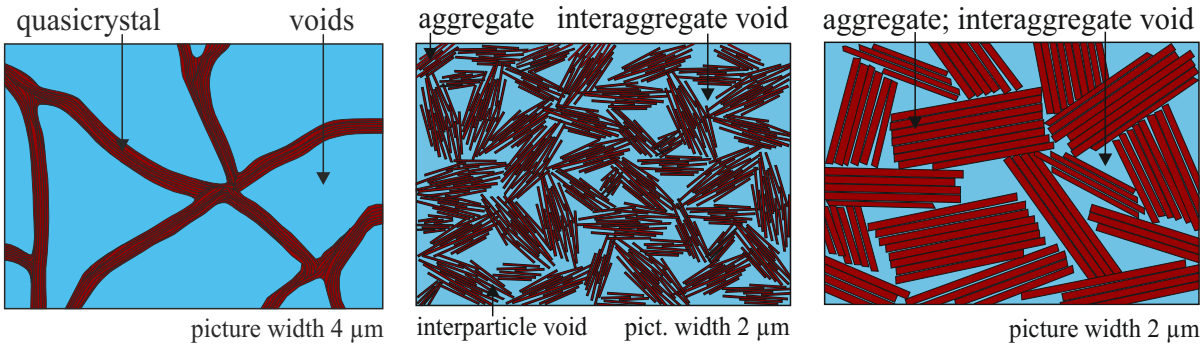

Figure 7.5.: Comparative illustration of initial fabric of the clays studied: (a) Calcigel bentonite, (b) NX illite, and (c) Spergau kaolin.

7.3. Observed volume change behaviour at macroscopic level

Fig. 7.6 presents the void ratio changes induced by mechanical loading and by suction increase for each clay separately. The air entry values ψ_{AEV} and the corresponding void ratios are marked in Figs. 7.6a, 7.6b, and 7.6c.

For Calcigel bentonite (Fig. 7.6a) and NX illite (Fig. 7.6b), it can be observed that the suction-void ratio and the vertical applied stress-void ratio relationships are nearly similar. Similar observations were made by Fleureau et al. (1993) and Marcial et al. (2002), and both studies attributed the similarity in the void ratio change induced by mechanical and suction loading to the validity of Terzaghi's effective stress concept (Terzaghi 1943) for suctions smaller than the air-entry value.

Suction increase beyond air entry value does not cause significant volume change of soils due to a reduction in effective stress (Lu & Likos 2006, Vesga 2008, Baille, Tripathy & Schanz 2014). Baille et al. (2014) have shown that an increase in applied suction beyond air-entry value causes a decrease in effective stress for Spergau kaolin and NX illite, whereas effective stress was shown to further increase at suctions beyond air-entry value. Contrary, the increase in applied vertical stress causes an increase in the effective stress of the clays for the purely mechanical loading. The differences in volume change observed in Spergau kaolin are on account of dissimilar effective stresses obtained by the different loading paths (see also discussion in chapter 10).

Figs. 7.7a and 7.7b show the observed volume change behaviour of the clays as obtained by purely mechanical loading and purely suction loading, respectively. In case of the former (Fig. 7.7a), the e-$\log \sigma_v$ curves are ordered according to the physico-chemical properties, such as the cation exchange capacity and the specific surface area, for the lower stress range up to 4 MPa. That is, Calcigel bentonite has the highest void ratio, followed by NX illite, and Spergau kaolin shows the smallest void ratio. In other words, greater is the specific surface and the cation exchange capacity of the clay, higher is the water absorption and greater is the void ratio of the clay at a given stress. At about 4 MPa, the e-$\log \sigma_v$ plot of NX illite crosses that of Calcigel bentonite and shows the highest void ratio until maximum applied stress of 20.6 MPa. This means, that for stresses greater than about 4 MPa, NX illite shows greater resistance to deformation than Calcigel bentonite. The void ratio of Spergau kaolin remains below that of Calcigel bentonite and NX illite throughout the whole stress range up to the maximum applied stress.

The applied suction versus void ratio data behaviour presented in Fig. 7.7b is somewhat different from the volume change behaviour of the saturated clays due to the purely mechanical loading. For applied suctions up to about 2 to 4 MPa, the curves are mutually ordered according to the physico-chemical properties. Again, the greater is the specific surface of the clay, the higher is the water absorption, and thicker is the diffuse double layer, and greater is the void ratio of the clay at a given suction. The curves cross each other between applied suctions of about 2 to 4 MPa. Thus, at applied suctions greater than about 2 to 4 MPa, Spergau kaolin shows the greatest resistance against deformation, followed by NX illite and Calcigel bentonite. This is in agreement with the reduction of effective stress at suctions greater than the air-entry value, leading to a reduction in volume change (see also discussion in chapter 10).

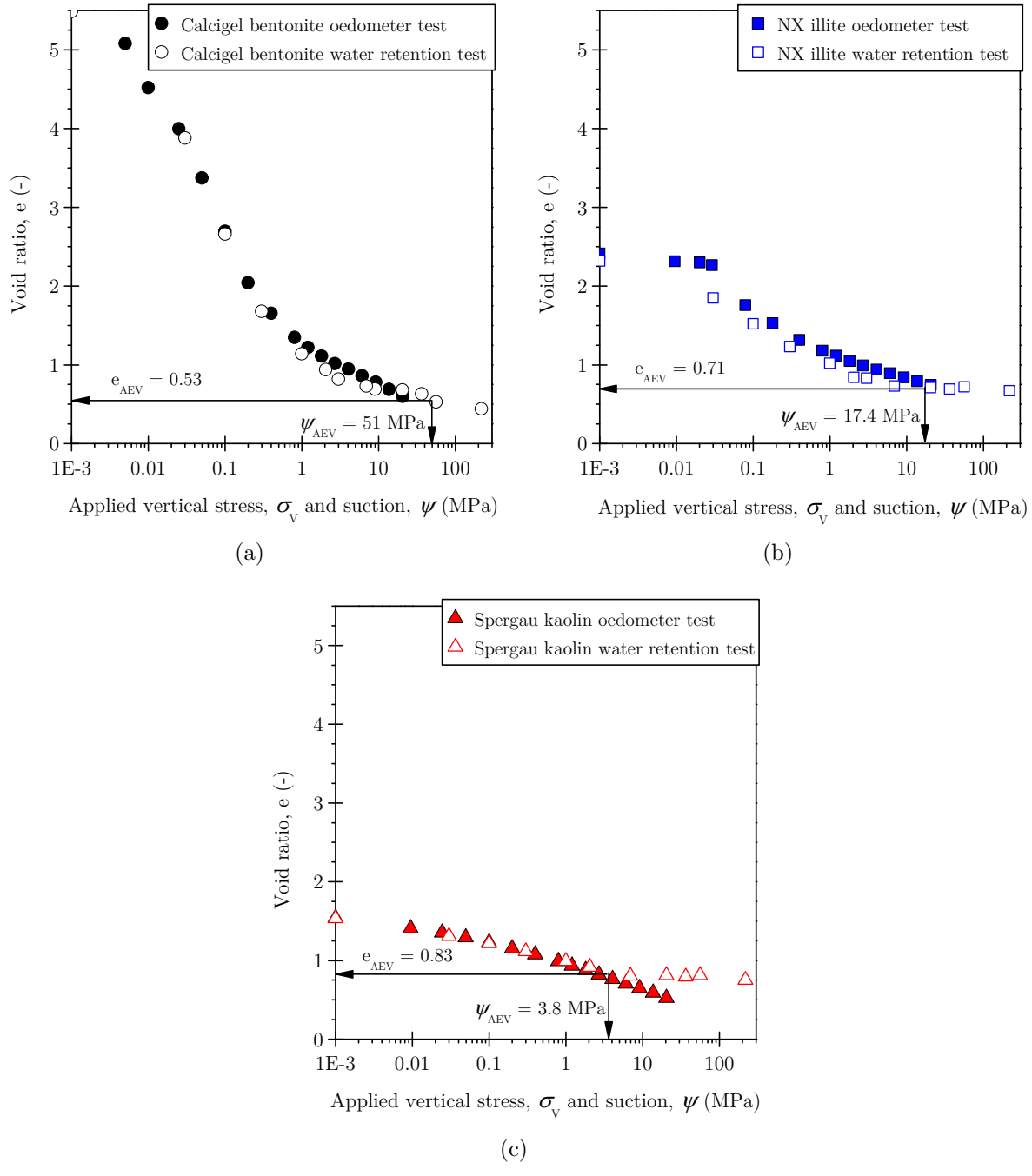

Figure 7.6.: Void ratio vs. applied suction and vertical stress for the clays: (a) Calcigel bentonite, (b) NX illite, and (c) Spergau kaolin.

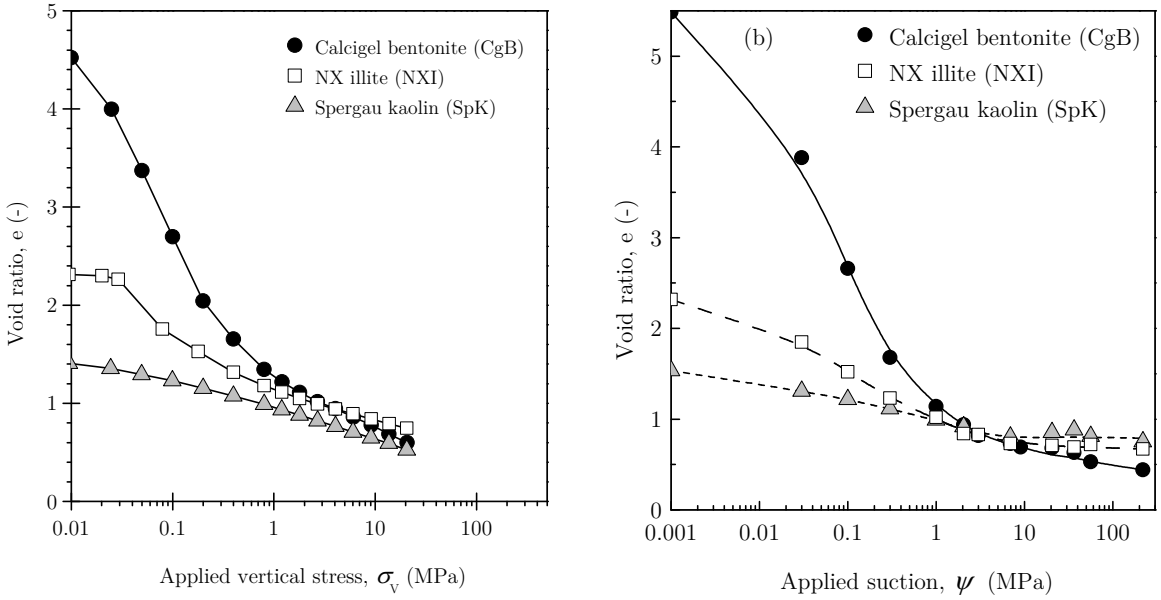

Figure 7.7.: Volume change due to vertical stress and suction increase: (a) vertical stress-void ratio plot, (b) suction-void ratio plot.

An interpretation of the results presented in Figures 7.6 and 7.7 based on micro-mechanical considerations is given in the following sections.

7.4. Effect of loading type

Figure 7.8 presents photomicrographs of the ESEM investigation of Calcigel bentonite and Spergau kaolin specimens submitted to vertical applied stresses of 2 and 20 MPa. The pictures of the initial state (Figs. 7.8a and 7.8b) are also shown. ESEM photomicrographs for NX illite under mechanical load are not available.

Fig. 7.9 presents the photomicrographs of the clays at shrinkage limit (SL) after oven drying in comparison to the photomicrographs at initial state corresponding to $1.1w_L$. The state of the specimens after oven drying can be considered to be equivalent to a very large suction of about 1000 kPa.

The fabric of Spergau kaolin at 2 and 20 MPa vertical applied stresses is shown in Figs. 7.8d and 7.8f, respectively. At both stress levels, the kaolin aggregates are squeezed together. Large pores existing at the initial state (Fig. 7.8b) were compressed, only few small pores remained.

For Calcigel bentonite, the pattern of the fabric at 2 and 20 MPa vertical applied stresses (Figs. 7.8c, 7.8e) as compared to the initial state (Fig. 7.8a) indicates an overall compression of the large pores between quasi-crystals. A pronounced orientation of the particles was not detected.

The anisotropic nature of the oedometric loading as compared to the isotropic suction loading is one reason for the higher deformation of the Spergau kaolin in the oedometer test beyond 4.0 MPa. Pores tend to orient themselves, leading to a smaller void ratio as compared to isotropic suction loading (see Figs. 7.8f vs. 7.9f). Additionally, in the oedometer test, the specimens remained saturated throughout the test and the re-orientation process was facilitated by lubrication in case of the granular type of kaolin aggregates.

In case of Calcigel bentonite, a large quasi-crystal of about 2000 nm thickness was observed at shrinkage limit (Fig. 7.9b). For Spergau kaolin, at both the initial state and at shrinkage limit, relatively large pores of about 2000 nm are visible (Figs. 7.9e and 7.9f). In case of NX illite, differences in the pattern are not very significant (Figs. 7.9c and 7.9d). Figures 7.10 and 7.11 present the pore size distribution (PSD) of the three clays obtained after the shrinkage limit tests, the former in terms of cumulative pore volume, the latter in terms of log. differential intrusion. Overall, the MIP results confirm the suction induced volume change for maximum applied suction obtained at macroscopic level (see Fig. 7.7b). Spergau kaolin shows the highest cumulative pore volume, followed by NX illite and Calcigel bentonite. The comparison with the global pore volume as determined by standard wax method (ASTMD4943-02 2002) and indicated by the dashed lines in Fig. 7.10 reveals that the existing pore space of Calcigel bentonite and NX illite could not be fully intruded by means of MIP. Only in case of Spergau kaolin, both measurement techniques lead to the same pore volume, indicating that the full range of existing pore space was detected by the MIP. About 17% of the pores in Calcigel bentonite and about 20% in case of NX illite are smaller in diameter than the detection limit of the MIP device of 8 nm (see Table 7.1).

The PSD of Spergau kaolin was found to be unimodal. This is consistent with the fact that pore space within a kaolin is on account of inter-domain pores. In case of illite, the unimodal curve shows a mean pore size of about 16 nm, representing the interaggregate pores. Intraaggregate (= interparticle) pores of the illite are to small for the detection limit of the MIP device and they belong to the 20% of not detected pore space. This indicates that a second pore family, probably representing the intraaggregate pores of about 3 nm diameter exists. Thus, the pore size distribution of NX illite should be bimodal in reality. The MIP curve obtained for Calcigel bentonite shows two mean pore diameters, one at

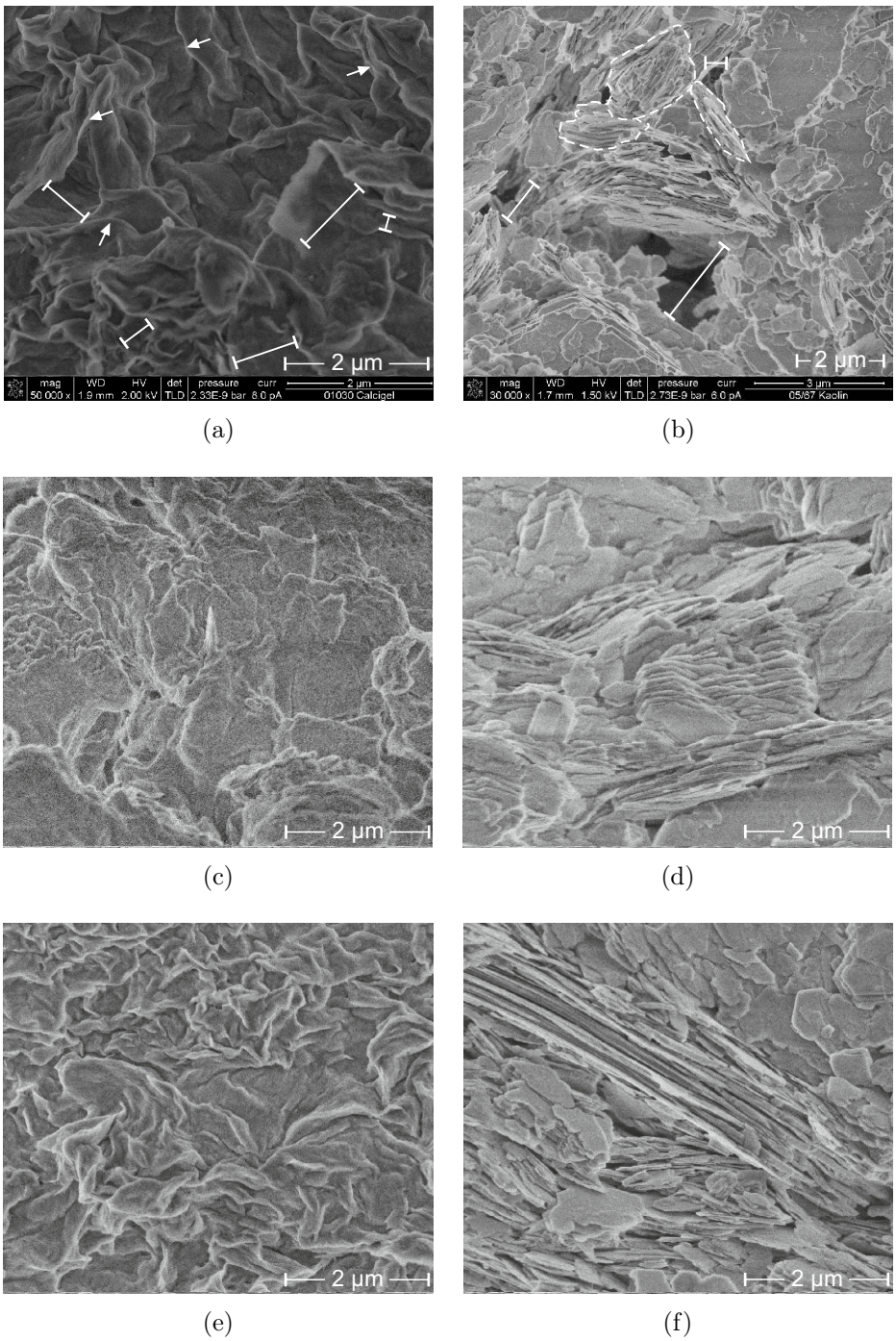

(a) (b) (c) (d) (e) (f)

Figure 7.8.: ESEM photomicrographs showing the effect of vertical applied stress for Calcigel bentonite (CgB) and Spergau kaolin (SpK): (a) CgB initial state, (b) SpK initial state, (c) CgB at 2 MPa, (d) SpK at 2 MPa, (e) CgB at 20 MPa, and (f) SpK at 20 MPa.

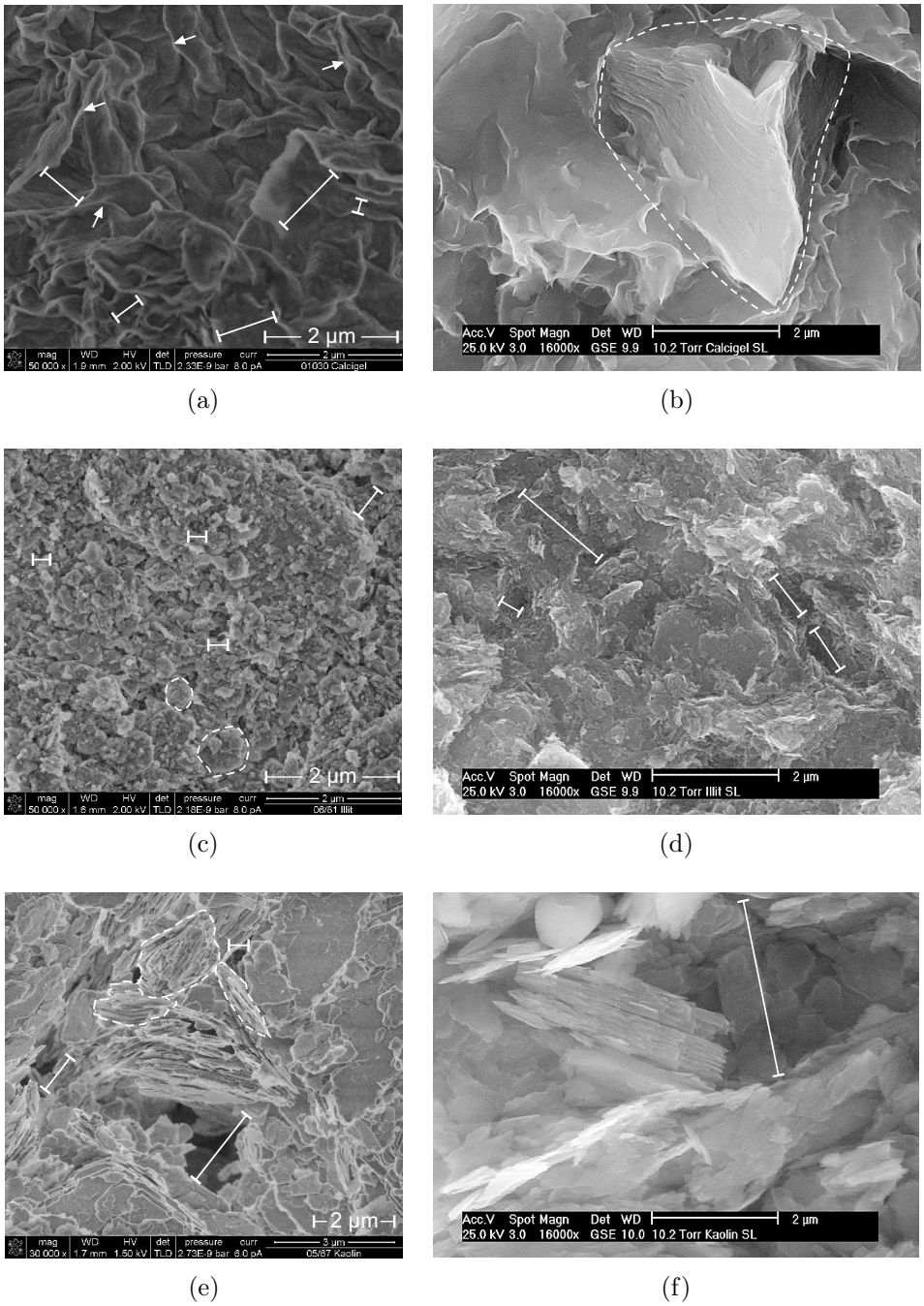

Figure 7.9.: ESEM photomicrographs of Calcigel bentonite (CgB), NX illite (NXI) and Spergau kaolin (SpK) at initial state and shrinkage limit (SL): (a) Cgb initial, (b) Cgb SL, (c) NXI initial, (d) NXI SL, (e) SpK initial, (f) SpK SL.

$2 \cdot 10^5$ nm (= 0.2 mm), and another at about 12 nm. The former one is rather large and is therefore considered to be an artefact due to fissures within the specimen. Considering a correction of the artefact by subtracting its volume from the total intruded volume, the percentage of non-intruded pores would then increase to 48% of the pores having a diameter smaller 8 nm. This indicates that the suction increase leads to a significant reduction in size of the initially large voids between the quasi-crystals from about 1 to 2 µm to about 12 nm or smaller. It is hypothesised that due to the flexible nature of the quasi-crystals enabling sliding of layers, volume continued to decrease after air entry suction was reached. Due to suction increase, the quasi-crystals simultaneously approach each other and unify to form larger quasi-crystals.

The PSD of Spergau kaolin at initially saturated condition, which was prepared using freeze-drying, is also presented in Fig. 7.10. There is a discrepancy between the total pore volume of 0.58 cm^3/g and the total pore volume measured by MIP. Since it is not expected that there are unavailable pores smaller than the detection limit for the kaolin sample, the discrepancy in total pore volume is probably due to the very soft nature of the specimen after freeze drying. This means, mercury was not intruded during the first stages of the test, but an isotropic compression of the specimen occured, due to the external stress exerted by the mercury on the specimen (Penumadu & Dean 2000). Thus, the resulting pore volume between 200 and 400 nm can not be considered as true intruded pore volume. However, the result qualitatively confirms the unimodal pore size distribution of the initially saturated kaolin.

Table 7.1.: Porosity values of the clays studied as determined by MIP and standard wax method

	Calcigel bentonite	NX illite	Spergau kaolin
Porosity, n_{MIP} [a]	18.0	35.0	44.6
Porosity, n_{wax} [b]	27.8	34.4	44.3

[a] determined from MIP data

[b] determined by wax method following ASTM D4943 (2003)

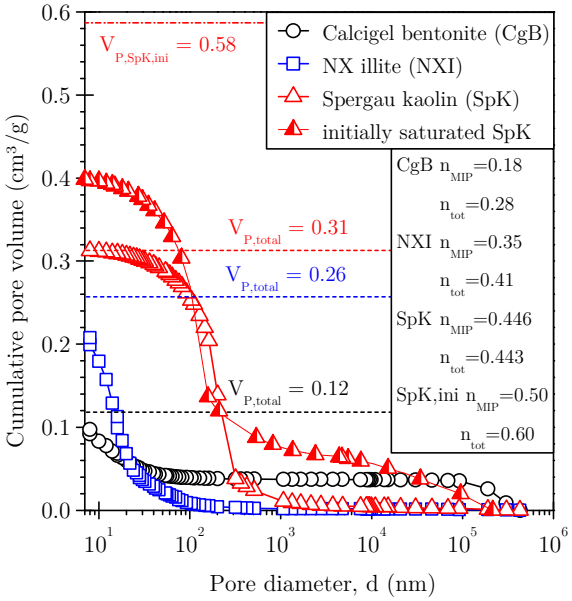

Figure 7.10.: MIP of the clays studied after shrinkage limit test in terms of cumulative pore volume.

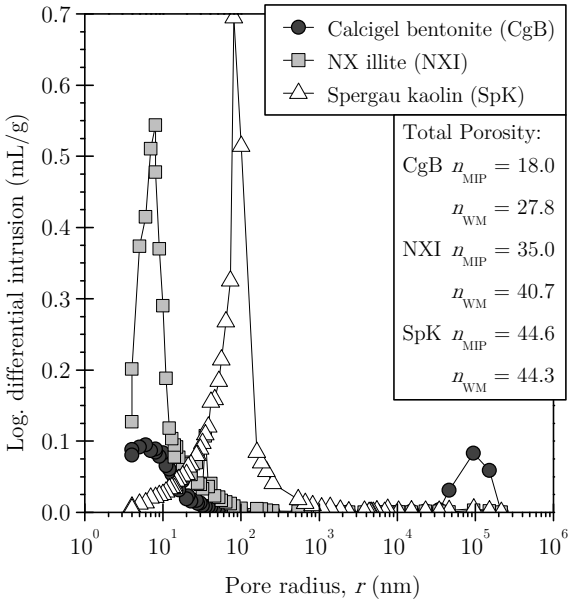

Figure 7.11.: MIP data of the clays studied after shrinkage limit test in terms of log differential intrusion.

7.5. Effect of mineralogy

In section 7.3, it was shown that the e-$\log \sigma_v$ curves (Fig. 7.7a) and the e-$\log \psi$ curves (Fig. 7.7b) are ordered according to the physico-chemical properties of the clays until about 2 to 4 MPa applied vertical stress or applied suction.

For the mechanical loading (see Fig. 7.7a), at about 4 MPa, the e-$\log \sigma_v$ plot of NX illite crosses that of $e - \log \sigma_v$ of Calcigel bentonite and shows the highest void ratio until maximum applied stress of 20.6 MPa. The void ratio of Spergau kaolin remains below that of Calcigel bentonite and NX illite throughout the whole stress range up to the maximum applied stress. The position of the Spergau kaolin curve below those of NX illite and Calcigel bentonite at applied stresses greater than 2 to 4 MPa is in accordance with its layer-to-layer distance of 0.72 nm as compared to 1.0 nm for illite, and 0.96 to 1.9 nm for Ca-montmorillonite, depending on the state of hydration in the interlayer space. However, the layer-to-layer distance can hardly be the reason for the greater void ratio of NX illite as compared to Calcigel bentonite, since the latter is not free of adsorbed water. Illite particles form irregular aggregates of strong stability with interparticle pore sizes of about 3 nm (Quirk & Aylmore 1971). Considering a the range of layer-to-layer thickness of hydrated Ca-montmorillonite up to 1.9 nm and the extinction of interparticle and interaggregate pores at maximum applied stress, pores between illite particles of 3 nm in size can explain the greater void ratio of NX illite as compared to Calcigel bentonite. This is true when the maximum applied mechanical stress of 21.6 MPa was not able to affect the interparticle pore size of the illite.

For purely suction loading (Fig. 7.7b), the curves of the clays cross each other between applied suctions of about 2 to 4 MPa. Thus, at applied suctions greater than about 2 to 4 MPa, Spergau kaolin shows the greatest resistance against deformation, followed by NX illite and Calcigel bentonite. This is in agreement with the reduction of effective stress at suctions greater than the air-entry value, leading to a reduction in volume change (see chapter 10). Regarding the micro-mechanical interpretation of the results presented in Fig. 7.7b, the structural features of the clays introduced in section 7.2 will be recalled. No interlayer space exists between the kaolin layers within a particle and the interparticle pore space in the kaolin clay is negligible. Thus, the measured global void ratio of Spergau kaolin is on account of the interaggregate voids only. During suction induced shrinkage, the aggregates approach each other leading to a reduction of inter-aggregate pore space. The shrinkage curve of Spergau kaolin (see Fig. 4.1d in section 4.2) is shaped similar to a pure crystalline material, with a linear primary shrinkage stage and zero residual

shrinkage. Similar results were obtained by Haines (1923) for a kaolin. Due to the relatively large size of the Spergau kaolin aggregates, a greater pore volume remains at the end of primary shrinkage, when the aggregates have come into contact and cease to shrink. The aggregates, which can be regarded as grains or particles, are in contact with each other and form a rigid structure which is not compressible due to any further suction increase, once shrinkage limit water content was reached. The comparison of the ESEM pictures of Spergau kaolin at initial state (Fig. 7.9e) and after shrinkage limit test (Fig. 7.9f) show that, even after oven drying, a significant amount of pore space exists within the clay. Contrary, the high mechanical stress in the oedometer test is able to overcome the friction between the domains and to further compress the structure formed by them.

The mechanism responsible for the suction induced volume change of NX illite is similar to that of Spergau kaolin, since the illite aggregates can be considered as rigid as well, and therefore, can be regarded as a stable entity with respect to the effect of increasing suction. Quirk & Aylmore (1971) noted that the average pore size between the illite particles within an aggregate was about 3 nm, even at very high suctions upon complete drying. The relatively large spacing between the particles within the aggregates is attributed to the bending and interleaving of the irregular crystals. From the above considerations it follows that the observed volume decrease of NX illite induced by suction increase would be mainly due to a reduction of the inter-aggregate pore space while the intraaggregate pore space remains constant. As suction increases, the rigid aggregates of NX illite approach each other until friction between them prevents any further volume reduction, without any internal structural change within the aggregates. The total pore space at high suctions arises from the voids within the aggregate (intraaggregate or interparticle voids) as well to some extent from the voids between the aggregates (inter-aggregate voids).

Contrary to a domain of illite or kaolin clay, a Ca-montmorillonite quasi-crystal is not rigid. As suction increases, firstly, the water within the large pores between the quasi-crystals is drained out and the pore size decreases while the amount and distance of the layers within the quasi-crystals remain unchanged. For suctions > 1 MPa, the number of layers within a quasi-crystal increased significantly. This means that the initial quasi-crystals associate to form larger aggregates. Only a further suction increase beyond 5 MPa reduces the layer-to-layer distance within the particle from 1.86 to 1.56 nm (Ben Rhaïem et al. 1987). In Fig. 7.9b, the formation of a large particle of the Calcigel bentonite after the shrinkage limit test is shown. It is hypothesized, that the flexible nature of Calcigel bentonite, enabling the formation of large aggregates with close layer-to-layer distances by

sliding of the layers, is responsible for the smaller global void ratio of Calcigel bentonite in the suction test and to some extend in the oedometer test. The rigid nature of the NX illite aggregates together with the fixed interparticle pore space of about 3 nm prevents shrinkage at higher suctions, contrary to Calcigel bentonite.

7.6. Summary

The measured volume change behaviour of Calcigel bentonite, NX illite and Spergau kaolin were compared and discussed based on micro-structural considerations. The effect of loading type and the effect of clay mineralogy on the observed volume change behaviour both at low and high applied stresses and suctions were brought out. Concurrent with earlier studies, the test results revealed that up to the air-entry value (AEV) of the clays equal magnitudes of applied vertical stress and suction brought clay specimens to nearly equal void ratios, whereas suction values greater than AEV were less effective in causing volume change.

Comparisons of environmental scanning electron photomicrographs (ESEM) of the clays at saturated state and at shrinkage limit clearly showed the influence of loading type and mineralogy on the evolution of fabric of the clays.

Spergau kaolin and NX illite mineral crystals form a rigid type of fabric dominated by frictional contacts between the aggregates. The quasi-crystals of Calcigel bentonite are flexible in nature. The internal layer-redistribution within the quasi-crystals during suction increase, i.e., the change of the ratio between interlayer pores and pores between the quasi-crystals, together with the flexible nature of the quasi-crystals enable the Calcigel bentonite to drain its water out of the pores while staying saturated up to large suction values, leading to smaller void ratios as compared to Spergau kaolin and NX illite in case of applied suction increase.

The mechanical loading of 2 to 20 MPa vertical applied stress caused a tight compression of the fabric of Spergau kaolin, where only negligible pore space was discernable. The anisotropic nature in the oedometer tests as compared to the isotropic suction loading lead to a particle re-orientation and a a smaller global void ratio as compared to the other clays. Re-orientation was not pronounced for Calcigel bentonite during mechanical loading. The intraaggregate pore space of the stable, rigid NX-illite aggregates, which are not affected by large suctions and stresses leads to a higher global void ratio of NX illite as compared to Calcigel bentonite for both types of loading.

8. Application of the physico-chemical theories

8.1. General

In the following chapter, the results of diffuse double layer calculations are presented. The calculated stress-void ratio or stress-dry density relationships are compared to those obtained from the swelling pressure experiments, the one-dimensional consolidation tests and from the unconfined water retention tests of the three clays. In the first section of this chapter, the theoretical stress-void ratio and dry density-stress relationships based on Gouy-Chapman diffuse double layer theory were directly calculated using the known physical and physico-chemical parameters of the clays studied and the pore fluid properties as input parameters. In the second section of this chapter, a modified approach (Tripathy et al. 2004, Schanz & Tripathy 2005, Tripathy & Schanz 2007)) was used to calculate the stress-void ratio and dry density-swelling pressure relationships based on diffuse double layer theory.

8.2. Procedure adopted based on diffuse-double layer approach

8.2.1. Equations based on classical Gouy-Chapman diffuse-double layer theory

The set of equations used and the needed entrance parameters for calculating the repulsive diffuse-double layer pressure for a given void ratio or dry density and vice versa is presented in the following (Verwey & Overbeek 1948, Bolt 1956, van Olphen 1977, Sridharan & Jayadeva 1982).

The following entrance parameter are needed:

- solid properties:
  - specific gravity, G_{S} (-)
  - specific surface area, A_{S} (m^2/g)
  - cation exchange capacity, CEC (meq/100g)
  - valency of the exchangeable cations, ν (-); for non-homoionic clays, the value of weighted average valency is used
- bulk fluid properties:
  - ion concentration, n_0 (m^{-3})
  - relative permittivity, ε_{r} (-); $\varepsilon_{\mathrm{r}} = 80.4$ for water at 20 °C; with $\varepsilon_{\mathrm{r}} = \varepsilon/\varepsilon_0$
    - permittivity of vacuum, $\varepsilon_0 = 8.8542 \cdot 10^{-12}$ $\mathrm{C}^2\mathrm{J}^{-1}\mathrm{m}^{-1}$
    - permittivity of the medium, ε ($\mathrm{C}^2\mathrm{J}^{-1}\mathrm{m}^{-1}$)
- other system parameters:
  - absolute temperature, T (K)
- physical constants:
  - Boltzmann constant, $k_B = 1.38 \cdot 10^{-23}$ J/K
  - elementary electron charge, $e' = 1.602 \cdot 10^{-19}$ C

Knowing the soil and fluid parameters presented above, the following equations were used:

$$R_{\mathrm{ddl}} = 2n_0 k_B T(\cosh u - 1) \tag{8.1}$$

$$-\left(\frac{dy}{d\xi}\right)_{x=0} = \frac{CEC}{S}\left(\frac{1}{2\varepsilon_0\varepsilon_{\mathrm{r}} n_0 k_B T}\right)^{1/2} \qquad \text{at} \quad x = 0,\ y = z \tag{8.2a}$$

$$-\left(\frac{dy}{d\xi}\right)_{x=0} = \left(2\cosh z - 2\cosh u\right)^{1/2} \tag{8.2b}$$

$$\int_z^u \frac{1}{(2\cosh y - 2\cosh u)^{1/2}}\, dy = \int_0^d d\xi = -Kd \tag{8.3}$$

$$K = \left(\frac{2n_0 e'^2 \nu^2}{\varepsilon_0 \varepsilon_r k_B T} \right)^{1/2} \tag{8.4}$$

$$e = G_S \rho_w A_S d \tag{8.5}$$

$$\rho_d = \frac{G_S \rho_w}{1+e} \tag{8.6}$$

where R_{ddl} is the repulsive pressure in N/m^2 , u is the nondimensional midplane potential, ξ is the distance function, where $\xi = Kx$, y is the nondimensional potential at a distance x from the particle surface, z is the nondimensional potential function at the surface ($x = 0$), K is the diffuse double layer parameter (m^{-1}), e is the void ratio of the clay, d is half the distance between the clay particles, ρ_d is the dry density, and ρ_w the density of water in Mg/m^3 The variables x, y, u, and z refer to the schematic given in Fig. 2.18a. The interparticle repulsive pressure for a given interparticle distance $2d$ is calculated by relating the non-dimensional midplane potential u to the nondimensional distance function Kd.

The following steps need to be performed: u is obtained by eq. 8.1 for a range of assumed interparticle pressures R_{ddl}, and the corresponding z values are obtained using eqs. 8.2a and 8.2b. Kd is then calculated by solving the integral in eq. 8.3 for the known z and u values corresponding to the considered range of R_{ddl} values. Knowing K from eq. 8.4 and Kd from eq. 8.3, d is obtained, which is related to the void ratio e by eq. 8.5. For the evaluation of swelling pressure data vs. dry density, eq. 8.6 is used to convert void ratio to dry density. The flowchart presented in Fig. 8.1 illustrates the procedure of calculation.

The theoretical u-Kd relationships are linear in an u-log Kd-plot (Sridharan & Jayadeva 1982). The theoretical repulsive pressure-void ratio and repulsive pressure-dry density relationships obtained using the above procedure were compared to their experimental counterparts of the clays studied (Calcigel bentonite, NX illite, Spergau kaolin). The results are presented in section 8.3.

8.2.2. Modified approach

In the modified approach of Tripathy et al. (2004), equations were proposed, which have been established based on swelling pressure-dry density data sets of various bentonites

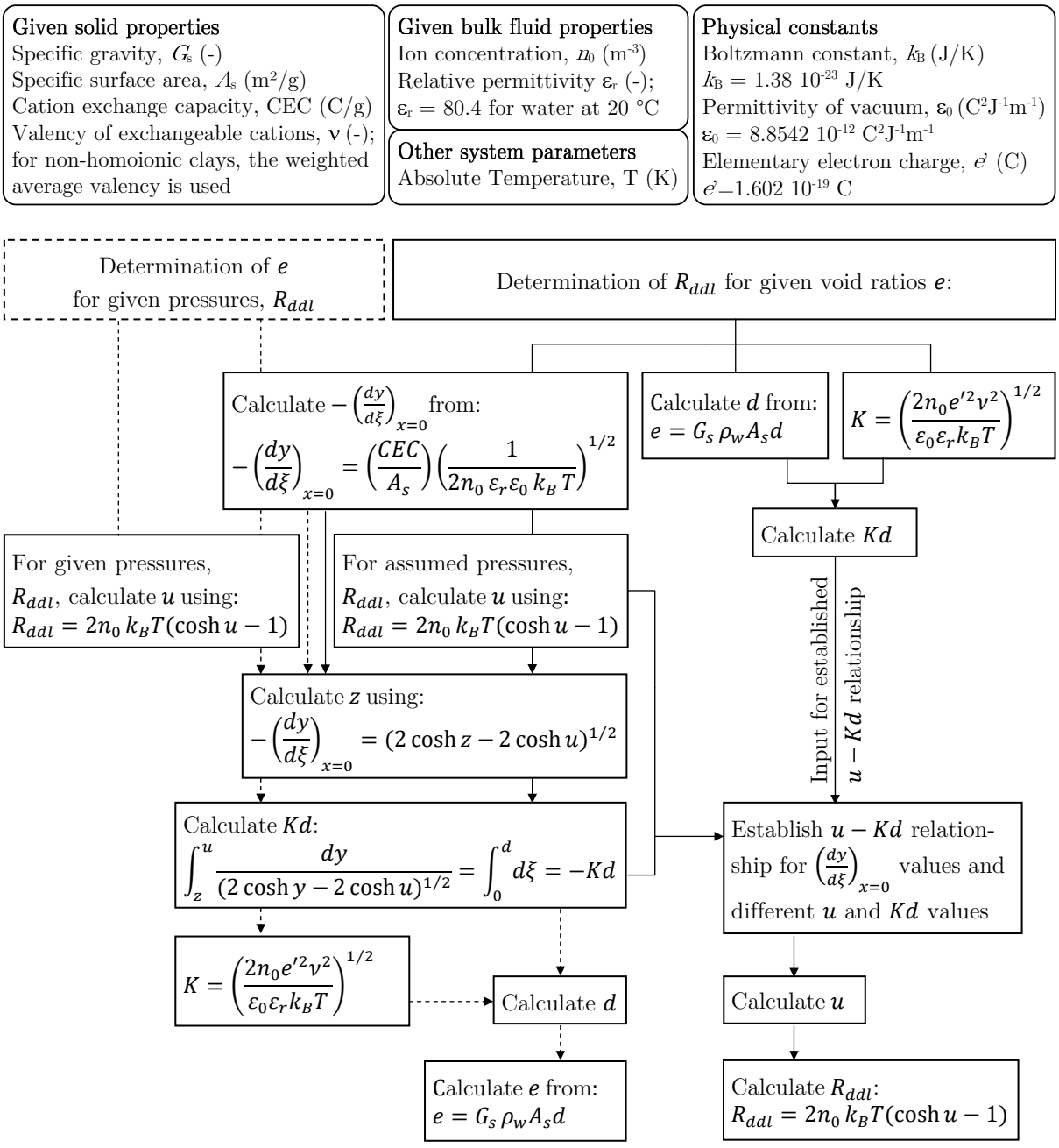

Figure 8.1.: Flowchart illustrating the procedures for calculation of repulsive pressures R_{ddl} for given void ratios e and vice versa.

reported in literature. The bentonites used for establishing the equations were MX80, Febex and Montigel, having an weighted average valency ν of 1.14, 1.73, and 1.97, respectively. In Tripathy et al. (2004), the bentonites Kunigel V1 ($\nu = 1.46$), Kunigel ($\nu = 1.5$), and Bentonite S-2 ($\nu = 1.1.66$).

The equations were established by back-calculating the u-Kd relationship from the respective experimental dry density-swelling pressure data: u was back-calculated from the measured swelling pressure values using eq. 8.1. From the corresponding dry densities, the Kd-values were calculated using eqs. 8.4, 8.5 and 8.6. Thus, an experimental u-$\log Kd$ plot was obtained for each clay, which was fitted to a linear equation of the form $u = A \lg(Kd) + B$, where A and B are the fitting parameters.

The experimental u-Kd relationships obtained by Tripathy et al. (2004) were:

$$u = -7.277 \lg(Kd) - 2.91 \qquad \text{for MX80} \quad \nu = 1.14 \tag{8.7a}$$

$$u = -10.427 \lg(Kd) - 7.72 \qquad \text{for Febex} \quad \nu = 1.73 \tag{8.7b}$$

$$u = -9.190 \lg(Kd) - 3.26 \qquad \text{for Montigel} \quad \nu = 1.97 \tag{8.7c}$$

Replacing the u-value in eq. 8.1 by eq. 8.7a, 8.7b or 8.7b leads to eq. 8.8a, 8.8b, and 8.8c for the corresponding range of valency.

$$p_s = 2n_0 k_B T[\cosh(-7.277 \lg(Kd) - 2.91) - 1] \quad \text{for} \quad \nu = 1.14 - 1.5 \tag{8.8a}$$

$$p_s = 2n_0 k_B T[\cosh(-10.427 \lg(Kd) - 7.72) - 1] \quad \text{for} \quad \nu = 1.66 - 1.73 \tag{8.8b}$$

$$p_s = 2n_0 k_B T[\cosh(-9.190 \lg(Kd) - 3.26) - 1] \quad \text{for} \quad \nu = 1.97 \tag{8.8c}$$

Similarly, (Tripathy & Schanz 2007) have established equations for the prediction of compressibility of bentonites. For this, the experimental u-Kd relationship for each clay was established based on the experimental void ratio-applied stress data in the range up to 500 kPa. The void ratios for the applied stresses greater than 500 kPa were then calculated using the experimental u-Kd relationships established in the low stress range smaller than 500 kPa.

In the present work, eq. 8.8c was verified with the experimental swelling pressure data of Calcigel bentonite. Further, based on the experimental high stress oedometer and water retention data of Calcigel bentonite, experimental u-Kd relationships from the data at low stresses and suctions was used to calculate the void ratio in the high stress and suction range. The results are discussed in section 8.4.

8.3. Gouy-Chapman diffuse double layer theory

In this section, the results of the calculations using the classical diffuse double layer equations are presented. The theoretical u-Kd relationships for Calcigel bentonite, NX illite and Spergau kaolin are shown in Figs. 8.2a, 8.2b and 8.2c, respectively. The comparison of the measured and calculated swelling pressures for the three clays is presented in Fig. 8.3.

For Calcigel bentonite (Fig. 8.3a), the calculated swelling pressure values are in reasonable agreement to the experimental values for dry densities up to about 1.55 g/cm^3. For greater dry densities, the theoretical swelling pressure values remain significantly below the experimental swelling pressures. The large discrepancy between the theoretical and experimental swelling pressures are attributed to the strong hydration forces developing due to the large amount of divalent exchangeable cations in Calcigel bentonite. A possible reason for the overestimation of the swelling pressures in the lower range of dry densities is the deviation of the true particle arrangement from the ideal homogeneous parallel particle arrangement. Thus, the value of total specific surface area used in the calculation might be greater than the specific surface area corresponding to the outer surfaces of the particles, where diffuse double layer is supposed to be active in case of calcium dominated bentonites.

In case of NX illite (Fig. 8.3b), the calculated swelling pressures are smaller than the measured swelling pressures for the full range of dry densities considered in the tests. This indicates that diffuse double layer is not controlling the behaviour. For Spergau kaolin (Fig. 8.3c), negligible swelling pressures are calculated by diffuse double layer theory, which was in accordance with the test results for initial dry densities up to about 1.3 g/cm^3. As discussed in section 5.2, diffuse double layer is not the relevant force component for explaining the observed swelling pressures at high dry densities.

Fig. 8.4 compares the measured volume change in terms of void ratio vs. applied vertical stress and void ratio vs. applied suction to the theoretical curve. Any prediction of a suction induced void ratio change using diffuse double layer would be only valid as long as

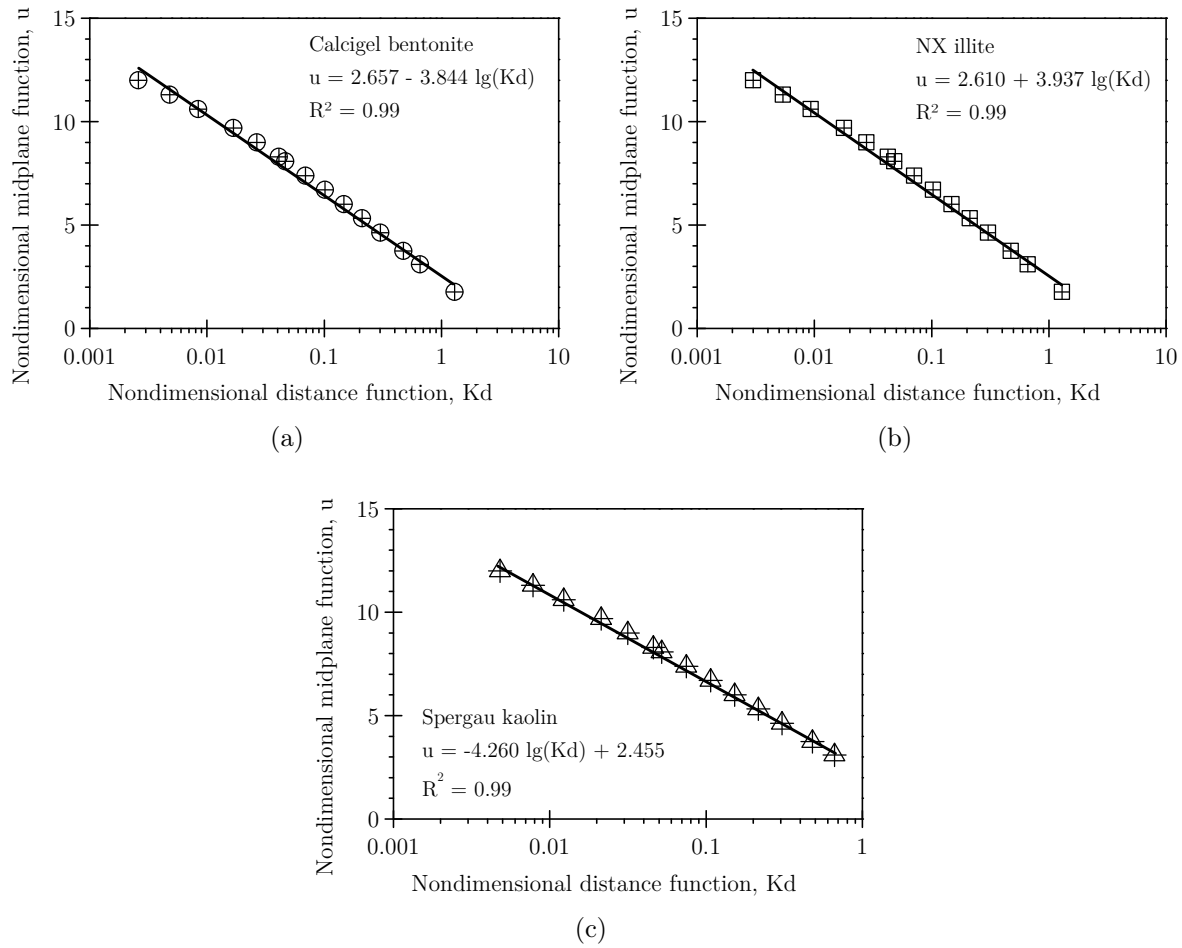

Figure 8.2.: Theoretical *u-Kd* relationships: (a) Calcigel bentonite, (b) NX illite, (c) Spergau kaolin.

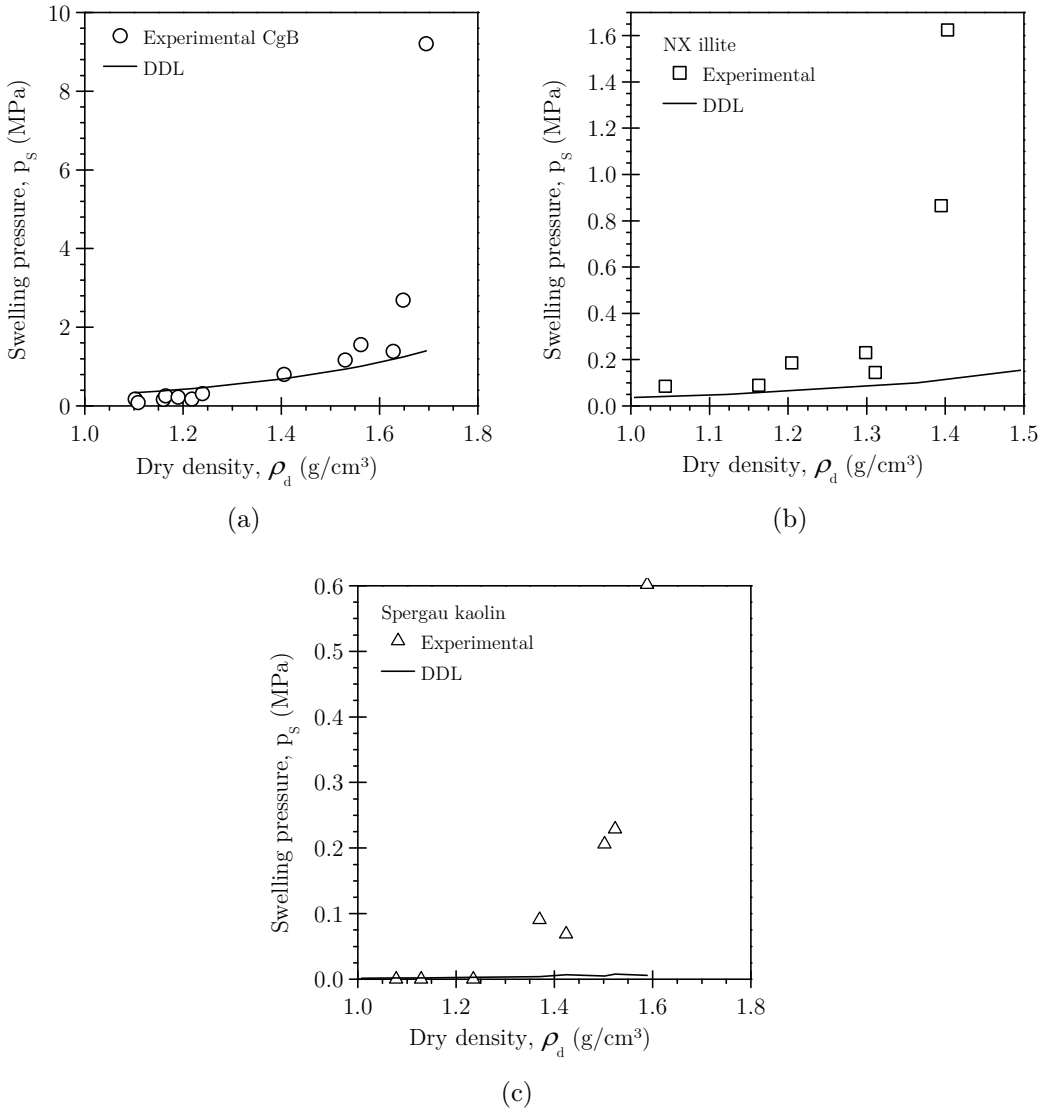

Figure 8.3.: Experimental and calculated swelling pressure vs. dry density plots: (a) Calcigel bentonite, (b) NX illite, (c) Spergau kaolin.

the clays are saturated (Tripathy & Schanz 2007). Considering the air-entry value ψ_{AEV}, this is the case up to a suction of 3.8 MPa for Spergau kaolin, 17.4 MPa for NX illite and 51.0 MPa for Calcigel bentonite.

The calculated curve of Calcigel bentonite crosses both experimental curves (Fig. 8.4a). The calculated void ratios are greater than the experimental ones for applied vertical stresses and suctions smaller than 0.1 MPa, and they are smaller than the experimental void ratios for applied stresses and suctions greater than about 0.4 MPa. Between 0.1 MPa and 0.4 MPa, the calculated void ratios agree reasonably well to the experimental curves. In the smaller stress and suction range, the deviation is attributed to the fabric, which consists of a network of large quasi-crystals enclosing large pores. The compressibility behaviour is controlled by the drainage of these pores. Possible diffuse double layers at the outer surface of the quasi-crystals would not overlap. At stresses and suctions greater than 0.4 MPa, deviation is attributed to the hydration of the calcium ions which manifest as a strong repulsive component at small layer and particle distances, thus leading to higher repulsive forces than predicted by diffuse double layer.

For Spergau kaolin and NX illite (Fig. 8.4b and 8.4c), it is obvious from the plots that diffuse double layer is not able to represent the volume change behaviour of these clays, which clearly indicates that the compressibility of illite and kaolinite is not governed by diffuse double layer.

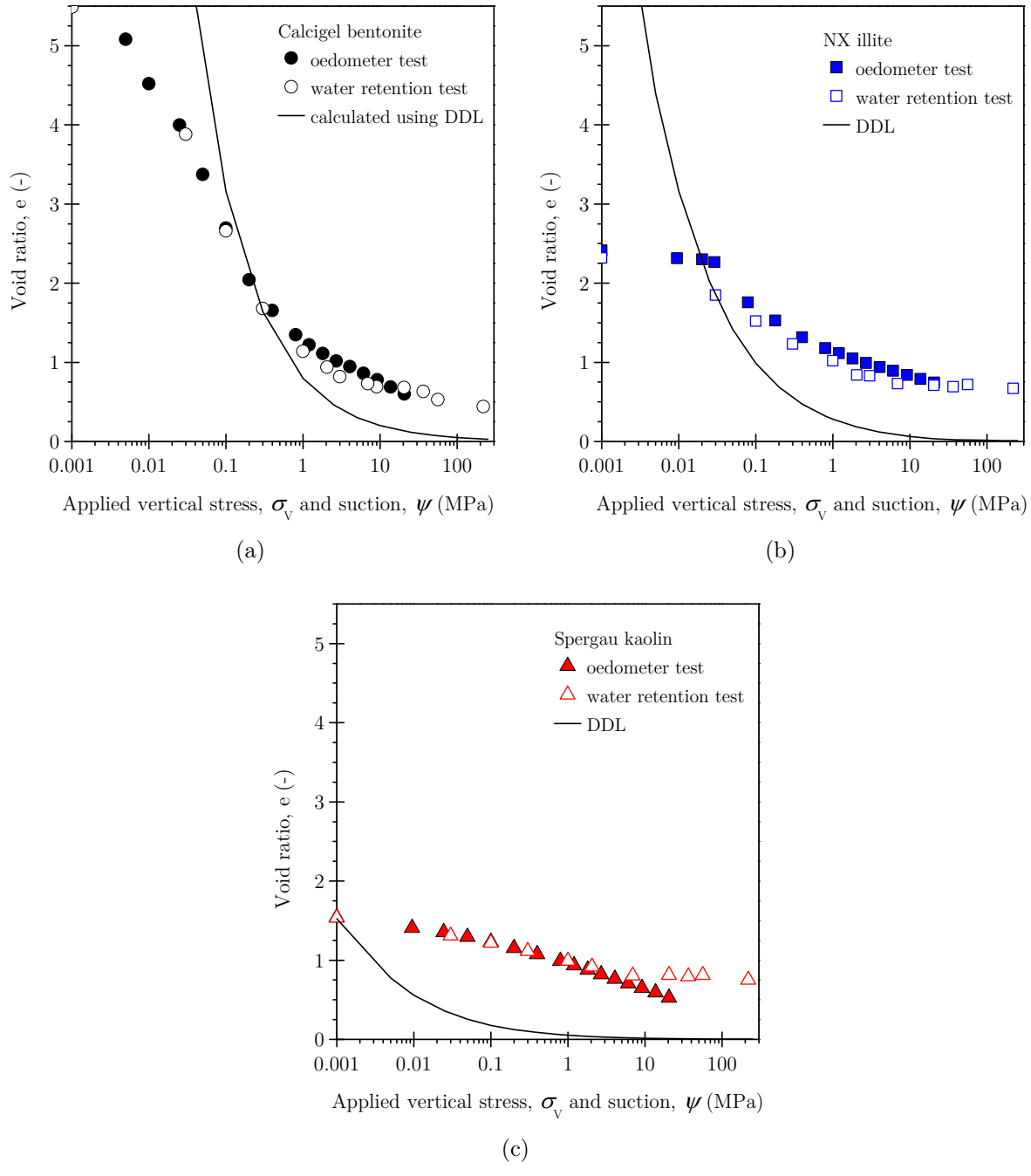

Figure 8.4.: Experimental and calculated void ratio vs. applied vertical stress or suction plots: (a) Calcigel bentonite, (b) NX illite, (c) Spergau kaolin.

8.4. Modified approach

The experimental swelling pressure-dry density relationship of Calcigel bentonite was used to establish a modified equation according to Tripathy et al. (2004) for the calculation of swelling pressures. They are given in eqs. 8.9a and 8.9b. The corresponding u-Kd relationship is illustrated in Fig. 8.5.

In Fig. 8.6, the predicted swelling pressures of the bentonites studied in Tripathy et al. (2004) and those of Calcigel bentonite from this study are plotted against the corresponding calculated swelling pressures. In Fig. 8.6a, the swelling pressures for Calcigel bentonite were calculated using the proposed eq. 8.8c (corresponding to eq. [22] in Tripathy et al. 2004, which was established based on data for Montigel bentonite). The calculated swelling pressures for Calcigel bentonite were much greater than the measured values, despite the similar average valency of both bentonites (1.97 for Montigel and 1.93 for Calcigel). A new equation was derived based on the swelling pressure data obtained in this study. Fig. 8.6b presents the calculated swelling pressures from the new equation. They obviously agree well to the experimental data; however, a third data set of swelling pressures of a bentonite of a similar valency should be found for verification of the new equation.

$$u = -9.325 \lg(Kd) - 4.866 \qquad \text{for Calcigel} \quad \nu = 1.93 \tag{8.9a}$$

$$p_s = 2n_0 k_B T[\cosh(-9.325 \lg(Kd) - 4.866) - 1] \quad \text{for} \quad \nu = 1.93 \tag{8.9b}$$

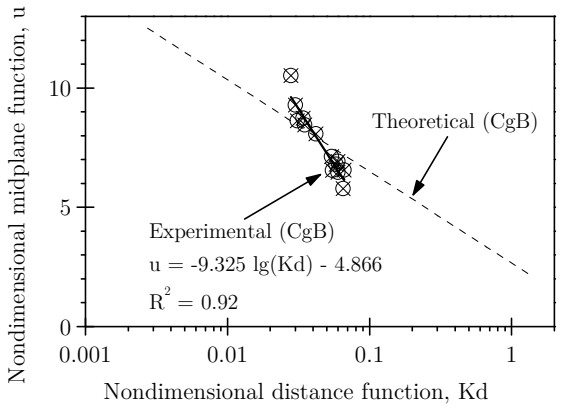

Figure 8.5.: Theoretical and experimental u-Kd relationships for Calcigel bentonite.

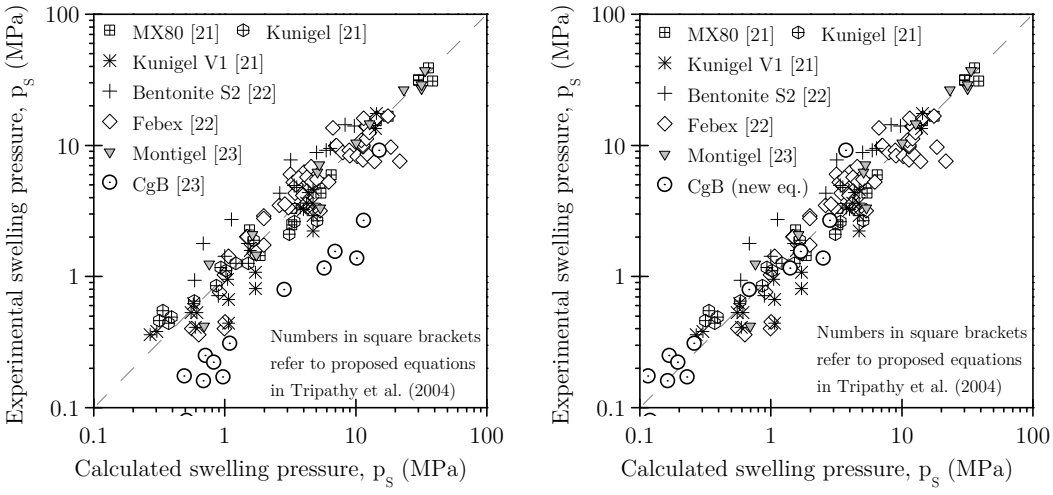

Figure 8.6.: Experimental vs. theoretical swelling pressures based on modified approach for bentonites: (a) using the suggested eqs. [21] to [23] in Tripathy et al. (2004) for all bentonites, (b) using new modified equation for Calcigel bentonite (CgB).

Similarly, modified equations were established from the experimental volume change data obtained in the oedometer test and in the unconfined water retention test to predict the behaviour at high stresses and suctions according to Tripathy & Schanz (2007). Figs. 8.7a and 8.8a present experimental u-Kd relationships derived from the oedometer test and the water retention test, respectively. The data points in the range of 25 to 400 kPa applied stress, and in the suction range from 30 to 300 kPa were used to establish the experimental u-Kd relationships. Eqs. 8.10a and 8.10b are for the oedometer data, eqs. 8.11a and 8.11b are for the water retention data.

$$u = -6.931 \lg(Kd) - 0.585 \tag{8.10a}$$

$$R_{\mathrm{ddl}} = 2n_0 k_B T[\cosh(-6.931 \lg(Kd) - 0.585) - 1] \tag{8.10b}$$

$$u = -6.424 \lg(Kd) - 0.173 \tag{8.11a}$$

$$R_{\mathrm{ddl}} = 2n_0 k_B T[\cosh(-6.424 \lg(Kd) - 0.173) - 1] \tag{8.11b}$$

Fig. 8.7b shows that the use of the modified equation improves the fit to the experimental points at high applied stresses, however, the calculated void ratios were slightly smaller than the experimental void ratios at maximum applied stress. Similarly, the modified equation for the suction induced volume change has improved the agreement to the experimental data points. It is to be noted that air starts to enter into the pores at a suction of about 8 MPa, and the fitted air-entry value was found to be 51 MPa. Only the data in the saturated range is relevant for the comparison between the calculations and experiments (Fig. 8.7b).

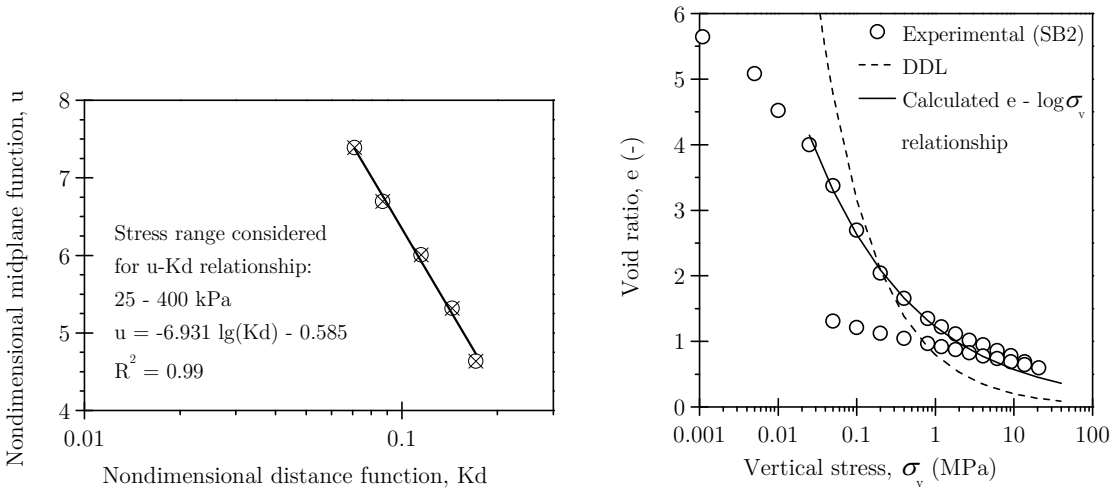

Figure 8.7.: Experimental (oedometer test) vs. calculated volume change for Calcigel bentonite: (a) the $u - Kd$ relationship derived from experimental oedometer data for a stress range of 25 to 400 kPa, (b) experimental and calculated e-log σ_v relationships.

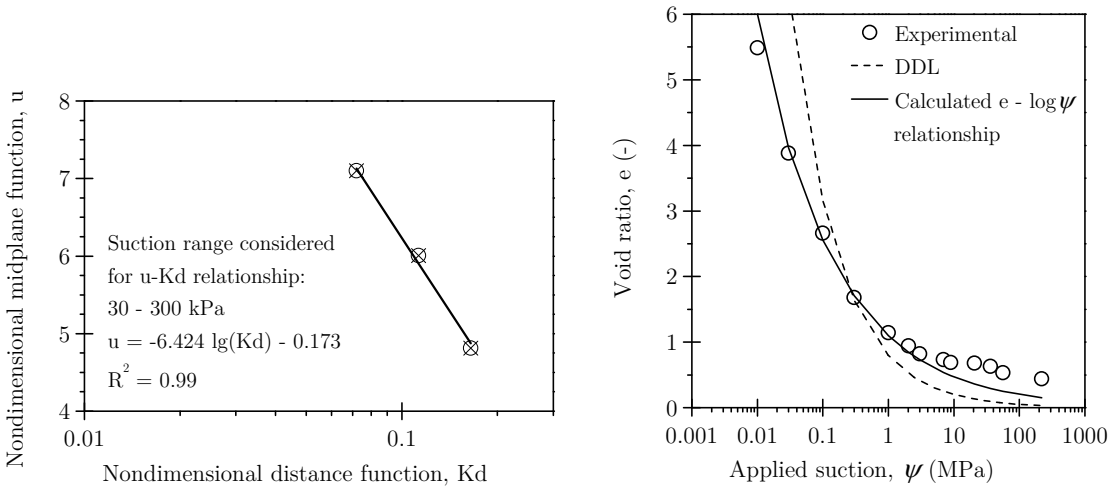

Figure 8.8.: Experimental (suction test) vs. calculated volume change for Calcigel bentonite: (a) the $u - Kd$ relationship derived from suction test data for a suction range of 30 to 300 kPa, (b) unconfined suction test data and calculated e-log ψ relationships.

8.5. Summary

The application of classical diffuse double layer theory was found to be relevant to some extent for Calcigel bentonite, but not relevant for NX illite and Spergau kaolin. Classical diffuse double layer calculations were found to represent reasonably well the experimental data in limited ranges of considered dry densities or applied stresses and suctions of Calcigel bentonite. The overestimation of swelling pressures for lower dry densities and the overestimation of void ratio in the low stress range of the one-dimensional consolidation test and in the low suction range of the water retention tests is attributed to the non-ideal particle arrangement in the compacted specimens and the slurry specimens. The significant deviations in calculated swelling pressures at high dry densities and applied stresses are attributed to the hydration forces manifest as strong repulsion in the swelling pressure test and as a greater resistance to volume change in the oedometer test. The use of the modified approach according to Tripathy et al. (2004) and Tripathy & Schanz (2007) could improve the agreement to the experimental data. However, diffuse double layer forces are not the single operating force within the clay-water system. Thus, the use of approaches based of diffuse double layer only can not be expected to represent the full range of observed phenomena, especially for small interparticle distances.

9. Additional repulsive pressures in clays

9.1. General

In this section, the interparticle repulsive pressures due to double layer repulsion, the interparticle attractive pressures, and the additional repulsive pressures at close clay platelet spacing in the clays studied (Calcigel bentonite, NX illite and Spergau kaolin) and in several reported highly plastic bentonites (MX 80, Febex, Bentonite S2, Kunigel, and Kunigel V1) were determined. The diffuse double layer repulsive pressures for the compacted clays were determined using the equations for the diffuse double layer theory of interacting platelets. The influence of valency of exchangeable cations on the theoretical net interparticle repulsive pressures is shown. The difference between the experimental swelling pressures and the theoretical net interparticle repulsive pressures at closer particle spacing were determined to account for the additional repulsive pressures that get generated within the clay systems. A fairly good correlation was obtained between the spacing between the bentonite platelets and the additional repulsive pressures below a bentonite platelet spacing of about 1.5 nm for the bentonites studied. For NX illite and Spergau kaolin, correlations differed significantly from that of the bentonites. For all three clays, additional repulsive pressures became significant for dry densities greater than the respective Proctor dry density of the clay.

9.2. Parameters influencing the net interparticle pressures

The diffuse double layer repulsive pressures for the compacted clays were determined using the equations for the diffuse double layer theory of interacting platelets (see chapter 8.3).

The attractive pressures for the same range of interlayer distances were calculated using the van der Waals-Hamaker equation (eq. 9.1). The difference between the experimental swelling pressures and the theoretical net interparticle pressures $R-A$ was determined to account for the additional repulsive pressures that get generated within the clay systems.

$$A = \frac{A_{\mathrm{h}}}{48\pi}\left[\frac{1}{d^3} + \frac{1}{(d+\delta)^3} - \frac{2}{(d+0.5\delta)^3}\right] \tag{9.1}$$

Parameter d is half of the interlayer distance, δ is the thickness of the clay particle, and A_{h} is the Hamaker constant ($= 6.11 \cdot 10^{-17}$ kN m for water as the bulk fluid). The value of A_{h} depends upon the dielectric constant, temperature and the degree of saturation of the clay system (Mitchell 1993, Sridharan & Venkat. Rao 1979). The thickness of the clay particles assumed was 1 nm for montmorillonite, 10 nm for NX illite, and 50 nm for Spergau kaolin. The latter two values were chosen based on the results of fabric investigation. In this study, no attempt was made to apply any restrictive rules to limit the double layer repulsion and attraction below a spacing of 1.0 nm. It is assumed that these forces do exist up to a spacing of 0.5 nm, whereas the additional repulsion co-exists and comes into operation at spacing smaller than 1.5 nm, as shown later in this chapter. In any case, such a presumption will indicate the relative importance of double layer repulsion, attraction, and the additional repulsive pressures at very close particle spacing. The dominance of attractive pressure over the repulsive pressure would primarily depend upon the type of exchangeable cations present in the clay media, specific surface area and cation exchange capacity. Since, these are the factors that contribute to the separation distance between the clay platelets and hence the repulsive pressure determination using diffuse double layer theory (see eqs. 8.1 to 8.6).

It may be expected that for a given clay system all other factors (G_{S}, A_{S}, CEC, n) except the valency of exchangeable cations, ν, remaining the same, the attractive pressure will be higher than that of the repulsive pressure at a larger particle spacing for divalent exchangeable cations ($\nu = 2$) than that of a clay containing monovalent exchangeable cations ($\nu = 1$). Reference is made to Fig. 9.1 to explain this. The repulsive pressure, attractive pressure and the net interparticle pressure for a clay ($A_{\mathrm{S}} = 800$ m^2/g, $G_{\mathrm{S}} = 2.7$, $CEC = 100$meq/100g, $n = 10^{-4}$ M) are calculated using eqs. 8.1 to 8.6 and 9.1, and are shown in Fig. 9.1. It can be seen that for the clay with divalent exchangeable cations the attractive pressures are higher than the repulsive pressures below a $2d$ spacing of about 1.25 nm, whereas this occurred at a $2d$ spacing of about 0.75 nm for the same bentonite with monovalent cations. This behaviour is attributed due to the suppressed interparticle distance in case of clays with the divalent exchangeable cations. The net interparticle

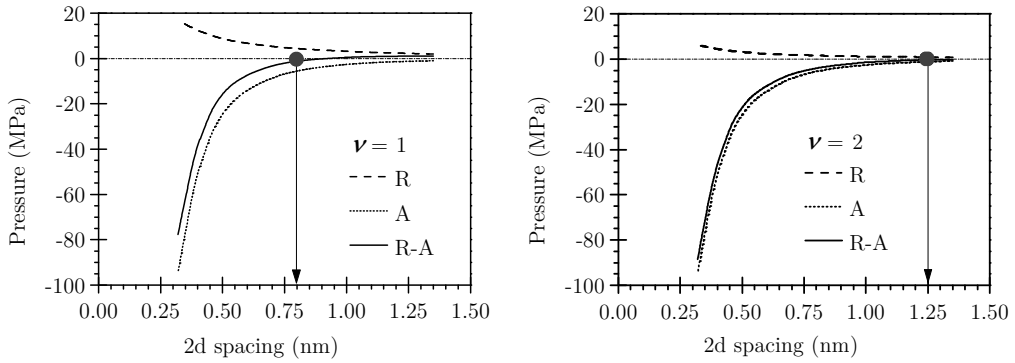

Figure 9.1.: Repulsive, attractive and net interparticle pressures for a clay-water system with two different valencies of exchangeable cations, ν: (a) $\nu = 1$, (b) $\nu = 2$.

pressure (i.e., repulsive minus attractive, $R - A$) goes negative at the corresponding platelet spacing. If a repulsive component of the forces within a compacted clay system is responsible for the development of the swelling pressure, a compacted clay system overpowered by the attractive pressure would tend to reduce its volume. However, this does not happen commonly in compacted expansive clays that show enormous swelling pressure at higher dry densities or lesser $2d$ spacing. Therefore, if at all, the attractive pressure is to be considered, it is then necessary to compute the additional repulsive pressure that is responsible for the swelling pressure of compacted clays at close platelet spacing.

Beside the diffuse double layer repulsion and the van der Waals attraction forces, other short-range repulsive forces exist in clay systems. These include the hydration or solvation forces at a particle distance smaller than 2 nm and Born repulsion. The Born component of the repulsive pressure strictly corresponds to the overlapping of electron clouds of adjacent atoms. Born repulsion increases sharply with decreasing interlayer distance. In most cases, the nature of these pressures are presented as exponential functions, power laws, and steep linear relations (Anderson & Lu 2001, Santamarina 2001*b*). For example, the Born repulsion can be calculated using eq. 9.2, where B is Born repulsion and n is a constant, and $2d$ is the distance between the layers.

$$F_{\mathrm{B}} = \frac{B}{(2d)^n} \tag{9.2}$$

Experimental compression data on various bentonites shown by Marcial et al. (2002) clearly indicated that the type of exchangeable cations affect the void ratio even at a stress as high as 30 MPa. In relatively dry clays, adsorbed cations occupy positions in

holes on the clay surfaces. On hydration, they surround themselves with water and move to the central region between the layers (Mitchell 1993). For a compacted bentonite system allowed to imbibe water under constant volume condition, this movement may be restricted. Therefore, no attempt was made to compute the Born repulsion alone from eq. 9.2, rather, an attempt was made to account for the theoretical double layer repulsive and the attractive pressures separately and the net pressures were then deducted from the experimental swelling pressures of the clays studied to obtain the additional repulsive pressures at close interparticle distances.

9.3. Materials used and procedure adopted for calculation of additional repulsive pressure

The swelling pressure results of five bentonites reported in literature and the swelling pressure results of Calcigel bentonite (see Fig. 5.1 were used for calculation of additional repulsive pressure. Further, the additional repulsive pressure of Spergau kaolin and NX illite were calculated using the experimental swelling pressures reported in section 5.2. The properties of the clays are shown in Table 9.1. The details of the experimental procedure for the constant volume swelling pressure measurements on the bentonites from literature are reported separately by Bucher & Müller-Vonmoos (1989), ENRESA (2000), Komine & Ogata (1996) and JNC (2000). The swelling pressure tests have been conducted using distilled water as the bulk fluid in all cases. The initial degree of saturation of the compacted bentonite samples varied between 20 to 60% for MX 80, 35 to 67% for Febex, 47% to 67% for Kunigel and Kunigel V1 and 17 to 92% for Calcigel bentonite. For Spergau kaolin and NX illite, the initial degree of saturation of the specimens were between 2 and 96% and 3 and 14%, respectively. The experimental swelling pressures of the bentonites are shown in Figs. 9.3 and 9.4 in the following section.

The theoretical repulsive pressures were calculated using eqs. 8.1 to 8.6. The attractive pressures were computed using eq. 9.1. The net repulsive minus the attractive pressures, $R - A$, were then computed.

The example of Calcigel bentonite shown in Fig. 9.2 is used to explain the further steps of the procedure. The calculated net theoretical interparticle pressure $R - A$ and the experimental swelling pressure p_s were plotted as a function of dry density and $2d$ spacing. Similar to the principle behaviour explained in section 9.2, the net interparticle pressure $R - A$ becomes negative with increasing dry density, whereas the measured swelling

Table 9.1.: Properties of the clays considered for determination of additional repulsive forces R_{add}

Bentonite	Specific gravity, G_S	Specific surface area, A_S (m^2/g)	Cation exchange capacity, CEC (meq/100g)	Weighted average valency, ν
MX 80	2.76 [a]	562 [a]	73 [a]	1.12
Febex	2.70 [b]	725 [b]	102 [b]	1.73
Bentonite S2	2.78 [b]	614 [b]	97 [b]	1.66
Kunigel	2.79 [c]	389 [c]	73.2 [c]	1.5
Kunigel V1	2.70 [d]	500 [d]	104.4 [d]	1.46
Calcigel bentonite	2.80	525	74	1.93
NX illite	2.71	154	26	1.92
Spergau kaolin	2.62	28	8	2.0

[a] Müller-Vonmoos & Kahr (1983), [b] ENRESA (2000),

[c] Komine & Ogata (1996), [d] JNC (2000)

pressure values increase with increasing dry density. The additional repulsive pressure correspond to the difference between the experimental swelling pressure p_s and the net interparticle pressure $R - A$. It was denoted as $|p_s - (R - A)| = R_{\text{add}}$ in Fig. 9.2a. The calculated values of R_{add} were plotted separately against $2d$ spacing as shown in Fig. 9.2b. The points were best-fitted using a potential equation (see eq. 9.2). The described procedure was adopted for all clays studied.

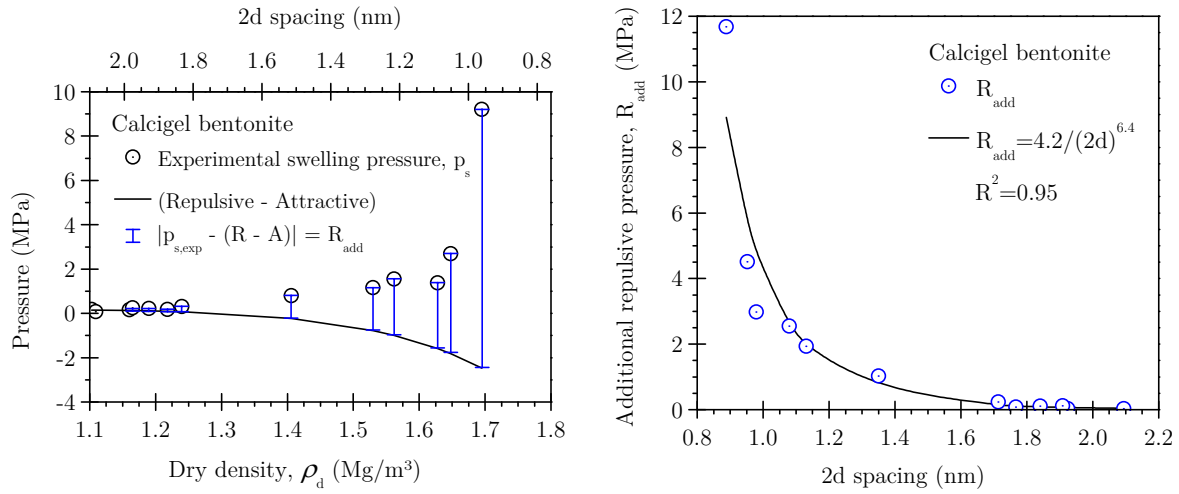

Figure 9.2.: Illustration of determination of additional repulsive pressures R_{add} using the example of Calcigel bentonite: (a) Calculation of the absolute difference between experimental swelling pressures and theoretical net interparticle pressures, $|p_{\text{s}} - (R - A)|$, (b) $|p_{\text{s}} - (R - A)|$ plotted as additional repulsive pressure versus $2d$ spacing.

9.4. Results

The experimental swelling pressure p_{s} and the net interparticle pressure $R - A$ for the bentonites studied are shown in Fig. 9.3, those for Spergau kaolin and NX illite are shown in Fig. 9.4. It can be clearly seen that the theoretical net interparticle pressure $R - A$ becomes negative for all the bentonites, whereas it remains in the repulsive regime with an insignificant magnitude for Spergau kaolin and NX illite. It is to be noted that the calculated $2d$ spacings corresponding to the respective dry densities are in a significantly higher range than those of the bentonites. For the bentonites, the $2d$ values corresponding to dry densities from 1.1 to 2.1 g/cm^3 are in the range from 2.1 to 0.4 nm, whereas dry densities of 1.0 to 1.5 g/cm^3 correspond to $2d$ values of 8.2 to 3.8 nm for NX illite, and to 47 to 22 nm for Spergau kaolin.

Fig. 9.3 shows the additional repulsive pressure versus the distance between clay platelets for spacing less than 2.0 nm for the bentonites studied. The additional repulsive pressure seems to be insignificant above a spacing of 1.5 nm. In other words, above a spacing of 1.5 nm, the repulsive minus the attractive pressures, $R - A$, give a fairly good matching to the experimental swelling pressures. Whereas, the additional repulsive pressure R_{add} increased with a decrease in the $2d$ spacing for all cases below a spacing of about 1.5 nm.

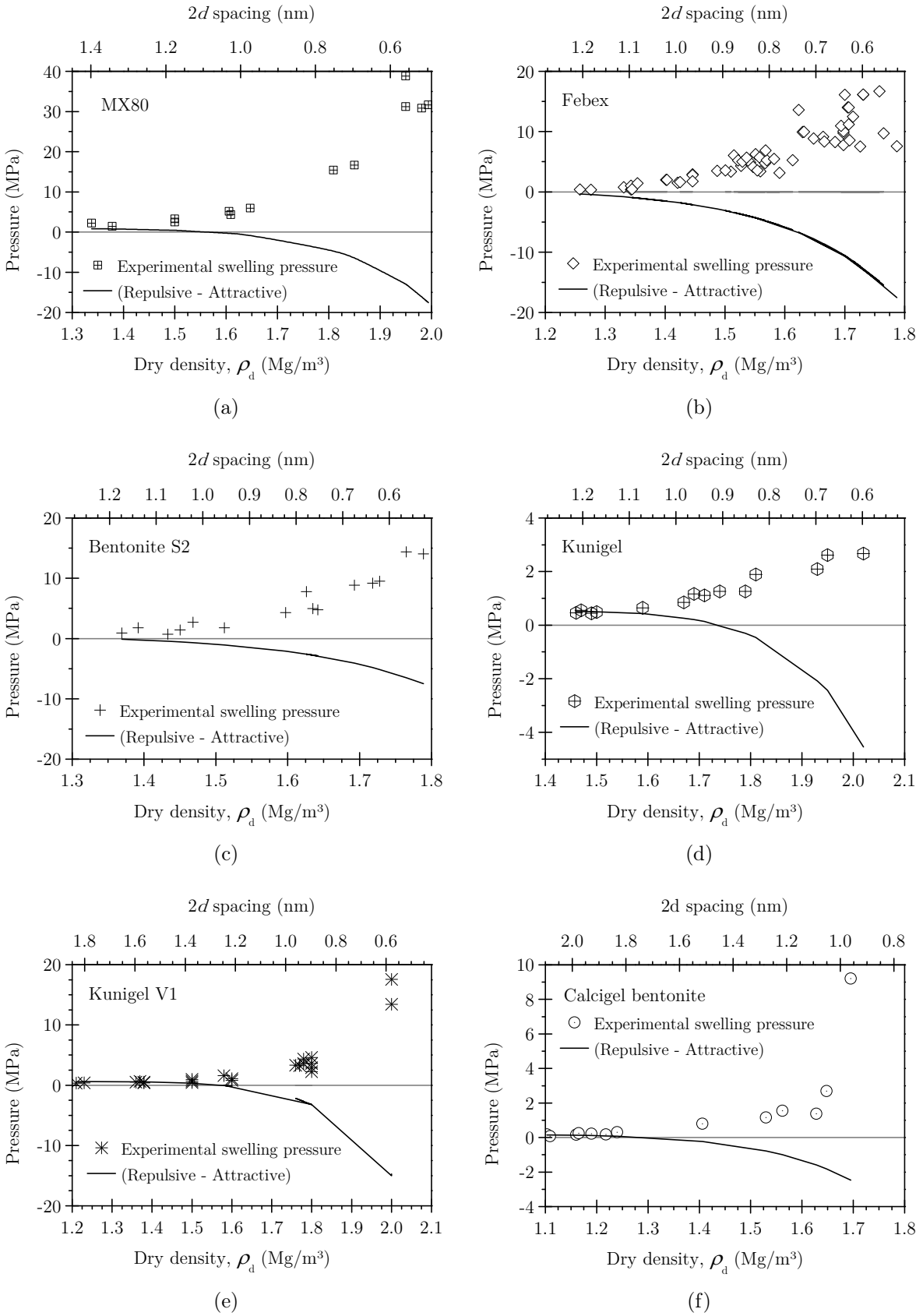

Figure 9.3.: Experimental swelling pressure and net interparticle pressure for bentonites: (a) MX 80, (b) Febex, (c) Bentonite S2, (d) Kunigel, (e) Kunigel V1, and (f) Calcigel.

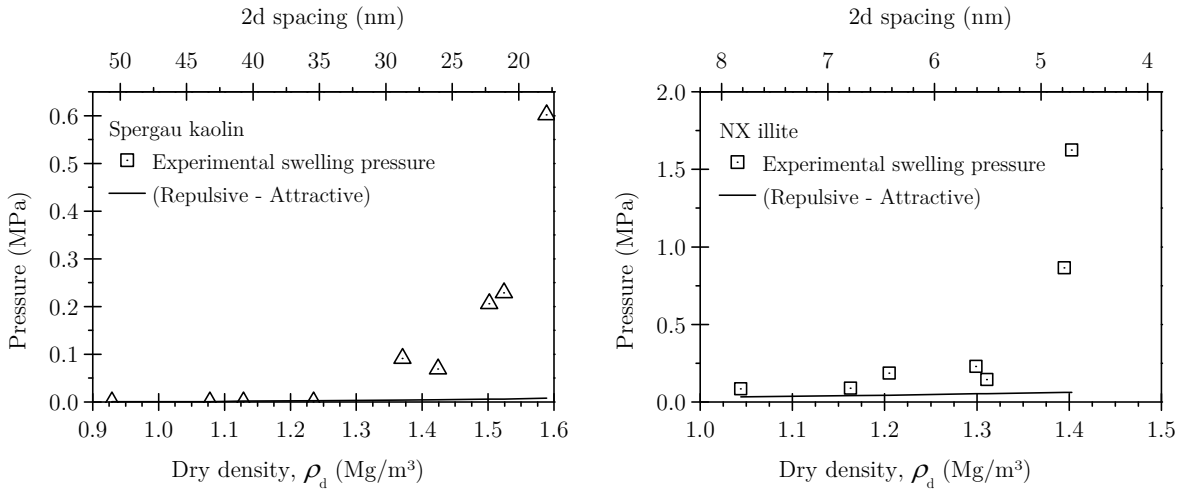

Figure 9.4.: Experimental swelling pressures and net interparticle pressures for Spergau kaolin and NX illite: (a) Spergau kaolin, (b) NX illite.

The spacing of 1.5 nm corresponds to different dry density values of the bentonites. This is expected since the platelet spacing depends upon the physical and mineralogical properties of the clays.

MX 80 bentonite showed the largest additional repulsive pressure, whereas Kunigel V1 showed the least. From Fig. 9.5a, the relationship between $2d$ spacing versus the additional repulsive pressure for each of the bentonites was obtained. The generalised relationship can be expressed in the form of eq. 9.3, where R_{add} is the additional repulsive pressure, and m and n are the parameters responsible for the magnitude of the additional repulsive pressure. The best fit for the bentonites studied is shown in Fig. 9.5b. The R_{add} versus $2d$ plot for each bentonite separately is presented in Annexe C. The values of the parameters m and n, and the correlation coefficient for each of the bentonites are shown in Table 9.2.

$$R_{\text{add}} = \frac{m}{(2d)^n} \tag{9.3}$$

It can be seen from eq. 9.3 and Table 9.2 that the additional repulsive pressure varies inversely with 4th to 6th power of the distance between the clay platelets. The increase in the repulsive pressure is found to be significantly below the spacing of 0.7 nm. The values of the numerator m (see eq. 9.3 and Table 9.2) and are plotted against the surface charge densities, Γ, of the bentonites in Fig. 9.8. The parameter m was found to decrease linearly with an increase in the surface charge density. Plotting the m-value of the clays

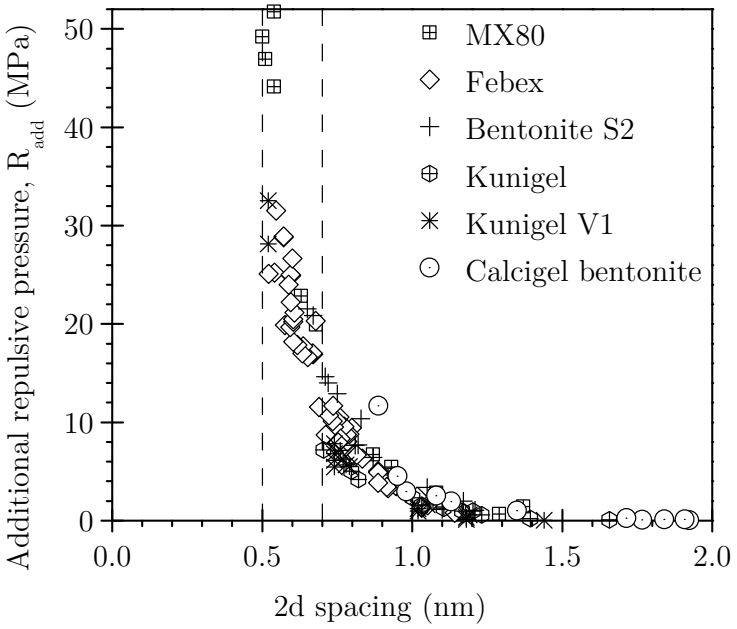

(a)

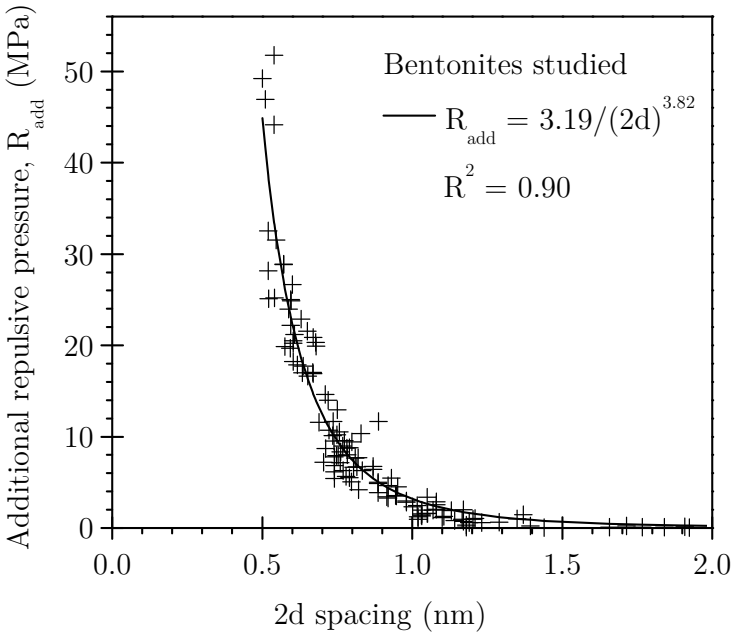

(b)

Figure 9.5.: Relationship for additional repulsive pressures of bentonite: (a) R_{add} versus $2d$-spacing for the bentonites studied, (b) best fit of R_{add} versus $2d$-spacing for the bentonites studied.

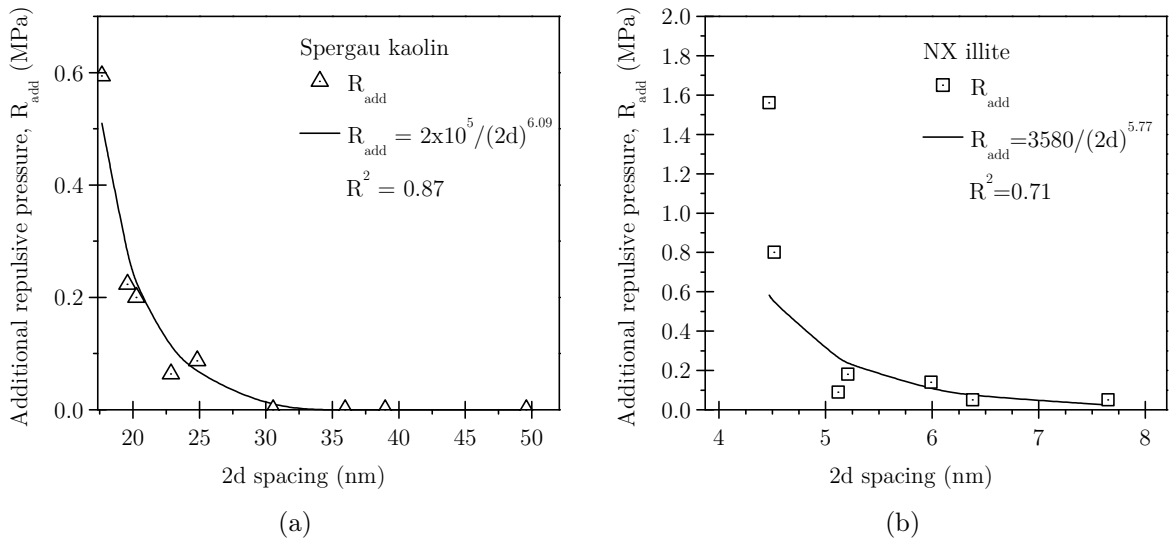

Figure 9.6.: Relationships and best fit equations for additional repulsive pressures of Spergau kaolin and NX illite: (a) Spergau kaolin, (b) NX illite.

Table 9.2.: Parameters m and n for the calculation of R_{add}

Bentonite	Surface charge density, Γ (μeq/m^2)	Dimensionless parameter m	n	R^2
MX 80	1.30	3.4	4.1	0.97
Febex	1.41	2.3	4.5	0.95
Bentonite S2	1.58	3.0	4.9	0.95
Kunigel	1.88	1.7	4.8	0.95
Kunigel V1	2.09	0.9	6.2	0.91
Calcigel bentonite	1.41	4.2	6.4	0.95
NX illite	1.69	3580	5.77	0.71
Spergau kaolin	2.86	$2 \cdot 10^5$	6.09	0.87

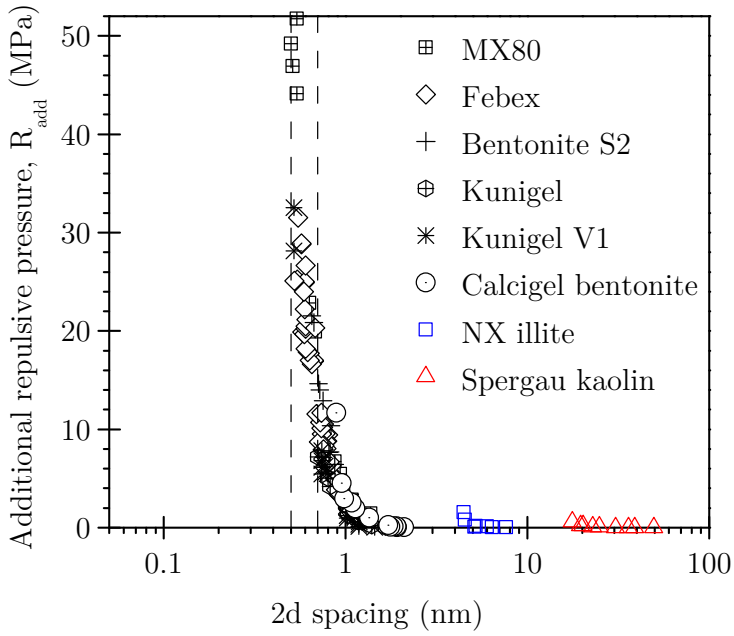

(a)

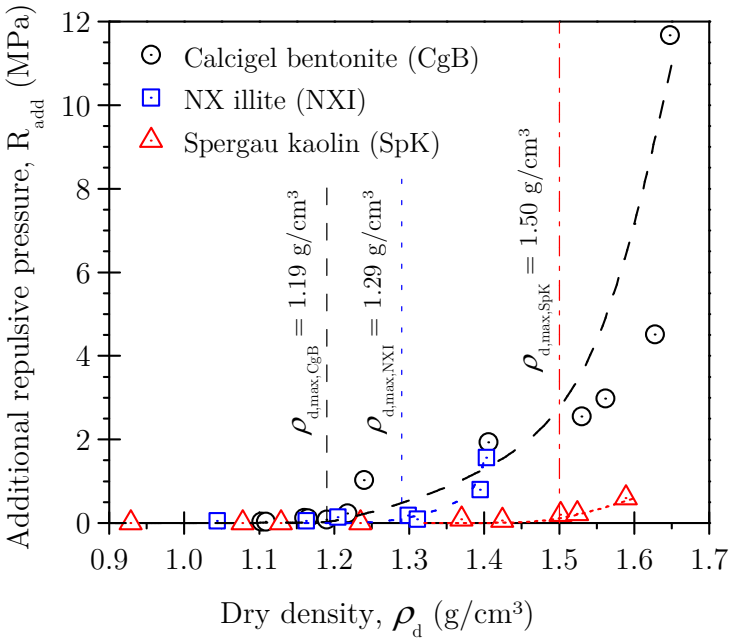

(b)

Figure 9.7.: Additional repulsive pressure vs. $2d$ spacing and dry density for Spergau kaolin, NX illite and the bentonites studied: (a) R_{add} vs. $2d$-spacing, (b) R_{add} vs. dry density.

separately against specific surface area (Fig. 9.9a), cation exchange capacity (9.9b) and surface charge density (9.9b), indicates a relationship of m to the specific surface area and the cation exchange capacity of the clays.

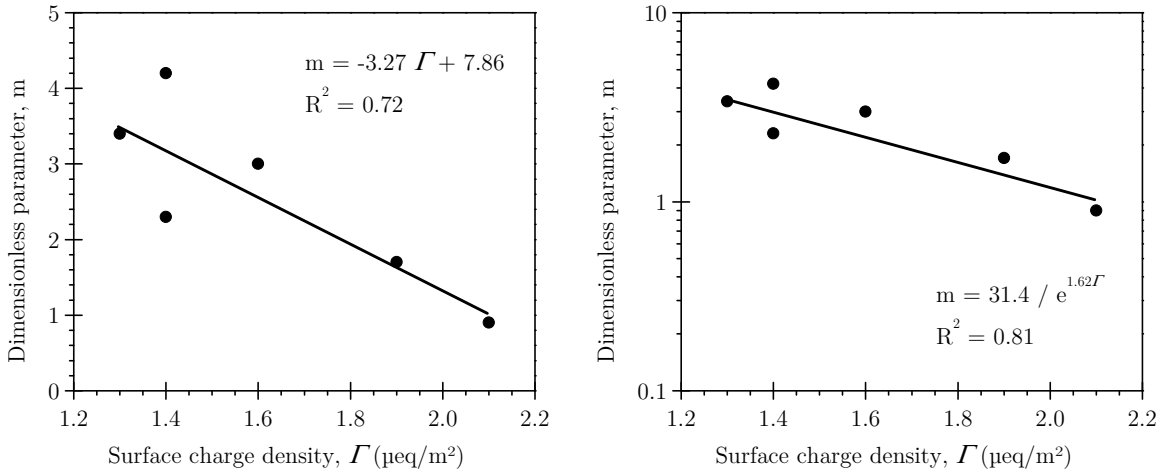

(a) (b)

Figure 9.8.: Surface charge density Γ versus parameter m and best fit for the bentonites studied: (a) m versus Γ and linear best fit, (b) $\log m$ versus Γ and exponential best fit.

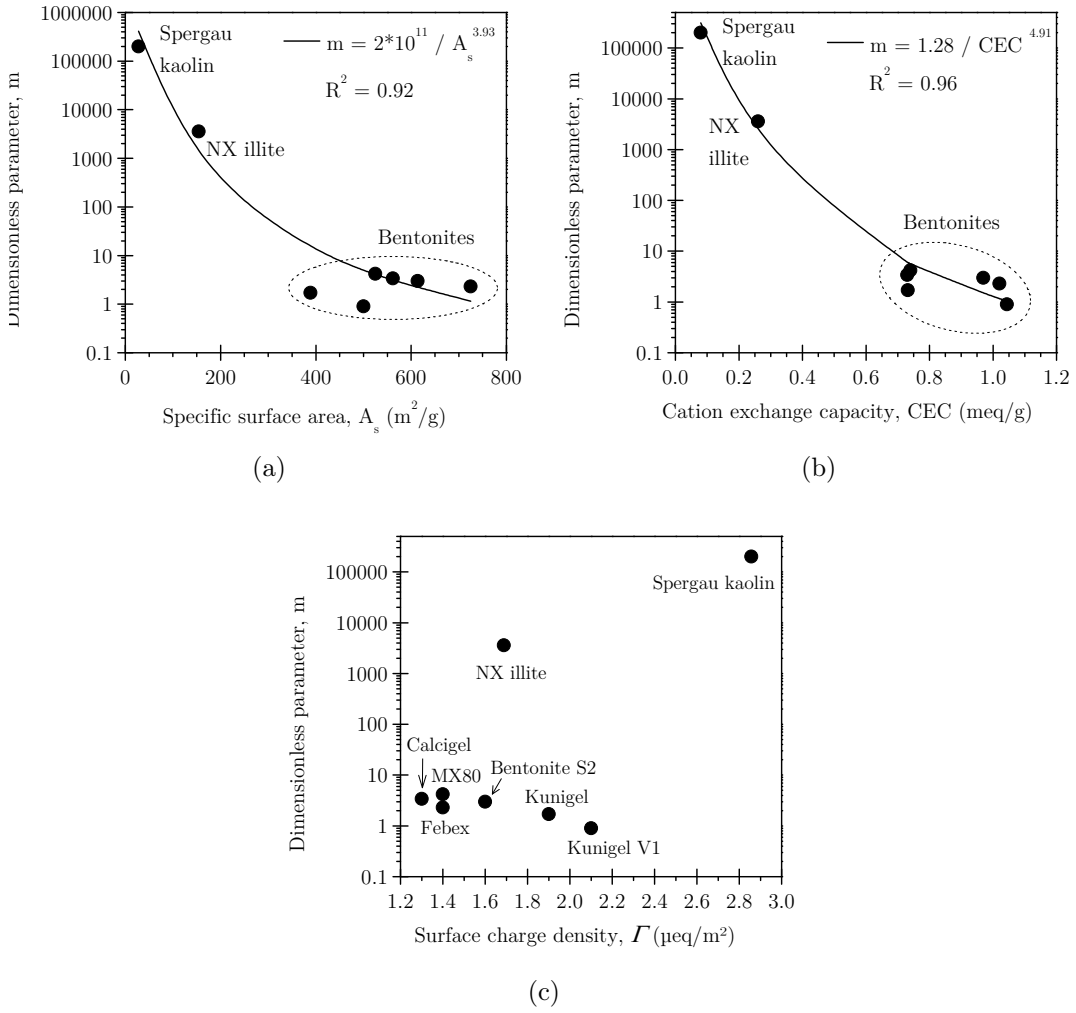

Figure 9.9.: Correlation of parameter m with A_S, CEC and Γ for Spergau kaolin, NX illite and the bentonites studied: (a) m versus A_S and best fit, (b) m versus CEC and best fit, (c) m versus Γ.

9.5. Summary

The repulsive and attractive pressures for several compacted clays from literature (MX 80, Febex, Bentonite S2, Kunigel and Kunigel V1) and for the clays of the present study (Calcigel bentonite, NX illite and Spergau kaolin) were calculated based on physico-chemical considerations. The additional repulsive pressures at close particle spacing were obtained by subtracting the theoretical net interparticle double layer repulsive pressures from the corresponding experimental swelling pressures of the clays. It is shown that the additional repulsive pressure contribute to the swelling pressure of compacted bentonites below a spacing of 1.5 nm, whereas their contribution is significant below a spacing of about 0.7 nm. The additional repulsive pressure was shown to have a near linear relationship with the surface charge density and varies inversely from 4th to 6th power of the platelet spacing. The additional repulsive pressures for Spergau kaolin and NX illite were found to be significantly smaller than those of the bentonites. It was shown that the repulsive pressures at short range are becoming relevant for dry densities greater than the proctor density. The additional repulsive pressure was shown to be related to the specific surface area and the cation exchange capacity independent of the mineral type.

10. Effective stress in clays

10.1. General

Effective stress is known to govern the mechanical behaviour of soils. Since many years, the determination of effective stress in unsaturated soils is an active field of research. One of the proposed approaches for determining effective stress of unsaturated soils is the suction stress approach. Distinction of the influence of clay mineral type on the shape of the suction stress characteristic curve (SSCC), magnitudes of minimum and maximum suction stress, and further, their influence on the effective stress of clays for a large range of suction has not been fully explored yet. In this context, and based on the experimental data for water retention and one-dimensional volume change behaviour of the clays with significantly different clay minerals, the influence of suction stress on the effective stress of clays is brought out in this part the study. The effective stress in the clays studied was determined based on the suction stress characteristic curves (SSCCs) of the clays. The SSCCs were determined based on the drying soil-water characteristic curves (SWCCs) of the clays for a suction range of 0.03 to about 219.0 MPa. One-dimensional compressibility behaviour of initially saturated clays was also studied by loading clay specimens up to a maximum vertical stress of 21.0 MPa. The effective stress-void ratio responses of the clays during the drying process were compared with their counterparts obtained for saturated condition. The differences in the observed behaviour due to the differences in mineralogy of the clays studied were highlighted.

10.2. Suction stress concept

Based on the suction stress approach (Lu et al. 2010), the effective stress of unsaturated soils can be calculated using equations 10.1 to 10.5 in conjunction with suction-effective degree of saturation SWCCs. The effective degree of saturation, S_e, at any suction (ψ) can be calculated by knowing the degree of saturation (S_r) and the residual degree of

saturation (S_{res}) from eq. 10.1. In order to obtain the fitting parameters α (inverse of the air-entry value (AEV), u_b) and the pore size distribution parameter (n), van Genuchten's (1980) model can be used to best-fit the SWCC (ψ versus S_e) (eq. 10.2). The suction stress (σ^s) corresponding to any S_e can be calculated from the closed-form expression (i.e., eq. 10.3). The effective stress (σ') can be calculated from eq. 10.4. In the absence of any external stress on soil specimens during SWCC tests and the pore air pressure (u_a) as a reference, eq. 10.4 reduces to eq. 10.5.

$$S_e = \frac{S_r - S_{res}}{1 - S_{res}} \tag{10.1}$$

$$S_e = \left[\frac{1}{1 + (\alpha\psi)^n}\right]^{1-\frac{1}{n}} \tag{10.2}$$

$$\sigma^s = -\frac{S_e}{\alpha}(S_e^{\frac{n}{1-n}} - 1)^{\frac{1}{n}} \qquad 0 \leq S_e \leq 1 \tag{10.3}$$

$$\sigma' = (\sigma - u_a) - \sigma^s \tag{10.4}$$

$$\sigma' = -\sigma^s \qquad \text{for} \qquad \sigma - u_a = 0 \tag{10.5}$$

The uniqueness of the SSCC determined from both shear strength and water retention tests has been examined (Lu et al. 2010, Oh et al. 2012). These studies have demonstrated the validity of the effective stress principle by showing that the effective stress based on the SSCC describes the same unique failure criterion as that for the saturated failure criterion. The measured SSCCs are shown to predict the salient features of soil-water retention curves within reasonable accuracy. Similarly, the SSCCs of soils, determined directly from water retention tests, also were found to accord well with the SSCCs determined directly from direct shear and triaxial shear-strength tests with the difference within several tens of kPa.

Variations of the shear strength and the tensile strength (i.e., the suction stress) with changes in the water content of unsaturated soils have been reported by several researchers (Mullins & Panayiotopoulos 1984, Lu, Wu & Tan 2007, Vesga 2008). Vesga (2008) measured the tensile strength of a kaolinite at several water contents from direct tensile

tests. It was shown that depending upon the state of water in the clay, a reduction in the water content was accompanied by a decrease in the suction stress, which remained nearly constant for a specified range of water content, and further increased. Accordingly, the volume of the clay was found to decrease, remained constant, and further increased during the drying process. The minimum volume in the clay was reached when the minimum suction stress was developed.

Lu et al. (2010) showed that, depending on the value of n (see eq. 10.2), the SSCC can be expected to exhibit two distinct regimes, such as that if $n = 2$, the suction stress monotonically decreases and if $n > 2$, the suction stress decreases and then increases with an increase in suction. Lu et al. (2010) stated that the α parameter dominantly controls the minimum value of suction stress and the suction value corresponding to that minimum, whereas the parameter n solely controls the effective degree of saturation corresponding to the minimum suction stress.

The magnitudes of interparticle repulsive pressure in clays depend upon the applied external stress, the specific surface area, the cation exchange capacity, the type of exchangeable cations present in the clay, and the pore-fluid characteristics. Similarly, the magnitude of van der Waals attractive force depends upon the separation distance between clay particles, the thickness of clay particles, the characteristics of the pore-fluid medium, and the degree of saturation. Additionally, the thickness of clay particles and the characteristics of pore fluid influence the fabric and structure of clays. During the drying process or with an increase in the applied stress on initially saturated clays the interparticle repulsive and attractive pressure increase. Tripathy et al. (2006) have shown that the van der Waals attractive pressure exceeds the interparticle double-layer repulsive pressure at low water contents or at low void ratios. At close particle spacing, additional forces on account of BornŠs repulsion and primary valence bond influence the volume change behaviour of clays. Among several factors, the clay mineral type is considered to directly influence the hydraulic and mechanical behaviour of clays.

10.3. Procedure adopted for the calculation of effective stress

Laboratory tests were carried out in order to study the unconfined water retention behaviour (see chapter 4), one-dimensional compressibility (see chapter 6), and suction stress behaviour of three initially saturated clays. The methods and the equipment used for the

tests were described in detail in the respective sections. The results of the unconfined water retention tests enabled calculating the effective stress in the clays undergoing the drying process. The material properties of the clays used (Calcigel bentonite, NX illite, Spergau kaolin) were described in detail in section 3.1. It was shown in Table 3.7 that the dominant mineral present in Calcigel bentonite is montmorillonite, illite in NX illite, and kaolinite in Spergau kaolin. The specific surface areas, cation exchange capacities, and the plasticity properties of the clays were found to be distinctly different (see Table 3.11).

The following procedure was adopted for the establishing the SSCCs: (*i*) based on the experimental data for the suction-water content and suction-void ratio SWCCs, the suction-effective degree of saturation SWCCs of the clays were established; the effective degree of saturation was calculated using eq. 10.1, (*ii*) the suction-effective degree of saturation SWCCs were best-fitted using van Genuchten's (1980) model using eq. 10.2 and further, the fitting parameters α and n were obtained, and (*iii*) suction stress values corresponding to all suctions considered and for the full range of effective degree of saturation was calculated using the closed-form expression proposed by Lu et al. (2010) (eq. 10.3). The effective stress corresponding to the applied suctions were calculated based on the suction stresses using eq. 10.5.

10.4. Results and discussion

10.4.1. Suction-water content SWCCs and volume change due to applied suctions

Figures 10.1a and 10.1b show the suction-water content SWCCs and applied suction versus void ratio plots of the clays studied, respectively. The shapes of the suction-water content SWCCs and suction versus void ratio responses of Calcigel bentonite and NX illite are found to be very similar; that is, a monotonic decrease in the water content and void ratio occurred with an increasing in the applied suction, whereas a decrease in the water content for Spergau kaolin was found to be abrupt between suctions of about 2.0 to 7.0 MPa. The residual zone is found to be distinct for Spergau kaolin, whereas it is indistinct for Calcigel bentonite and NX illite.

In order to verify the compatibility between the experimental results from osmotic and vapour equilibrium techniques, comparisons of water contents of the clays at applied suctions of 3.0 and 9.0 MPa in the osmotic tests and at applied suctions of 2.0 and

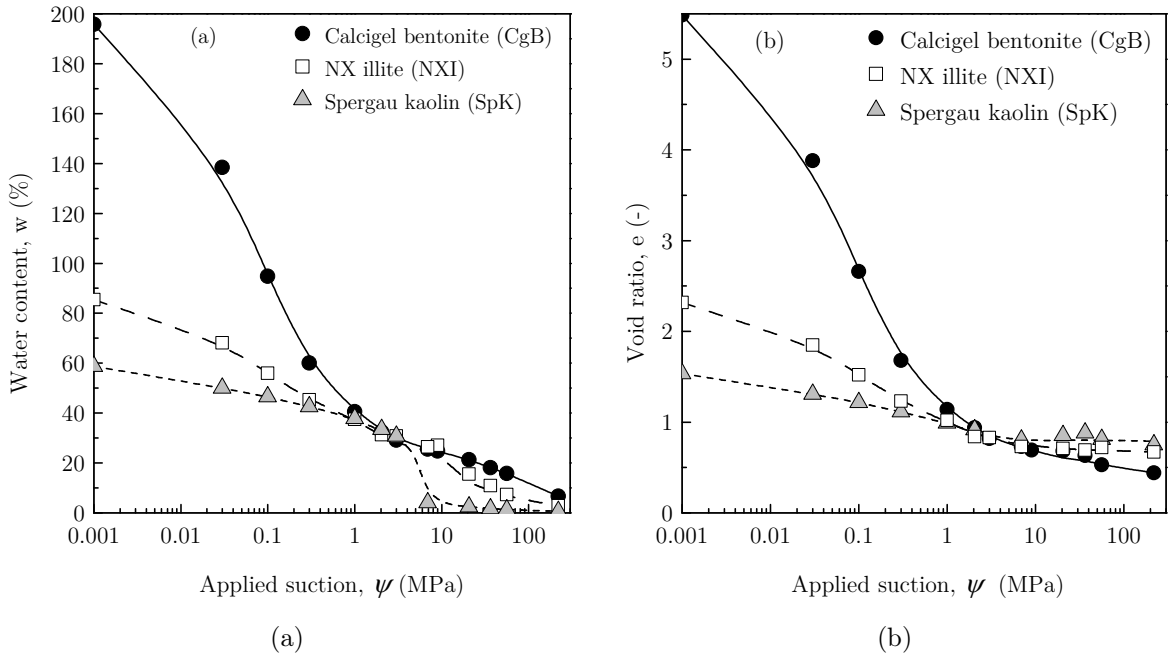

(a) (b)

Figure 10.1.: Suction induced water content and void ratio changes: (a) water content vs. suction, (b) void ratio vs. suction; Baille et al. (2014).

6.9 MPa in the vapour equilibrium tests were carried out. The results showed that, the water content decrease for Calcigel bentonite and NX illite was consistent in the osmotic and vapour equilibrium techniques in the overlapping suction range, whereas the water content of Spergau kaolin at 6.9 MPa was 4.0% as compared to 30.8 and 26.8% at applied suctions of 3.0 and 9.0 MPa in the osmotic tests. An insignificant decrease in the water content for Spergau kaolin in the osmotic tests at high applied suctions is attributed due to a discontinuity in water phase between the clay specimens and PEG solutions. It is hypothesized that the air-water interface retreated inwards from the surfaces of the clay specimens once the AEV of the clay was reached. This was found to be not an issue for the other two clays, in which cases, it will be shown later that, the AEVs of the clays were greater than the maximum applied suction in the osmotic tests (i.e., 9.0 MPa). The trend curves in Fig. 10.1a for Spergau kaolin was drawn based on the results from the vapour equilibrium tests at high applied suctions. At high applied suctions (>10.0 MPa), the water contents of Calcigel bentonite remained greater than that of NX illite and Spergau kaolin.

For applied suctions smaller than 2.0 MPa, the equilibrium void ratios and water contents of the clays were found to be arranged according to the liquid limits of the clays in the order of Calcigel bentonite, NX illite, and Spergau kaolin. For applied suctions greater

than 2.0 MPa, the ordering of the suction versus void ratio plots was found to be changed with the void ratios of Spergau kaolin remained distinctly greater than the void ratios of NX illite and Calcigel bentonite.

10.4.2. Volume change in oedometer and suction tests

Figures 10.2a, 10.2b, and 10.2c show for each clay, the void ratio changes due to an increase in the applied vertical stress in one-dimensional compressibility tests (applied vertical stress σ versus e, where e is the void ratio) and an increase in the applied suction on the void ratio of the clays in suction tests. For comparison, the suction-water content SWCCs of the clays are also shown in the relevant plots in Fig. 10.2. The void ratio axes in Fig. 10.2 (see right-hand side y-axes) were scaled to match the water contents on the left-hand side y-axis for fully saturated conditions.

For any clay, the oedometer compression path and the suction versus void ratio response were found to be very similar within a range of applied vertical stress or applied suction (i.e., up to about 2.0 to 4.0 MPa for Spergau kaolin, 10.0 to 20.0 MPa for NX illite, and up to about 21.0 MPa for Calcigel bentonite). This indicates that an applied suction and vertical stress of equal magnitudes caused similar volume changes of the clays within the specified stress ranges. The results are in agreement with the test results for various clays reported in the literature (Fredlund & Rahardjo 1993, Fleureau et al. 1993, Tripathy, Bag & Thomas 2010). For suctions less than the noted values, the suction-water content SWCC and suction versus void ratio response for any clay were found to be similar and the clays remain saturated. At high applied suctions, the suction versus void ratio plots of Spergau kaolin and NX illite remained distinctly above that of the corresponding applied vertical stress-void ratio curves and suction-water content SWCCs. Deviations of the suction versus void ratio responses from the corresponding saturated compression paths can be considered for approximately determining the AEVs of soils (Fredlund & Rahardjo 1993, Tripathy et al. 2010).

For any clay, the oedometer compression path and the suction-void ratio relationship were found to be very similar within a range of applied vertical stress or applied suction (i.e., up to about 2.0 to 4.0 MPa for Spergau kaolin, 10.0 to 20.0 MPa for NX illite, and up to about 21.0 MPa for Calcigel bentonite). This indicates that an applied suction and vertical stress of equal magnitudes caused similar volume changes of the clays within the specified stress ranges. The results are in agreement with the test results for various clays reported in the literature (Fredlund & Rahardjo 1993, Fleureau et al. 1993, Tripathy

et al. 2010). For suctions less than the noted values, the suction-water content SWCC and suction-void ratio relationship for any clay were found to be similar and the clays remained saturated. At high applied suctions, the suction-void ratio SWCCs of Spergau kaolin and NX illite remained distinctly above that of the corresponding applied vertical stress-void ratio curves and suction-water content SWCCs. Deviations of the suction-void ratio relationship from the corresponding saturated compression paths can be considered for approximately determining the AEVs of soils (Fredlund & Rahardjo 1993, Tripathy et al. 2010).

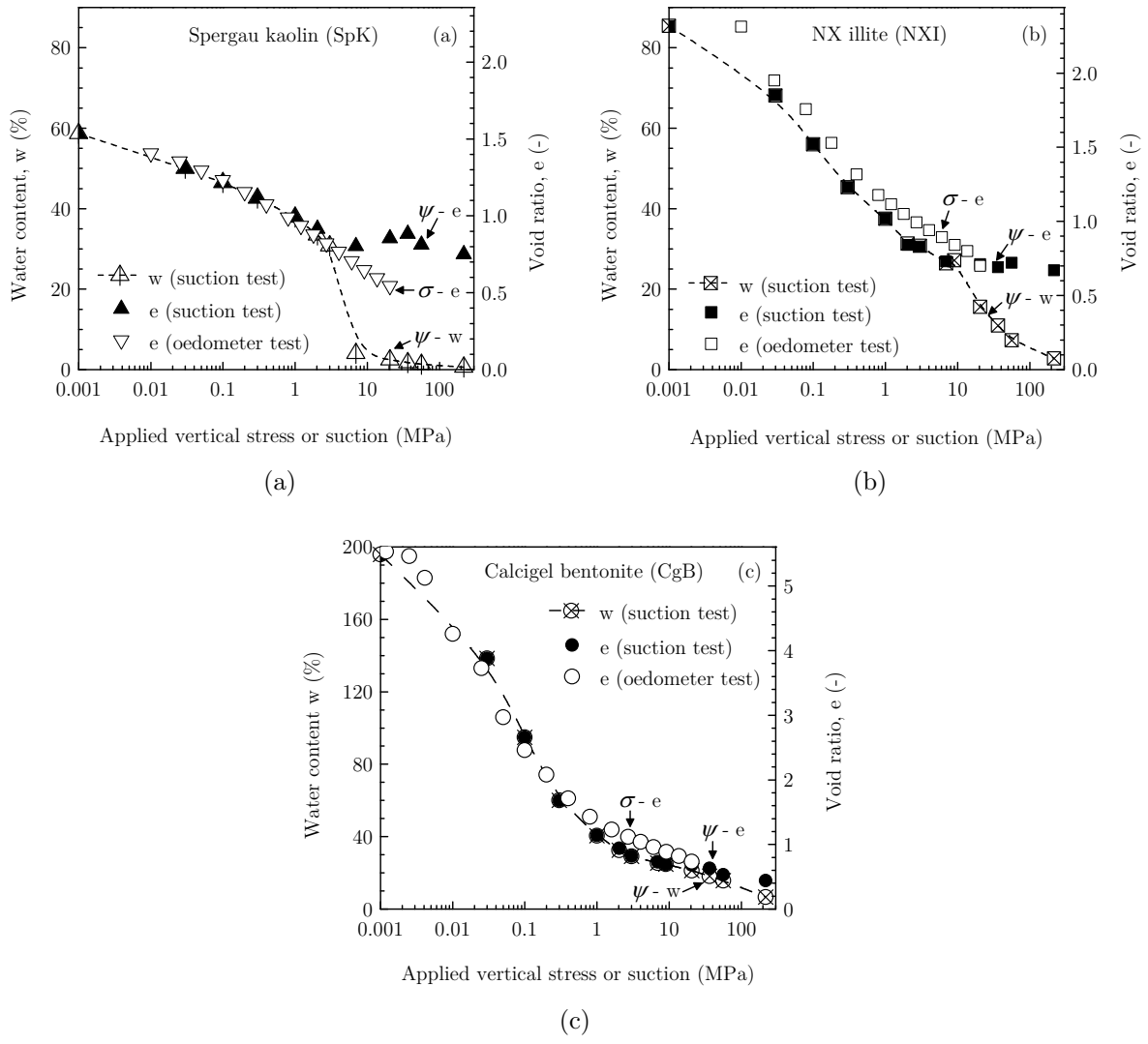

Figure 10.2.: Void ratio changes depending on loading type and suction induced water content change: (a) Spergau kaolin, (b) NX illite, (c) Calcigel bentonite; Baille et al. (2014).

10.4.3. Influence of mineralogy on suction stress characteristic curve

Figures 10.3a to 10.3c present the SWCCs and the SSCCs in terms of the effective degree of saturation for Spergau kaolin, NX illite and Calcigel bentonite, respectively. The fitting parameters (α and n), and the air-entry fitting parameters (i.e., u_b values) of the clays that were derived from the SWCCs are shown in the corresponding plots. The fitting parameters were used to calculate the suction stress values shown in Fig. 10.4b. The maximum value of suction was set to 1000 MPa for all clays, which is the value of total suction generally correspond to zero water content for many soils (Croney & Coleman 1961). Figure 10.4a, 10.4b and 10.4c show the suction-effective degree of saturation SWCCs, the SSCCs in terms of the effective degree of saturation, and the SCCCs in terms of suction of the clays, respectively. Figure 10.5 shows the results presented in Fig. 10.4c in log-log plot in order to better highlight the salient features of the SSCCs (in terms of suction) of the clays studied.

The shapes of the SWCCs of Spergau kaolin and NX illite are found to be similar (Figs. 10.3a, 10.3b, and 10.4a). However, the applied suction needed to desaturate NX illite was greater (17.4 MPa) as compared to that required for Spergau kaolin (3.8 MPa). The residual suction was found to be about 8.0 MPa for Spergau kaolin and about 80.0 MPa for NX illite. In case of Calcigel bentonite (Figs. 10.3c and 10.4a), the air-entry fitting parameter (u_b) was found to be 51.0 MPa. The residual zone was found to be indistinct for Calcigel bentonite indicating that the continuity in the water phase persisted even at high applied suctions. At a suction of 1000 MPa, the effective degree of saturation for Calcigel bentonite was found to be about 0.2 (i.e., about 20%). The results in this study for Calcigel bentonite are concurrent with the results for several other bentonites reported in the literature (Fleureau et al. 1993).

Figures 10.3a, 10.3b, and 10.4b show that, the shapes of SSCCs (in terms of the effective degree of saturation) for Spergau kaolin and NX illite are similar and correspond to down-and-up characteristic of suction stress, similar to that has been observed for sands and silts (Lu et al. 2010). However, the induced magnitude of suction stress during the drying process is found to differ quite significantly for the clays. Suction stress decreased (i.e., became more negative) with an increase in suction, but the clays remained fully saturated. In this regime, applied suctions and suction stresses were equal. The minimum values of suction stress were found to be about 2.0 MPa for Spergau kaolin and about 12.0 MPa for NX illite. A decrease in the effective degree of saturation caused the suction stress

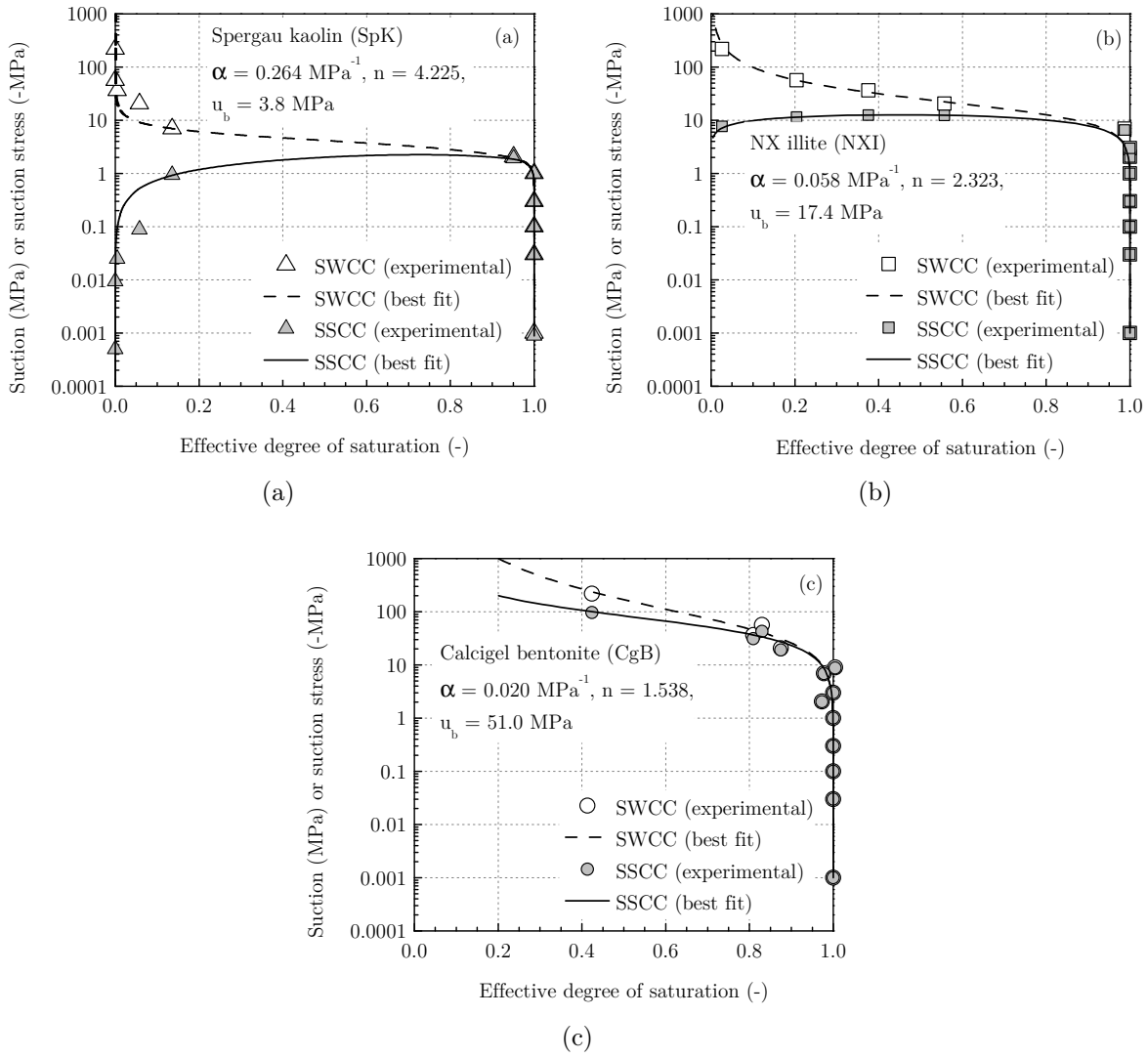

Figure 10.3.: Soil-water characteristic curve (SWCC) and suction stress characteristic curve (SSCC) of the clays studied: (a) Spergau kaolin, (b) NX illite, (c) Calcigel bentonite; Baille et al. (2014).

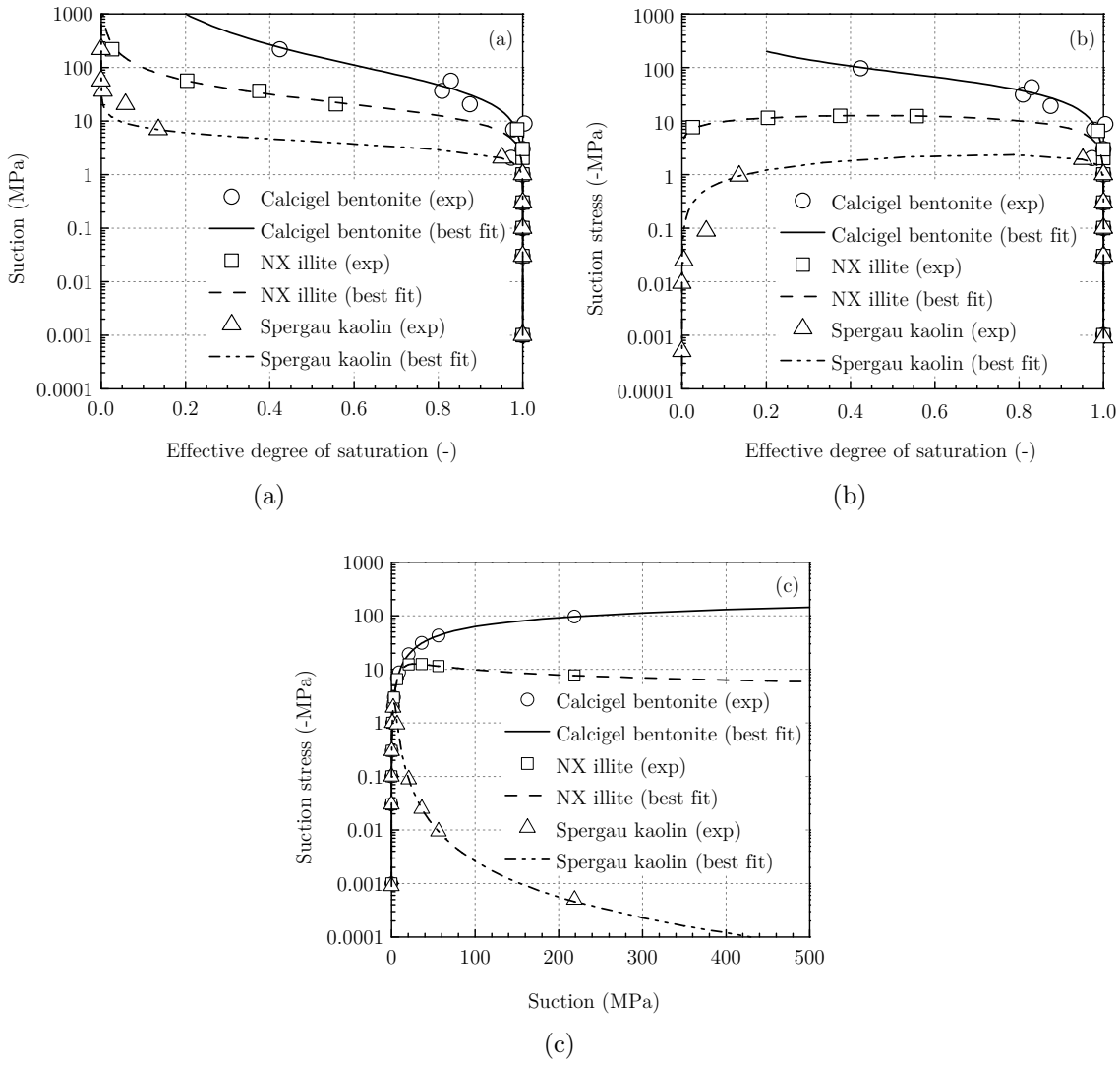

Figure 10.4.: Comparison of the SWCCs and SSCCs of the clays studied: (a) SWCCs in terms of suction vs. effective degree of saturation, (b) SSCCs in terms of effective degree of saturation, (c) SSCCs in terms of suction; Baille et al. (2014).

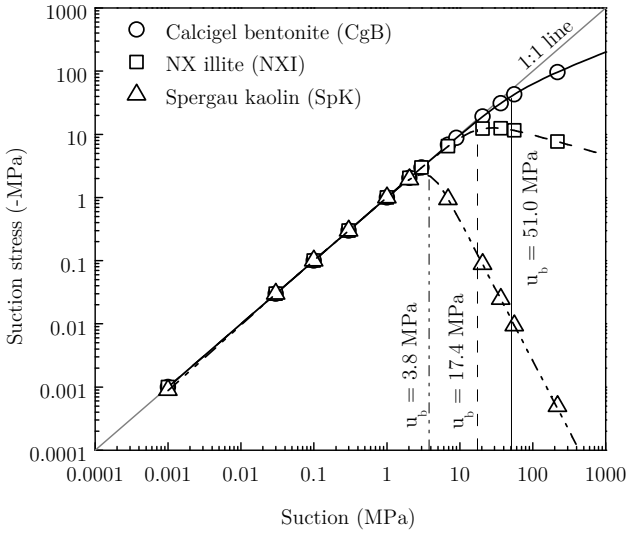

Figure 10.5.: SSCCs in terms of suction for the clays studied (*log-log* scale); Baille et al. (2014).

to increase (less negative) for Spergau kaolin, whereas the suction stress remained nearly unaltered for a large range of effective degree of saturation for NX illite. For fully dried state (suction approximately equal to 1000 MPa), the values of suction stress for Spergau kaolin and NX illite were found to be about zero and 5.0 MPa, respectively.

The SSCC in terms of the effective degree of saturation for Calcigel bentonite presented in Figs. 10.3c and 10.4c showed a somewhat different characteristic as compared to the SSCCs of Spergau kaolin and NX illite. Suction stress decreased with an increase in applied suction and the clay remained fully saturated up to about a suction of 51.0 MPa. Further, with a decrease in the effective degree of saturation, suction stress decreased monotonically. The shape of the SSCC for Calcigel bentonite was found to be similar to that of the characteristic SSCC for clays, as noted by Lu et al. (2010). At a suction of 1000 MPa, the suction stress of Calcigel bentonite was found to be about 200 MPa as against zero and 5.0 MPa for Spergau kaolin and NX illite, respectively. The shapes of SSCCs (in terms of suction) for Calcigel bentonite and Spergau kaolin were found to be distinctly different (see Figs. 10.4c and 10.5), whereas the shape of the SSCC for NX illite remained intermediately between the other two clays. The results presented in Figs. 10.1 to 10.5 clearly showed that the mineralogy of clays significantly influences the shape and the salient features of the SWCC (i.e., AEV and residual zone) and SSCC (i.e., the minimum and maximum suction stresses) during the drying process.

Water saturated clay minerals usually form clay aggregates. Among several other factors, the liquid limit of clays is primarily dependent upon the specific surface areas of the clays. Clays with thicker clay particles possesses lesser specific surfaces, lesser cation exchange capacities, thinner electrical double-layer, smaller liquid limits, and usually exhibit less volumetric deformations upon subjected to external stresses (van Olphen 1963, Lambe & Whitman 1969, Sridharan & Jayadeva 1982, Mitchell & Soga 2005). Once the electrical double-layer among clay particles are pushed aside, the shearing resistance offered against volumetric deformation is on account of the van der Waals attractive force and the chemical cementation effects. Lu & Likos (2006) stated that, with no external stress and pore water pressure, the short-range forces arising from Born and steric repulsion (i.e., the bonding stress) counterbalance the physico-chemical forces in saturated soils. Similarly, for a soil undergoing the drying process under zero external stress, the suction stress is comprised of the bonding stress at the saturated state and the changes in physico-chemical stresses due to desaturation, capillary stress arising from surface tension, and negative pore-water pressure (Lu & Likos 2006, Lu et al. 2010). The current study showed that, the suction stress of the clays studied is in order of a few megapascals to several tens of megapascals. The SSCCs of Spergau kaolin and NX illite were found to be similar to that of sands and silts, respectively. However, the minimum suction stresses attained by the clays are found to be about two to three orders of magnitude greater than that for typical silty soils which indicates that contributions of the physico-chemical stresses to the suction stress for these clays are quite significant. The characteristic down-and-up shape of the SSCC for Spergau kaolin indicates that, at high applied suctions the dominant components of suction stress are the surface tension forces and forces arising from the negative pore water pressure. On the other hand, a monotonic decrease of suction stress with decreasing effective degree of saturation for Calcigel bentonite dictates dominant active local forces (Lu & Likos 2006) for a large range of applied suction.

Recalling that, clays composed of kaolinite, illite, and montmorillonite may exhibit expansion or compression upon inundation with fluids. The SSCCs of the clays presented in Fig. 10.5 qualitatively indicate that a decrease in suction stress due to a decrease in suction from very dry state of the clays would increase the effective stress (equations 10.4 and 10.5) which in turn would tend to cause compression of Spergau kaolin and NX illite, whereas a decrease in suction causing an increase of suction stress aids decreasing the effective stress which in turn would tend to cause swelling of Calcigel bentonite.

10.4.4. Influence of suction stress on effective stress

Figures 10.6a to 10.6c show the effective stress-void ratio results from the consolidation tests (both loading and unloading) and the effective stress-void ratio results based on the suction stress that in turn, were calculated from the drying SWCCs for Spergau kaolin, NX illite, and Calcigel bentonite, respectively. For the sake of clarity, trend lines with arrows are shown in Fig. 10.6 to distinguish the drying paths of the clays from the saturated loading and unloading paths. The void ratios of the clays presented in Fig. 10.6 for the drying paths are the measured values at various applied suctions.

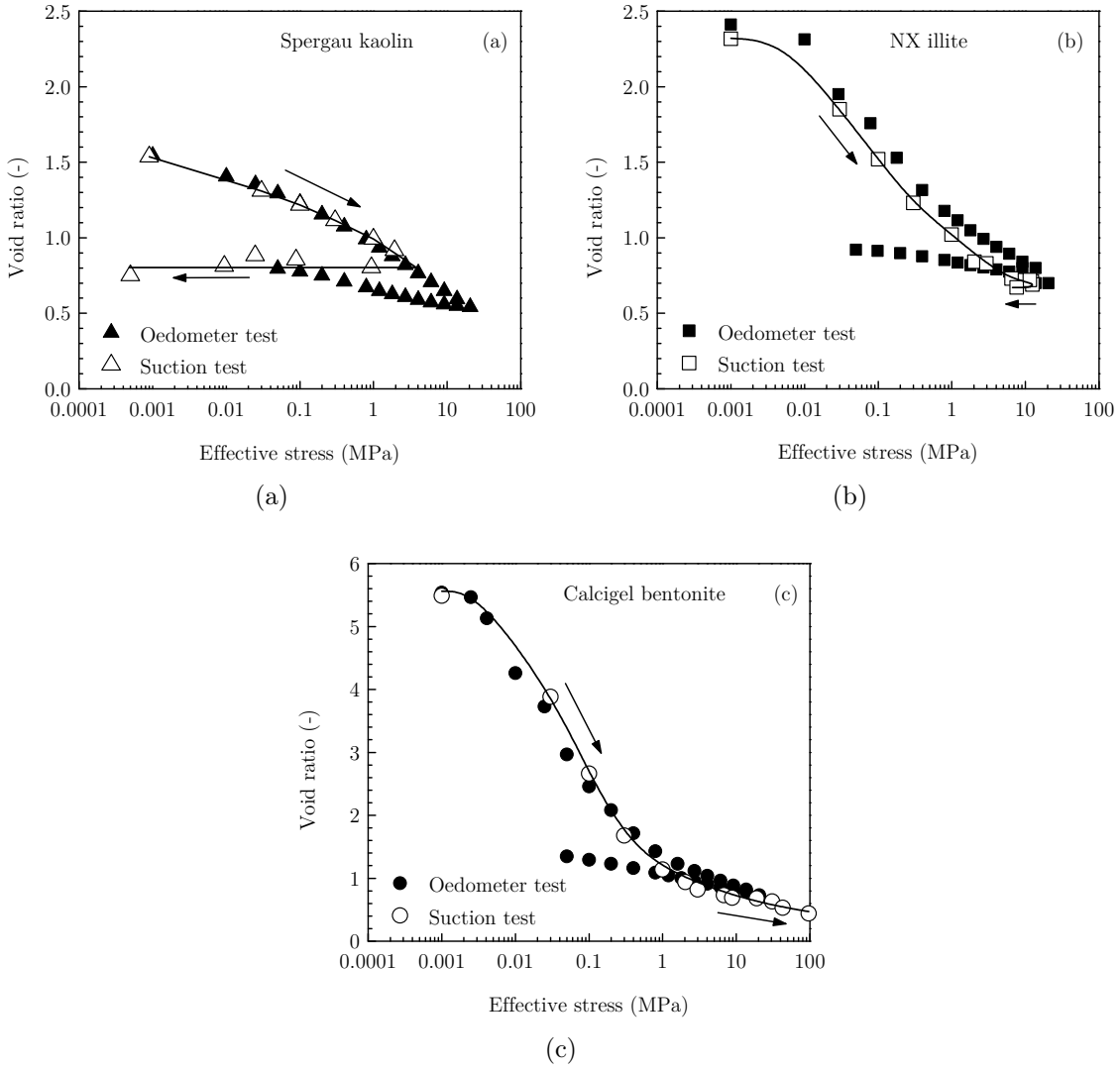

Figure 10.6.: Void ratio versus effective stress: (a) Spergau kaolin, (b) NX illite, (c) Calcigel bentonite; Baille et al. (2014).

Figures 10.6a and 10.6b clearly show that, the void ratio decrease for Spergau kaolin and NX illite for an increase in the effective stress on account of an increase in the vertical stress in one-dimensional consolidation tests and due to a decrease in the suction stress in the drying tests (see Figs. 10.3a, 10.3b, 10.4 and 10.5) is similar until the effective stress corresponding to minimum suction stress of the clays were reached (i.e., 2.0 MPa for Spergau kaolin and 12.0 MPa for NX illite). Further, the void ratios of the clays continued to decrease with an increase in the effective stress in consolidation tests, whereas the effective stress corresponding to the drying paths are found to decrease concurrent with an increase in the suction stress (see Figs. 10.3a, 10.3b, 10.4 and 10.5). For Calcigel bentonite, the effective stress-void ratio plots for one-dimensional loading and the effective stress-void ratio plot for the drying path are similar up to an effective stress of 21.0 MPa. Note that for Calcigel bentonite, suction stress decreased monotonically upon an increase in suction (see Figs. 10.3c, 10.4 and 10.5). Hence, in this case, the effective stress during the drying process continued to increase. The results presented in Fig. 10.6 clearly showed that, suction increase beyond the AEVs of soils is less effective in producing volume change of unsaturated soils primarily due to a decrease in the effective stress on account of an increase in the suction stress. A decrease in the effective stress depends upon the magnitude of the minimum suction stress attained by the soil. Vesga (2008) noted that a decrease in the effective stress during the drying process caused an increase in the void ratio of a kaolinite. However, in this study, this was not evident from the test results for Spergau kaolin and NX illite.

The slopes of the unloading paths of Spergau kaolin and NX illite and the corresponding slopes of the effective stress-void ratio paths (decreasing effective stress paths only) of unsaturated specimens were found to be dissimilar (Fig. 10.6). This indicates that, the impact of same effective stress reduction (unloading and suction stress increase) generated different void ratio changes of the clays. The differences in the slopes can be attributed due to a difference in the saturation states of the clays.

10.5. Summary

Suction stress characteristic curves (SSCCs) of three clays, each possessing significant proportion of one of the clay minerals from montmorillonite, illite, and kaolinite were established based on the drying soil-water characteristic curves (SWCCs) of the clays. The SSCCs of the clays enabled determining effective stress changes in the clays during the drying process. The SWCCs of the clays for a suction range of 0.03 to 219.0 MPa were

established from osmotic and vapour equilibrium tests. One-dimensional compressibility behaviour of the clays was studied by loading clay specimens up to a maximum vertical stress of 21.0 MPa for comparing with the effective stress-void ratio responses of the clays during the drying process. The study showed that the shape of SSCC and the magnitudes of minimum and maximum suction stress strongly depend upon the mineralogy and the properties of clays. Suction stress was found to decrease, remained nearly constant, and further increased with an increase in suction for the clays with kaolinite and illite as the dominant clay minerals, whereas it decreased monotonically with an increasing suction for the montmorillonite clay. A decrease in the suction stress caused an increase in the effective stress, which in turn was found to reduce the void ratios of the clays. For applied suctions smaller than the air-entry values of the clays, equal magnitudes of suction stress and effective stress in consolidation tests produced similar volume change. Suction changes beyond the air-entry value were found to be less effective in producing volume change of unsaturated soils primarily due to a decrease in the effective stress on account of an increase in the suction stress. Considerable magnitude of suction stress was noted at very high suctions for the clays with minerals illite and montmorillonite.

11. Summary and conclusions

In the present work, the influence of the mineralogy and the related physicochemical and microstructural properties on the hydromechanical behaviour of various clays possessing significant proportion of one of the clay minerals from kaolinite, illite, and montmorillonite over a wide range of stress and suction was experimentally investigated. Theoretical approaches considering the physico-chemical properties of the clays based on diffuse double layer theory were used to analyse the experimental data. The influence of mineralogy on effective stress in clays was assessed using suction stress approach.

The swelling pressures and one-dimensional compressibility behaviour of compacted clays were studied. Several initial compaction conditions of the clays were considered. A newly developed high stress oedometer device was used to measure the swelling pressures of compacted specimens upon saturation under constant volume condition. Further, the compacted saturated specimens were submitted to one cycle of loading and unloading. The maximum applied vertical stress during the consolidation tests was 25 MPa. The void ratio-swelling pressure data and the compression-decompression paths of the compacted saturated specimens were compared with the compression-decompression path of the corresponding initially saturated clay specimen subjected to a maximum vertical pressure of 21 MPa. The effects of initial compaction conditions and the vertical pressures on the compression index, the decompression index, the calculated coefficient of consolidation, and the saturated coefficient of permeability were brought out in detail. The following conclusions were drawn from the study.

Initial compaction conditions clearly affected the swelling pressure of Calcigel bentonite specimens. At the same water content, the swelling pressure increased with an increase in the dry density. Also, at the same dry density, the swelling pressure was found to decrease with an increase in the water content indicating that the influence of molding water on the fabric of the clay can be quite significant. The test results are concurrent with the reported studies on the swelling pressure of compacted expansive clays. As expected, NX illite and Spergau Kaolin have shown zero or negligible swelling pressures at smaller initial dry densities. Initial water content had no effect on the swelling pressures measured

for Spergau kaolin and NX illite. Irrespective of the mineral type, the clays showed significantly greater swelling pressures at high initial dry densities, which are attributed to short range repulsive forces being dominant at close particle spacings.

The void ratio-swelling pressure data and the corresponding compression paths of the compacted saturated bentonite specimens remained distinctly below that of the void ratio-vertical pressure compression path of the initially saturated specimen even at very large pressures. The differences in the void ratios of the compacted saturated and the initially saturated Calcigel bentonite at pressures smaller than 1000 kPa are attributed to the differences in the micro- and macro-structural void ratios of the initial saturated and compacted saturated specimens, whereas at pressures greater than 1000 kPa, the void ratio differences are primarily due to the dissimilar interlayer void ratios. Similarly, compression paths of the compacted saturated NX illite and Spergau kaolin specimens remained distinctly below that of the void ratio-vertical pressure compression path of the initially saturated specimen even at very large pressures. This is attributed to the compaction conditions of the specimens with density values above the Proctor curve.

The e-$\log \sigma'_{\mathrm{v}}$ relationship for the initially saturated Calcigel bentonite specimen subjected to a vertical pressure of 21 MPa showed two distinctly different values of C_{c} similar to that reported in the literature. The e-$\log \sigma'_{\mathrm{v}}$ relationships for compacted saturated bentonite specimens were found to be nearly linear for the range of pressure considered in the study. The C_{c} values of the compacted saturated bentonite specimens were found to decrease with an increase in the initial dry density. On the other hand, the initial compaction conditions marginally affected the decompression index indicating that the influence of initial compaction conditions on the fabric and structure of bentonite was very nearly eliminated at large pressures.

The e-$\log \sigma'_{\mathrm{v}}$ relationship for the initially saturated Spergau kaolin specimen showed that stress range had only a slight effect on the C_{c} values. For the initially saturated NX illite specimen, a bilinear behaviour was observed, where the C_{c} value at high stresses was found to be half of that at low stresses. For the compacted saturated Spergau kaolin and NX illite specimens, the C_{c} values were only marginally affected by the initial compaction conditions. Likewise, no effect on the decompression index was found.

In case of Calcigel bentonite, with an increase in the applied pressure or a decrease in the void ratio, c_{v} was found to decrease for both initially saturated specimen and compacted saturated specimens; however, at large pressures, c_{v} increased for the initially saturated specimen, whereas it remained nearly constant for the compacted saturated specimens. The effect of initial compaction conditions on c_{v} was found to be nearly indiscernible at

void ratios smaller than 0.5 indicating the similarity in the fabric and structure of the bentonite specimens at very large pressures. Qualitatively, a similar behaviour was found for the NX illite specimens, with c_v values being about an order of magnitude greater than those of Calcigel bentonite. The behaviour was found to be different for Spergau kaolin, where the c_v-value was found to decrease and with increasing applied pressure or a decrease in the void ratio; the initial increase of c_v-value observed for the specimens with smaller dry density require a verification.

The variation of coefficient of permeability with the void ratio was found to be distinctly bilinear for the initially saturated Calcigel bentonite specimen, whereas for the compacted saturated specimens the relationship was found to be nearly linear and remained within a narrow band. The coefficient of permeability of NX illite and Spergau kaolin were found to vary linearly with void ratio within a band. For the three clays studied, the compacted saturated specimens were found to be more permeable than the initially saturated specimens at all void ratios considered in this study.

Osmotic and vapour equilibrium techniques were used for establishing drying water retention characteristic curves for a suction range of 30 kPa to 219.7 MPa. Volume measurements of the clays during the drying process enabled establishing the shrinkage curves and the suction-degree of saturation relationships. Mineralogy was found to significantly influence the shape and salient features of the water retention curves of the clays. The volume change was compared to that obtained from one-dimensional consolidation tests, where initially saturated clay specimens were step-wise loaded to a maximum vertical stress of 21.6 MPa. Concurrent with earlier studies, the test results revealed that up to the air-entry values of the clays equal magnitude of applied vertical stress and suction brought clay specimens to nearly equal void ratios, whereas suctions greater than the air-entry values were less effective in causing volume change. The differences in observed void ratios between the clays in the oedometer test are related to mineralogical features, such as layer-to-layer distance and microstructure of the clays.

Comparisons of environmental scanning electron (ESEM) photomicrographs of the clays at saturated state and at shrinkage limit clearly showed the influence of mineralogy on fabric and structure of the clays and fabric changes due to the drying process. Mercury intrusion porosimetry (MIP) studies at shrinkage limit showed the difference in pore size distributions of the clays. Similarly, ESEM studies clearly showed some significant differences in fabric and structure of the clays due to applied vertical stress and applied suction, particularly for applied suctions greater than the air-entry value of the clays. Spergau kaolin and NX illite mineral crystals form a rigid type of fabric dominated by

frictional contacts between the aggregates. The quasi-crystals of Calcigel bentonite are flexible in nature. The internal layer-redistribution within the quasi-crystals, i.e., the change of the ratio between interlayer pores and pores between the quasi-crystals, together with the flexible nature of the quasi-crystals enable the Calcigel bentonite to drain its water out of the pores while staying saturated up to large suction values, leading to smaller void ratios as compared to Spergau kaolin and NX illite. The anisotropic mechanical loading until 20 MPa vertical applied stress caused a tight compression of the fabric of Spergau kaolin; only negligible pore space was discernable at this state. For Calcigel bentonite, an overall compression of the large pores between quasi-crystals was observed. A pronounced orientation of the particles at higher stress level was not detected.

The application of classical diffuse double layer theory was found to be relevant to some extent for Calcigel bentonite, but not relevant for NX illite and Spergau kaolin. Classical diffuse double layer calculations were found to represent reasonably well the experimental data in limited ranges of considered dry densities or applied stresses and suctions of Calcigel bentonite. The overestimation of swelling pressures for lower dry densities and the overestimation of void ratio in the low stress range of the one-dimensional consolidation test and in the low suction range of the water retention tests is attributed to the non-ideal particle arrangement in the compacted specimens and the slurry specimens. The significant deviations in calculated swelling pressures at high dry densities and applied stresses are attributed to the hydration forces manifest as strong repulsion in the swelling pressure test and as an increasing resistance to volume change in the oedometer test at applied stresses > 2 MPa. The use of the modified approach according to Tripathy et al. (2004) and Tripathy & Schanz (2007) could improve the agreement to the experimental data. However, diffuse double layer forces are not the single operating force within the clay-water system. Thus, the use of approaches based of diffuse double layer only can not be expected to represent the full range of observed phenomena, especially for small interparticle distances.

The repulsive and attractive pressures for several compacted clays from literature (MX 80, Febex, Bentonite S2, Kunigel and Kunigel V1) and for the clays of the present study were calculated based on physico-chemical considerations. The additional repulsive pressures at close particle spacing were obtained by subtracting the theoretical net interparticle double layer repulsive pressures from the corresponding experimental swelling pressures of the clays. It is shown that the additional repulsive pressure contribute to the swelling pressure of compacted bentonites below a spacing of 1.5 nm, whereas their contribution is significant below a spacing of about 0.7 nm. The additional repulsive pressure was shown

to have a near linear relationship with the surface charge density and varies inversely from 4th to 6th power of the platelet spacing. The additional repulsive pressures for Spergau kaolin and NX illite were found to be significantly smaller than those of the bentonites. It was shown that the repulsive pressures at short range are becoming relevant for dry densities greater than the proctor density. The additional repulsive pressure was shown to be related to the specific surface area and the cation exchange capacity independent of the mineral type.

Suction stress characteristic curves (SSCCs) of the clays were established based on the drying soil-water characteristic curves (SWCCs) of the clays for a suction range of 0.03 to 219.0 MPa. The SSCCs of the clays enabled determining effective stress changes in the clays during the drying process. One-dimensional compressibility behaviour of the clays up to a maximum vertical stress of 21.6 MPa was used for comparing with the effective stress-void ratio responses of the clays during the drying process. The study showed that the shape of SSCC and the magnitudes of minimum and maximum suction stress strongly depend upon the mineralogy and the properties of clays. Suction stress was found to decrease, remained nearly constant, and further increased with an increase in suction for the clays with kaolinite and illite as the dominant clay minerals, whereas it decreased monotonically with an increasing suction for the montmorillonite clay. A decrease in the suction stress caused an increase in the effective stress, which in turn was found to reduce the void ratios of the clays. For applied suctions smaller than the air-entry values of the clays, equal magnitudes of suction stress and effective stress in consolidation tests produced similar volume change. Suction changes beyond the air-entry value were found to be less effective in producing volume change of unsaturated soils primarily due to a decrease in the effective stress on account of an increase in the suction stress. Considerable magnitude of suction stress was noted at very high suctions for the clays with minerals illite and montmorillonite.

The following recommendations for further studies are given:

The SWCC of the clays should be determined for the full cycle of drying and wetting. This enables the validation of the applied effective stress concept for the wetting path. Also, shear tests at controlled suction and tensile tests of the clays can be carried out to investigate a possible influence of the stress path for the effective stress determination based on suction stress concept. Further, based on the obtained experimental data, other approaches for determining effective stress in soils can be verified.

An investigation of the unloading behaviour is recommended by submitting the clays to an identical loading path in terms of effective stress, but separately induced by increase

in mechanical load and by an increase in suction. Does unloading from these stress states result in the same magnitude of volume change?

Models for the prediction of the stress-void ratio relationships which are based on physico-chemical properties of the clays, should be able to take into account other mechanisms than diffuse double layer, such as short range forces at close particle spacings, to fully represent hydromechanical clay behaviour. Also, specific site properties like non-uniform charge distribution, or edge charges of varying sign as the case for kaolin clays should be considered. Diffuse double layer models including the effect of the Stern layer (Tripathy 2013) or the triple layer model (TLM) of Gonçalvèz et al. (2007) are examples for research in this direction.

The observation of fabric during the hydromechanical loading, e.g. during unconfined hydration of bentonites, is still a challenge. The internal redistribution of fabric during bentonite hydration and desorption is of importance for the permeability of the bentonites. Fabric and permeability at various stages during hydration and desorption should be simultaneously determined.

A. Time-compression and time-decompression curves

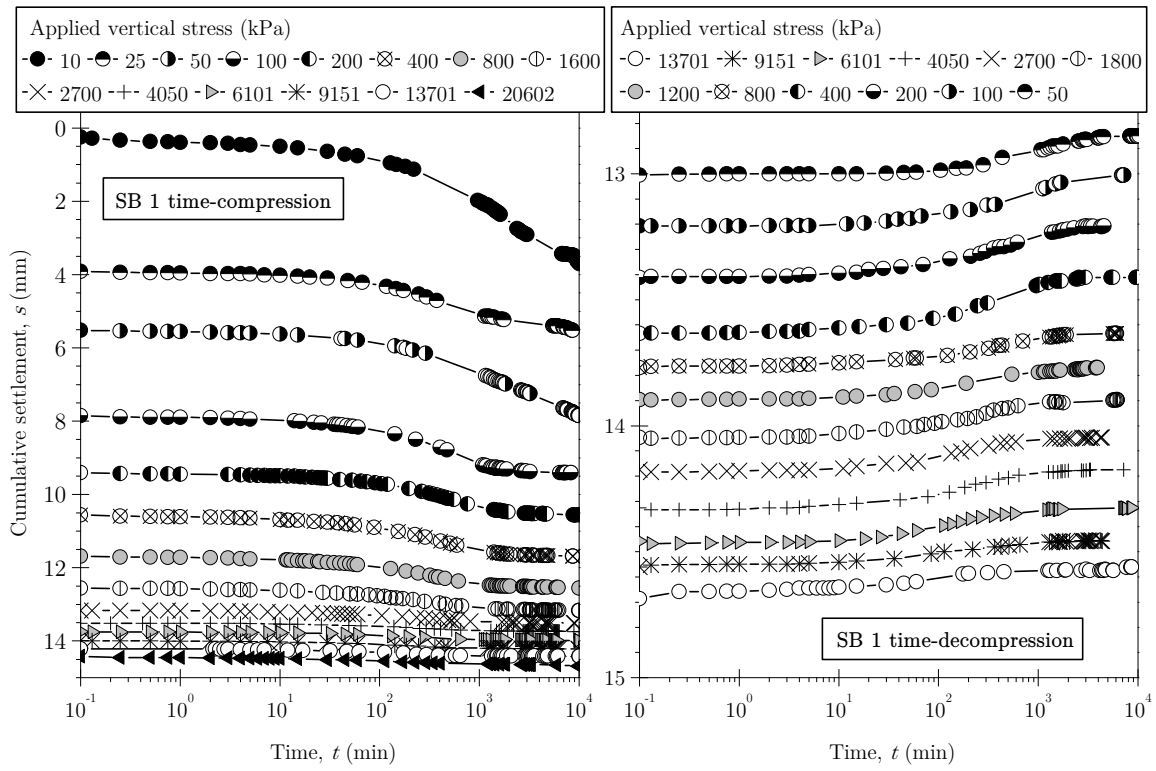

(a)

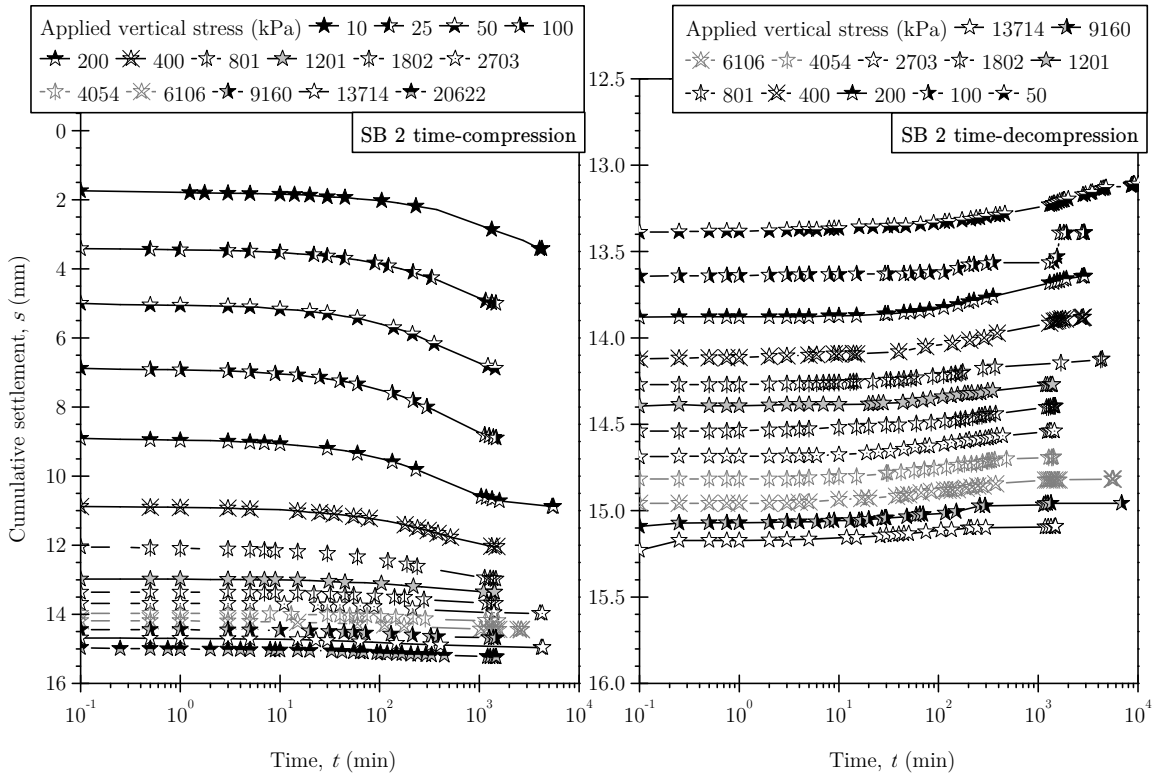

(b)

Figure A.1.: Time-compression and time-decompression curves: (a) Calcigel bentonite specimen SB 1, (b) Calcigel bentonite specimen SB 2.

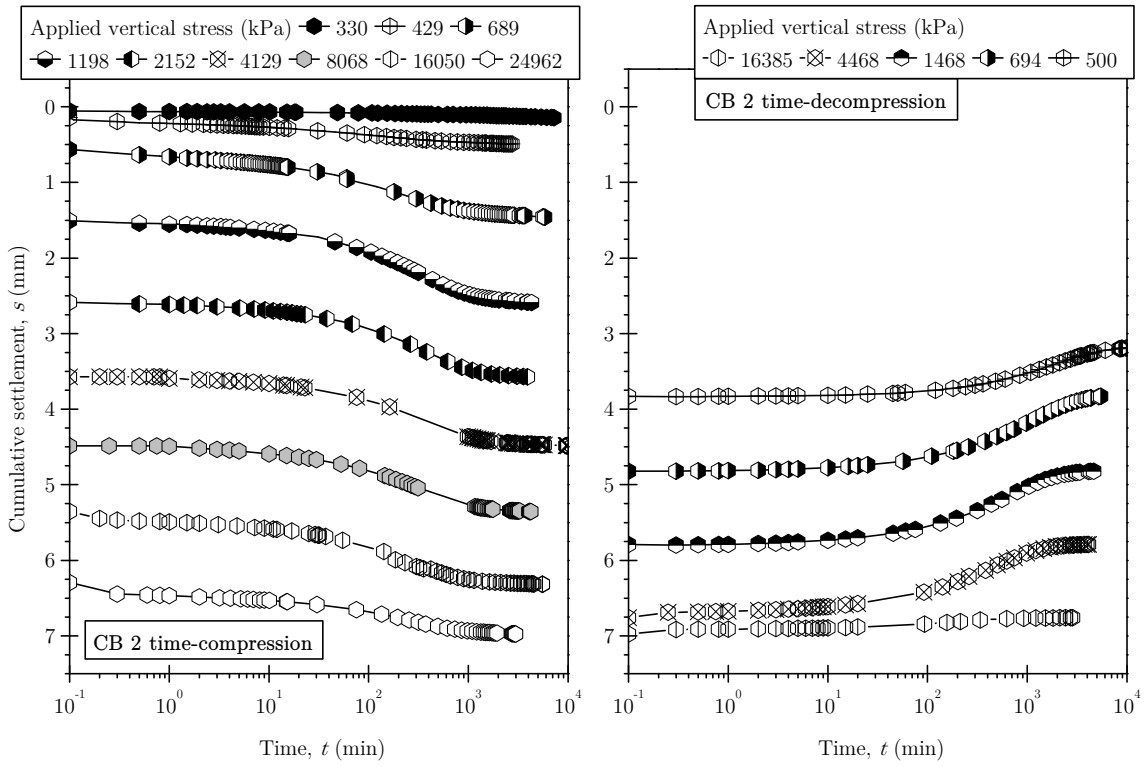

(a)

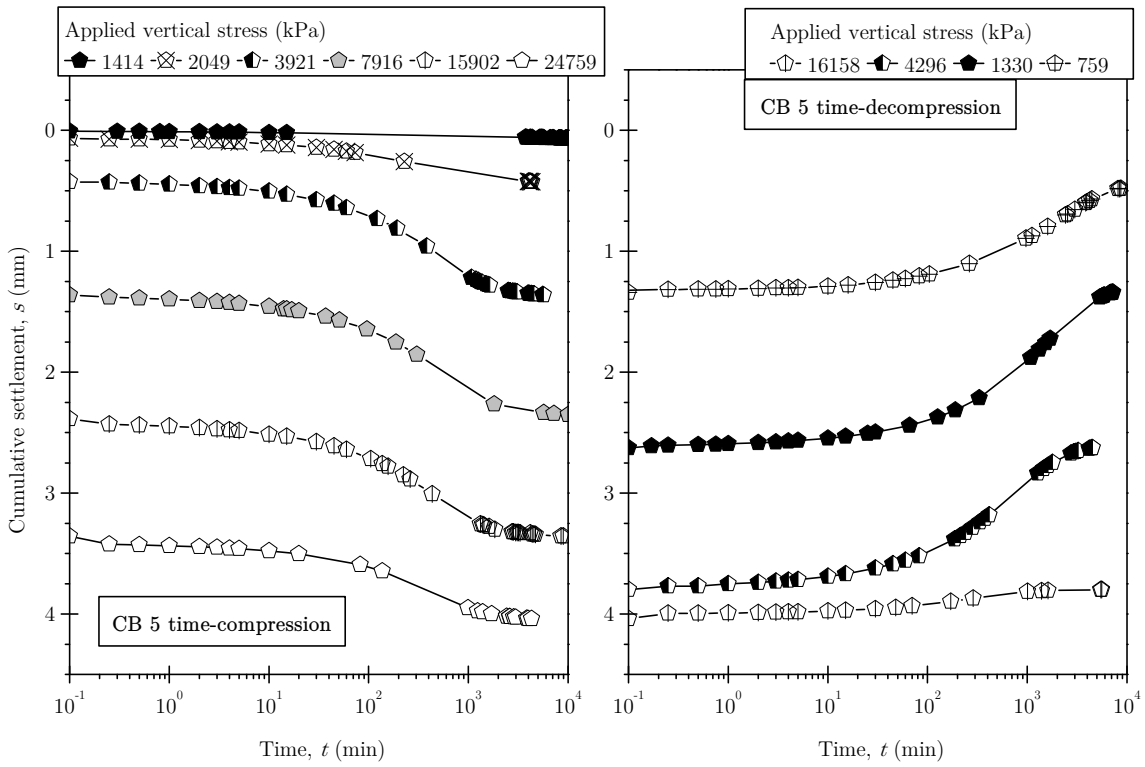

(b)

Figure A.2.: Time-compression and time-decompression curves: (a) Calcigel bentonite specimen CB 2, (b) Calcigel bentonite specimen CB 5.

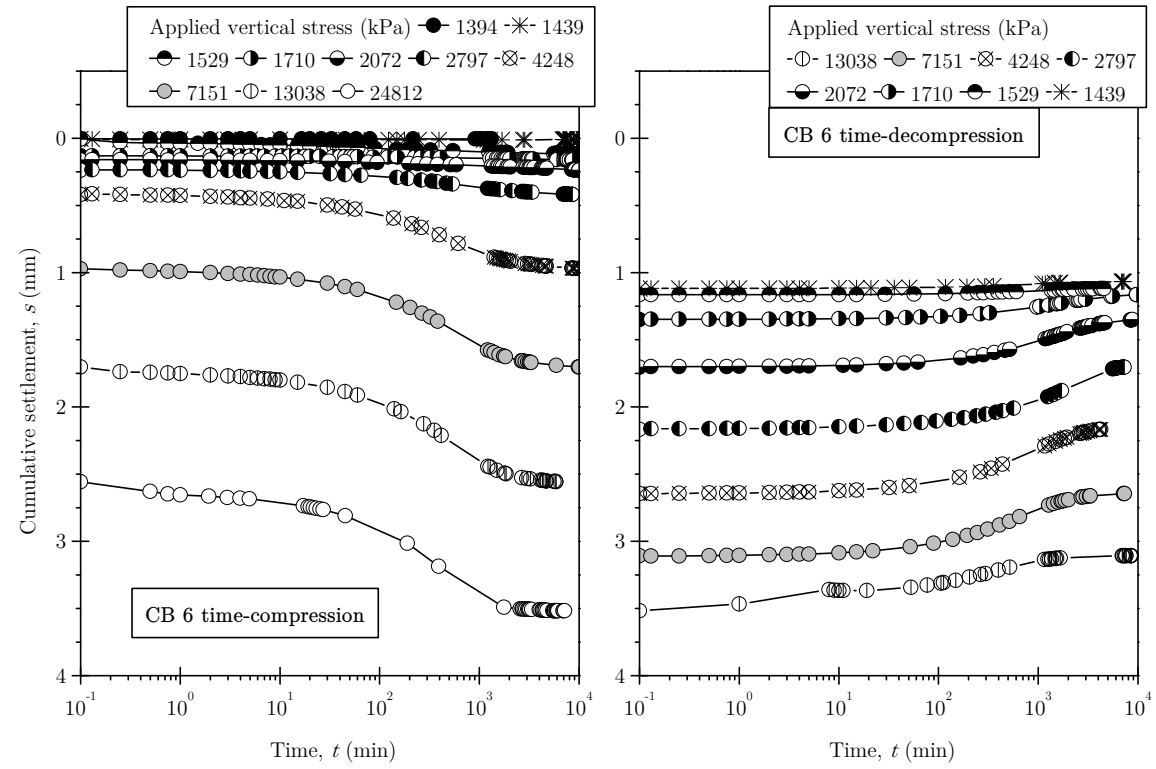

(a)

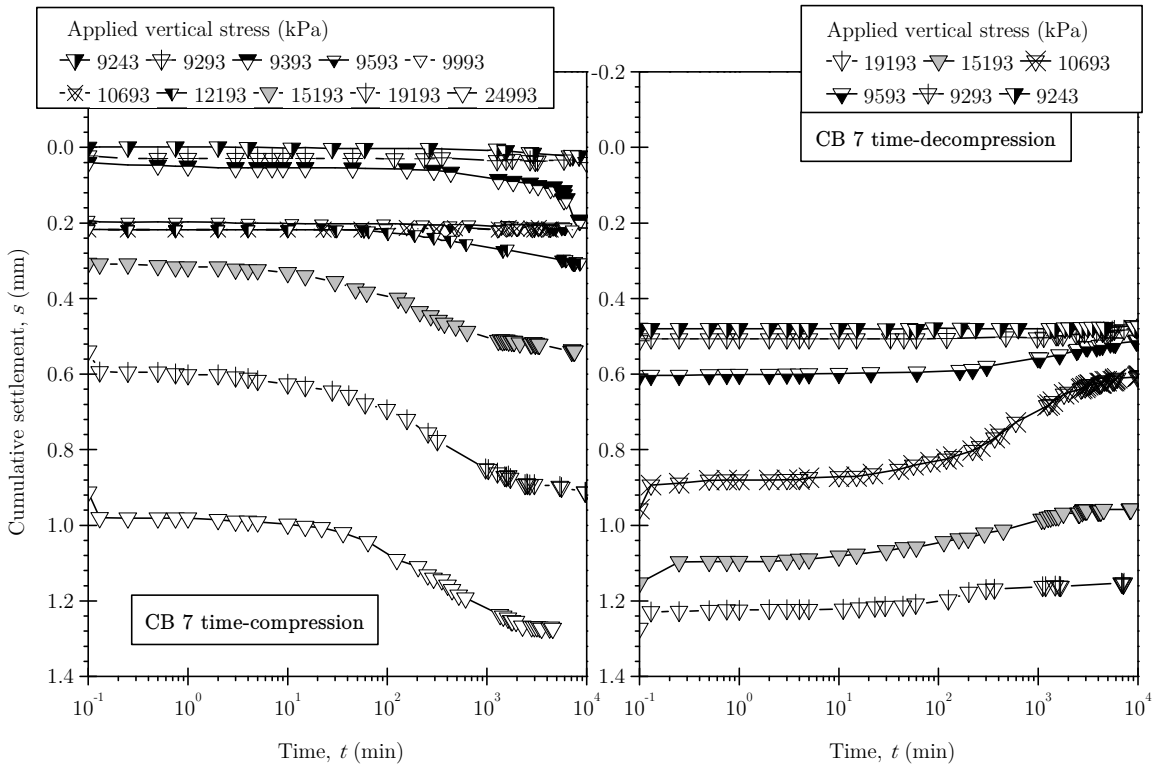

(b)

Figure A.3.: Time-compression and time-decompression curves: (a) Calcigel bentonite specimen CB 6, (b) Calcigel bentonite specimen CB 7.

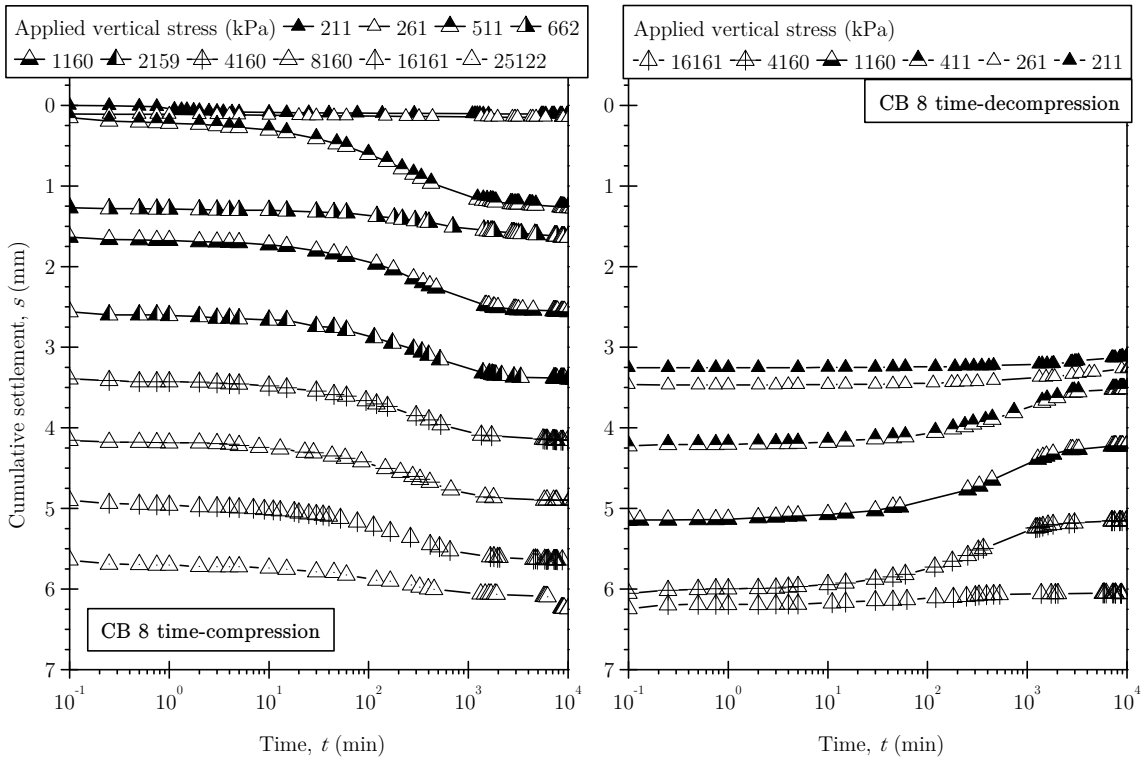

(a)

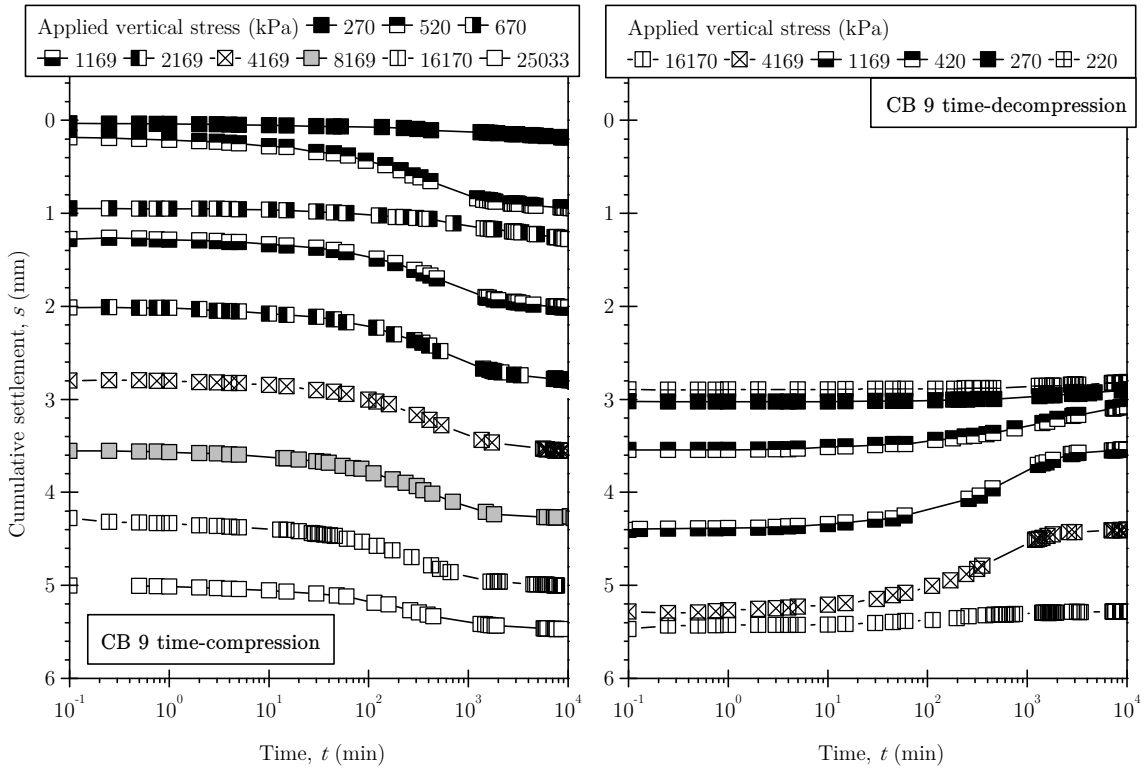

(b)

Figure A.4.: Time-compression and time-decompression curves: (a) Calcigel bentonite specimen CB 8, (b) Calcigel bentonite specimen CB 9.

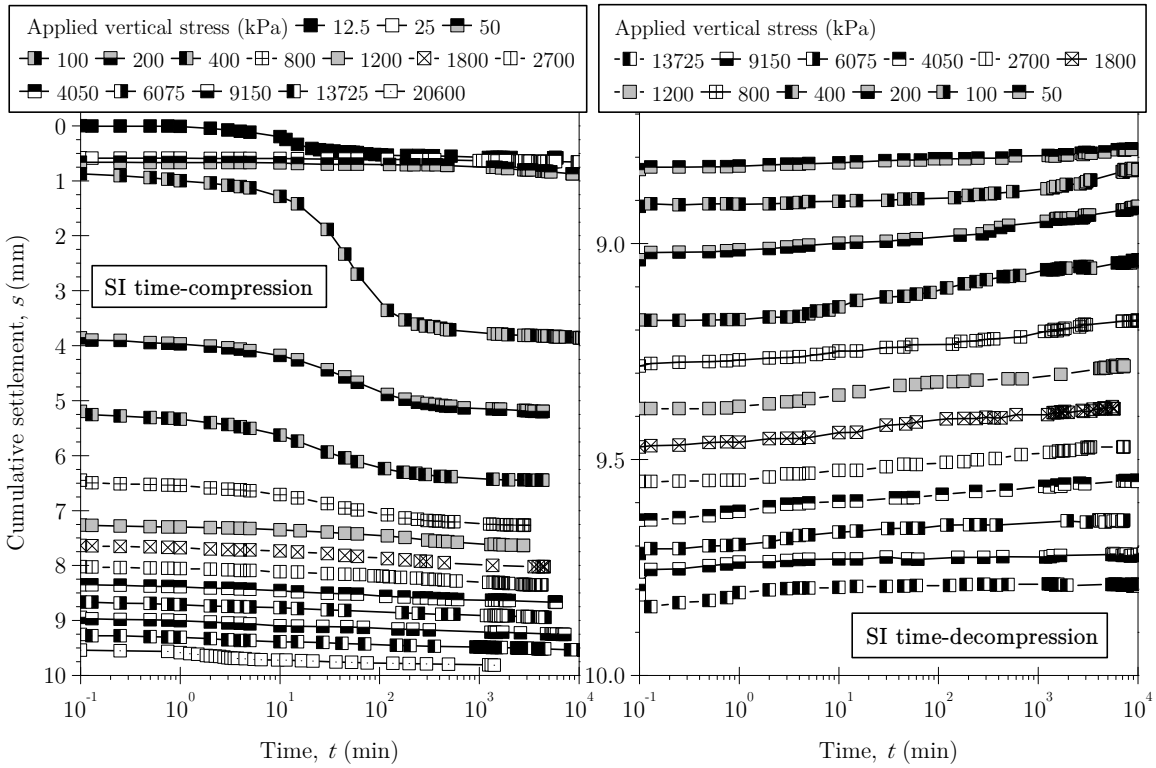

Figure A.5.: Time-compression and time-decompression curves: NX illite specimen SI

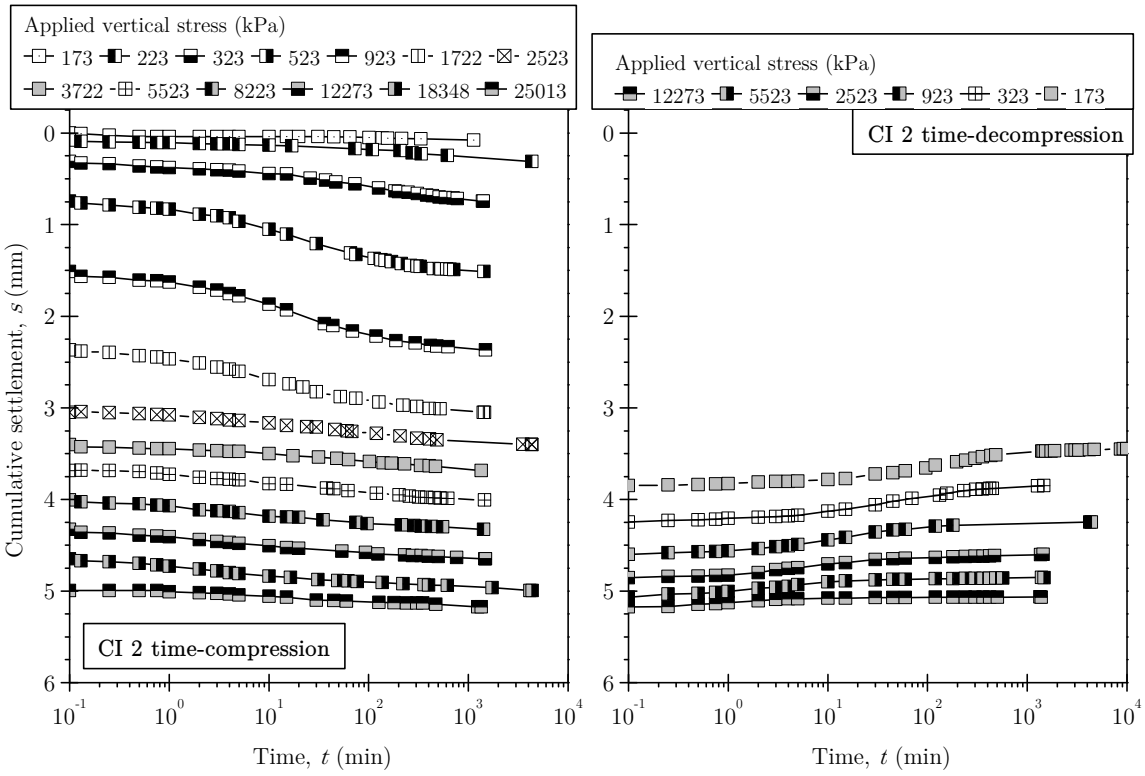

(a)

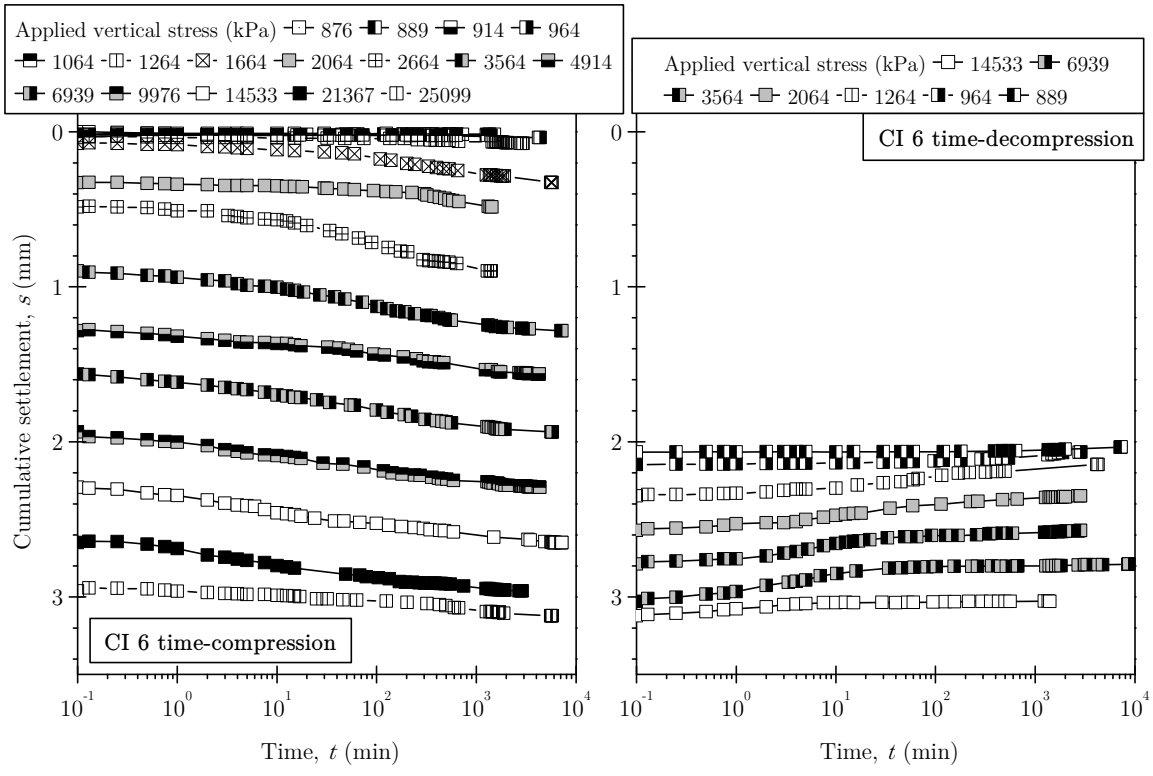

(b)

Figure A.6.: Time-compression and time-decompression curves: (a) NX illite specimen CI 2, (a) NX illite specimen CI 6.

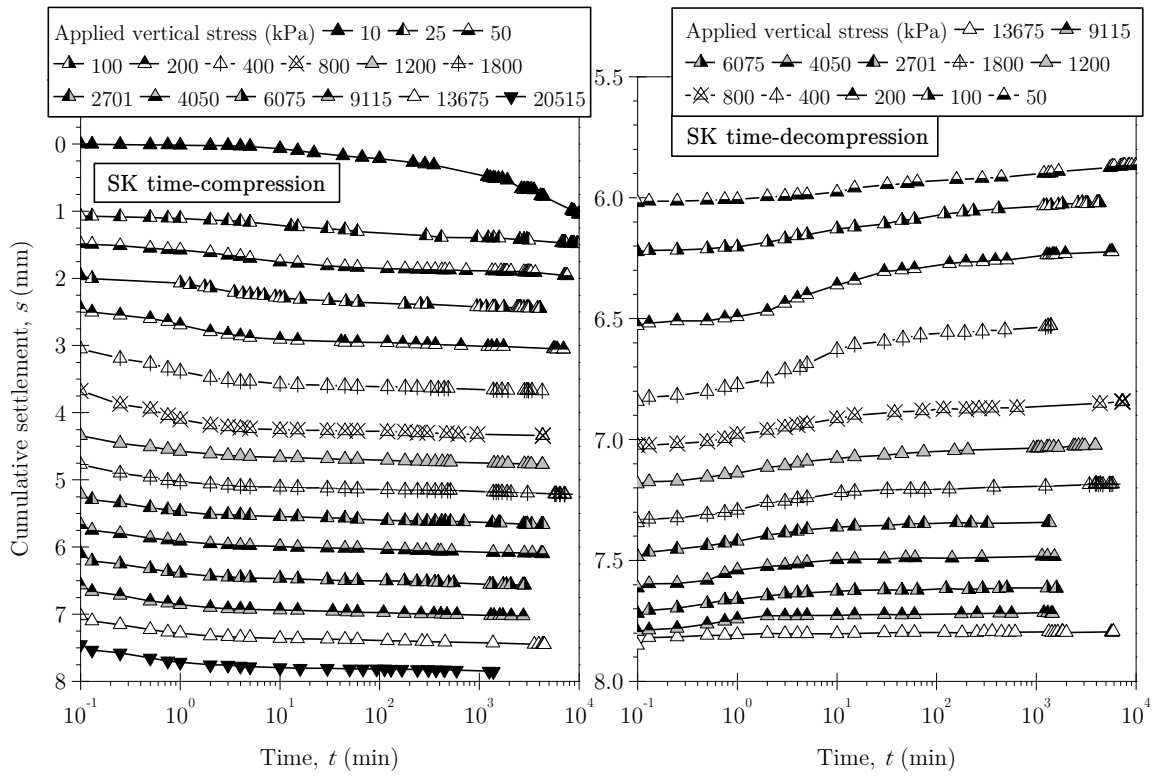

Figure A.7.: Time-compression and time-decompression curves: Spergau kaolin specimen SK

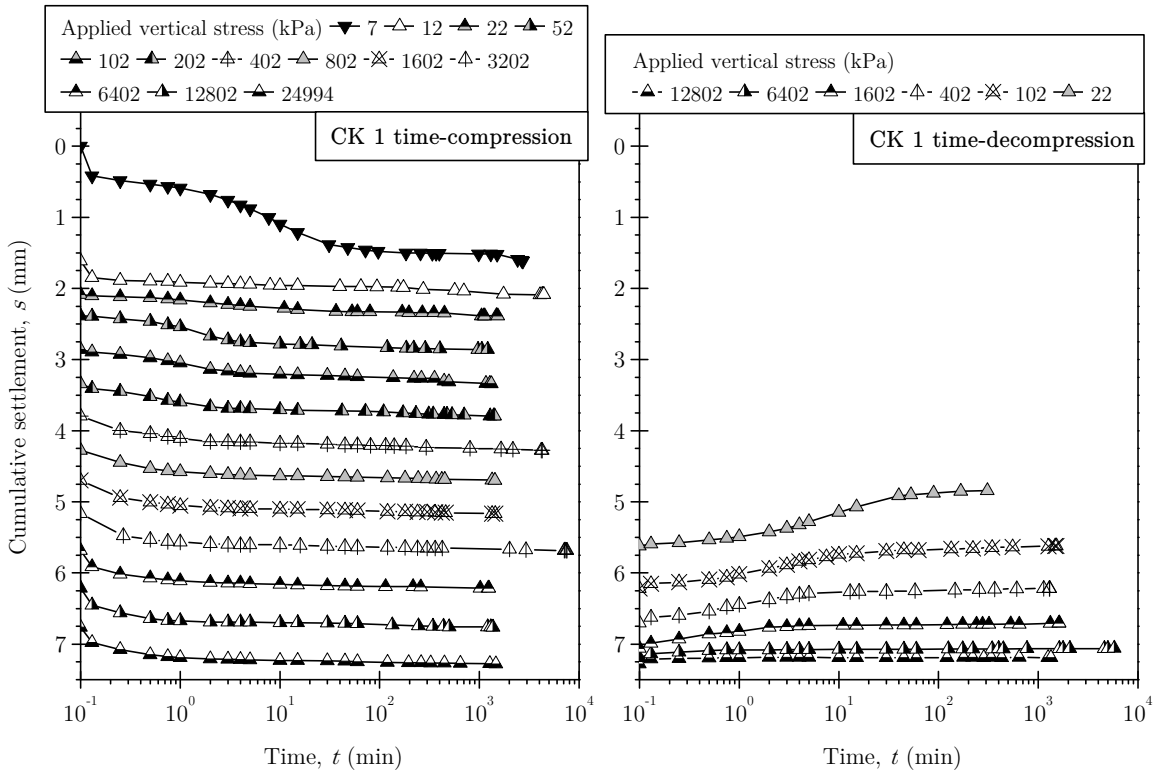

(a)

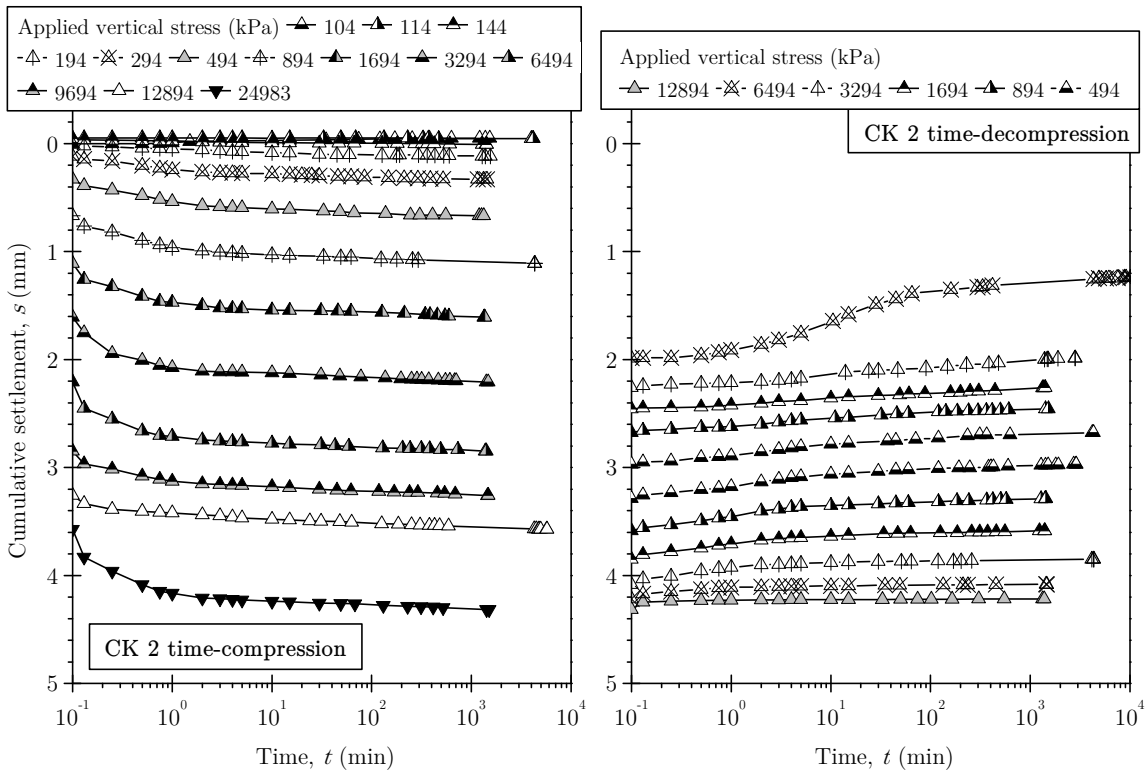

(b)

Figure A.8.: Time-compression and time-decompression curves: (a) Spergau kaolin specimen CK 1, (b) Spergau kaolin specimen CK 2.

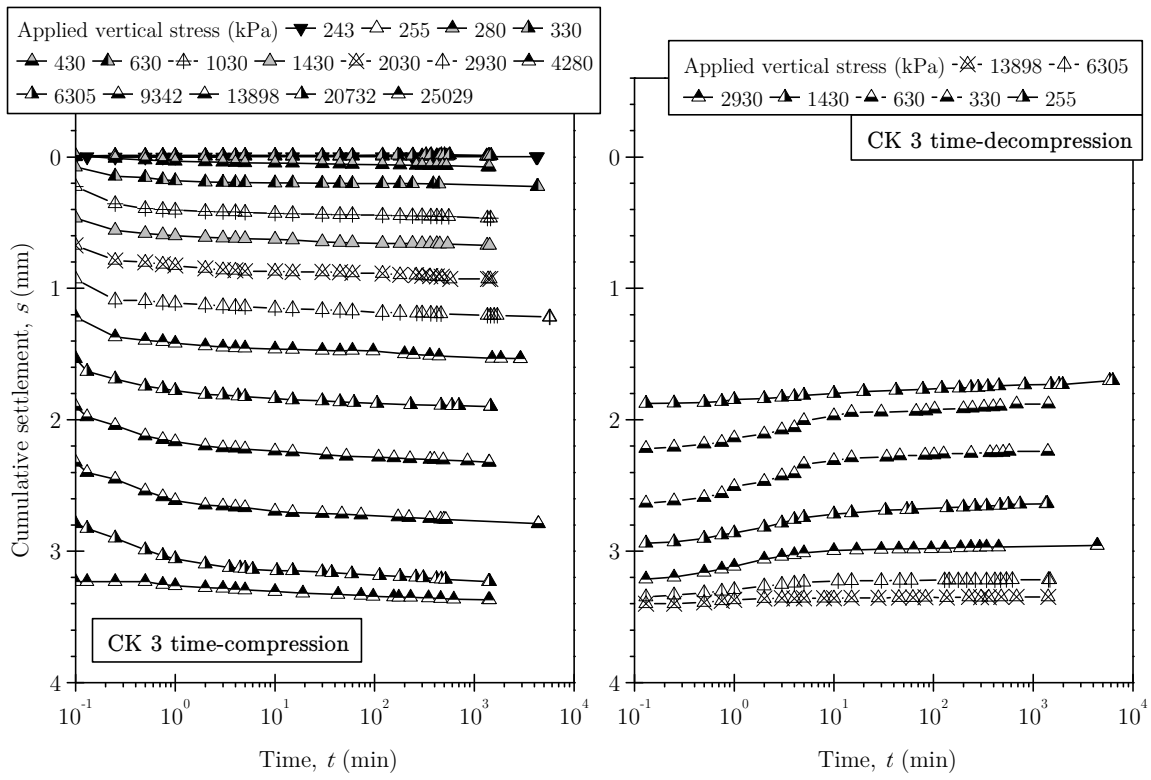

(a)

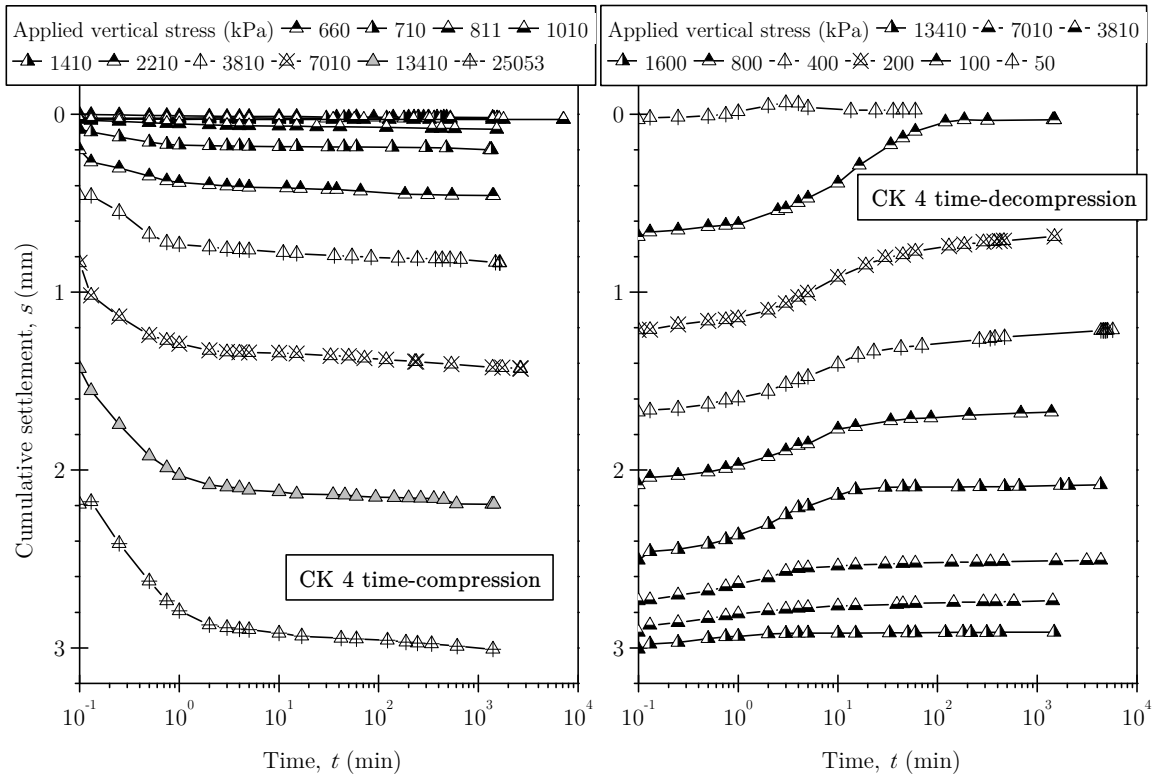

(b)

Figure A.9.: Time-compression and time-decompression curves: (a) Spergau kaolin specimen CK 3, (b) Spergau kaolin specimen CK 4.

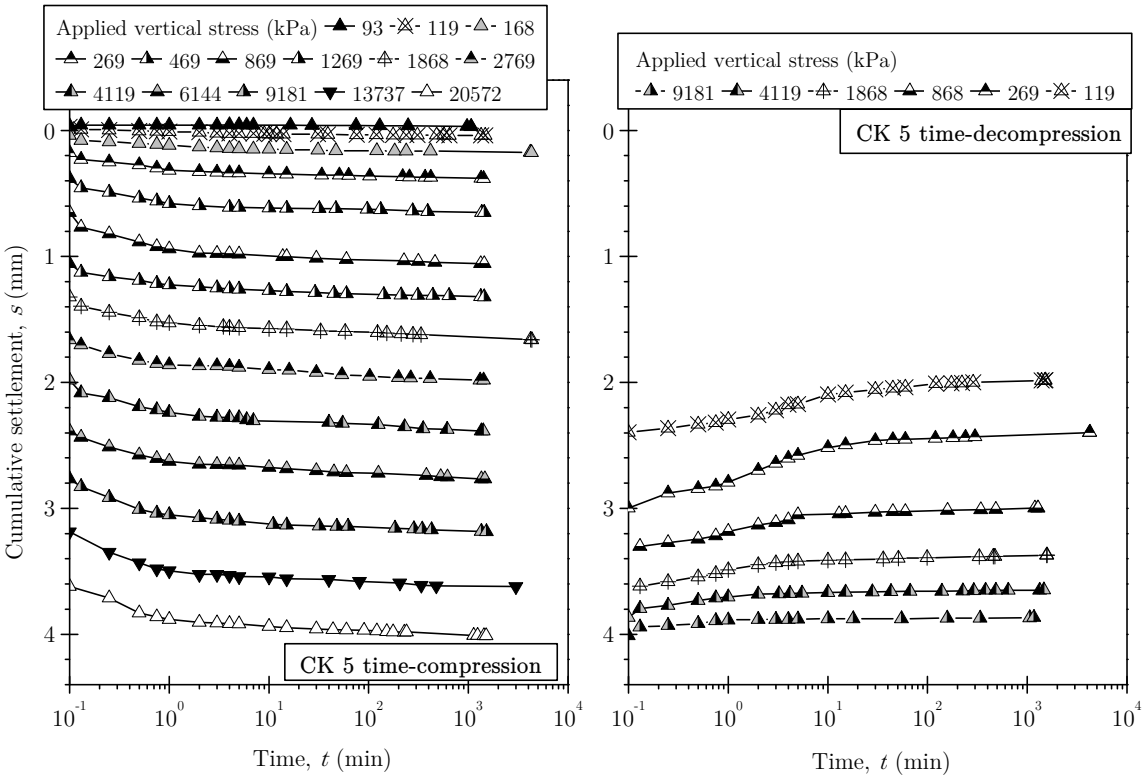

(a)

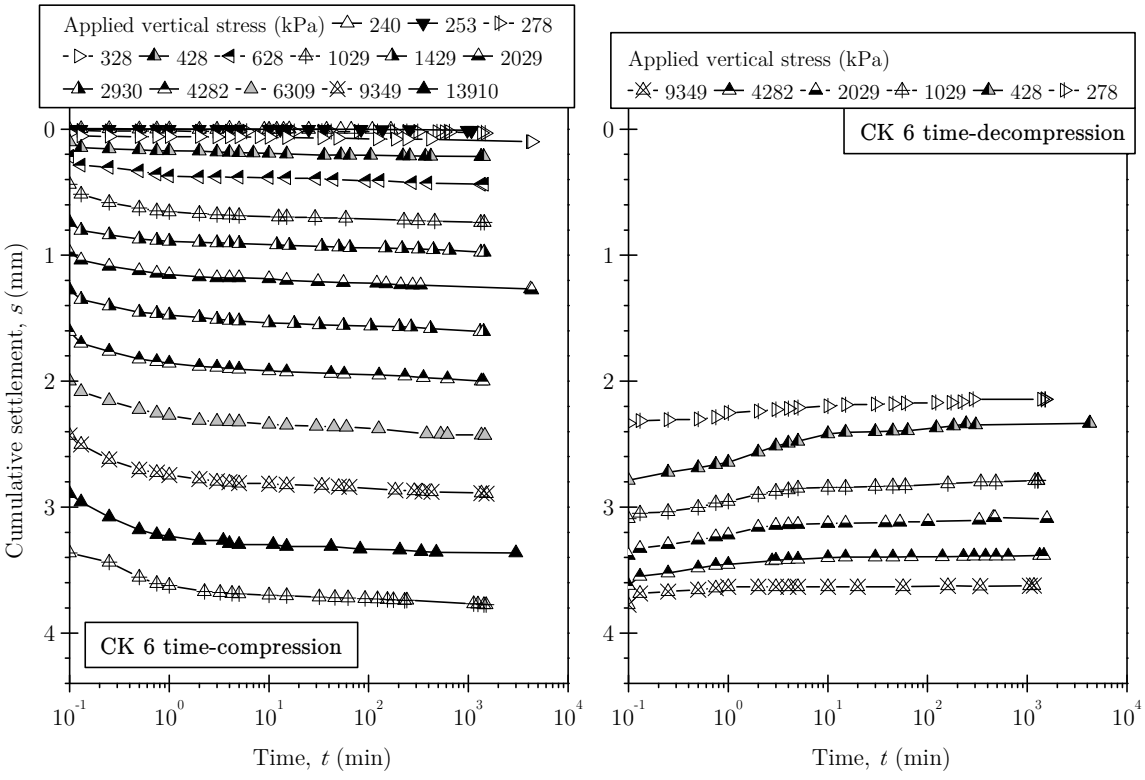

(b)

Figure A.10.: Time-compression and time-decompression curves: (a) Spergau kaolin specimen CK 5, (b) Spergau kaolin specimen CK 6.

B. Water retention tests with vapour equilibrium technique: time-water content and time-mass curves

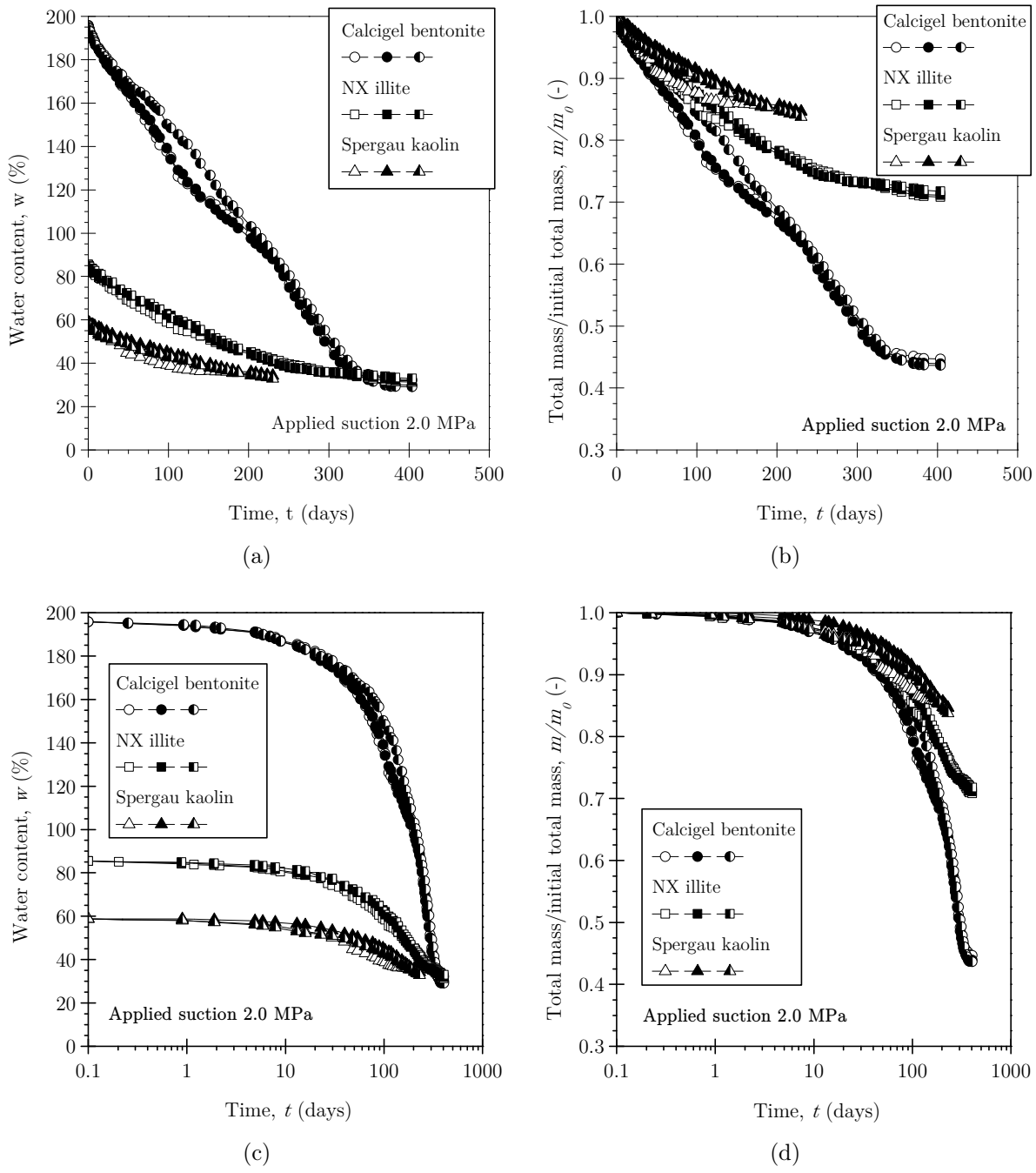

Figure B.1.: Time-water content and time-mass plots at 2.0 MPa suction: (a) t-w plot linear time scale, (b) t-m/m_0 plot linear time scale, (c) t-w plot log time scale, and (d) t-m/m_0 plot log time scale.

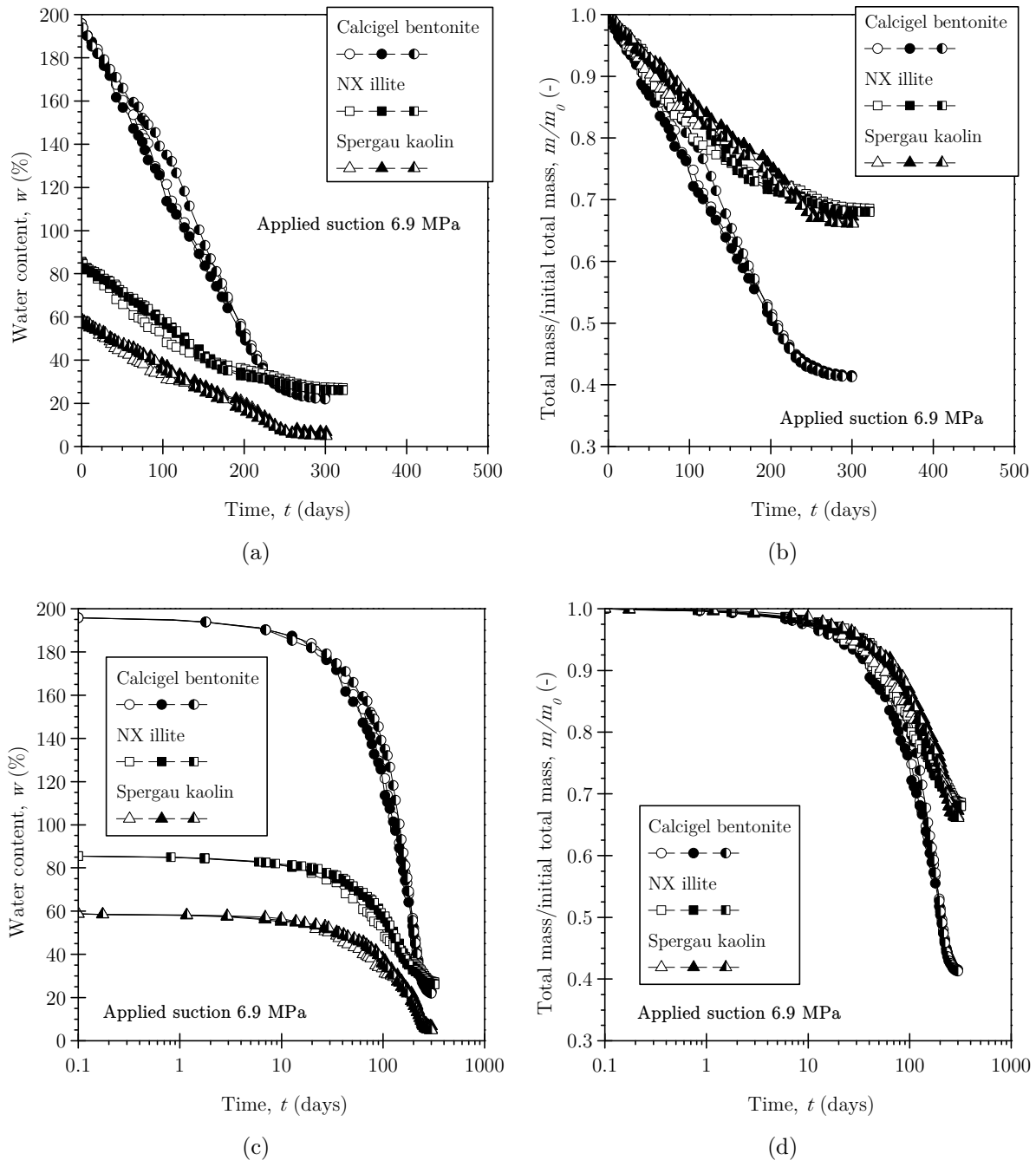

Figure B.2.: Time-water content and time-mass plots at 6.9 MPa suction: (a) t-w plot linear time scale, (b) t-m/m_0 plot linear time scale, (c) t-w plot log time scale, and (d) t-m/m_0 plot log time scale.

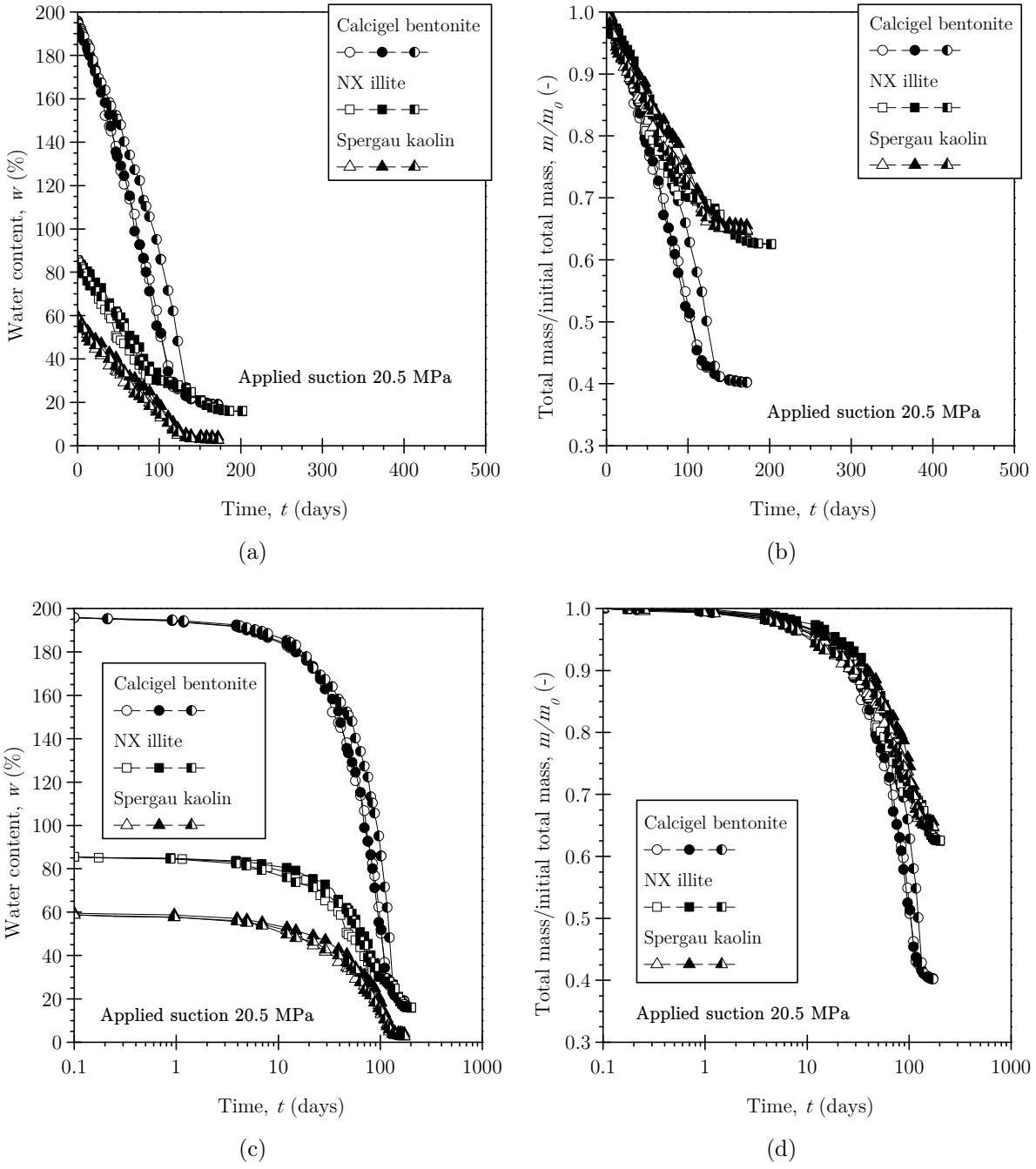

Figure B.3.: Time-water content and time-mass plots at 20.5 MPa suction: (a) t-w plot linear time scale, (b) t-m/m_0 plot linear time scale, (c) t-w plot log time scale, and (d) t-m/m_0 plot log time scale.

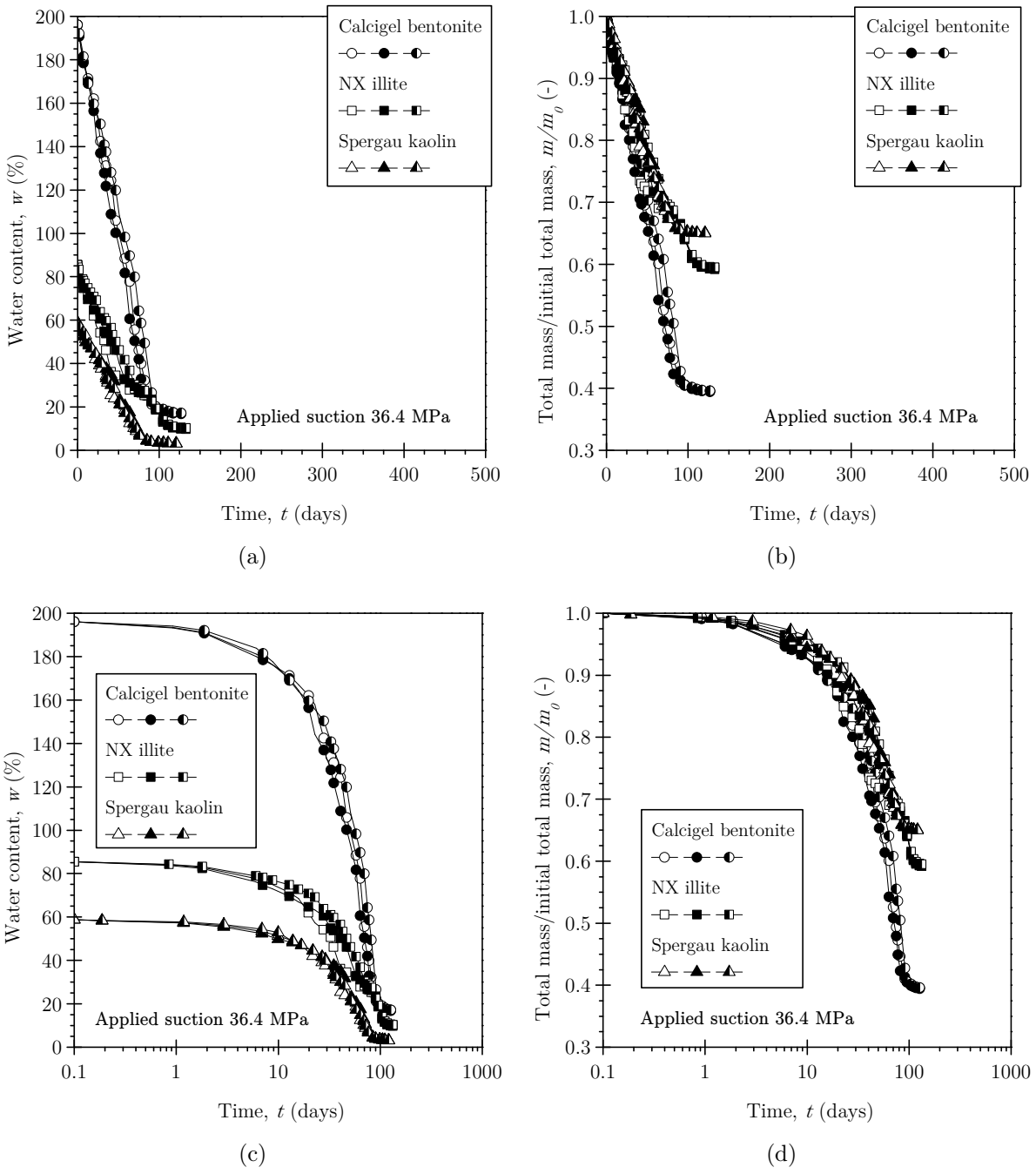

Figure B.4.: Time-water content and time-mass plots at 36.4 MPa suction: (a) t-w plot linear time scale, (b) t-m/m_0 plot linear time scale, (c) t-w plot log time scale, and (d) t-m/m_0 plot log time scale.

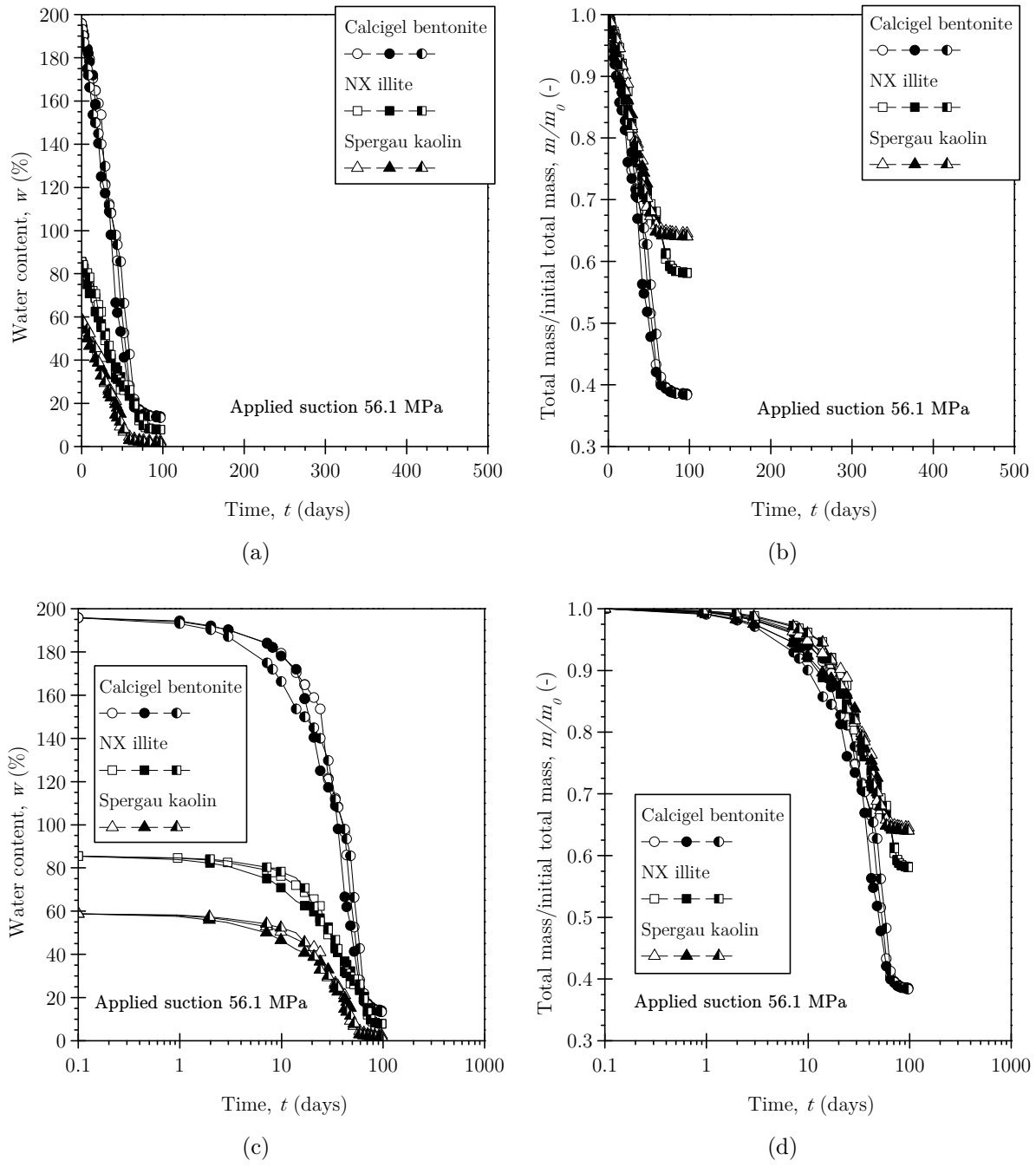

Figure B.5.: Time-water content and time-mass plots at 218.7 MPa suction: (a) t-w plot linear time scale, (b) t-m/m_0 plot linear time scale, (c) t-w plot log time scale, and (d) t-m/m_0 plot log time scale.

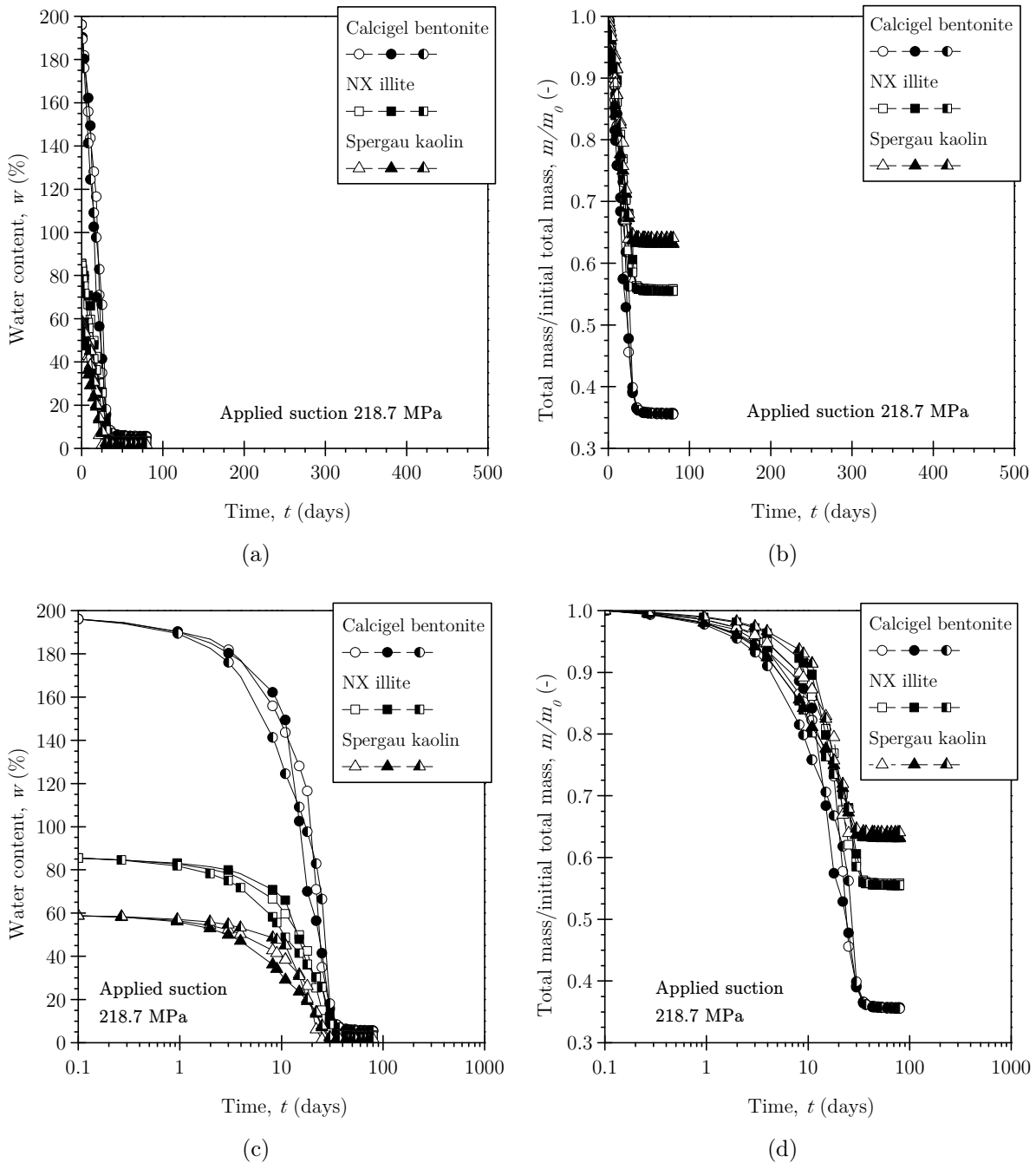

Figure B.6.: Time-water content and time-mass plots at 218.7 MPa suction: (a) t-w plot linear time scale, (b) t-m/m_0 plot linear time scale, (c) t-w plot log time scale, and (d) t-m/m_0 plot log time scale.

C. Additional repulsive pressure versus interparticle distance plots

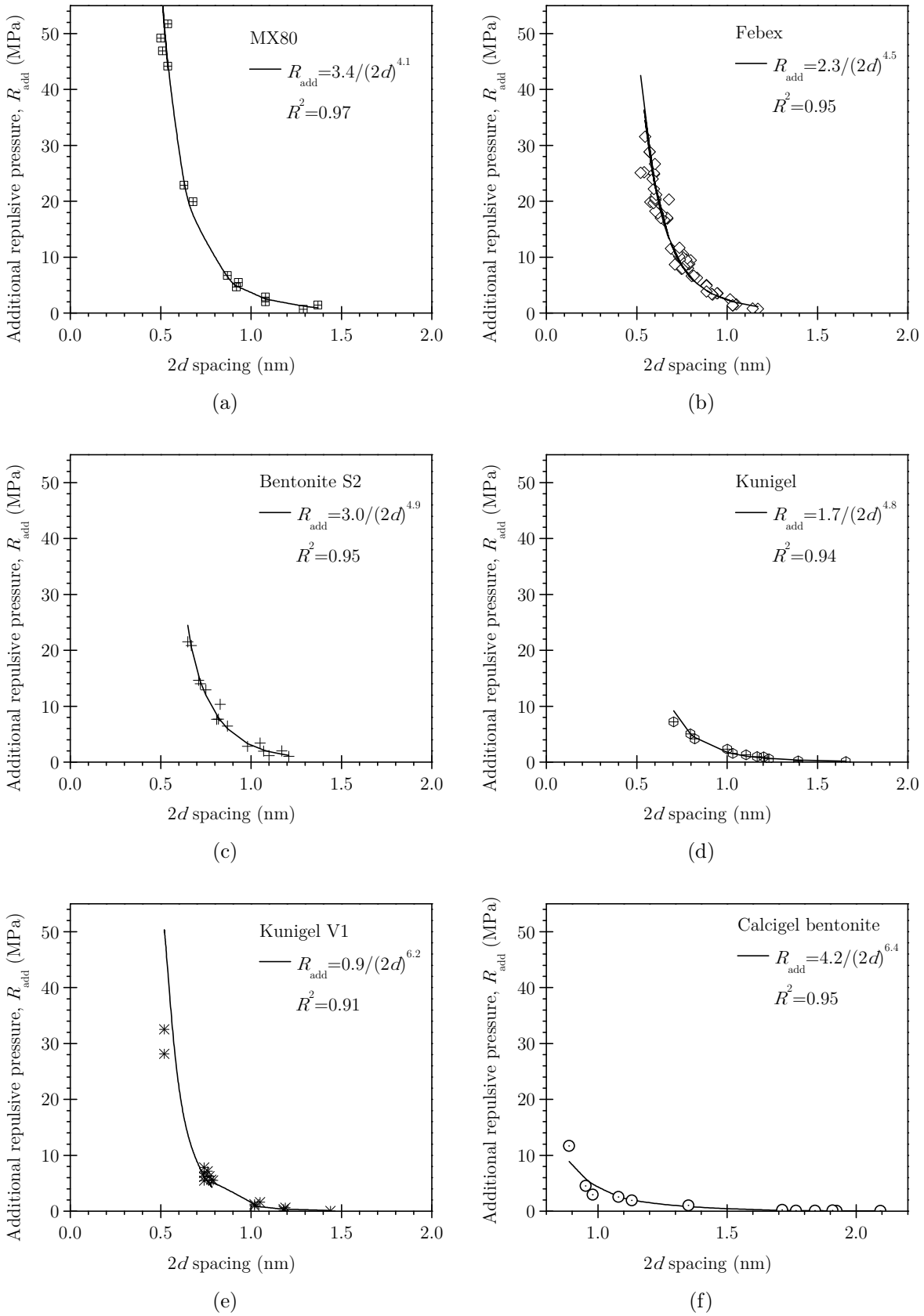

Figure C.1.: Equations for additional repulsive pressure for the bentonites studied: (a) MX 80, (b) Febex, (c) Bentonite S2, (d) Kunigel, (e) Kunigel V1, and (f) Calcigel.

D. Correlation of parameters m and n with physico-chemical properties

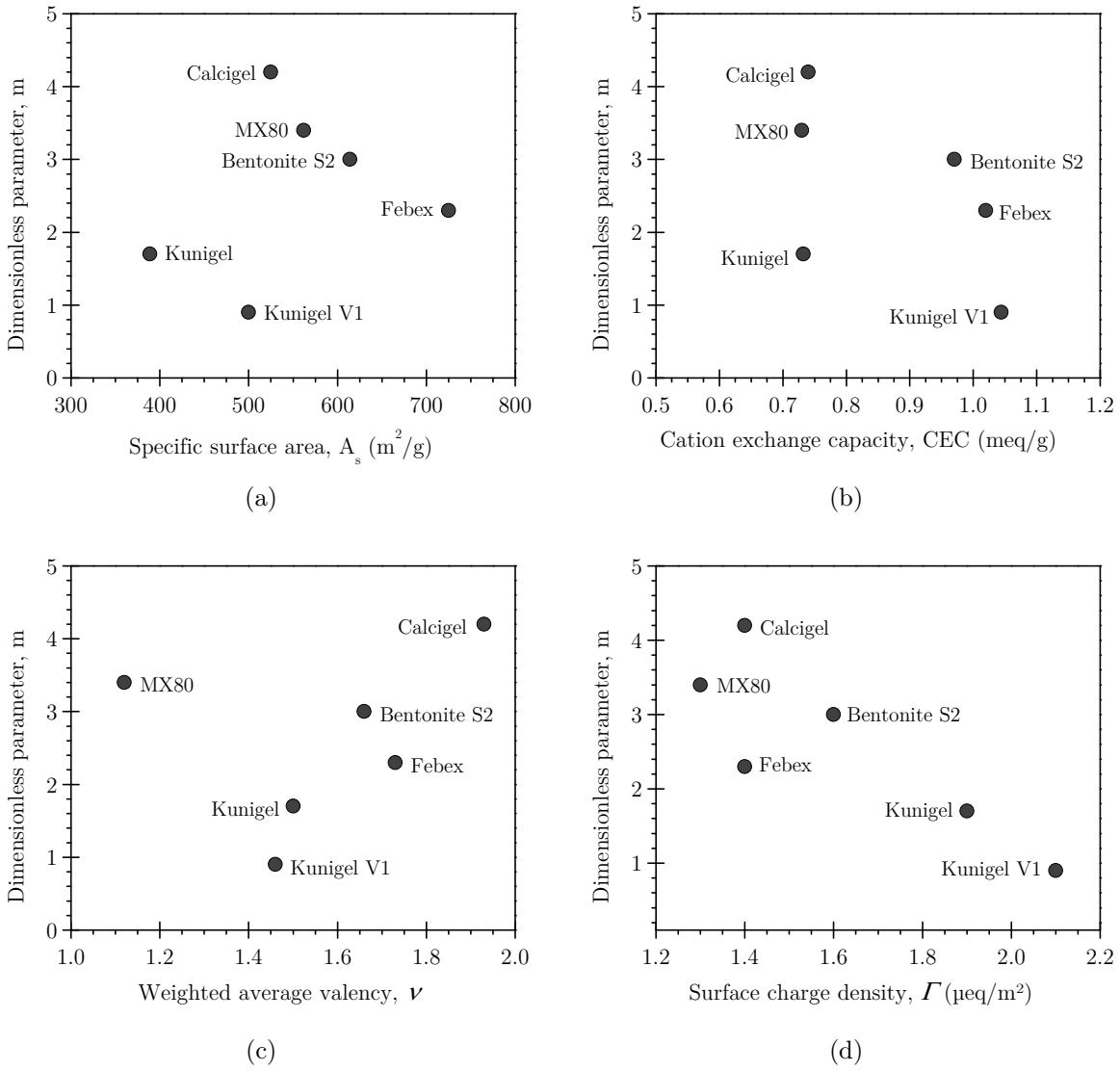

Figure D.1.: Correlation of parameter m with physico-chemical properties for bentonites: (a) m-A_S, (b) m-CEC, (c) m-ν, and (d) m-Γ.

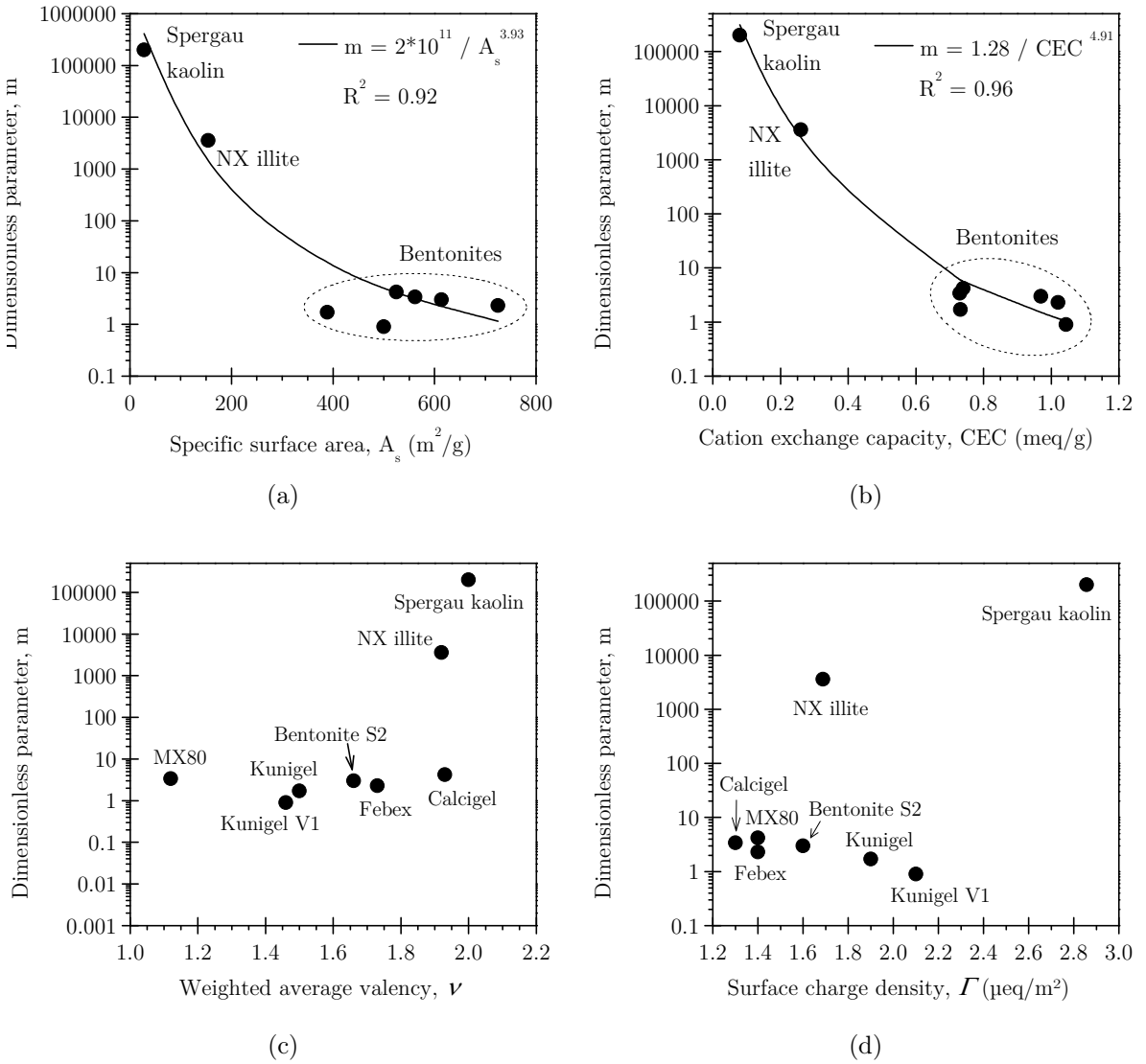

Figure D.2.: Correlation of parameter m with physico-chemical properties for the clays studied: (a) m-A_S, (b) m-CEC, (c) m-ν, and (d) m-Γ.

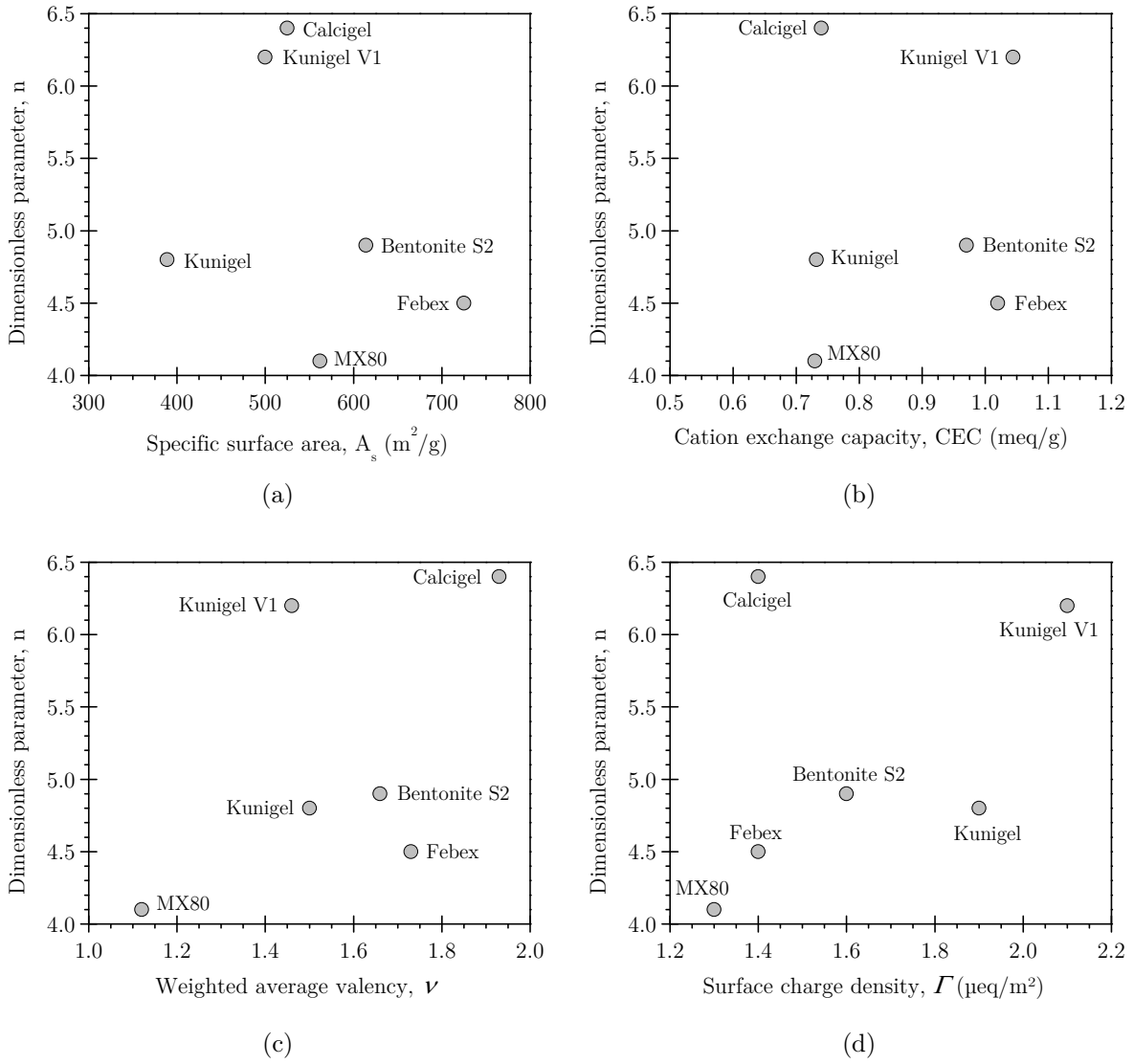

Figure D.3.: Correlation of parameter n with physico-chemical properties for bentonites: (a) n-A_S, (b) n-CEC, (c) n-ν, and (d) n-Γ.

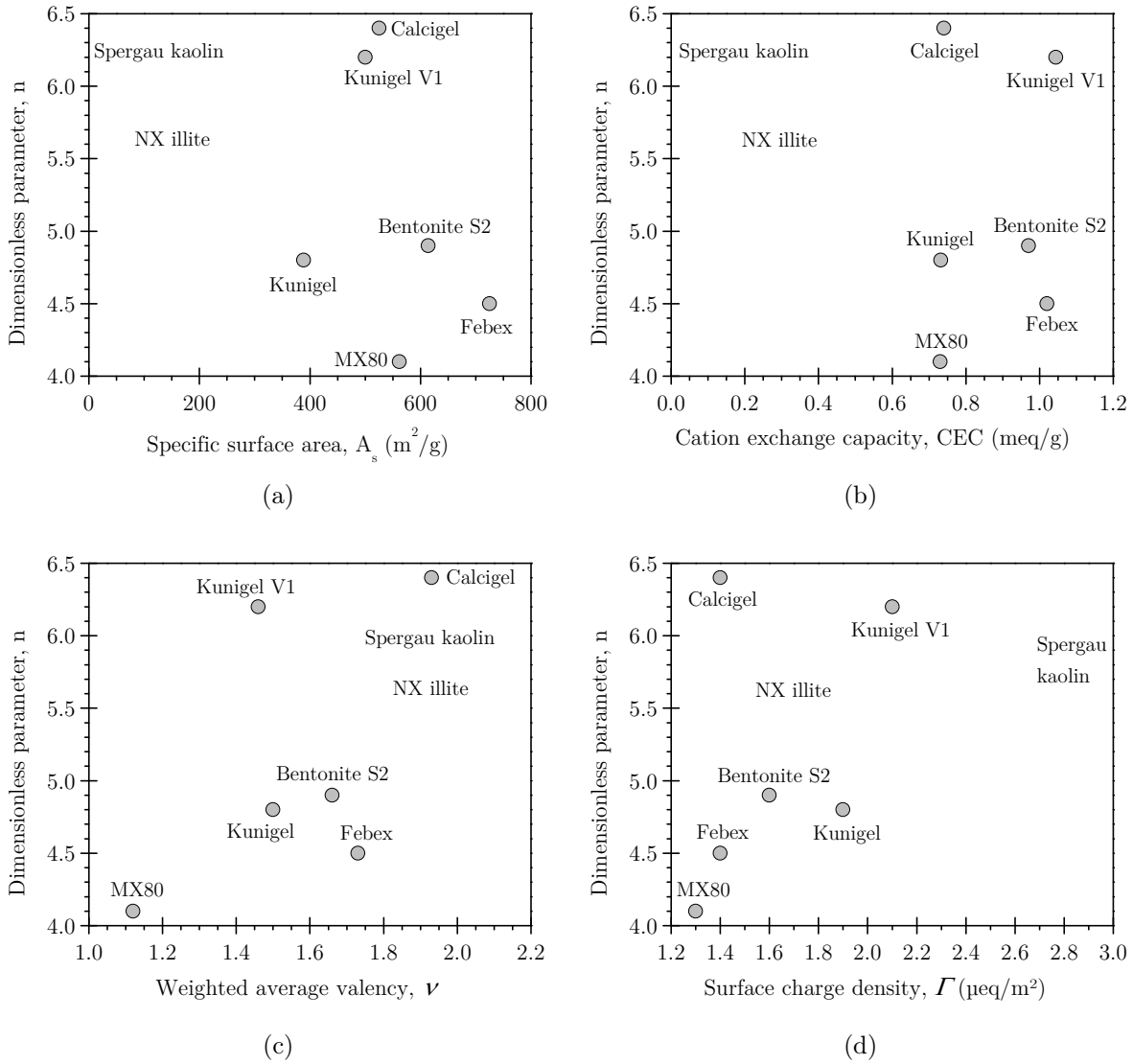

Figure D.4.: Correlation of parameter n with physico-chemical properties for the clays studied: (a) n-A_S, (b) n-CEC, (c) n-ν, and (d) n-Γ.

Bibliography

Abdullah, W., Al-Zou'bi, M. & Alshibli, K. (1997), 'On the physicochemical aspects of compacted clay compressibility', *Can. Geotech. J.* **34**, 551–559.

Achari, G., Joshi, R., Bentley, L. & Chatterji, S. (1999), 'Prediction of the hydraulic conductivity of clays using the electric double layer theory', *Can. Geotech. J.* **36**, 783–792.

Agus, S. S. (2005), An Experimental Study on Hydro-Mechanical Characteristics of Compacted Bentonite-Sand Mixtures, PhD thesis, Bauhaus-Universität Weimar.

Agus, S. & Schanz, T. (2005*a*), 'Comparison of four methods for measuring total suction', *Vadose Zone Journal* **4**(4), 1087–1095.

Agus, S. & Schanz, T. (2005*b*), Effect of shrinking and swelling on microstructures and fabric of a compacted bentonite-sand mixture, *in* 'Proceedings of International Conference on Problematic Soils', Eastern Mediterranean University, Famagusta, N. Cyprus, Famagusta, N. Cyprus.

Ahmed, S., Lovell, C. & Diamond, S. (1974), 'Pore sizes and strength of compacted clays', *ASCE J. Geotech. Eng. Division* **100**, 407–425.

Al-Mukhtar, M., Belanteur, N., Tessier, D. & Vanapalli, S. K. (1996), 'The fabric of a clay soil under controlled mechanical and hydraulic stress states', *Applied Clay Science* **11**, 99–115.

Al-Mukhtar, M., Qi, Y., Alcover, J.-F. & Bergaya, F. (1999), 'Oedometric and water-retention behavior of highly compacted unsaturated smectites.', *Canadian Geotechnical Journal* **36**, 675–684.

Anandarajah, A. (2000), 'Numerical simulation of one-dimensional behaviour of a kaolinite', *Géotechnique* **50**(5), 509–519.

Anandarajah, A. & Chen, J. (1997), 'Van der waals attractive force between clay particles in water and contaminants', *Soils and Foundations* **37**(2), 27–37.

Anandarajah, A. & Lu, N. (1991), 'Numerical study of the electrical double-layer repulsion between non-parallel clay particles of finite length', *International Journal for Numerical and Analytical Methods in Geomechanics* **15**, 683–703.

Anderson, M. T. & Lu, N. (2001), 'Role of microscopic physicochemical forces in large volumetric strains for clay sediments', *Journal of Engineering Mechanics* **127**(7), 710–719.

ASTMD2435-96 (1996), 'Standard test method for one-dimensional consolidation properties of soils', in 1998 Annual Book of ASTM Standards, Vol. 04.08.

ASTMD4546-08 (2008), 'Standard test methods for one-dimensional swell or collapse of cohesive soils', in 2008 ASTM Volume 04.08 Soil and Rock (I).

ASTMD4943-02 (2002), 'Standard test method for shrinkage factors of soils by the wax methods (d4943)', in 2005 Annual Book of ASTM Standards, Vol. 04.08.

ASTMD698 (2000), 'Standard test methods for laboratory compaction characteristics of soil using standard effort', in 2005 Annual Book of ASTM Standards, Vol. 04.08.

Aylmore, L. & Quirk, J. (1959), 'Swelling of clay-water systems', *Nature* **183**, 1752–1753.

Aylmore, L. & Quirk, J. (1962), 'The structural status of clay systems', *Clays and Clay Minerals* **9**, 104–130.

Aylmore, L. & Quirk, J. (1967), 'The micropore size distributions of clay mineral systems', *Journal of Soil Science* **18**(1), 1–17.

Bailey, S., Brindley, G., Johns, W., Martin, R. & Ross, M. (1971), 'Clay mineral society report of nomenclature committee 1969-1970', *Clays and Clay Minerals* **19**, 132–133.

Baille, W., Tripathy, S. & Schanz, T. (2014), 'Effective stress in clays of various mineralogy', *Vadose Zone Journal* **13**(5), 1–10.

Barbour, S. (1998), 'Nineteenth canadian geotechnical colloquium: The soil-water characteristic curve: a historical perspective', *Canadian Geotechnical Journal* **35**(5), 873–894.

Barden, L. & Sides, G. (1970), 'Engineering behaviour and structure of compacted clay', *Journal of the Soil Mechanics and Foundations Division, ASCE* **96**(SM4), 1171–1200.

Barkas, W. W. (1946), 'Some elastic constants and swelling pressures of natural wood and of its gel materials', *Trans. Faraday Soc.* **42**, 137.

Ben Rhaïem, H., Pons, C. & Tessier, D. (1987), Factors affecting the microstructure of smectites. role of cations and history of applied stresses., *in* L. G. Schultz, H. van Olphen & F. A. Mumpton, eds, 'Proceedings of the International Clay Conference Denver 1985', The Clay Minerals Society, Bloomington, Indiana 47405, U.S.A., pp. 292–297.

Bergaya, F. & Lagaly, G. (2013), *Basics*, Vol. 1 of *Handbook of Clay Science*, Elsevier Ltd., chapter 1.

Bishop, A. (1954), 'The use of pore water coefficients in practice', *Géotechnique* **4**, 148–152.

Blackmore, A. & Warkentin, B. (1960), 'Swelling of calcium montmorillonite', *Nature* **186**(4727), 823–824.

Bolt, G. (1956), 'Physico-chemical analysis of the compressibility of pure clays.', *Géotechnique* **6**(2), 86–93.

Bolt, G. H. (1955), 'Analysis of the validity of the gouy-chapman theory of the electric double layer', *Proceedings of the Soil Science Society of America* **19**, 285–288.

Bolt, G. & Miller, R. (1955), 'Compression studies of illite suspensions', *Soil Science Society of America Proceedings* **19**, 285Ű288.

Bolt, G. & Miller, R. (1958), 'Calculation of total and componanet potentials of water in soil', *Transactions of the American Geophysical Union* **39**(5), 917–928.

Brackley, I. (1973), Swell pressure and free swell in a compacted clay, *in* 'Proc. 3rd Int. Conf. Expansive Soils, Haifa, Israel', Vol. 1, Academic Press, Jerusalem, p. 169Ű176.

Bruand, A. & Prost, R. (1987), 'Effect of water content on the fabric of a soil material: an experimental approach', *Journal of Soil Science* **38**, 461–472.

Brunauer, S., Emmett, P. & Teller, E. (1938), 'Adsorption of gases in multi-molecular layers', *Journal of American Chemical Society* **60**, 309–319.

Bucher, F. & Müller-Vonmoos, M. (1989), 'Bentonite as a containment barrier for the disposal of highly radioactive wastes', *Applied Clay Science* **4**(2), 157–177.

Buckingham, E. (1907), *Studies on the movement of soil moisture*, Vol. 38 of *Bureau of Soils-Bulletin*, Washington, Govt. Print. Off., United States.

Carter, D., Heilman, M. & Gonzalez, C. (1965), 'Ethylene glycol monoethyl ether for determining surface area of silicate minerals', *Soil Science* **100**, 356–360.

Casagrande, A. (1932), 'The structure of clay and its importance in foundation engineering', *Journal of the Boston Society of Civil Engineers Section* **19**, 168–221.

Cerato, A. & Lutenegger, A. (2002), 'Determination of surface area of fine-grained soils by the ethylene glycol monoethyl ether (egme) method', *Geotechnical Testing Journal* **25**(3), 1–7.

Chapman, D. L. (1913), 'A contribution to the theory of electrocapillarity', *Philos. Mag.* **25**(6), 475–481.

Chen, F. H. (1988), *Foundations on expansive soils*, 2nd edn, Elsevier Science Publishing Co., Inc., New York.

Collins, K. & McGown, A. (1974), 'The form and function of microfabric features in a variety of natural soils', *Géotechnique* **24**(2), 223–254.

Croney, D. & Coleman, J. (1961), Pore pressure and suction in soils, *in* 'In Proceedings of the Conference on Pore Pressure and Suction in Soils', Butterworths, London, pp. 31–37.

Cui, Y. J. & Delage, P. (1996), 'Yielding and plastic behaviour of an unsaturated compacted silt', *Géotechnique* **46**(2), 291–311.

Cuisinier, O. & Laloui, L. (2004), 'Fabric evolution during hydromechanical loading of a compacted silt', *International Journal for Numerical and Analytical Methods in Geomechanics* **28**, 483–499.

Cuisinier, O. & Masrouri, F. (2004), 'Testing the hydromechanical behavior of a compacted swelling soil', *Geotechnical Testing Journal* **27**(6), 1–9.

Cuisinier, O. & Masrouri, F. (2005), 'Hydromechanical behaviour of a compacted swelling soil over a wide suction range', *Engineering Geology* **81**, 204–212.

Delage, P. (2007), Microstructure features in the behaviour of engineered barriers for nuclear waste disposal, *in* T. Schanz, ed., 'Experimental Unsaturated Soil Mechanics', Springer Proceedings in Physics, Vol. 112, Springer, Berlin Heidelberg, pp. 11–32.

Delage, P., Audiguier, M., Cui, Y. & Howat, M. (1996), 'The microstructure of a compacted silt', *Can. Geotech. J.* **33**, 150–158.

Delage, P. & Cui, Y. J. (2008), 'An evaluation of the osmotic method of controlling suction', *Geomechanics and Geoengineering* **3**(1), 1–11.

Delage, P., Howat, M. & Cui, Y. (1998), 'The relationship between suction and swelling properties in a heavily compacted unsaturated clay', *Engineering Geology* **50**(1), 31–48.

Delage, P. & Lefebvre, G. (1984), 'Study of the structure of a sensitive champlain clay and of its evolution during consolidation', *Can. Geotech. J.* **21**, 21–35.

Delage, P., Marcial, D., Cui, Y. & Ruiz, X. (2006), 'Ageing effects in a compacted bentonite: a microstructure approach', *Géotechnique* **56**(5), 291–304.

Delage, P. & Pellerin, F. (1984), 'Influence de la lyophilisation sur la structure d'une argile sensible du québec', *Clay Minerals* **19**, 151–160.

Derjaguin, B. V. & Landau, L. D. (1941), 'The theory of stability of strongly charged lyophobic sols and the adhesion of strongly charged particles in solutions of electrolyte', *Acta Physicochimica (URSS)* **14**, 633–662.

Devineau, K., Bihannic, I., Michot, L., Villiéras, F., Masrouri, F., Cuisinier, O., Fragneto, G. & Michau, N. (2006), 'In situ neutron diffraction analysis of the influence of geometric confinement on crystalline swelling of montmorillonite', *Applied Clay Science* **31**, 76–84.

Di Maio, C., Santoli, L. & Schiavone, P. (2004), 'Volume change behaviour of clays: the influence of mineral composition, pore fluid composition and stress state', *Mechanics of Materials* **36**, 435–451.

Diamond, S. (1970), 'Pore size distributions in clays', *Clays and Clay Minerals* **18**, 7–23.

DIN18122T1 (1997), 'Soil, investigation and testing - consistency limits - part 1: Determination of liquid limit and plastic limit'.

DIN18122T2 (2000), 'Soil - investigation and testing - part 2: Determination of the shrinkage limit'.

DIN18123 (1996), 'Soil, investigation and testing - determination of grain-size distribution'.

DIN18124 (1997), 'Soil, investigation and testing - determination of density of solid particles - capillary pyknometer, wide mouth pycnometer'.

Dineen, K. & Burland, J. B. (1995), A new approach to osmotically controlled oedometer testing, *in* 'Proceedings of the 1st International Conference on Unsaturated Soils', Vol. 2, Paris, pp. 459–465.

Dixon, D. & Gray, M. (1985), The engineering properties of buffer material., Technical Report TR-350, Fuel Waste Technology Branch, Whiteshell Laboratories., Pinawa, Man.

Dohrmann, R. (1997), Kationenaustauschkapazität von Tonen. Bewertung bisheriger Analysenverfahren und Vorstellung einer neuen und exakten Silber-Thioharnstoff-Methode., PhD thesis, RWTH Aachen, Aachen. in German.

Drits, V. & Sakharov, B. (1976), *X-Ray structure analysis of mixed-layer minerals*, Academy of Science, Moscow, Moscow. (in Russian).

Dyal, R. & Hendricks, S. (1950), 'Total surface of clays in polar liquids as a characteristic index', *Soil Science* **69**, 421–432.

Edlefsen, N. & Anderson, A. (1943), 'Thermodynamics of soil moisture.', *Hilgardia* **15**, 31–298.

ENRESA (2000), Febex project. full-scale engineered barriers experiment for a deep geological repository for high level radioactive waste in crystalline host rock. final report., Technical Report Publicación Técnica ENRESA 1/2000, ENRESA, Madrid.

Fleureau, J.-M., Kheirbek-Saoud, S., Soemitro, R. & Taibi, S. (1993), 'Behaviour of clayey soils on drying-wetting paths', *Can. Geotech. J.* **30**, 287–296.

Fleureau, J.-M., Verbrugge, J.-C., Huergo, P. J., Gomes Correia, A. & Kheirbek-Saoud, S. (2002), 'Aspects of the behaviour of compacted clayey soils on drying and wetting paths', *Canadian Geotechnical Journal* **39**(6), 1341–1357.

Fredlund, D. (2006), 'Unsaturated soil mechanics in engineering practice', *Journal of Geotechnical and Geoenvironmental Engineering* **132**(3), 286–321.

Fredlund, D. G. & Rahardjo, H. (1993), *Soil Mechanics for Unsaturated Soils*, John Wiley & Sons, Inc.

Fredlund, D. & Morgenstern, N. (1977), 'Stress state variables for unsaturated soils', *J. Geotech. Eng. Div. Am. Soc. Civ. Eng.* **103**, 447–466.

Fredlund, D. & Xing, A. (1994), 'Equation for the soil-water characteristic curve', *Can. Geotech. J.* **31**, 521–532.

Gens, A. & Alonso, E. (1992), 'A framework for the bahaviour of unsaturated expansive clays', *Canadian Geotechnical Journal* **29**, 1013–1032.

Gonçalvèz, J., Rousseau-Gueutin, P. & Revil, A. (2007), 'Introducing interacting diffuse layers in tlm calculations: A reappraisal of the influence of the pore-size on the

swelling pressure and the osmotic efficiency of compacted bentonites', *Journal of Colloid and Interface Science* **316**(1), 92–99.

Gouy, M. (1910), 'Sur la constitution de la charge électrique à la surface d'un électrolyte', *Journal de Physique* **4**(IX), 457–468.

Gray, M., Cheung, S. & Dixon, D. (1984), The influence of sand content on swelling pressures and structure developed in statically compacted na-bentonite, Technical Report 7825, Atomic Energy of Canada Limited, Mississauga, Ont.

Griffiths, F. & Joshi, R. (1990), 'Clay fabric response to consolidation', *Applied Clay Science* **5**, 37–66.

Grim, R. (1962), 'Clay mineralogy', *Science* **135**, 890–898.

Grim, R. E. (1968), *Clay Mineralogy*, 2nd edition edn, McGraw-Hill Book Company.

Güven, N. (1992), Molecular aspects of clay-water interactions., *in* N. Güven & R. Pollastro, eds, 'Clay-water interface and its rheological implications. CMS Workshop lectures', Vol. 4, Clay Minerals Society, Boulder, CO, pp. 2–79.

Haines, W. B. (1923), 'The volume-changes associated with variations of water content in soil', *The Journal of Agricultural Science* **13**, 296–310.

Hamaker, H. (1937), 'The london-van der waals attraction between spherical particles', *Physica* **IV**(10), 1058–1072.

Herbert, H.-J. & Moog, H. (2002), Untersuchungen zur quellung von bentonit in hochsalinaren lösungen., Technical Report GRS-179, Gesellschaft für Anlagen und Reaktorsicherheit (GRS) mbH, Berlin.

Hiemenz, P. (1977), *Principles of colloid and surface chemistry*, Dekker, New York.

Hilf, J. (1956), An investigation of pore water pressure in compacted cohesive soils, Tech Memo 654, Bureau of Reclamation (US).

Holmes, J. (1955), 'Water sorption and swelling of clay blocks', *Journal of Soil Sciences* **6**, 200–208.

Hueckel, T. (1992), 'On effective stress concepts and deformation in clays subjected to environmental loads: Discussion', *Canadian Geotechnical Journal* **29**, 1120–1125.

Imbert, C. & Villar, M. (2006), 'Hydro-mechanical response of a bentonite pellets/powder mixture upon infiltration', *Applied Clay Science* **32**, 197–209.

Ingles, O. (1968), *Soil chemistry relevant to the engineering behaviour of soils, Chapter I, Soil Mechanics, Selected Topics*, Elsevier, New York.

Israelachvili, J. (1992), *Intermolecular and Surface Forces*, 2nd edn, Academic Press, London-San Diego.

Israelachvili, J. & Pashley, R. (1983), 'Molecular layering of water at surfaces and origin of repulsive hydration forces', *Nature* **306**, 249–250.

Jasmund, K. & Lagaly, G. (1993), *Tonminerale und Tone: Struktur, Eigenschaften, Anwendung und Einsatz in Industrie und Umwelt*, Steinkopff-Verlag.

JNC (2000), H12: Project to establish the scientific and technical basis for hlw disposal in japan; supporting report 2: Repository design and engineering technology, Technical Report JNC-TN1410-2000-003, Japan Nuclear Cycle Development Institute (JNC), Tokyo.

Kakinoki, J. & Komura, Y. (1952), 'Intensity of x-ray diffraction by one-dimensionnaly disordered crystals', *J. Phys. Soc. Japan* **7**, 30–35.

Kassiff, G. & Ben Shalom, A. (1971), 'Experimental relationship between swell pressure and suction', *Géotechnique* **21**(3), 245–255.

Kaufhold, S., Dohrmann, R., Ufer, K. & Meyer, F. (2002), 'Comparison of methods for the quantification of montmorillonite in bentonites', *Applied Clay Science* **22**, 145–151.

Khalili, N., Geiser, F. & Blight, G. (2004), 'Effective stress in unsaturated soils: Review with new evidence', *Int. J. Geomech.* **4**(2), 115–126.

Kjellander, R., Marcelja, S., Pashley, R. & Quirk, J. (1988), 'Double-layer correlation forces restrict calcium-clay swelling', *Journal of Physical Chemistry* **92**, 6489–6492.

Komine, H. & Ogata, N. (1996), 'Prediction for swelling characteristics of compacted bentonite', *Canadian Geotechnical Journal* **33**, 11–22.

Komine, H.and Ogata, N. (1994), 'Experimental study on swelling characteristics of compacted bentonite', *Canadian Geotechnical Journal* **31**(4), 478–490.

Laird, D. (2006), 'Influence of layer charge on swelling of smectites', *Applied Clay Science* **34**, 74–87.

Lambe, T. (1958*a*), 'Compacted clay: Engineering behavior', *Transactions of the American Society of Civil Engineers (ASCE)* **125**, 718–741.

Lambe, T. (1958*b*), 'Compacted clay: Structure', *Transactions of the American Society of Civil Engineers (ASCE)* **125**, 682–706.

Lambe, T. (1960), A mechanistic picture of shear strenght in a clay, *in* 'Proceedings of the ASCE Conference on Shear Strength of Cohesive Soils', Boulder, Colorado, pp. 503–532.

Lambe, T. & Whitman, R. (1969), *Soil Mechanics*, John Wiley & Sons, Inc.

Leonards, G. (1961), *Foundation Engineering*, McGraw-Hill Book Co., New York.

Leong, E. & Rahardjo, H. (1997), 'Review of soil-water characteristic curve equations', *Journal of Geotechnical and Geoenvironmental Engineering* **123**(12), 1106–1117.

Leong, E., Tripathy, S. & Rahardjo, H. (2003), 'Total suction measurement of unsaturated soils with a device using the chilled-mirror dew-point technique', *Géotechnique* **53**(2), 173–182.

Leong, E., Tripathy, S. & Rahardjo, H. (2004), 'A modified pressure plate apparatus', *Geotechnical Testing Journal* **27**(3), 322–331.

Leroy, P. & Revil, A. (2004), 'A triple-layer model of the surface electrochemical properties of clay minerals', *Journal of Colloid and Interface Science* **270**, 371Ű380.

Likos, W. J. (2004), 'Measurement of crystalline swelling in expansive clay', *Geotechnical Testing Journal* **27**(6), 1–7.

Likos, W. J. & Lu, N. (2006), 'Pore-scale analysis of bulk volume change from crystalline interlayer swelling in na+ and ca2+-smectite', *Clays and Clay Minerals* **54**(4), 516–529.

Likos, W. & Lu, N. (2001), 'Automated measurement of total suction characteristics in high-suction range: Application to assessment of swelling potential', *Transportation Research Record: Journal of the Transportation Research Board* **1755**(1), 119–128.

Likos, W. & Lu, N. (2003), 'Automated humidity system for measuring total suction characteristics of clay', *Geotechnical Testing Journal* **26**(2), 179–190.

Likos, W. & Lu, N. (2012), Characterizing physical properties of clay by water vapor sorption, *in* 'GeoCongress 2012, State of the Art and Practice in Geotechnical Engineering', pp. 1175–1184.

Likos, W. & Wayllace, A. (2010), 'Porosity evolution of free and confined bentonites during interlayer hydration', *Clays and Clay Minerals* **58**(3), 399–414.

Lloret, A., Villar, M., Sànchez, M., Gens, A., Pintado, X. & Alonso, E. (2003), 'Mechanical behaviour of heavily compacted bentonite under high suction changes', *Géotechnique* **53**, 27–40.

Low, P. (1959), 'Viscosity of water in clay systems', *Clays and Clay Minerals* **8**(1), 170–182.

Lu, N. & Anandarajah, A. (1992), 'Empirical estimation of double-layer repulsive force between two inclined clay particles of finite length', *Journal of Geotechnical Engineering* **118**(4), 628–634.

Lu, N., Godt, J. W. & Wu, D. T. (2010), 'A closed-form equation for effective stress in unsaturated soil', *Water Resources Research* **46**(W05515), 1–14.

Lu, N. & Likos, W. (2004), *Unsaturated Soil Mechanics*, John Wiley & Sons, Inc., Hoboken, New Jersey.

Lu, N. & Likos, W. J. (2006), 'Suction stress characteristic curve for unsaturated soil', *Journal of Geotechnical and Geoenvironmental Engineering* **132**(2), 131–142.

Lu, N., Wu, B. & Tan, C. (2007), 'Tensile strenght characteristics of unsaturated sands', *J. Geotech. Geoenv. Eng.* **133**(2), 144–154.

MacEwan, D. (1954), 'Short-range electrical forces between charged colloid particles', *Nature* **174**, 39–40.

Madsen, F. & Müller-Vonmoos, M. (1985), 'Swelling pressure calculated from mineralogical properties of a jurassic opalinum shale, switzerland', *Clays and Clay Minerals* **33**(6), 501–509.

Marcial, D., Delage, P. & Cui, Y. J. (2002), 'On the high stress compression of bentonites', *Canadian Geotechnical Journal* **39**(4), 812–820.

Martin, R. (1960), Adsorbed water on clay: a review, *in* A. Swineford & P. Franks, eds, 'Proceedings of the Ninth National Conference on Clays and Clay Minerals 1960', International Series of Monographs on Earth Sciences, Pergamon Press, Symposium Publ. Division, 1962, Lafayette, Indiana, pp. 28–70.

McQueen, I. S. & Miller, R. (1974), 'Approximating soil moisture characteristics from limited data: Empirical evidence and tentative model', *Water Resources Research* **10**(3), 521–527.

Meier, L. & Kahr, G. (1999), 'Determination of the cation exchange capacity (cec) of clay minerals using the complexes of copper(ii) ion with triethylenetetramine and tetraethylenepentamine', *Clays and Clay Minerals* **47**(3), 386–388.

Mesri, G. & Olson, R. (1971), 'Consolidation characteristics of montmorillonite', *Géotechnique* **21**(4), 341–352.

Mitchell, J. K. (1993), *Fundamentals of Soil Behaviour*, 2 edn, John Wiley & Sons, Inc.

Mitchell, J. & Soga, K. (2005), *Fundamentals of Soil Behavior*, 3rd edn, John Wiley and Sons, Inc., Hoboken, New Jersey.

Müller-Vonmoos, M. & Kahr, G. (1982), Bereitstellung von bentonit für laboruntersuchungen, Technischer Bericht 82-04, Nagra.

Müller-Vonmoos, M. & Kahr, G. (1983), Mineralogische untersuchungen von wyoming bentonit mx-80 und montigel, Technischer Bericht 83-12, Nagra, Baden/Schweiz.

Monroy, R., Ridley, A., Dineen, K. & Zdrakovic, L. (2007), 'The suitability of the osmotic technique for the long term testing of partly saturated soils', *Geotechnical Testing Journal* **30**(3), 220Ű226.

Montes-H, G., Duplay, J., Martinez, L., Geraud, Y. & Rousset-Tournier, B. (2003), 'Influence of interlayer cations on the water sorption and swellingŰshrinkage of mx80 bentonite', *Applied Clay Science* **23**(5Ű6), 309–321.

Moore, D. (1996), 'Comment on: definition of clay and clay mineral: joint report of the aipea nomenclature and cms nomenclature committees', *Clays and Clay Minerals* **44**, 710–712.

Morgenstern, N. & Balasubramonian, B. (1980), Effects of pore fluid on the swelling of clay-shale, *in* D. Snethen, ed., 'Proceeding 4th International Conference on Expansive Soil', ASCE, Denver, CO, pp. 190–205.

Moriwaki, T. & Wada, Y. (2001), Quantitative evaluation of microstructure of clays, *in* K. Adachi & M. Fukue, eds, 'Clay Science for Engineering Proc. of the int. Symp. on suction, swelling, permeability and structure of clays', A.A. Balkema, Rotterdam/Brookfield, Shizuaoka, Japan, p. 606.

Mualem, Y. (1976), 'A new model for predicting the hydraulic conductivity of unsaturated porous media', *Water Resources Research* **12**, 593–622.

Mullins, C. & Panayiotopoulos, K. (1984), 'The strength of unsaturated mixtures of sand and kaolin and the concept of effective stress', *Journal of Soil Science* **35**, 459–468.

Nagaraj, T. & Srinivasa Murthy, B. (1983), 'Rationalization of skempton's compressibility equation', *Géotechnique* **33**(4), 433–443.

Newman, A. (1987), *Chemistry of Clays and Clay Minerals*, Mineral. Soc., London.

Nickel, E. (1995), 'The definition of a mineral', *Canadian Mineralogist* **33**, 689–690.

Nikooee, E., Habibagahi, G., Hassanizadeh, S. & Ghahramani, A. (2013), 'Effective stress in unsaturated soils: A thermodynamic approach based on the interfacial energy and hydromechanical coupling', *Transport in Porous Media* **96**, 369–396.

Ninham, B. (1980), 'Long-range vs. short-range forces. the present state of play.', *Physical Chemistry* **84**(12), 1423–1430.

Norrish, K. & Quirk, J. (1954), 'Crystalline swelling of montmorillonite - use of electrolytes to control swelling', *Nature* **173**, 255–256.

Nuth, M. & Laloui, L. (2008), 'Effective stress concept in unsaturated soils: Clarification and validation of a unified framework', *Int. J. Numer. Anal. Meth. Geomech.* **32**, 771–801.

Oh, S., Lu, N., Kim, Y., Lee, S. & Lee, S. (2012), 'Relationship between the soil-water characteristic curve and the suction stress characteristic curve: Experimental evidence from residual soils', *J. Geotech. Geoenviron. Eng.* **138**, 47–57.

Olson, R. E. & Mesri, G. (1970), 'Mechanisms controlling the compressibility of clay', *ASCE Journal of the Soil Mechanics and Foundations Division* **96**(6), 1863–1878.

Osipov, V. & Sokolov, V. (1978), 'Structure formation in clay sediments', *Bulletin of the International Association of Engineering Geology* **18**, 83–90.

Palomino, A. & Santamarina, J. (2005), 'Fabric map for kaolinite: Effects of ph and ionic concentration on behavior', *Clays and Clay Minerals* **53**(3), 209–222.

Pashley, R. (1981), 'Dlvo and hydration forces between mica surfaces in li+, na+, k+, and cs+ electrolyte solutions: A correlation of double-layer and hydration forces with surface cation exchange properties', *Journal of Colloid and Interface Science* **83**(2), 531–546.

Pellerin, F. (1979), 'La porosimétrie au mercure appliquée à l'étude géotechnique des sols et des roches', *Bulletin de Liaison des Laboratoires des Ponts et Chaussées* **106**, 105–116.

Penumadu, D. & Dean, J. (2000), 'Compressibility effect in evaluating the pore-size distribution of kaolin clay using mercury intrusion porosimetry', *Canadian Geotechnical Journal* **37**, 393–405.

Plançon, A. & Tchoubar, C. (1976), 'Étude des fautes d'empilement dans les kaolinites partiellement désordonnées', *J. Appl. Cryst.* **9**, 279–285.

Pleysier, J. & Juo, A. (1980), 'A single-extraction method using silver-thiourea for measuring exchangeable cations and effective cec in soils with variable charges', *Soil Science* **129**(4), 205–211.

Pons, C. H. (1980), Mise en evidence des rélations entre la texture et la structure dans les systèmes eau-smectite par diffusion aux petits angles du rayonnement X synchrotron, PhD thesis, Univ. Orléans.

Pusch, R. (1977), Required physical and mechanical properties of buffer masses., Technical report 33, KBS, Swedish Nuclear Fuel Supply Co., Stockholm.

Pusch, R. (1982), 'Mineral–water interactions and their influence on the physical behavior of highly compacted na bentonite', *Can. Geotech. J.* **19**, 381–387.

Pusch, R. & Karnland, O. (1990), Preliminary report on longevity of montmorillonite clay under repository related conditions, Technical report 90-44, Clay Technology AB, Lund.

Pusch, R., Karnland, O. & Hökmark, H. (1990), Gmm - a general microstructural model for qualitative and quantitative studies of smectite clays, Technical report 90-43, Clay Technology AB, Lund.

Quirk, J. P. & Aylmore, L. A. G. (1971), 'Domains and quasi-crystalline regions in clay systems', *Soil Sci. Soc. Am. Proc.* **35**, 652–654.

Radhakrishna, H., Chan, H., Crawford, A. & Lau, K. (1989), 'Thermal and physical properties of candidate buffer-backfill materials for a nuclear fuel waste disposal vault', *Can. Geotech. J.* **26**, 629–639.

Romero, E. (1999), Characterisation and thermo-hydro-mechanical behaviour of unsaturated Boom clay: an experimental study, PhD thesis, Universitat Polytècnica de Catalunya.

Romero, E., Gens, A. & Lloret, A. (1999), 'Water permeability, water retention and microstructure of unsaturated compacted boom clay.', *Engineering Geology* **54**(1-2), 117–127.

Saiyouri, N., Hicher, P. & Tessier, D. (2000), 'Microstructural approach and transfer water modelling in highly compacted unsaturated swelling clays', *Mechanics of Cohesive-Frictional Materials* **5**, 41–60.

Saiyouri, N., Tessier, D. & Hicher, P. (2004), 'Experimental study of swelling in unsaturated compacted clays', *Clay Minerals* **39**, 469Ű479.

Santamarina, J. C. (2001*a*), Soil behavior at the microscale: Particle forces, *in* 'Proceedings of the Symposium of Soil Behavior and Soft Ground Construction, in honor of Charles C. Ladd', MIT.

Santamarina, J. C. (2001*b*), *Soils and waves*, John Wiley & Sons.

Santamarina, J., Klein, K., Wang, Y. & Prencke, E. (2002), 'Specific surface: determination and relevance', *Canadian Geotechnical Journal* **39**, 233–241.

Schanz, T. & Tripathy, S. (2005), Soil-water characteristic curves of clays from physico-chemical concepts, *in* H. Bilsel & Z. Nalbantoglu, eds, 'Proceedings of International Conference on Problematic Soils', Vol. 1, Eastern Mediterranean University, Famagusta, N. Cyprus, pp. 219–228.

Schanz, T. & Tripathy, S. (2009), 'Swelling pressure of a divalent-rich bentonite: Diffuse double-layer theory revisited', *Water Resources Research* **45**(2), W00C12.

Schofield, R. K. (1935), The pf of the water in soil, *in* 'Trans. 3rd Int. Congr. Soil Sci. 3rd', Vol. II, pp. 38–48.

Sides, G. & Barden, L. (1971), 'The microstructure of dispersed and flocculated samples of kaolinite, illite, and montmorillonite', *Can. Geotech. J.* **8**(3), 391–399.

Skempton, A. (1953), The colloidal activity of clay, *in* 'Proceedings of the Third International Conference on Soil Mechanics and Foundation Engineering', Vol. I, Zürich, pp. 57–61.

Sposito, G. & Prost, R. (1982), 'Structure of water adsorbed on smectites', *Chemical Reviews* **82**(6), 553–573.

Sridharan, A. (1968), Some studies on the strenght of partly saturated clays, PhD thesis, Purdue University.

Sridharan, A. (2002), Engineering behaviour of clays: Influence of mineralogy, *in* C. Di Maio, T. Hueckel & B. Loret, eds, 'Chemo-Mechanical Coupling in Clays; From Nano-Scale to Engineering Applications', Swets & Zeitlinger, Lisse, pp. 3–27.

Sridharan, A., Altschaeffl, A. & Diamond, S. (1971), 'Pore size distribution studies', *Journal of the Soil Mechanics and Foundations Division, ASCE* **97**(SM5), 771–787.

Sridharan, A. & Jayadeva, M. (1982), 'Double layer theory and compressibility of clays', *Géotechnique* **32**(2), 133–144.

Sridharan, A. & Rao, G. (1973), 'Mechanisms controlling volume change of saturated clays and the role of the effective stress concept', *Géotechnique* **23**(3), 359–382.

Sridharan, A., Rao, S. & Murthy, N. (1986), 'Compressibility behaviour of homoionized bentonites', *Géotechnique* **36**(4), 551–564.

Sridharan, A., Sreepada Rao, A. & Sivapullaiah, P. (1986), 'Swelling pressure of clays', *Geotechnical Testing Journal* **9**(1), 24–33.

Sridharan, A. & Venkat. Rao, G. (1979), 'Shear strength behaviour of saturated clays and the role of the effective stress concept', *Géotechnique* **29**(2), 177–193.

Sridharan, A. & Venkatappa Rao, G. (1971), 'Effective stress theory of shrinkage phenomena', *Canadian Geotechnical Journal* **8**(4), 503–513.

Stern, O. (1924), 'Zur theorie der elektrolytischen doppelschicht', *Zeitschrift für Elektrochemie* **30**, 508–516.

Suzuki, S., Prayongphan, S., Ichikawa, Y. & Chae, B. (2005), 'In situ observations of the swelling of bentonite aggregates in nacl solution', *Applied Clay Science* **29**, 89–98.

Tarantino, A. & De Col, E. (2008), 'Compaction behaviour of clay', *Géotechnique* **58**(3), 199–213.

Terzaghi, K. (1925), *Erdbaumechanik auf bodenphysikalischer Grundlage*, Deuticke, Leipzig.

Terzaghi, K. (1936), The sehearing resistance of saturated soils and the angle between the planes of shear, *in* 'International Conference on Soil Mechanics and Foundation engineering', Harvard University press, Cambridge, MA.

Terzaghi, K. (1943), *Theoretical soil mechanics*, Wiley, New York.

Tessier (1990*a*), *Soil Colloids and Their Associations in Aggregates*, Plenum Press, New York, chapter 14 Behaviour and Microstructure of Clay Minerals, pp. 387–415.

Tessier, D. (1984), Étude expérimentale de l'organisation des matériaux argileux, PhD thesis, L'université de Paris VII, Paris, France.

Tessier, D. (1990*b*), *Matériaux argileux: Structure, propriétés et applications*, Société francaise de minéralogie et de cristallographie, chapter Organisation des materiaux argileux en relation avec leur comportement hydrique, pp. 387–445.

Tessier, D. & Pedro, G. (1976), 'Les modalités de l'organisation des particules dans les matériaux argileux', *Science du Sol* **2**, 85–99.

Thom, R., Sivakumar, R., Sivakumar, V., Murray, E. & Mackinnon, P. (2007), 'Pore size distribution of unsaturated compacted kaolin: the initial states and final states following saturation', *Géotechnique* **57**(5), 469–474. Technical Note.

Tovey, N. & Wong, K. (1980), 'The microfabric of deformed kaolin', *Journal of Microscopy* **120**(3), 329–342.

Tripathy, S., B. R. . T. H. R. (2013), 'Effect of stern-layer on the compressibility behaviour of bentonites', *Acta Geotechnica* **online**, 1–13.

Tripathy, S., Bag, R. & Thomas, H. (2010), Desorption and consolidation behaviour of intially saturated clays, *in* E. Alonso & A. Gens, eds, 'Proceedings of the 5th International Conference on Unsaturated Soils', Taylor & Francis, Barcelona, Spain, pp. 381–386.

Tripathy, S., Kessler, W. & Schanz, T. (2006), Determination of interparticle repulsive pressures in clays, *in* G. Miller, C. Zapata, S. Houston & D. Fredlund, eds, 'Proceedings of the Fourth International Conference on Unsaturated Soils', Carefree, Arizona, USA, pp. 2198–2209.

Tripathy, S. & Schanz, T. (2007), 'Compressibility behaviour of clays at large pressures', *Can. Geotech. J.* **44**, 355–362. Note.

Tripathy, S., Sridharan, A. & Schanz, T. (2004), 'Swelling pressures of compacted bentonites from diffuse double layer theory', *Canadian Geotechnical Journal* **41**, 437–450.

Tripathy, S., Subba Rao, K. & Fredlund, D. (2002), 'Water content - void ratio swell-shrink paths of compacted expansive soils', *Canadian Geotechnical Journal* **39**, 938–959.

Tuller, M. & Or, D. (2003), 'Hydraulic functions for swelling soils: pore scale considerations', *Journal of Hydrology* **272**, 50–71.

van Genuchten, M. T. (1980), 'A closed-form equation for predicting the hydraulic conductivity of unsaturated soils', *Soil Sci. Soc. Am. J.* **44**, 892–898.

van Olphen, H. (1963), *An introduction to clay colloid chemistry*, 1st edn, John Wiley & Sons, New York London Sydney Toronto.

van Olphen, H. (1977), *An introduction to clay colloid chemistry*, 2nd edn, John Wiley & Sons, New York London Sydney Toronto.

Vanapalli, S., Fredlund, D. & Pufahl, D. (1996), 'The relationship between the soil-water characteristic curve and the unsaturated shear strength of a compacted glacial till', *Geotechnical Testing Journal* **19**(3), 259–268.

Verwey, E. & Overbeek, J. (1948), *Theory of the stability of lyophobic colloids*, Elsevier, Amsterdam.

Vesga, L. F. (2008), 'Equivalent effective stress and compressibility of unsaturated kaolinite clay subjected to drying', *Journal of Geotechnical and Geoenvironmental Engineering* **134**(3), 366–378.

Villar, M. (2000), Caracterización termo-hidro-mecánica de una bentonita de Cabo de Gata Universidad Complutense, Madrid, Spain., PhD thesis, Universidad Complutense, Madrid, Spain.

Wang, Y.-H. & Siu, W.-K. (2006*a*), 'Structure characteristics and mechanical properties of kaolinite soils. i. surface charges and structural characterizations', *Canadian Geotechnical Journal* **43**, 587–600.

Wang, Y.-H. & Siu, W.-K. (2006*b*), 'Structure characteristics and mechanical properties of kaolinite soils. ii. effects of structure on mechanical properties', *Canadian Geotechnical Journal* **43**, 601–617.

Warkentin, B. P., Bolt, G. M. & Miller, R. D. (1957), 'Swelling pressure of montmorillonite', *Soil Sci. Soc. Am. J.* **21**, 495–497.

Warr, L. & Berger, J. (2007), 'Hydration of bentonite in natural waters: Application of "confined volume" wet-cell x-ray diffractometry', *Physics and Chemistry of the Earth* **32**, 247–258.

Weaver, C. & Pollard, L. (1973), *The chemistry of clay minerals*, Vol. 15 of *Developments in sedimentology*, Elsevier Scientific Publishing Company, Amsterdam.

Williams, J. & Shaykewich, C. (1969), 'An evaluation of polyethylene glycol (p.e.g.) 6000 and p.e.g. 20,000 in the osmotic control of soil water matric potential', *Canadian Journal of Soil Science* **49**, 397–401.

Yong, R. (1999), 'Soil suction and soil-water potentials in swelling clays in engineered clay barriers', *Engineering Geology* **54**, 3–13.

Yong, R. & Mohamed, A. (1992), 'A study of particle interaction energies in wetting of unsaturated expansive clays', *Canadian Geotechnical Journal* **29**(6), 1060–1070.

Yong, R. & Warkentin, B. (1966), *Introduction to soil behaviour*, Transportation research board, Washington.

Zur, B. (1966), 'Osmotic control of the matric soil-water potential: I soil-water system.', *Soil Science* **102**(6), 394–398.

Schriftenreihe des Lehrstuhls für Grundbau, Boden- und Felsmechanik der Ruhr-Universität Bochum

Herausgeber: H.L. Jessberger

1 (1979) **Hans Ludwig Jessberger**
Grundbau und Bodenmechanik an der Ruhr-Universität Bochum

2 (1978) **Joachim Klein**
Nichtlineares Kriechen von künstlich gefrorenem Emschermergel

3 (1979) **Heinz-Joachim Gödecke**
Die Dynamische Intensivverdichtung wenig wasserdurchlässiger Böden

4 (1979) **Poul V. Lade**
Three Dimensional Stress-Strain Behaviour and Modeling of Soils

5 (1979) **Roland Pusch**
Creep of soils

6 (1979) **Norbert Diekmann**
Zeitabhängiges, nichtlineares Spannungs-Verformungsverhalten von gefrorenem Schluff unter triaxialer Belastung

7 (1979) **Rudolf Dörr**
Zeitabhängiges Setzungsverhalten von Gründungen in Schnee, Firn und Eis der Antarktis am Beispiel der deutschen Georg-von-Neumayer- und Filchner-Station

8 (1984) **Ulrich Güttler**
Beurteilung des Steifigkeits- und Nachverdichtungsverhaltens von ungebundenen Mineralstoffen

9 (1986) **Peter Jordan**
Einfluss der Belastungsfrequenz und der partiellen Entwässerungs-möglichkeiten auf die Verflüssigung von Feinsand

10 (1986) **Eugen Makowski**
Modellierung der künstlichen Bodenvereisung im grundwasserdurchströmten Untergrund mit der Methode der finiten Elemente

11 (1986) **Reinhard A. Beine**
Verdichtungswirkung der Fallmasse auf Lastausbreitung in nichtbindigem Boden bei der Dynamischen Intensivverdichtung

12 (1986) **Wolfgang Ebel**
Einfluss des Spannungspfades auf das Spannungs-Verformungsverhalten von gefrorenem Schluff im Hinblick auf die Berechnung von Gefrierschächten

13 (1987) **Uwe Stoffers**
Berechnungen und Zentrifugen-Modellversuche zur Verformungsabhängigkeit der Ausbaubeanspruchung von Tunnelausbauten in Lockergestein

14 (1988) **Gerhard Thiel**
Steifigkeit und Dämpfung von wassergesättigtem Feinsand unter Erdbebenbelastung

15 (1991) **Mahmud Thaher**
Tragverhalten von Pfahl-Platten-Gründungen im bindigen Baugrund,
Berechnungsmodelle und Zentrifugen-Modellversuche

16 (1992) **Rainer Scherbeck**
Geotechnisches Verhalten mineralischer Deponieabdichtungsschichten
bei ungleichförmiger Verformungswirkung

17 (1992) **Martin M. Bizialiele**
Torsional Cyclic Loading Response of a Single Pile in Sand

18 (1993) **Michael Kotthaus**
Zum Tragverhalten von horizontal belasteten Pfahlreihen aus langen Pfählen in Sand

19 (1993) **Ulrich Mann**
Stofftransport durch mineralische Deponieabdichtungen:
Versuchsmethodik und Berechnungsverfahren

20 (1992) **Festschrift anlässlich des 60. Geburtstages von**
Prof. Dr.-Ing. H. L. Jessberger
20 Jahre Grundbau und Bodenmechanik an der Ruhr-Universität Bochum

21 (1993) **Stephan Demmert**
Analyse des Emissionsverhaltens einer Kombinationsabdichtung im Rahmen der
Risikobetrachtung von Abfalldeponien

22 (1994) **Diethard König**
Beanspruchung von Tunnel- und Schachtausbauten in kohäsionslosem Lockergestein
unter Berücksichtigung der Verformung im Boden

23 (1995) **Thomas Neteler**
Bewertungsmodell für die nutzungsbezogene Auswahl von Verfahren zur Altlastensanierung

24 (1995) **Ralph Kockel**
Scherfestigkeit von Mischabfall im Hinblick auf die Standsicherheit von Deponien

25 (1996) **Jan Laue**
Zur Setzung von Flachfundamenten auf Sand unter wiederholten Lastereignissen

26 (1996) **Gunnar Heibrock**
Zur Rissbildung durch Austrocknung in mineralischen Abdichtungsschichten
an der Basis von Deponien

27 (1996) **Thomas Siemer**
Zentrifugen-Modellversuche zur dynamischen Wechselwirkung zwischen Bauwerken
und Baugrund infolge stoßartiger Belastung

28 (1996) **Viswanadham V. S. Bhamidipati**
Geosynthetic Reinforced Mineral Sealing Layers of Landfills

29 (1997) **Frank Trappmann**
Abschätzung von technischem Risiko und Energiebedarf bei Sanierungsmaßnahmen
für Altlasten

30 (1997) **André Schürmann**
Zum Erddruck auf unverankerte flexible Verbauwände

31 (1997) **Jessberger, H. L. (Herausgeber)**
Environment Geotechnics, Report of ISSMGE Technical Committee TC 5
on Environmental Geotechnics

Herausgeber: Th. Triantafyllidis

32 (2000) **Triantafyllidis, Th. (Herausgeber)**
Boden unter fast zyklischer Belastung: Erfahrung und Forschungsergebnisse (Workshop)

33 (2002) **Christof Gehle**
Bruch- und Scherverhalten von Gesteinstrennflächen mit dazwischenliegenden Materialbrücken

34 (2003) **Andrzej Niemunis**
Extended hypoplastic models for soils

35 (2004) **Christiane Hof**
Über das Verpressankertragverhalten unter kalklösendem Kohlensäureangriff

36 (2004) **René Schäfer**
Einfluss der Herstellungsmethode auf das Verformungsverhalten von Schlitzwänden in weichen bindigen Böden

37 (2005) **Henning Wolf**
Zur Scherfugenbänderung granularer Materialien unter Extensionsbeanspruchung

38 (2005) **Torsten Wichtmann**
Explicit accumulation model for non-cohesive soils under cyclic loading

39 (2008) **Christoph M. Loreck**
Die Entwicklung des Frischbetondruckes bei der Herstellung von Schlitzwänden

40 (2008) **Igor Arsic**
Über die Bettung von Rohrleitungen in Flüssigböden

41 (2009) **Anna Arwanitaki**
Über das Kontaktverhalten zwischen einer Zweiphasenschlitzwand und nichtbindigen Böden

Herausgeber: T. Schanz

42 (2009) **Yvonne Lins**
Hydro-Mechanical Properties of Partially Saturated Sand

43 (2010) **Tom Schanz (Herausgeber)**
Geotechnische Herausforderungen beim Umbau des Emscher-Systems
Beiträge zum RuhrGeo Tag 2010

44 (2010) **Jamal Alabdullah**
Testing Unsaturated Soil for Plane Strain Conditions: A New Double-Wall Biaxial Device

45 (2011) **Lars Röchter**
Systeme paralleler Scherbänder unter Extension im ebenen Verformungszustand

46 (2011) **Yasir Mawla Hammood Al-Badran**
Volumetric Yielding Behavior of Unsaturated Fine-Grained Soils

47 (2011) **Usque ad finem**
Selected research papers

48 (2012) **Muhammad Ibrar Khan**
Hydraulic Conductivity of Moderate and Highly Dense Expansive Clays

49 (2014) **Long Nguyen-Tuan**
Coupled Thermo-Hydro-Mechanical Analysis: Experiment and Back Analysis

50 (2014) **Tom Schanz**
Ende des Steinkohlenbergbaus im Ruhrrevier: Realität und Perspektiven für die Geotechnik
Beiträge zum RuhrGeo Tag 2014

51 (2014) **Usque ad finem**
Selected research papers

52 (2014) **Houman Soleimani Fard**
Study on the Hydro-Mechanical Behavior of Fiber Reinforced Fine Grained Soils,
with Application to the Preservation of Historical Monuments

53 (2014) **Wiebke Baille**
Hydro-Mechanical Behaviour of Clays - Significance of Mineralogy